Catalytic transformations of bio-derived C_5/C_6 platform molecules to monomers and fuel additives

A THESIS SUBMITTED TO THE
UNIVERSITY OF PUNE

FOR THE DEGREE OF
DOCTOR OF PHILOSOPHY
(IN CHEMISTRY)

BY
Mr. Amol M. Hengne

Research Guide
Dr. Chandrashekhar V. Rode
Chief Scientist

CHEMICAL ENGINEERING AND PROCESS DEVELOPMENT DIVISION
CSIR- NATIONAL CHEMICAL LABORATORY
PUNE- 411 008, INDIA

October-2013

सीएसआयआर–राष्ट्रीय रासायनिक प्रयोगशाला
(वैज्ञानिक तथा औद्योगिक अनुसंधान परिषद)
डॉ. होमी भाभा मार्ग, पुणे – 411 008. भारत
CSIR-NATIONAL CHEMICAL LABORATORY
(Council of Scientific & Industrial Research)
Dr. Homi Bhabha Road, Pune - 411008. India

Certificate of the Guide

Certified that the work incorporated in the thesis entitled **"Catalytic transformations of bio-derived C_5/C_6 platform molecules to monomers and fuel additives"** submitted by **Mr. Amol M. Hengne** was carried out by the candidate under my supervision/guidance. Such material as has been obtained from other sources has been duly acknowledged in the thesis.

Date: 21-10- 2013

Dr. Chandrashekhar V. Rode
(Supervisor/Research Guide)

डॉ. चं. व. रोडे/Dr. C. V. RODE
वैज्ञानिक/Scientist
राष्ट्रीय रासायनिक प्रयोगशाला
National Chemical Laboratory
पुणे/ PUNE-411 008.

Communication Channels
NCL Level DID : 2590
NCL Board No. : +91-20-25902000
EPABX : +91-20-25893300
: +91-20-25893400
FAX
Director's Office : +91-20-25902601
COA's Office : +91-20-25902660
COS&P's Office : +91-20-25902664
WEBSITE
www.ncl-india.org

Declaration by the Candidate

I declare that the thesis entitled **"Catalytic transformations of bio-derived C_5/C_6 platform molecules to monomers and fuel additives"** submitted by me for the degree of Doctor of Philosophy is the record of work carried out by me during the period from 24-12-2010 to 21-10-2013 under the guidance of **Dr. C. V. Rode** and has not formed the basis for the award of any degree, diploma, associateship, fellowship, titles in this or any other University or other institution of Higher learning.

I further declare that the material obtained from other sources has been duly acknowledged in the thesis.

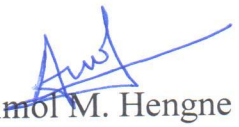

Amol M. Hengne

Date: 21-10-2013

CSIR-National Chemical Laboratory,

Pune-411 008

Dedicated to my beloved Family and Friends...

ACKNOWLEDGEMENT

I wish to place on record my immense and sincere gratitude to my guide ***Dr. Chandrashekhar V. Rode,*** *Chief Scientist, Chemical Engineering and Process Development Division, CSIR-National Chemical Laboratory (NCL), Pune, for his invaluable guidance, help, advice, encouragement and continuous support, throughout my PhD. I really admire the way he handled the scientific and nonscientific things with perfection and sincerity. There is no doubt that I learnt so many things from him especially how to analyze and get valuable information even from small things, and how to solve a problem.*

I am very much grateful to the Chair, Chemical Engineering and Process Development Division, Dr. V. V. Ranade, for providing me all the divisional facilities required for my research work.

I would like to thank Dr. S. Pal, Director, NCL, Pune, who gave me an opportunity to work in this esteemed research laboratory and providing all infrastructural facilities. I am also very much thankful to Council of Scientific and Industrial Research (CSIR) India for awarding me the research fellowship.

I am very much grateful to Dr. H. S. Potdar, Dr. M. Shirai, (AIST, Sendai, Japan), Dr. K. R. Patil, Dr. P. N. Joshi, Dr. Wadgaonkar,Dr. R. C. Chikate, Dr. B. B. Kale, Dr. B. L. V. Prasad, for their valuable discussions and facilities that they offered to me to complete this work.

My deepest and heartiest thanks goes to all my seniors and friends, Dr. Vikas, Dr. Jayprakash Nadgeri, Dr. Ajit Garade, Dr. Vivek Mate, Dr. S. Vijayanand, Narayan Biradar, Ajay Jha, Sumit Kamble, Sachin Sakate, Ajay Ghalwadkar, Atul Malawadkar, Rameshwar Swami, Virendra Patil, Rajan Pandya, Datta Mhamane, Anurag Sunda, Mahadev Patil, Sachin Jadkar, Pravin Mohite, Nitin Kore, Rupak Patil, Nilesh Tangale, Tejansh Chandole, Nagesh Hengne, Pradeep Biradar, Shivanand Patil, Abhijit, Sameer Joshi, Yogesh Suryavanshi, Ms. Rasika Mane, Mrs. Aparna Potdar, Ms. Sharada Kondawar, Ms. Mandakini Biswal, Ms. Priyanka Patil, Ms. Shobha Birajdar, Mrs. Chetana Patil, Ms. Chaitali Bagade, and Mrs. Pallavi Deshmukh, all research scholars

and friends in NCL who are not named in person, for their valuable suggestions and helping hand.

It is a pleasure for me to thank my NCL friends Hanumant Gurav, Dhanraj, Pradip Pachfule, Pradeep Lasonkar, Munshi, Balaji Jadhav, Sharad Gotmukhale, Prakash Korake, Samadhan, Ms. Trupti Kotbagi.

Also I express my special thanks to all scientific and non-scientific staff of NCL, Mr. David Soloman, Mr. Raheja, Mr. Dure, Mr. Chinnadurai, Mr. Kamble, and Mr. Patne.

This thesis would not have been possible without the strong faith, support and encouragement of my family. I wish to express my deep sense of gratitude to my parents for always providing unconditional support and helping me over the years. I would like to thank my wife for being patience and support me during the tough writing stage of the thesis.

Hengne Amol Mahalingappa

List of contents

List of tables

List of schemes

List of figures

Abbreviations

LA	Levulinic acid
MeLA	Methyl levulinate
IPALA	Isopropyl levulinate
Butyl LA	Butyl levulinate
GVL	γ- valerolactone
1, 5 PDO	1, 5 pentane diol
MTHF	Methyl tetrahydrofuran
PA	Pentanoic acid
VA	Valeric Acid/Valerates
FA	Formic acid
4-Hyd-MeLA/4 MeLA	4 hydroxy methyl levulinate
4-Hyd-LA	4 hydroxy Levulinic acid
4 Hyd-IPA LA	4 hydroxy isopropyl levulinate
FAL	Furfuryl alcohol
FFR	Furfural
5-HMF	5-hydroxy methyl furfural
MeOH	Methanol
EtOH	Ethanol
n-PrOH	n-Propanol
CTH	Catalytic transfer hydrogenation
MIM	1 Methyl imidazolium
MMT	Montmorillonite
NMP	N -Methyl 2-pyrollidonium
[BMIm-SH]	1-Butyl sulfonic acid, 3-methyl imidazolium
ILs	Ionic liquids
PLA	Polylactic acid or polylactide
1,2-PDO	1,2-propanediol
EG	Ethylene glycol
SO_4–ZrO_2	Sulfated zirconia

BET	Brunauer, Emmett and Teller
XRD	X-ray diffraction
TEM	Transmission electron microscopy
HR-TEM	High-resolution transmission electron microscopy
SAED	Selected area electron diffraction
EDS	Energy-dispersive X-ray spectroscopy
SEM	Scanning electron microscope
ICP-AES	Inductively coupled plasma atomic emission spectroscopy
XPS	X-ray photoelectron spectroscopy
ESCA	Electron Spectroscopy for Chemical Analysis
EXAFS	Extended X-ray absorption fine structure
XANES	X-ray absorption near edge structure
FT-IR	Fourier transform infrared spectroscopy
TG and DTA	Thermogravimetric and differential thermal analysis
NH_3-TPD	Temperature programmed desorption of ammonia
Py-IR	Pyridine infrared
TPR	Temperature programmed reduction
WGSR	Water gas shift reaction
LHSV	Liquid hourly space velocity
WHSV	Weight hourly space velocity
GC	Gas chromatography
HPLC	High performance liquid chromatography
FID	Flame ionization detector
TCD	Thermal conductivity detector
FFAP	Free fatty acid phase
HP-5	Hewlett Packard-5
TOF	Turnover frequency
NL	Normal liter
APR	Aqueous phase reforming
TOS	Time on stream

ABSTRACT OF THESIS

"Catalytic transformations of bio-derived C_5/C_6 platform molecules to monomers and fuel additives"

The cheapest, most abundant, and fastest growing form of terrestrial biomass is lignocellulosic biomass, which is composed of cellulose, hemicellulose and lignin [1]. Pentoses as well as hexoses derived from carbohydrate feedstock are processed to obtain important C_5-C_6 platform molecules such as levulinic acid (LA), itaconic acid (IA) and furfuryl alcohol (FAL) [2]. Hence one of the major subject areas in biomass conversion is aimed at designing, developing new catalytic systems for selective transformation of C_5 and C_6 molecules into specialty monomers and fuels/fuel additives. Oxygen atoms present in the bio-derived molecules poses an interesting challenge of selective hydro-deoxygenation by designing appropriate catalyst systems and at the same time with less number of processing steps as compared to the fossil derived hydrocarbons [3-8]. Downstream processing of LA and furfuryl alcohol gives several useful molecules such as lactone (GVL) and esters of levulinic acid (methyl levulinate) which are sustainable commodity chemicals having great commercial importance as solvents in lacquers and can be converted in to a variety of monomers and fuel/fuel additives [9-11].

My PhD work aims at developing various non-noble catalytic systems, their characterization and evaluation for the hydrogenation of bio-derived C_5/C_6 platform molecules to the corresponding lactones and diols having applications as fuel and/or fuel additives. The study also involves preparation of noble metal catalysts for understanding the role of support in the activity and stability of the catalysts. The thesis contains total 7 chapters among which, **Chapter 1** deals with introduction of rational for biorefineries, role of catalysis in biorefineries, and importance of heterogeneous catalysts. This chapter also covers the literature survey on the hydrogenation of LA, IA and 5-methyl FAL. At the end of this chapter, the objectives and scope of this thesis are given. **Chapter 2** includes experimental procedure of the preparation of noble/non-noble metals (Ru, Ag, Cu and Ni) catalysts using various supports such as C, ZrO_2, montmorillonite (MMT), SiO_2 and Al_2O_3. Experimental setup and procedure for hydrogenation reactions in batch

and continuous reactors under high and atmospheric pressure conditions are given in detail. Various characterization techniques used for the prepared catalyst include BET N_2 adsorption, Chemisorption, XRD, Raman, XPS, SEM and HRTEM. The analytical techniques such as GC and HPLC used for the analysis of liquid and gaseous reactants and products in this work are also described.

Chapter 3 contains the screening of a series of supported noble metal catalysts studied for the hydrogenation of methyl levulinate. We evaluated the activity of Ru on various supports (C, Al_2O_3 and SiO_2) for the hydrogenation of methyl levulinate. Among the three supports studied, carbon supported ruthenium catalyst showed the highest conversion of methyl levulinate 95% which was about 5–13 times higher than the ruthenium on silica and alumina respectively, and the highest selectivity 91% was achieved for GVL. TPR and XPS studies revealed that Ru^0 species were in less concentration or absent in case of less active Ru/SiO_2 and Ru/ Al_2O_3 catalysts, due to either encapsulation of Ru with silica or due to some other stable species such as $Ru(OH)_3$ formed on the surface [12].

Chapter 4 deals with the systematic development of non noble metal catalysts for the hydrogenation of levulinic acid and its methyl ester. The nanocomposites of $Cu–ZrO_2$ and $Cu–Al_2O_3$ quantitatively catalyzed the hydrogenation of levulinic acid and its methyl ester to give 90–100% selectivity to γ-valerolactone in methanol and water respectively. In our unique approach, copper leaching was completely suppressed in the case of the $Cu–ZrO_2$ catalyst in methanol in spite of the substrate loading was increased from 5 to 20% w/w. The excellent recyclability of the $Cu–ZrO_2$ catalyst with complete LA conversion and >90% GVL selectivity makes it a sustainable process having a commercial potential. This was also established by continuous hydrogenation of levulinic acid and its ester over $Cu-ZrO_2$ catalyst, to achieve complete conversion of levulinic acid/its ester with 90-95% selectivity to GVL [13].

Chapter 5 contains studies on development of two new catalyst systems for catalytic transfer hydrogenation (CTH) of levulinic acid to GVL using two different H_2 donors, viz. isopropanol (IPA) and formic acid. We systematically explored the suitability of various supports such as montmorilonite (MMT), Al_2O_3, SiO_2, ZnO and C for Ni for hydrogenation of LA to GVL using isopropanol as a solvent and also as a

hydrogen donor. Ni /MMT showed complete conversion with highest selectivity (>99%) to GVL within 1h due to its highest Bronsted acidity. As formic acid is co-generated during the production levulinic acid by hydrolysis of bio-derived hexose (glucose via 5-hydroxymethyl furfural), we report here for the first time, bi-metallic Ag, Ni catalysts in combination with zirconia for aqueous LA:FA mixture hydrogenation with complete conversion of LA and highest selectivity (> 99%) to GVL. In this study, the role of co-metal was found to be crucial for decomposition of formic acid to give nascent hydrogen without CO formation. Synergetic effect of Ag-Ni was suggested by the H_2-TPR profile. This catalyst (Ag-Ni/ZrO_2) was also tested for HCOOH mediated selective reductive transformation of other biomass-derived compounds ranging from C_3 (glycerol) to C_6 (5-Methyl furfural) molecules to the respective value added hydrogenated products.

In chapter 6, we report the catalytic alcoholysis/hydrogenation for single pot conversion of furfuryl alcohol to GVL via esters of LA by using the combination of sulfonic acid-functionalized ionic liquids (SO_3H-ILs) and carbon supported Ru, Re, Ir and Ag catalysts. 5%Ru/C+ [BMIm-SO3H][HSO4] showed the complete dehydration of furfuryl alcohol with 95% selectivity to methyl levulinate followed by hydrogenation to GVL (68%) in a batch reactor. The Bronsted acidity of ILs was varied by varying the anions such as $ClSO_3H$, SO_3H, PTSA and TFA with the same cation, MIMH for the first step alcoholysis of furfuryl alcohol to methyl levulinate. Effect of process parameters such as catalyst loading, substrate loading, metal loading and H_2 pressure was carried out for both steps i) alcoholysis of furfuryl alcohol to methyl levulinate ii) single pot conversion of FAL to GVL [14].

Chapter 7 summarizes the results presented in all the chapters and general conclusions arrived at from the discussed results.

References

1. M. J. Climent, A. Corma, S. Iborra, Green Chem. 13 (2011) 520.
2. J. J. Bozell, G. R. Petersen, Green Chem. 12 (2010) 539.
3. I. T. Horvath, H. Mehdi, V. Fabos, L. Boda and L. T. Mika, Green Chem. 10 (2008) 238.
4. G. W. Huber, S. Iborra, A. Corma, Chem. Rev., 106 (2006) 4044.
5. E. Manzer, Appl. Catal. A: Gen. 272 (2004) 249.
6. J. P. Lange, J. Z. Vestering, R. J. Haan, Chem. Commun. (2007) 3488.
7. R. W. Christian, H. D. Brown, R. M. Hixon, J. Am. Chem. Soc. 69 (1947) 1961.
8. H. A. Schutte, R. W. Thomas, J. Am. Chem. Soc. 52 (1930) 3010.
9. R. A. Bourne, J. G. Stevens, J. Ke, M. Poliakoff, Chem. Commun. 2007, (4632).
10. J. P. Lange, R. Price, P. M. Ayoub, J. Louis, L. Petrus, L. Clarke, H. Gosslink, Angew. Chem., Int. Ed. 49 (2010) 4479.
11. R. J. Hann, J. P. Lange, US, 0046399, (2011).
12. A. M. Hengne, C. V. Rode, Green Chem. 14 (2012) 1064.
13. A. M. Hengne, N.S. Biradar, C. V. Rode, Catal. Lett. 142 (2012) 779.
14. A. M. Hengne, S. B. Kamble, C. V. Rode, Green Chem. 15 (2013) 2540–2547.

Chapter 1

Introduction and literature survey

1.1. Biomass

The term "biomass" means any organic matter that is available on a renewable or recurring basis (excluding old-grown timber), including dedicated energy crops, trees, agricultural food, feed crop residues, aquatic plants, wood and wood residues, animal wastes, and other waste materials [1, 2]. Biomass has a complex composition and its primary separation leads to three main components, the subsequent treatment and processing of which produces a whole range of products similar to that obtained from petro-resources. Petro chemistry involves processing of well defined chemically pure starting material viz. hydrocarbons obtained from petro-refineries. This is an integrated complex in which basic chemicals, intermediates, and sophisticated products are produced [3]. However, the starting material being simple hydrocarbons, their transformations to various functional groups invariably require to overcome large energy barriers. In principle, petroleum refineries can be transferred to biorefineries using biomass feedstock however the later, in contrast to petroleum feedstock contains C:H:O:N in different ratios. This characteristic of biomass feedstock enables its processing at lower energy input than that for petroleum feedstock as shown in Figure 1.1. Biorefineries combine the essential technologies analogous to petro refinery, which convert biological raw materials into the industrial intermediates and final products. Thus biomass can be suitably modified for its subsequent processing to obtain specific target products [4]. Plant biomass consists of the basic precursors such as carbohydrates, lignin, proteins, fats, vitamins, dyes, flavors, aromatic essences of different chemical structures. A technically feasible separation process which would enable to separate the above precursors and the subsequent processing of the basic compounds is currently at fairly advanced research and development stage. Worldwide, approximately 170 billion tones of biomass is produced per year by photosynthesis, which consists of three major components i) Cellulose: high molecular weight polymers of glucose that are held rigidly together as bundles of fibers to provide material strength [5]. The cellulose typically accounts for some 40 wt% of the lignocellulose.

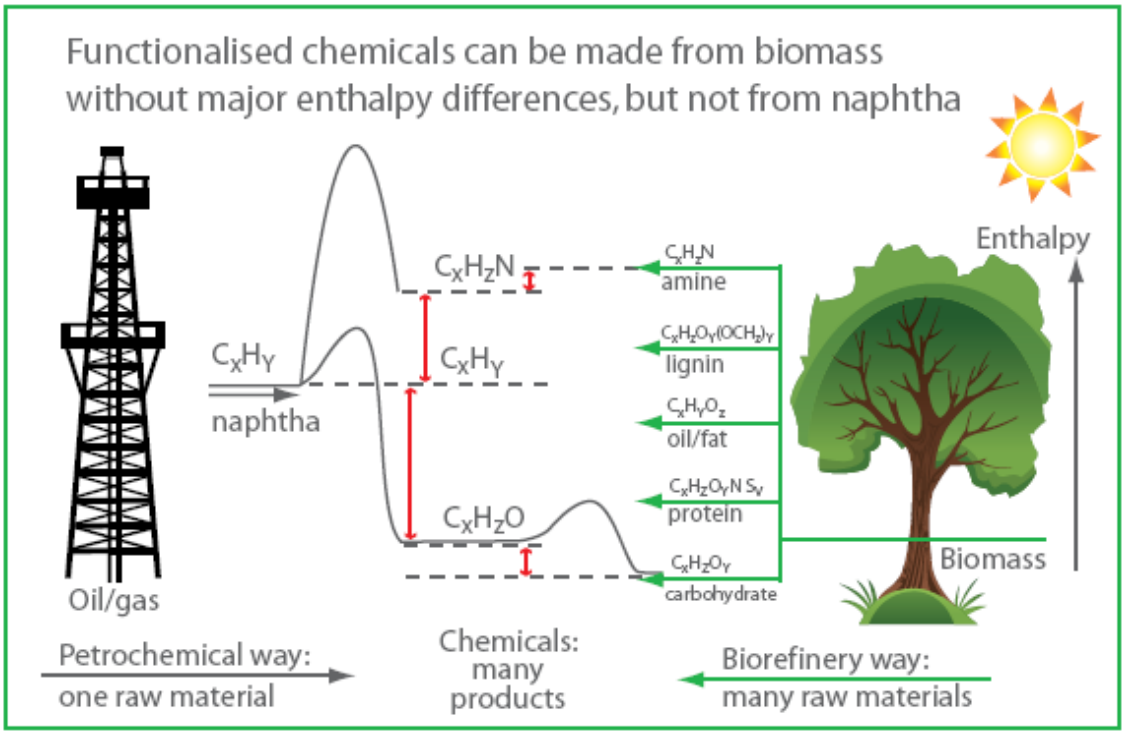

Figure 1.1. Energy barriers between petrorefinery Vs biorefinery [6, 7]

ii) Hemicellulose: shorter polymers of various sugars that glue the cellulose bundles together. It usually accounts for some 25 wt% of the lignocellulose. iii) Lignin: a tri-dimensional polymer of propyl-phenol that is embedded in and bound to the hemicellulose. It provides rigidity to the structure. It accounts for some 20 wt% of the lignocellulose. Thus, 75% lignocellulosic biomass is part of carbohydrates, of which only 3-4% is used for food and nonfood sectors. Hence, there is a vast scope to develop technologies for conversion of unutilized biomass to chemicals, fuels and materials [8-10].

1.2. Integrated biorefinery

The term "Biorefinery" was first defined in the year 1997 as the complex (to fully integrated) systems of sustainable, environmentally and resource-friendly technologies for the comprehensive materials and energy production [10, 11]. The original term used in Germany "complex construction and systems" was substituted by "fully integrated systems". The US Department of Energy (DOE) uses the following definition [12, 13].

"A biorefinery is an overall concept of a processing plant where biomass feedstocks are converted and extracted into a spectrum of valuable products based on the petrochemical refinery."

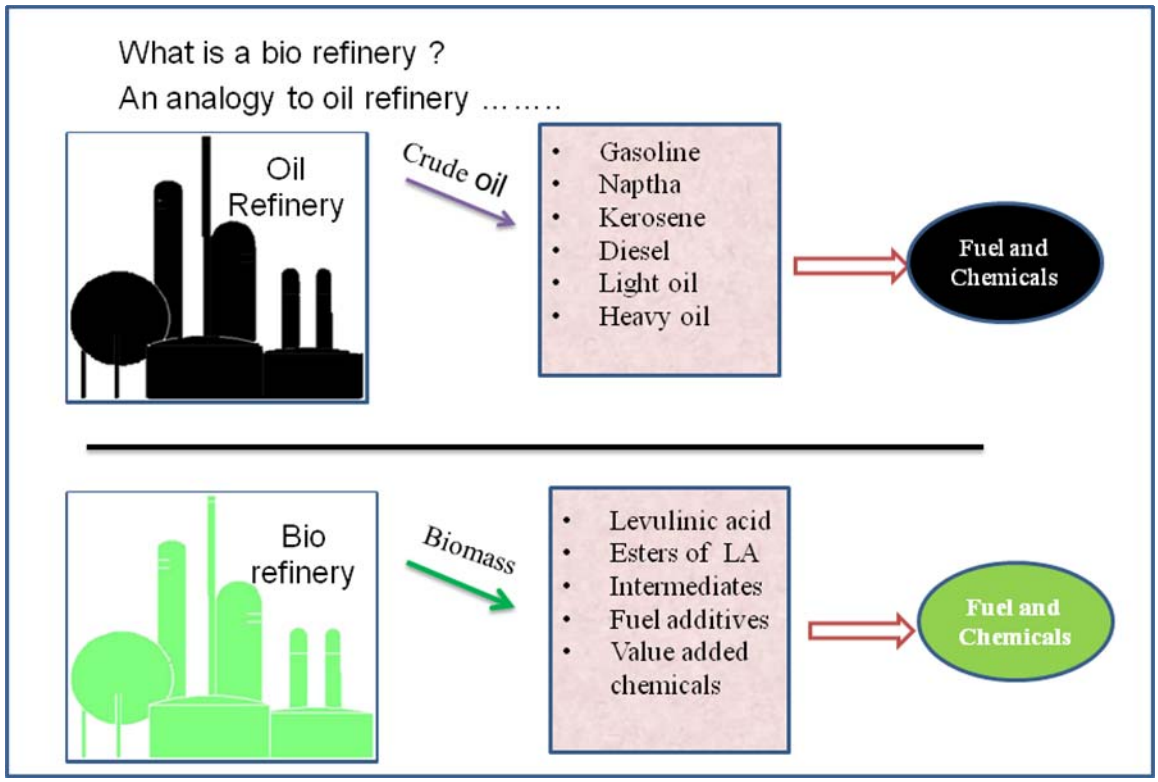

Figure 1.2. Biorefinery concept [15, 16]

The American National Renewable Energy Laboratory (NREL) published the definition [14]. "A biorefinery is a facility that integrates biomass conversion processes and equipment to produce fuels, power, and chemicals. The biorefinery concept is analogous to today's petroleum refineries, which produce multiple fuels and products from petroleum as shown in Figure 1.2 biorefineries have been identified as the most promising route to the creation of a new domestic bio-based industry [17, 18]. From the start of biorefinery concept, several technological advances have been made according to which the biorefineries are termed as follows.

i) Generation-I biorefinery: This involves a dry milling plant for ethanol production. It uses whole grain as a feedstock hence, competing seriously with the food chain. Other drawbacks of this technology are, it has a fixed processing capability and produces a

fixed amount of ethanol, feed. Therefore, this technology can be used for restricted purposes only [11].

ii) Generation-II biorefinery: This is the current wet milling technology however it also uses grain feedstock, yet has the capability to produce a variety of end products depending on product demand. Such products include starch, high-fructose corn syrup, ethanol, corn oil, plus corn gluten feed, and meal. This type of biorefinery opens up numerous possibilities to connect industrial product lines with existing agricultural production units. Due to more value added product diversity other than ethanol, "Generation-II biorefineries" have existing plants like Nature Works PLA facility and Iogen's wheat straw to ethanol plant.

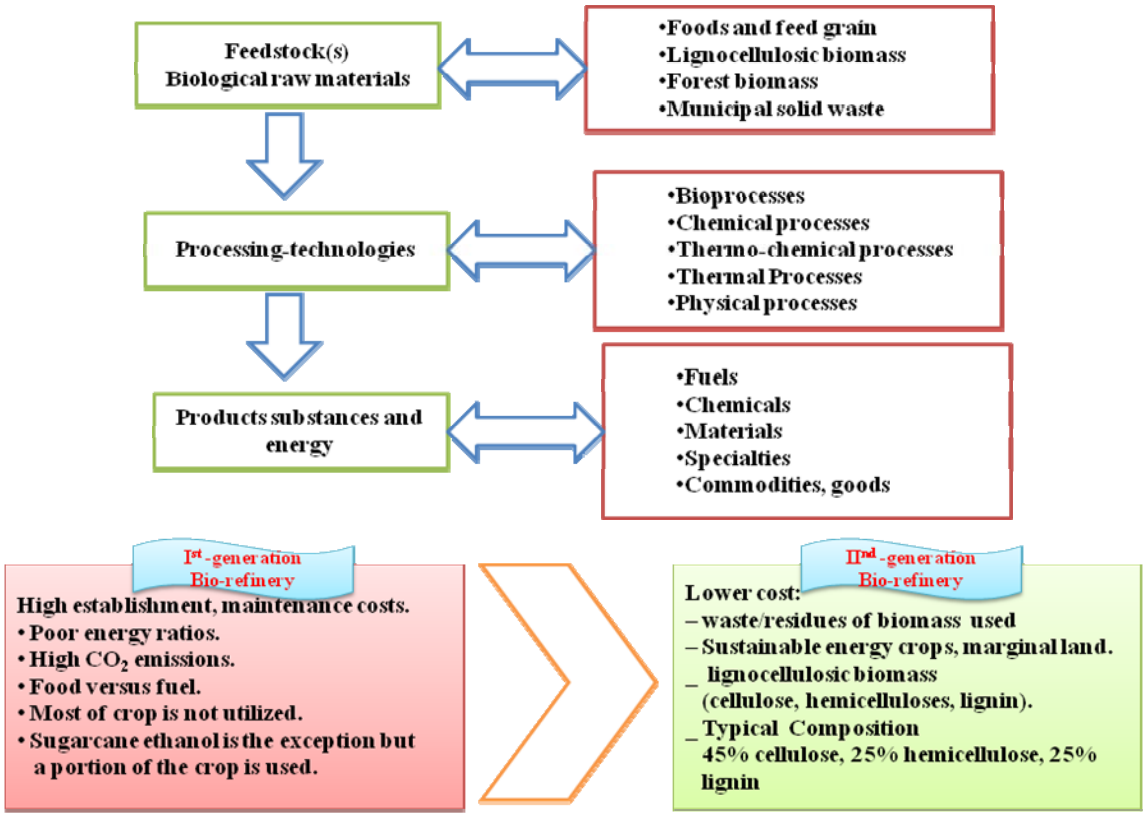

Figure 1.3. Generations of biorefinery

iii) Generation-III are more advanced biorefineries although have not yet been built but will use agricultural or forest biomass to produce multiple products streams, for example, ethanol for fuels, chemicals, and plastics. Figure 1.3 shows the details of the

types of the biorefineries particularly highlighting comparison between Generation-I and Generation-II [19].

1.2.1. Challenges in biorefinery development [20-26]

- Bio-based chemical production is challenged by a lack of matured conversion technology although; promising hypothetical scenarios integrating fuels and chemicals do exist.
- Conversion of renewable carbon to chemicals is the least developed and most complicated of all biorefinery operations, especially when compared to conversion processes available for nonrenewable hydrocarbons.
- Biobased chemical production is challenged by an overabundance of targets. Integrated biorefinery development is still in its infancy, and as such has yet to identify a core group of primary chemicals and secondary intermediates analogous to those used by the petrochemical industry.
- The range of potential targets includes structures already made by the chemical industry (and thus demonstrated as commercial products) as well as new structures formed from biorefinery building blocks.
- Rational selection of processes for existing opportunities and available expertise is necessary.

1.3. Biomass compositions

The details of biomass composition shown in Figure 1.4 in terms of its percentage range depending on the biomass feedstock and chemical structure are given below.

1.3.1. Lignin

It is an amorphous polymer composed of methoxylated phenylpropane structures such as coniferyl alcohol, sinapyl alcohol, and coumaryl alcohol [27]. These compounds provide strength and structural rigidity to plants as well as form a hydrophobic vascular system for the transportation of water and solutes [28]. The other two fractions, hemicellulose and cellulose are surrounded by lignin, which if desired can first be de-polymerized by a

pretreatment step so that the cellulose and hemicellulose portions can be accessed easily for further upgradation [29]. Although lignin can be isolated, it is not readily amenable to upgrading strategies. One option for lignin utilization is to burn it directly to produce heat and electricity. Heat and power obtained from burning lignin and other residual solids are more than enough to drive the biofuel production process [30]. In addition, lignin can serve as a chemical feedstock in the production of phenolic resins [31-34]. Pyrolysis strategies for lignin have been reported for the production of bio-oils and aromatics [35-37].

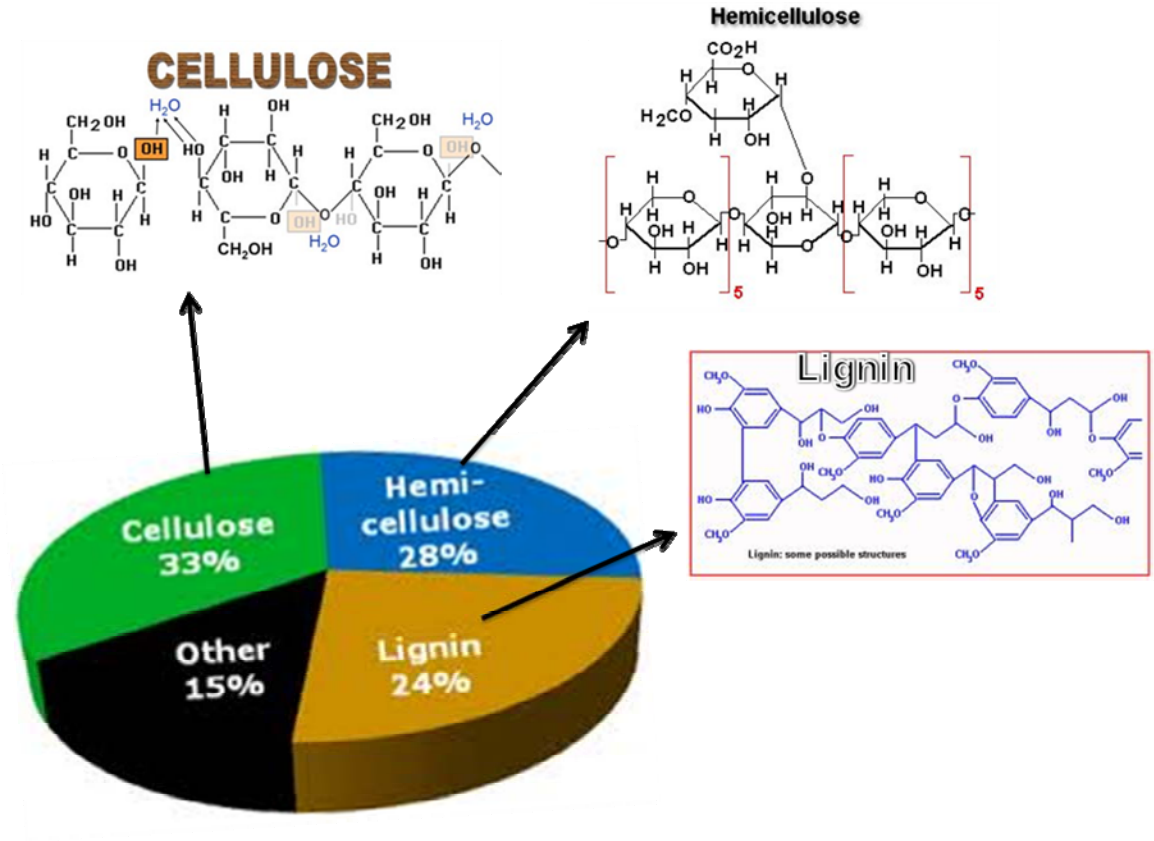

Figure 1.4. Biomass compositions [38]

1.3.2. Cellulose

Polymer composed of glucose units linked via β-glycosidic bonds, providing the structure with a rigid crystallinity that inhibits hydrolysis is known as cellulose. Cellulose is more accessible to hydrolysis in untreated biomass before the removal of lignin and hemicellulose. High yields of glucose (>90% of theoretical maximum) can be

achieved by enzymatic hydrolysis of cellulose after biomass pretreatment. Harsher conditions using solutions of mineral acids (H_2SO_4) at elevated temperatures can be applied to hydrolyze cellulose; however, these conditions lead to the formation of degradation products such as hydroxymethylfurfural (HMF) levulinic acid, and greater extent of insoluble humins [39].

1.3.3. Hemicellulose

It is an amorphous polymer generally comprised of five different sugar monomers: D-xylose (the most abundant), L-arabinose, D-galactose, D-glucose, and D-mannose [31]. If separate processing of cellulose is desired to increase the effectiveness of the cellulose hydrolysis steps in the production of glucose, the hemicellulose fraction of biomass can be removed during pretreatment. The pretreatment process aims to preserve the xylose obtained from hemicellulose and inhibits the formation of degradation and dehydration products. Compared to hydrolysis of crystalline cellulose, hemicellulose extraction/hydrolysis is an easier process and allows for high yields of sugar [40, 41].

1.4. Processes for lignocellulosic biomass conversion

Current strategies for the conversion of lignocellulosic biomass into liquid hydrocarbon fuels involve three major primary routes: pyrolysis, gasification and aqueous-phase hydrolysis as shown in Figure 1.5. Out of the three strategies, the first two are the thermal processes involving biomass decomposition by manipulating high temperature conditions to yield selectively liquid products usually called bio-oils (Figure 1.6). Bio-oils are currently the cheapest form of liquid fuels that can be made from lignocellulosic biomass. It was in 1970, that the researchers first found the reaction conditions that maximize liquid bio-oil yields. There are two major routes to produce bio-oils, viz. fast pyrolysis and liquefaction. The first approach involves the conversion of biomass to synthesis gas, a mixture of CO and H_2 which serves as a precursor of liquid hydrocarbon fuels by Fisher Tropsch synthesis [42-44]

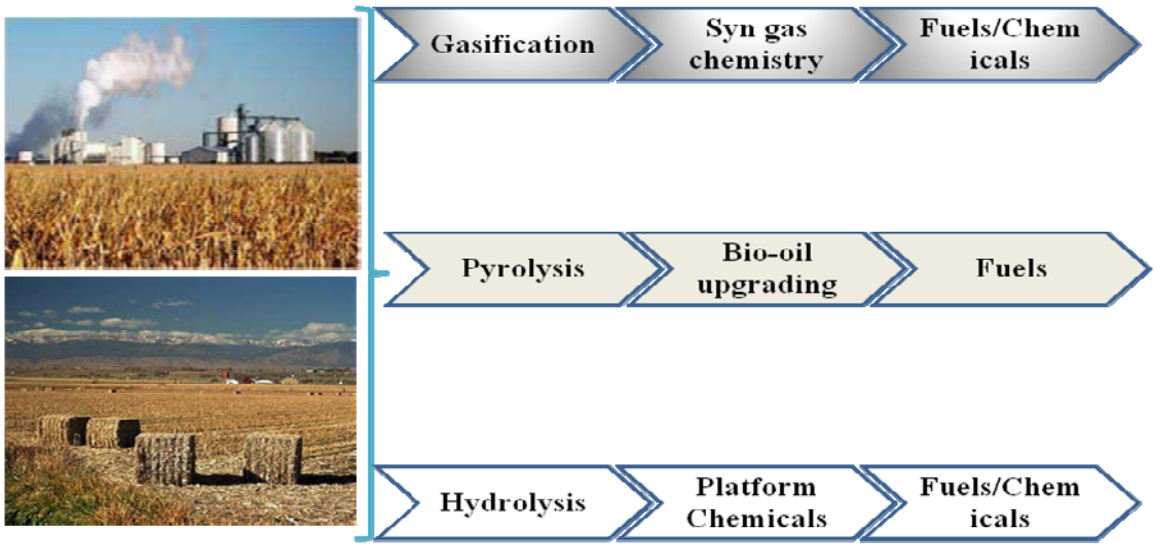

Figure 1.5. Processes for production of fuels and chemicals from biomass

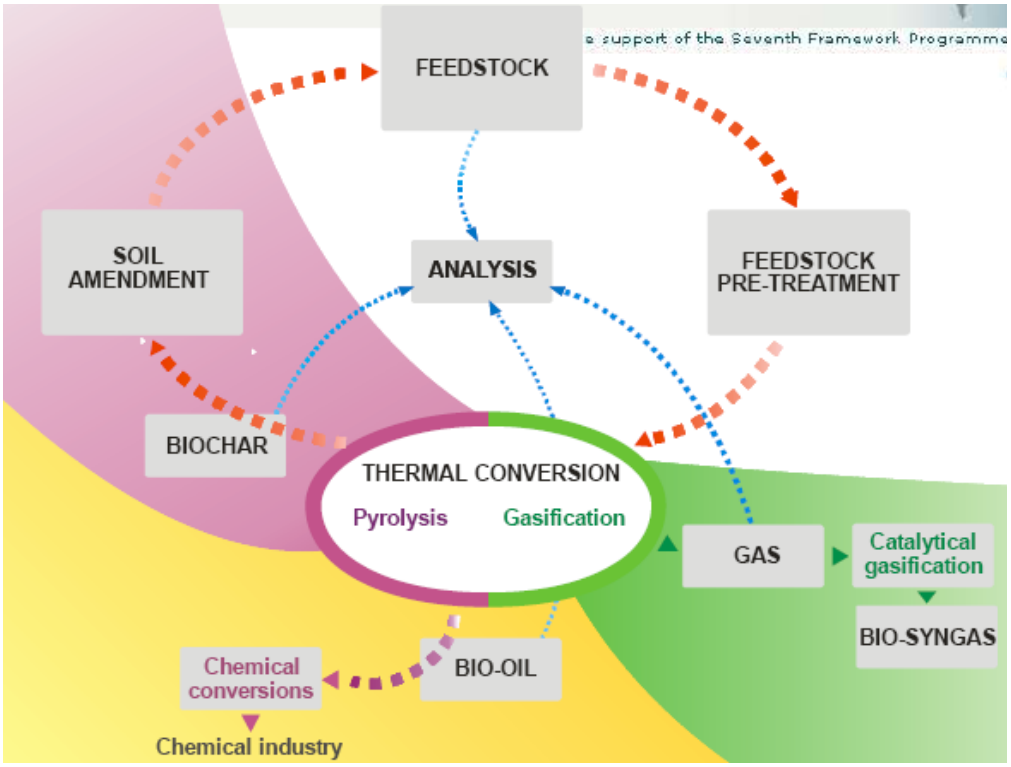

Figure 1.6. Thermal decomposition [42]

1.4.1. Pyrolysis

Fast pyrolysis is the thermal depolymerization process in which biomass is rapidly heated in absence of oxygen with short residence time at atmospheric pressure. Depending on the reaction conditions, reactor design, and type of biomass feedstock, the distribution of products varies in the gas, liquid, and solid phases [45]. The keys to maximize yields of bio-oils are: rapid heating, high heat transfer rate, short residence time, moderate reaction temperature (ca. 500 ^{o}C), and rapid cooling of pyrolysis vapors. An advantage of fast pyrolysis is that it is economical for use on a small scale (i.e. 50–100 tons-biomass per day). Figure 1.7 shows a portable fast pyrolysis reactor for liquid fuels production. This portable unit can easily access the biomass source, which significantly reduces costs in transportation of feedstocks [46, 47].

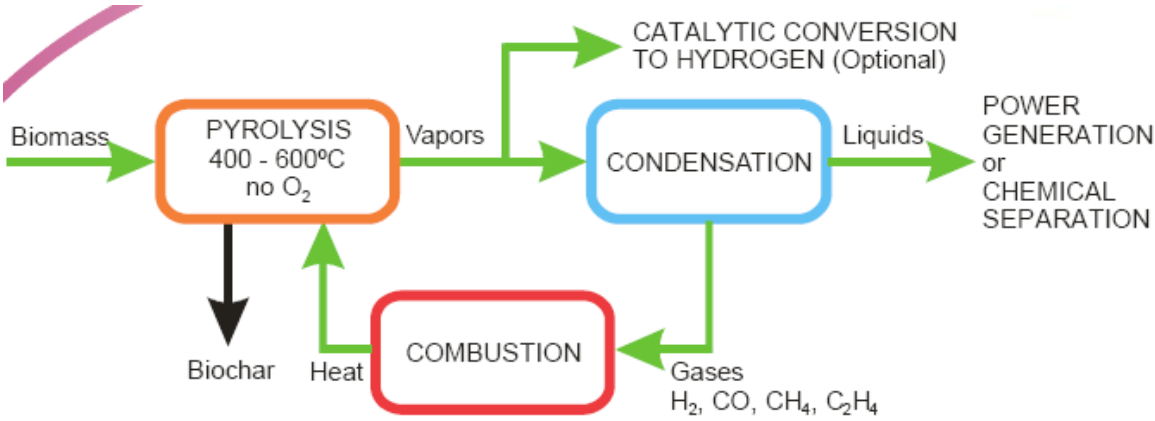

Figure 1.7. Pyrolysis of biomass

1.4.2. Gasification

This process for conversion of lignocelluloses is carried out by increasing temperature and/or pressure under controlled atmosphere, usually in the absence of catalysts. As shown in Figure 1.8, in biomass gasification, the plant material is converted to synthesis gas (i.e., a mixture of CO and H_2) at high temperatures (i.e., > 800 ^{o}C) via partial combustion in the presence of an oxidizing agent. To obtain alkanes suitable for use as liquid fuels, gasification is followed by Fischer-Tropsch synthesis. Instead of liquid alkanes, H_2 can be obtained as the end product by converting the CO present in the

synthesis gas to CO_2 and H_2 via the water gas shift reaction ($CO + H_2O$ or $CO_2 + H_2$) followed by purification [44, 48].

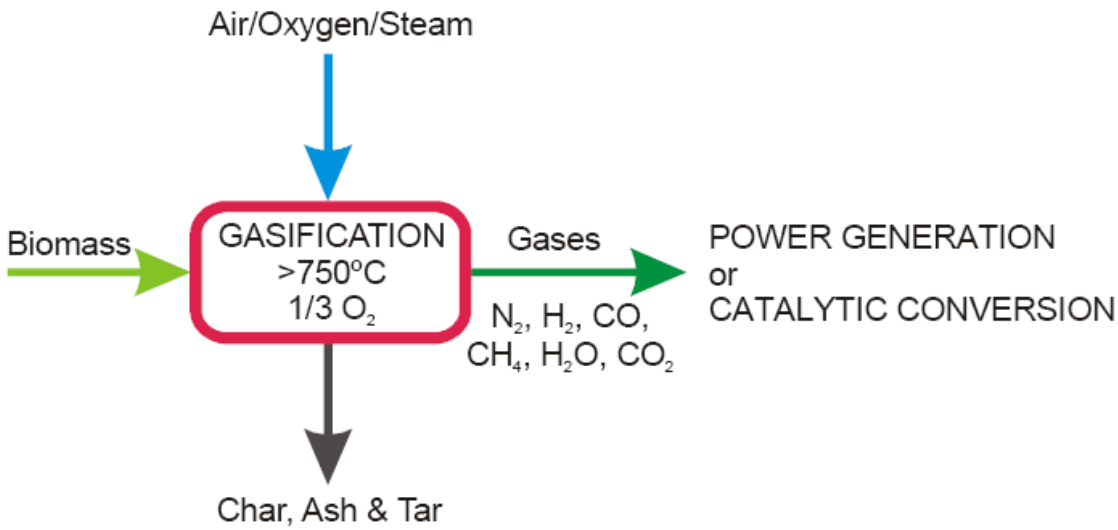

Figure 1.8. Gasification of biomass

1.4.3. Liquefaction

Liquefaction is an alternative pathway for the production of bio-oils, and this approach is summarized in Figure 1.9. Liquefaction consists of the catalytic thermal decomposition of large molecules to unstable shorter species that polymerize again into a bio-oil. Biomass is mixed with water and basic catalysts like sodium carbonate, and the process is carried out at lower temperatures than pyrolysis (250–450 ^oC) but higher pressures (5–20 atm) and longer residence times. These factors combine to make liquefaction a more expensive process; however, the liquid product obtained contains less oxygen (12–14%) than the bio-oil produced by pyrolysis and typically requires less extensive processing. However, problems exist associated with the complexity of the bio-oil product, leading to unsuitability for long term storage. Different approaches such as hydrodeoxygenation or steam reforming have been proposed to upgrade the bio-oils and to solve the stability issues. The hydrogen required by these upgrading strategies can be obtained by aqueous reforming of biomass releasing CO_2, thereby decreasing the dependence on external sources of hydrogen. It has also been proposed that bio-oils can serve as appropriate feedstocks for co-processing in petroleum refineries, particularly as

both hydro-treating and steam reforming are common practices in petroleum processing [49-51].

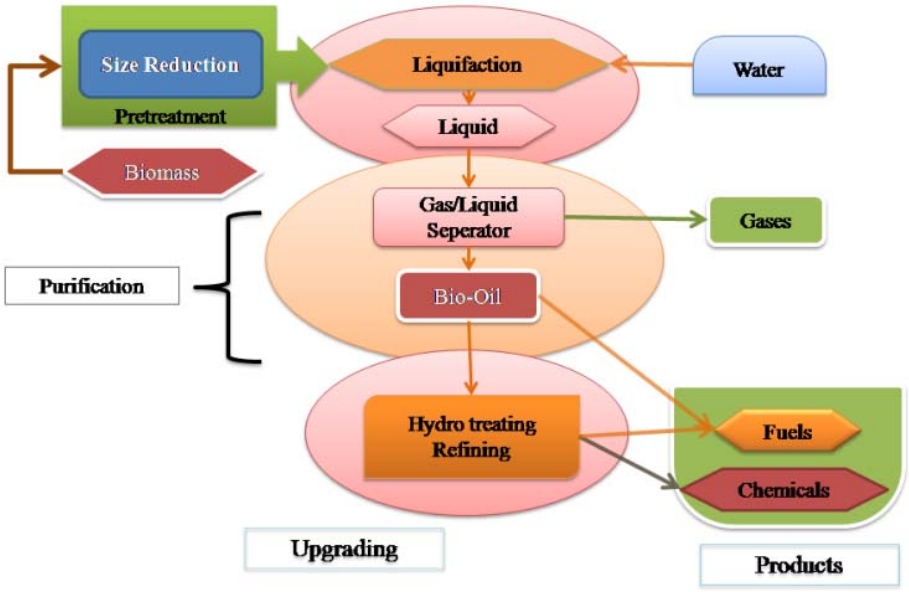

Figure 1.9. Liquefaction of biomass

1.4.4. Aqueous phase hydrolysis

Hydrolysis pathways are appropriate for lignocellulose processing if higher selectivity is desired in biomass utilization for example, in the production of chemical intermediates or targeted hydrocarbons for transportation fuel. Selective transformations require isolation of sugar monomers, a step which is complex and expensive for lignocellulosic feedstocks. Once sugar monomers are isolated however, they can be processed efficiently at relatively mild conditions by a variety of catalytic routes. Lignin utilization remains a challenge, although it makes a suitable feedstock for phenolic resins bio-oil/aromatic production through pyrolysis or catalytic fast pyrolysis, or heat and power production [52]. Aqueous phase processes for the conversion of carbohydrate-derived compounds are potentially attractive in that they do not require concentration of the aqueous solution and generally yield a gas phase or hydrophobic product that separates spontaneously from water, which reduces the cost of separation steps in the catalytic processing strategies. The primary motivation of the chemical route is the targeted reduction of the high oxygen content of carbohydrates (10 to 44%) by different reactions

such as hydrogenolysis, dehydration or hydrogenation to obtain hydrocarbons with increased energy density [53-55].

Four main processing units are needed for biomass conversion via syngas routes: a biomass gasifier, a gas clean-up unit, a water gas shift (WGS) reactor in certain cases, and finally a syngas converter [56]. The gasification unit converts the biomass at high temperature (600–900 ^{o}C) with oxidants (e.g., oxygen or steam). Syngas is the major product from the gasifier, accompanied by impurities such as tars, ammonia, hydrogen sulfide, and particulates. These impurities can have an adverse effect on downstream processing hence, they must be removed by different chemical and physical treatments. Although clean-up has been intensively studied, additional research is needed. Unlike gasification, pyrolysis and liquefaction take place under an inert atmosphere and lower temperatures (300-700 ^{o}C). The result of pyrolysis or liquefaction is a viscous liquid denoted as bio-oil, mixed with solid char. The elemental composition of bio-oil is similar to that of biomass, and it is composed of a complex mixture (more than 300 species) of highly oxygenated hydrocarbons and a substantial amount of water. Due to its high oxygen content, bio-oil cannot be utilized directly as a fuel and needs further upgrading reactions to lower the oxygen content, such as hydrodeoxygenation reactions [57-60].

The aforementioned thermo chemical approaches allow for the simultaneous processing of cellulose, hemicellulose and lignin, and these methods are generally preferred due to simplicity of operation and low costs. On the other hand, the simultaneous processing of components of biomass limits flexibility and does not allow us to take full advantage of the different chemical and physical properties of the hemicellulose and cellulose fractions, which is important for establishing biomass-based chemical and fuel industries. Therefore, it is desirable to separate different portions of the biomass through different pretreatment strategies, which are best carried out in the aqueous phase and thus referred to as aqueous-phase processing strategies.

1.4.5. Aqueous phase hydrolysis techniques

By separating the cellulose, hemicellulose and lignin portions of biomass, it becomes possible to combine chemical and biological routes as well. For instance, cellulose-derived C6 sugars can be processed through established routes to produce platform chemicals, selected fuel and fuel additives. Whereas, hemicellulose-derived C_5 sugars, which are more difficult to process enzymatically can be converted via chemical routes to value added chemicals. Hydrolysis can occur with concentrated or dilute acids, enzymes, or thermochemical procedures for the production of chemicals and fuels [61-64].

Three variations of hydrolysis techniques for lignocellulose decomposition with their corresponding characteristics are given below.

1.4.5.1 Acid hydrolysis

- Catalysts to break glycosidic bonds at low/high temperatures.
- Applicable to many feedstocks.
- Non-selective hence, producing undesirable byproducts.
- Scale-up strategies possible.

1.4.5.2. Enzymatic hydrolysis

- Theoretically highly selective, high monomer yields.
- Current costs are high due to enzyme losses and pretreatment steps.
- Treatment of waste materials may be more difficult.
- Current techniques focus on multiple reactors
- Variety of microorganisms/enzymes for hydrolysis/fermentation.

1.4.5.3. Thermal hydrolysis (e.g. steam auto hydrolysis)

- Only suitable for hemicelluloses.

1.5. Building blocks and their commercial potential

A large number of functionalized molecules can be obtained from lignocellulose decomposition, which varies chemically. From these numerous molecules, a team from Pacific Northwest National Laboratory (PNNL) and NREL identified a list of twelve chemicals having potential industrial applications as given in Figure 1.10. A shorter list of 30 potential candidates was selected from a list of more than 300 candidates, using an iterative review process based on the petrochemical model of building blocks, chemical data, known market data, properties, performance of the potential candidates, and previous industry experience of the team at PNNL and NREL. The final selection of 12 building blocks was made, the criteria of which are given in Table 1.1. The reported block chemicals can be produced from sugar by biological and chemical conversions.

Hydrolysis → Platform Chemicals

Name	Structure	Name	Structure
Glycerol	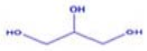	Levulinic acid	
3-hydroxypropionic acid	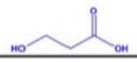	Glutamic acid	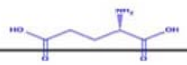
Succinic acid		Itaconic acid	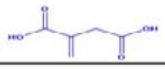
Fumaric acid	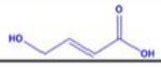	Xylitol	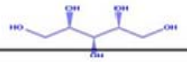
Malic acid	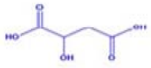	Sorbitol	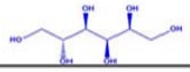
Aspartic acid	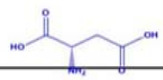	Glucaric acid	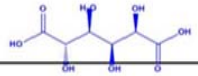
3-hydroxybutrolactone	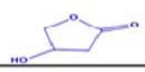	2,5-furan dicarboxylic acid	

Figure 1.10. Bio-derived Platform molecules

These building blocks can be subsequently converted to several high value chemicals and/or materials. The unique features of these building-block chemicals are that these are the molecules with multiple functional groups with a potential to be transformed into new families of useful molecules. The broad classification of these twelve sugar-based building blocks includes 1,4-diacids (succinic, fumaric, and maleic), 2,5-furandicarboxylic acid, 3-hydroxypropionic acid, aspartic acid, glucaric acid, glutamic acid, itaconic acid, levulinic acid, 3-hydroxybutyrolactone, glycerol, sorbitol, and xylitol/arabinitol [65-69].

Table 1.1. Criteria for inclusion in US DOE platform molecules [70]

Sr.No.	Criteria used in evaluating biobased product opportunities from carbohydrates
1	A high level of reported research identifies both broad technology areas and structures of importance to the biorefinery.
2	The compound illustrates a broad technology applicable to multiple products. As in the petrochemical industry, the most valuable technologies are those that can be adapted for the production of several different structures.
3	The technology provides direct substitutes for existing petrochemicals. Products recognized by the chemical industry provide a valuable interface with existing infrastructure and utility.
4	The technology is applicable to high volume products. Conversion processes leading to high volume functional equivalents or utility within key industrial segments will have particular impact.
5	A compound exhibits strong potential as a platform for the production of several derivatives offering commercial flexibility for biorefinery implementation.
6	Scale up of the product or a technology to pilot, demo, or full scale is underway. The impact of a bio-based product and the technology for its production is greatly enhanced upon scale up.
7	The bio-based compound is an existing commercial product, prepared at intermediate or commodity levels. Research leading to production improvements or new uses for existing bio-based chemicals expands their utility.
8	The compound may serve as a primary building block of the biorefinery. The petrochemical refinery is built on a small number of initial building blocks: olefins, BTX, methane, CO. Those compounds that are able to serve an analogous role in the biorefinery will be of high importance.
9	Commercial production of the compound from renewable carbon is well established. The potential utility of a given compound is improved if its manufacturing process is already recognized within the industry.

A second-tier group of building blocks was also identified as viable candidates for commercial applications. These include gluconic acid, lactic acid, malonic acid, propionic acid, the triacids citric and aconitic, xylonic acid, acetoin, furfural, levuglucosan, lysine, serine, and threonine. Recommendations for moving forward include, examining top value products from biomass components for example, aromatic compounds, polysaccharides, and oils; evaluating technical challenges in more detail especially comparing chemical Vs biological conversion.

1.6. Catalysis and Biorefinery

1.6.1 New directions in catalysis for energy and fuels

The past 50 years of catalysis research have primarily addressed how to add functionality to non-renewable fossil fuel resources and chemicals [71-74]. One notable exception being the treatment of the gaseous effluent from combustion processes. In general, the crude oil and natural gas feedstocks used for fuel and petrochemical production, are not particularly reactive hence, these molecules have to be "activated." The most common means of activation is through cracking-type reactions. This cracking is performed at elevated temperatures and leads to shorter chain molecules and compounds that contain a small fraction of unsaturated C–C bonds, which can be exploited for subsequent catalytic transformations. The new catalytic processes that allow the effective utilization of renewable biomass derived compounds by: (i) taking advantage of the high inherent functionality of these compounds, and (ii) selectively removing the excess functionality of these compounds. This strategy involves

1. Selective cleavage of C-O bonds Vs. C-C bonds
2. Selective dehydration
3. Selective hydrogenation of specific C=C, C=O groups, and hydrogenolysis of COH groups
4. Selective condensation processes, such as aldol condensation
5. Selective oxidation of specific -C-OH groups to –C=O groups

It is essential to develop new catalysts for the above processes that are stable under high temperature (e.g., 150-250 ^{o}C) aqueous conditions. Along with the catalysts, development of new supports and active phases that do not sinter and do not leach into an aqueous environment is also one of the desirable attributes for biorefinery catalysts [75, 76]. In contrast, biorenewable feedstocks already contain quite a number of functional groups that can be used for chemical transformations, which necessitates a new paradigm of how to design heterogeneous catalysts that can do selective chemistry in the presence of multiple reactive functional groups within a reactant molecule as shown in Figure 1.11. Designing heterogeneous catalysts for the conversion of biorenewable feedstocks, e.g., carbohydrates, lipids, and lignin, creates new challenges and opportunities for developing new catalyst technology [77-81].

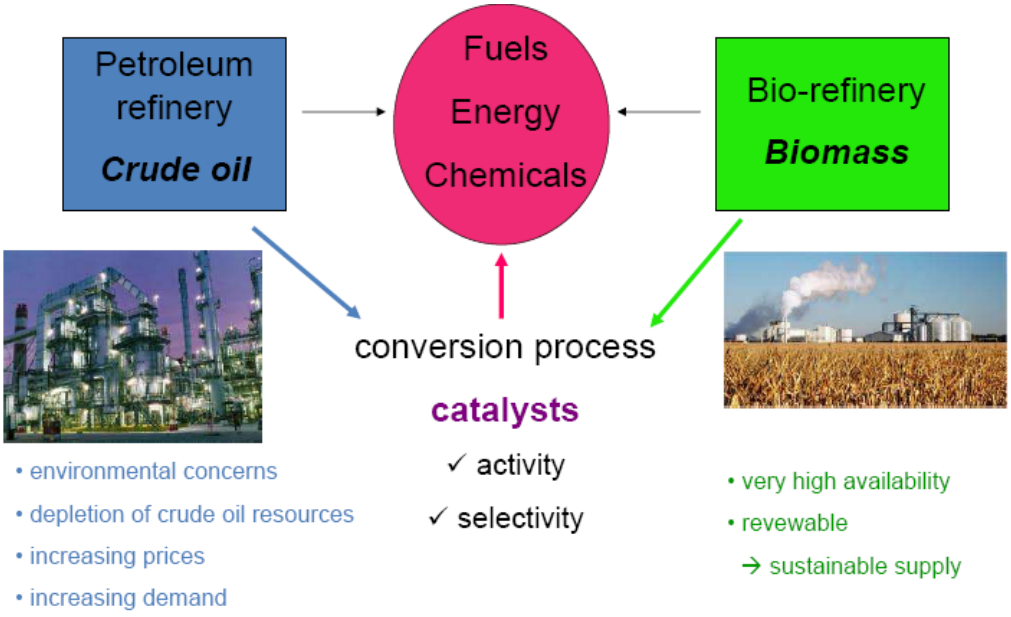

Figure 1.11. Comparison of petro-refinery with bio-refinery [86]

The fine and specialty chemical market has been confronted with the challenge of selectively converting substrates containing multiple reactive groups, which has commonly been addressed through the use of homogeneous catalysts or biocatalysts. Given the high value of fine and specialty chemicals, these types of catalyst systems may be afforded sometimes. Nevertheless, the cost, temperature limitations, and separation issues created by using homogeneous catalysts and biocatalysts undoubtedly

restrict their applications in bio-renewable feedstock conversions where the separation of catalyst and product mixture is critical from sustainable process point of view [82]. The development of heterogeneous catalyst systems is at a fairly advanced stage for biomass conversion involving selective hydrogenation, selective oxidation, isomerization, reforming, etc. however, improvement and /or development of multifunctional, efficient catalyst systems particularly with non-noble metals is still a challenge for dehydration, decarboxylation, decarbonylation, hydrogenolysis, esterification, ketonization, etc. [83-86]. Another challenge is the presence of multiple functional groups in biomass-derived compounds, leading to poor volatility of compounds at relevant reaction temperatures. This property commonly leads to the requirement of condensed phase reaction systems, which is in marked contrast to the primarily gas-phase reaction systems used for hydrocarbon processing. The resulting liquid-solid interfaces place new demands on materials regarding their catalytic properties, stability and transport properties, which are further exacerbated when the condensed phase solvent is water. Due to their high oxygen content, biorenewable feedstocks are effectively hydrogen deficient relative to hydrocarbons, so three-phase reaction systems consisting of a solid catalyst, liquid solvent/reactant mixture and hydrogen gas will commonly need to be employed to generate products that replace those from hydrocarbons [87, 88].

As discussed earlier, bio-renewable feedstocks can be in different forms according to which the reactions for their downstream processing will vary. The different types of reactions required for conversion of carbohydrates and their derivatives are described in the following sections.

1.6.2. Types of catalytic reactions for conversion of carbohydrate derived platform molecules

1.6.2.1. Hydrolysis

Hydrolysis is one of the major processing reactions of polysaccharides in which the glycosidic bonds between the sugar units are cleaved to form simple sugars like glucose, fructose, and xylose and partially hydrolyzed dimer, trimers, and other oligomers as

shown in Scheme 1.1. The challenge is to identify the reaction conditions and catalysts to convert a diverse set of polysaccharides (such as cellulose, hemicellulose, starch, inulin, and xylan) obtained from a variety of biomass sources [89].

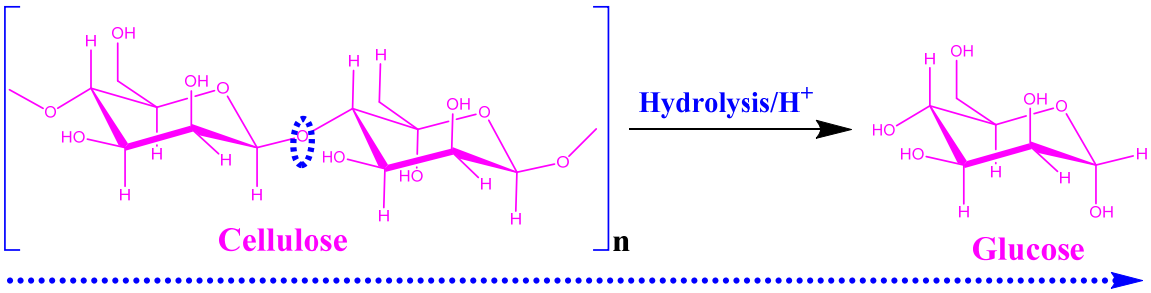

Scheme 1.1. Hydrolysis of cellulose to glucose

1.6.2.2. Isomerization

Isomerization of carbohydrates is typically carried out in the presence of base catalysts at mild temperatures and in different solvents. The conversion of glucose into fructose is widely practiced for the production of high-fructose corn syrup as seen from Scheme 1.2. In addition, HMF selectivity from glucose can be improved by isomerization of glucose to fructose [90].

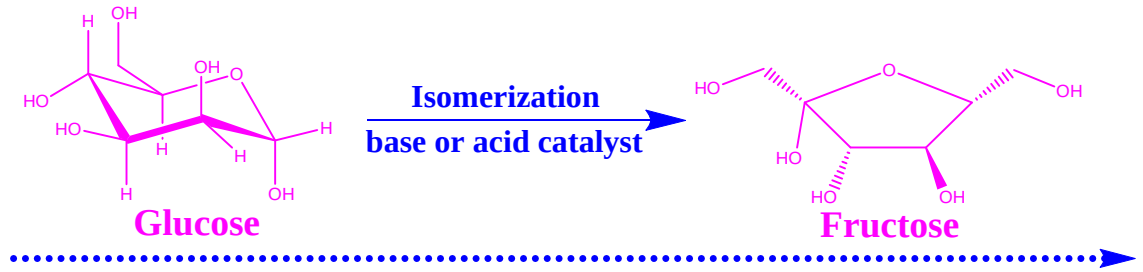

Scheme 1.2. Isomerization of glucose to fructose

1.6.2.3. Dehydration

Dehydration reactions of carbohydrates and carbohydrate derived molecules comprise an important class of reactions in the field of biomass chemistry. Dehydration of hexoses has been studied in water, organic solvents, biphasic systems, ionic liquids, and near- or supercritical water, using a variety of catalysts such as mineral and organic acids, organocatalysts, salts, and solid acid catalysts such as ion-exchange resins and zeolites

to produce various platform chemicals such as 5- hydroxyl-methyl furfural as seen from Scheme 1.3 [91].

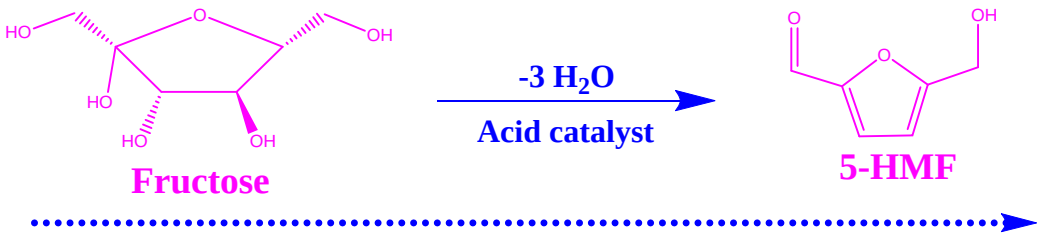

Scheme 1.3. dehydration of fructose to 5-HMF

1.6.2.4. Hydration reaction

A typical reaction pathway for the hydration of 5-HMF by the acid catalyzed decomposition is given in Scheme 1.4 which involves ring opening reaction of 5-HMF to produce a mixture of LA and FA in a 1:1 molar ratio. This implies that both LA and FA are stable under the reaction conditions employed and do not decompose to other products [92].

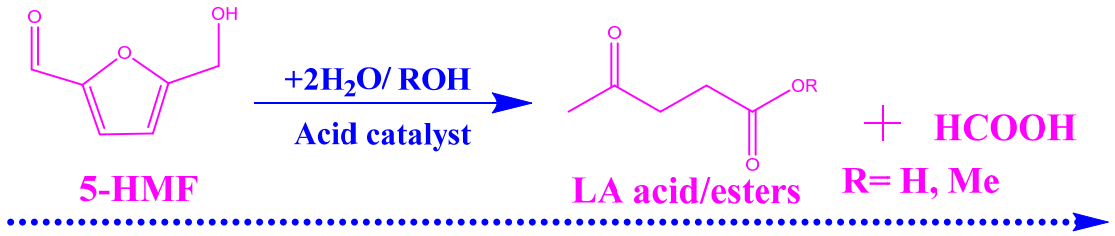

Scheme 1.4. Hydration of 5-HMF to LA acid/esters

1.6.2.5. Hydrogenation

Selective hydrogenation of C=O bond for example, of levulinic acid and furfural leads to 4-hydroxy LA, GVL and furfuryl alcohol. Hydrogenation reactions are carried out in the presence of a metal catalyst such as Pd, Pt, Ni, Ru and Cu at moderate temperatures (97–147 ^{o}C) and moderate pressures (10– 30 bar) to saturate C=C, C=O, and C-O-C bonds. Selectivity for the hydrogenation reaction depends on factors such as solvent, partial pressure of hydrogen, and the nature of the catalyst. For hydrogenation of levulinic acid to GVL as shown in Scheme 1.5, Ru/C has been reported to be advantageous compared

to other metal catalysts as it is known to be active for aliphatic carbonyl group hydrogenation [93].

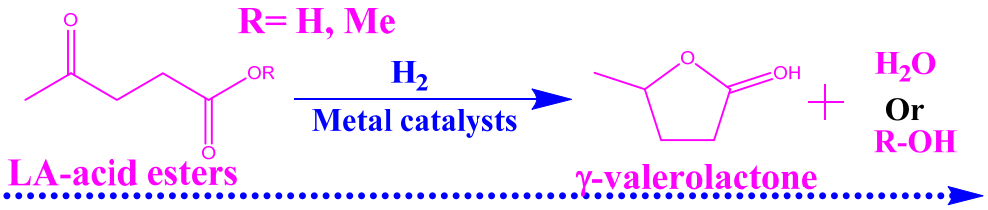

Scheme 1.5. Hydrogenation of LA acid/esters to GVL

1.6.2.6. Reforming Reactions

The production of hydrogen for fuel cells, ammonia synthesis, and other industrial operations is an essential feature of future biorefineries, similar to current petroleum refineries. Pyrolysis of solid biomass followed by reforming of bio-oils and biomass gasification are known technologies for H_2 production [94]. In addition, it has recently been shown that aqueous-phase reforming (APR) can be used to convert sugars and sugar alcohols with water into H_2 and CO_2 as shown below in Scheme 1.6.

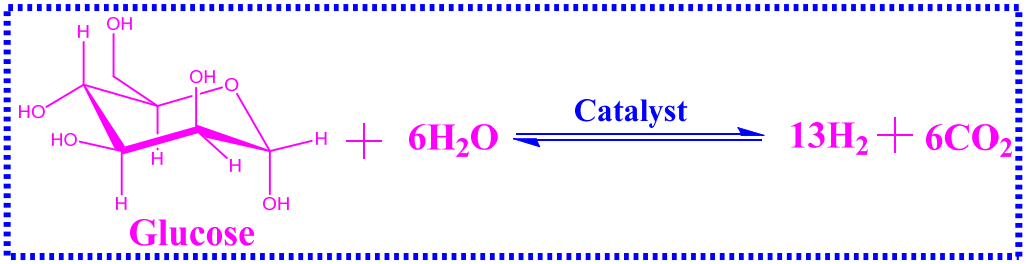

Scheme 1.6. Reforming of glucose

1.6.2.7. Aldol Condensation

Aldol condensation is a C-C bond forming reaction generally carried out to form larger molecules at mild temperatures (27-100 ^{o}C) in the presence of a base or an acid catalyst. It has been shown that various carbohydrate-derived carbonyl compounds such as furfural, HMF, dihydroxyacetone, acetone, and tetrahydrofurfural can be condensed in

aqueous and organic solvents to form larger molecules (C_7–C_{15}) that can be subsequently converted into diesel fuel as shown in Scheme 1.7 [82, 83].

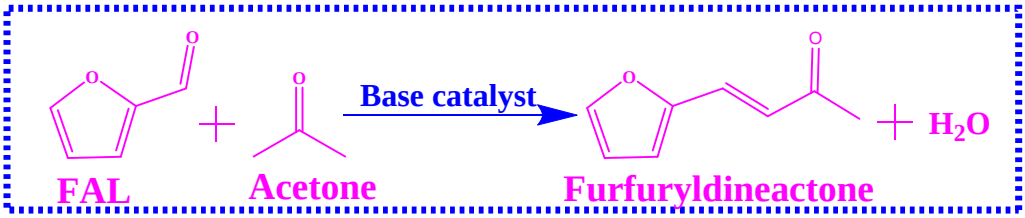

Scheme 1.7. Aldol condensation of furfural

1.6.2.8. Hydrogenolysis

The objective of hydrogenolysis is to selectively break targeted C=C and/or C-O bonds, thereby producing more valuable polyols and/or diols. Lower polyols such as ethylene glycol (EG), 1,2-propanediol (1,2-PDO), and 1,3- propanediol (1,3-PDO) have potential applications in the polymer industry as shown in Scheme 1.8 [48]. The Hydrogenolysis of C=C and C-O bonds in polyols occurs in the presence of hydrogen (14–300 bar) at temperatures from 130 to 220 ^{o}C usually, under basic or acidic conditions and with supported metal catalysts including Ru, Pd, Pt, Ni, and Cu [95, 96].

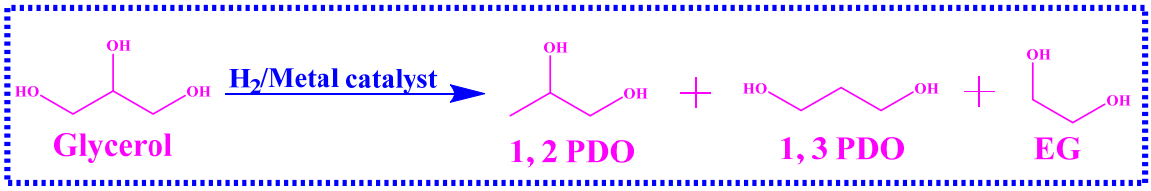

Scheme 1.8. Hydrogenolysis of glycerol

1.6.3. Key factors affecting the activity of solid catalysts in biomass conversion

In the following sections, we will address the key aspects when a heterogeneously catalyzed process for biomass conversion is considered. Today, there is a significant need to rapidly develop new technologies that will allow us to convert our biomass-derived resources into fuels and chemicals. In this respect, a large amount of applied research has been done but primarily focusing on empirical exploration. However, few studies have focused on the fundamentals of biomass refining. These essential studies

are critical for advanced improvements in biofuels quality, process optimization, as well as integration with petrochemical infrastructures. Efficient catalysts that are selective, stable and active for conversion of biomass-derived feedstocks must be developed by combining fundamental studies with applied research. Various factors affecting the catalyst activity involved in catalytic conversion of biomass derived platform chemicals to fuels and value added chemicals are as follows.

1.6.3.1. Reaction media

As stated in the preceding section, biomass conversion is expected to be carried out in different solvents. Considering that biomass components are relatively polar molecules, polar solvents or dispersants should be required for their chemical processing, at least in the initial stages of biomass conversion when the O/C ratio is still high. This brings new requirements with respect to the catalyst stability. Direct analogy from petrochemical industry may not be relevant because the catalysts involved there, are for high temperature gas phase reactions for the conversion non-polar hydrocarbons. Unlike this, biomass conversion reactions involve aqueous medium hence problems such as substantial swelling and stability in terms of metal leaching of the catalyst and/or supports are to be resolved appropriately [97, 98]. This can be also dealt with by simultaneously choosing the suitable reaction medium.

1.6.3.2. Catalyst composition

The development of strategies for the stabilization of the catalyst against leaching also requires tailoring of its structural and textural properties. In addition, many of the biomass components possess strong chelating groups, which can facilitate leaching and poisoning of the catalytically active phases. Very careful choice of catalyst components is therefore mandatory, and the diversity of biomass will make this problem even more challenging. Furthermore, the resistance of the solid catalysts against polar solvents as well as under different pH conditions is another significant issue, since the chemical processing of biomass should mainly be carried out in liquid phase because of the polymeric nature of most biomass components [99].

1.6.3.3. Hydrophilicity/hydrophobicity

Surface hydrophobicity and hydrophilicity of a solid determines the range of its potential catalytic applications since the key catalytic steps of adsorption and desorption depend strongly on these properties. Several functional groups present on solid surfaces, such as hydroxyl (–OH), carboxyl (–COOH), carbonyl (C=O), ether (R–O–R), alkyl, and ionic species (H^+, Na^+, Cl^-, SO_4^{--}) strongly affect the surface polarity. On the majority of solid surfaces, not only are hydrophilic and hydrophobic sites alone are present, but both sites can coexist in close local proximity [100]. Biomass derived molecules involve hydrophilic or hydrophobic molecules, or even both properties in different parts of the same molecule. Therefore, tuning of the surface properties is also necessary to optimize the adsorption and desorption processes and thus the overall catalytic transformation. The reduction of the oxygen content in biomass by dehydration and hydrogenation are associated with the elimination of water. Water is also a convenient dispersant for lignocellulosic materials, since the accessibility of their functional groups is enhanced under sub- and supercritical conditions by partial dissolution of the cellulose fraction [101]. However, severe poisoning of the acid sites by water is likely to occur [102]. Therefore, development of new water-tolerant solid acids with tailored porosity and adjusted surface polarity will be essential for industrial applications of biomass transformation processes.

1.6.3.4. Bi-functional nature

The potential bi-functionality of solid catalysts opens up a window of several possibilities to carry out complex transformations in a one-pot process. In principle, this means reduction of unit operations and intensification of processes [103]. Furthermore, one-pot processes make possible the efficient utilization of cascade reactions and multistep conversions Solid catalysts provide the possibility of combining in a single catalyst, several types of active sites, which would in principle be incompatible in homogeneous catalysis. For instance, solids can carry both acidic and basic sites on their surfaces as the rigidity of the surface make these sites distant enough to allow their co-existence on the same surface.

Since majority of the twelve platform molecules contain carboxylic acid functional group, the representative examples of C_3 to C_5 acids for transformation to value added products via catalytic hydrogenation are discussed below.

1.7. Platform chemicals [organic acids from biomass]

1.7.1. Lactic acid (C_3)

In 1895 industrial fermentation process was developed for lactic acid by the pharmaceutical entrepreneur A. Boehringer [104]. Lactic acid (2-hydroxypropanoic acid) is the most widely occurring carboxylic acid in nature [105]. The world's annual production was 1.2×10^5 tons per year in 2005, 90% of which was produced by bacterial fermentation of biomass, with the remainder synthesized by hydrolysis of lactonitrile. Traditionally lactic acid has been used in food and food-related applications; however, since the early 1990s the lactic acid market has been expanding steadily at a rate of 4×10^4 tons per year as a result of the development and commercialization of new applications. The new uses are related to the industrial production of polymers and chemicals. In particular, lactic acid because of its bi-functionality, can be converted through a variety of reactions to such compounds as acetaldehyde, acrylic acid and polylactic acid (PLA). Scheme 1.9 showed lactic acid hydrogenation to produced 1, 2 propanediol, propanoic acid and 2-propanol by using metal catalyzed hydrogenation reactions [106].

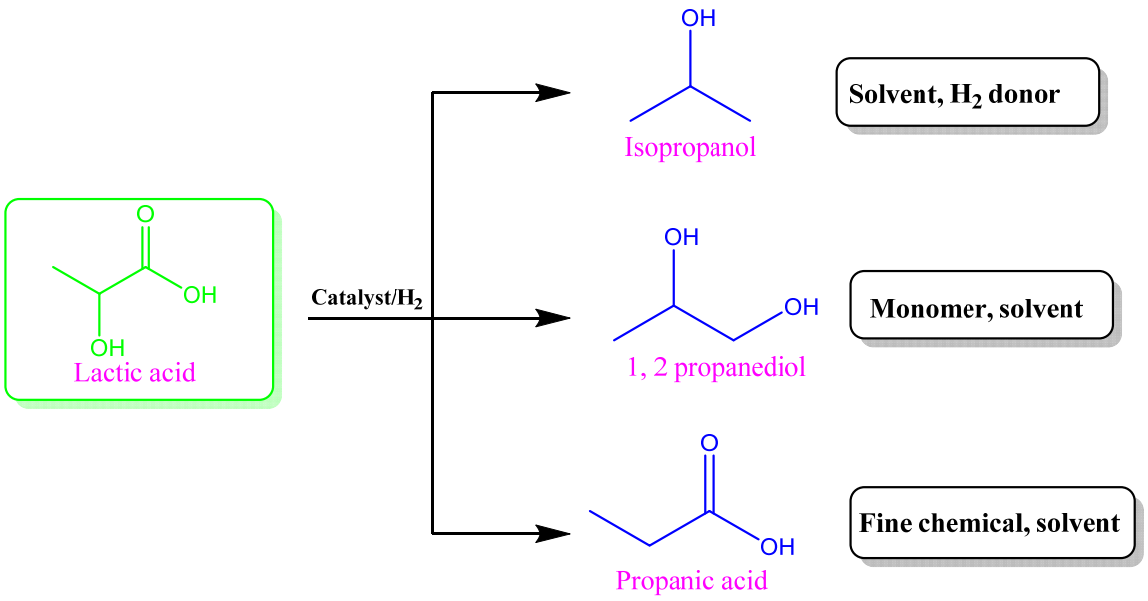

Scheme 1.9. Catalytic hydrogenation of lactic acid

1.7.2. Succinic acid (C_4).

Succinic acid is a widely investigated chemical building block available from biochemical transformation of biorefinery sugars [107]. Using (anaerobiospirillum succinici producens) as the fermentative organism and a three stage continuous cell recycle bioreactor, optimized processes producing 10.4 g L^{-1} h^{-1} and a final concentration of 83 g L^{-1}, equivalent to 1.35 mol succinic acid per mol of sugar. Recombinant E. coli also gives effective production of succinate from glucose (1.3 moles succinate per mol glucose). An alternative E. coli strain originally developed by the US Department of Energy [108] has been licensed by Bioamber, which recently commissioned a 2000 tonne per year production facility.

Succinic acid offers strong potential as a platform chemical, the use of succinic acid as a platform chemical is summarized in Scheme 1.10. Direct hydrogenation of succinic acid and its succinate esters are precursors for known petrochemical products such as 1,4-butanediol, tetrahydrofuran, γ-butyrolactone or various pyrrolidinone derivatives [109]. The market potential for succinic acid and its immediate derivatives has been projected to be as much as 245 X 10^3 tonnes per year, with an estimated market size for succinic acid-derived polymers being as high as 25 X 10^6 tonnes per year.

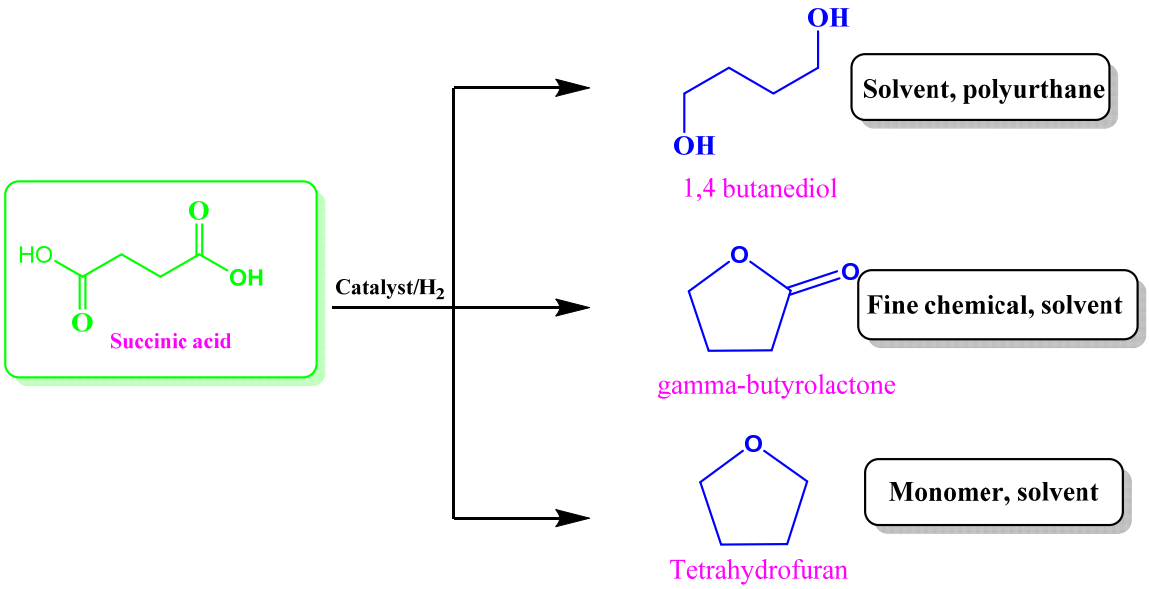

Scheme 1.10. Catalytic hydrogenation of succinic acid

1.7.3. Levulinic acid (C_5)

1.7.3.1. Physical properties of levulinic acid

In 1840 the Dutch Professor G. J. Mulder (who also introduced the name "protein") synthesized levulinic acid (4-oxopentanoic acid, γ-ketovaleric acid) by heating fructose with hydrochloride for the first time [110]. The former term "levulose" for fructose gave the levulinic acid its name as well as it contains two reactive C=O functional groups one as a keto and other as a carboxylic acid, and the molecule as such can be converted to various value added products having applications as fuels and chemicals [111].

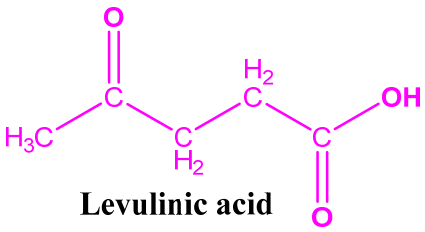

Levulinic acid

It is one of the principle compounds for the application of biorefinery, due to its easy production from biomass, with high yield as compared to 5-hydroxy methyl furfural and its reactivity to transform to value added derivatives. Levulinic acid has been well known since the 1870s when many of its reactions (e.g. esters) were established however, its commercial use never reached to any significant volume until 1940s when

commercial levulinic acid production began in an autoclave in the United States by A. E. Staley [112]. The physical properties of levulinic acid are given in Table 1.2.

Table 1.2. Physical properties of levulinic acid

Melting point (^{o}C)	37
Boiling point (^{o}C)	246
Density (Kg/L^{-1})	1.134
Vapor pressure	1 mm Hg (102 ^{o}C)
Refractive index	n20/D 1.439 (Lit)
Freezing point	280 ^{o}F
Heat of vaporization	0.58 KJ Mol^{-1}
Heat of Fusion	79.8 KJ Mol^{-1}

One of the major objectives of this work was to study the hydrogenation of levulinic acid to GVL, the details of levulinic acid production and its downstream processing are discussed in the following section.

1.7.3.2. Production and downstream conversion of levulinic acid

1.7.3.2.1. Production of LA and esters of LA

Starting from biomass carbohydrate raw material, the following routes are possible: 1) The indirect production of ethyl levulinate through acid hydrolysis of cellulosic constituents using mild acid catalysts to hexose sugars (glucose, sucrose, starch, fructose and inulin) then followed by isomerization and dehydration using strong acids with loss of water molecules to intermediate 5-HMF and then further rehydration of the later to levulinic acid and formic acid. After separation and purification of levulinic acid it undergoes esterification in an alcohol medium. 2) Direct production of ethyl levulinate is possible via hydrolysis of cellulosic constituents in alcohol medium. 3) Alternate and more beneficial route for the production of levulinic acid and its esters involves acidic treatment of pentoses such as xylose and arabinose from hemicelluloses to deliver furfural and then subsequent catalytic reduction to furfuryl alcohol followed by its rehydration in aqueous/alcoholic medium [113,114].

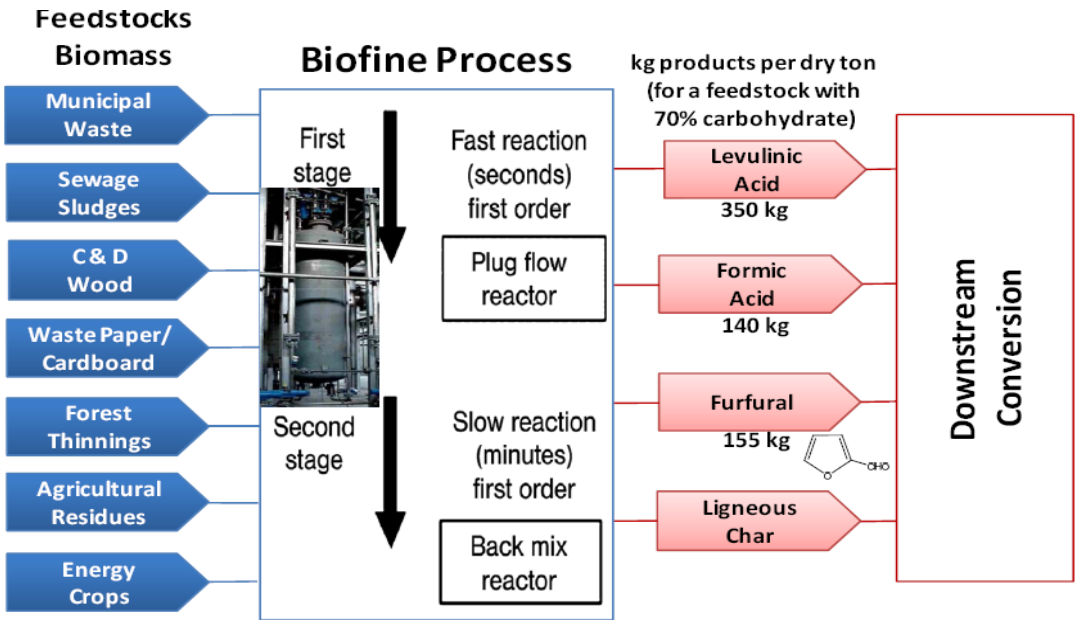

Scheme 1.12. Catalytic hydrogenation of succinic acid [124]

The highest potential of commercialization is offered by the well known Biofine process which has been scaled up to a pilot level production of levulinic acid as shown in Figure 1.12 [115-120]. It provides an interesting approach to convert lignocellulose biomass to valuable platform chemicals, specifically levulinic acid (C_6 fraction) and furfural (C_5 fraction), that can subsequently be upgraded to liquid biofuels by different routes. In this process, the biomass feedstock is mixed with sulfuric acid (1.5–3 wt%) and introduced into the first plug-flow reactor where hydrolysis of the carbohydrates to intermediates (HMF) takes place at 210–220 ^{o}C and 25 bar with a short residence time (12 s) to minimize the formation of degradation products. Subsequently in a second reactor, the intermediates are converted to levulinic acid and formic acid at 190–200 ^{o}C and 14 bar, with a residence time close to 20 min. These conditions have been optimized to remove formic acid, as well as furfural arising from dehydration of the C_5 sugars present in biomass. Final yields to levulinic acid are around 70–80% of the theoretical maximum, and correspond to 50% of the mass of the C_6 sugars. The remaining mass is collected as formic acid (20%) and a solid residue called humins (30%), produced by degradation reactions of the large number of intermediates and Klason lignin. The properties and the amount of this solid residue depend on the feedstock used, and normally this solid is burnt to produce heat and electricity. Optimization of the Biofine process for the

utilization of inexpensive raw materials could decrease the price of LA to 8–20 ¢/kg, increasing the scope of its potential commercialization [121]. Pilot plants in the United States and Italy have used paper waste, agricultural residues, and organic municipal wastes with successful results. Figure 1.13 shows different pathways to upgrade levulinic acid into different liquid fuels, and the following sections describe the preparation strategies and applications of these products [122, 123].

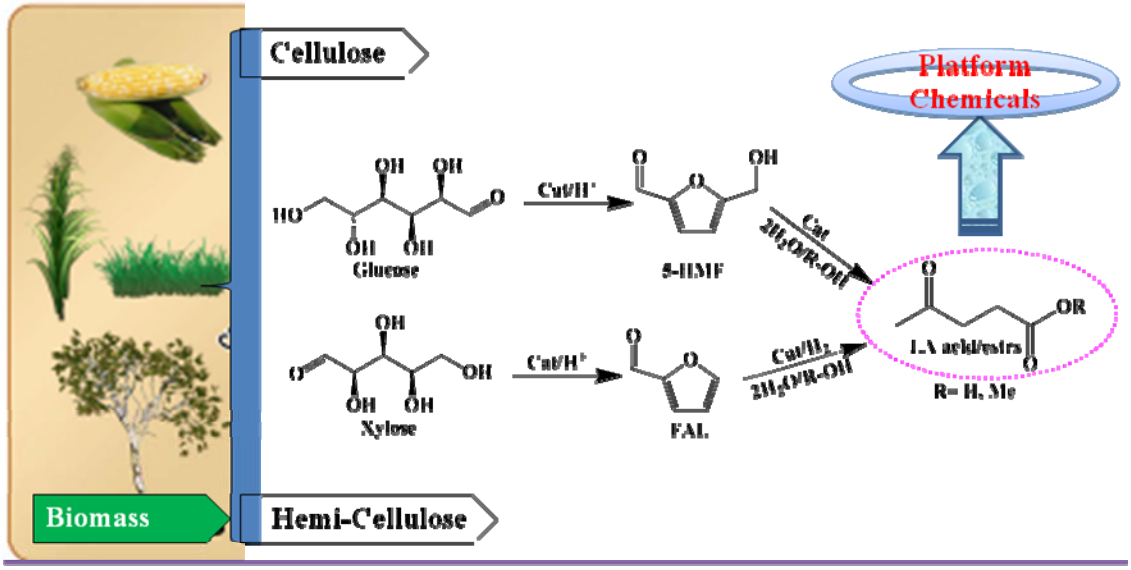

Figure 1.13. Production of levulinic acid and its esters from biomass

1.7.3.2.2. Routes for hydrogenation of levulinic acid/esters

Figure 1.14 shows GVL synthesis from LA involving the first step of hydrogenation to give an intermediate, 4-hydroxy levulinic acid followed by its subsequent cyclization which is a sustainable commodity chemical having great commercial importance due to its applications as a solvent in lacquers, as a food additive and can be converted to a variety of monomers [124]. It is also considered as a potential fuel additive for replacing ethanol in gasoline–ethanol blends. Levulinic acid (LA) can be converted to methyltetrahydrofuran (MTHF), a fuel extender and a part of P-series fuels. MTHF can be blended up to 70% with gasoline without modification of current internal combustion engines. The lower heating value of MTHF compared with gasoline is compensated by its higher specific gravity, which results in similar mileage to that achieved with

gasoline. Direct conversion of levulinic acid to MTHF is possible; however, improved yields can be achieved through indirect routes, which proceed through the production of γ-valerolactone as an intermediate. γ-valerolactone can be reduced to 1,4-pentanediol and subsequently dehydrated to MTHF [125].

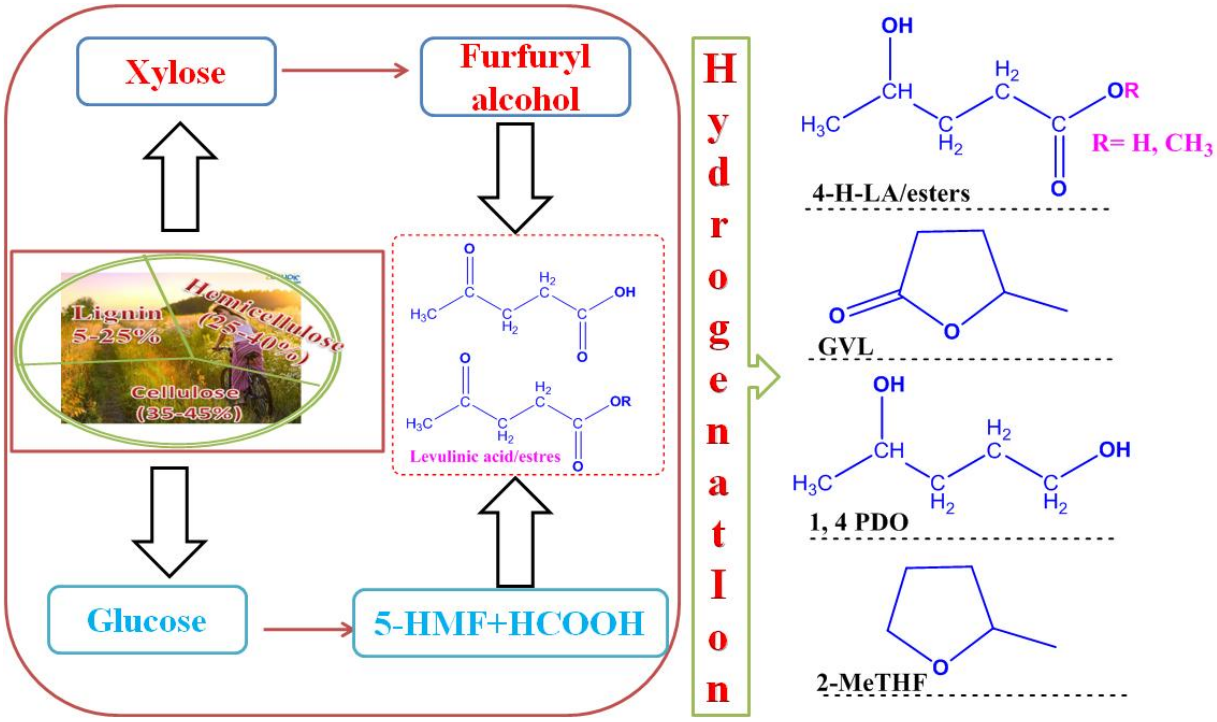

Figure 1.14. Catalytic hydrogenation of levulinic acid and its esters

Another processing option for LA is the production of methyl and ethyl esters that can be blended with diesel fuel. This esterification can be carried out at room temperature during LA storage in the presence of methanol or ethanol. Various acid catalysts have been studied to increase yields and reaction rates [126]. Studies conducted by Biofine and Texaco have demonstrated that the 21:79 formulation, a mixture containing 20% ethyl levulinate, 79% Diesel and 1% of other co-additives, can be used in diesel engines. These reactions are carried out at relatively low temperatures (100–270 ^{o}C) and high pressures (50–150 bars), and both homogeneous and heterogeneous catalysts have been studied for this process [127]. LA is solid at room temperature (melting point = 30 ^{o}C) and different solvents, such as ethyl ether, dioxane and water, have been used to

facilitate the pumping. This reduction is normally carried out using external H2 however, In situ hydrogen production through decomposition of the formic acid, produced as a by-product in the production of levulinic acid, is a promising alternative. The use of formic acid as a hydrogen donor in aqueous solutions reduces the need for external H_2 in the production of GVL and eliminates the need for LA purification strategies. Both the aspects ultimately contribute to a lower overall cost for the production of GVL. Although, the mechanism of the hydrogen transfer has not been definitively established, one proposition is that a metal-format formed decomposes into CO2 and a metal-hydride that reacts with LA to form 4- hydroxypentanoic acid, which then forms GVL by cyclization. A second alternative is that formic acid is decomposed into CO_2 and molecular H_2 and the latter then carries out the hydrogenation [128, 129].

1.7.3.2.3. GVL and its products as fuel and chemicals

Figure 1.15 shows GVL can be used directly as a liquid fuel or as an additive to current petroleum fuels similar to ethanol. Mixtures of 90 vol% conventional gasoline with 10 vol% GVL or 10 vol% ethanol were compared by Horvath et al. and they observed that the mixture with GVL had a lower vapor pressure, which improved the combustion at similar octane numbers. A major issue with using GVL as a pure fuel is its high water solubility; however, water can be distilled from the GVL as there is no azeotrope formation in contrast to ethanol. GVL can be further hydrogenated to produce fuel additives, such as MTHF and 1,4 pentanediol as shown in Figure 1.14. Biomass-derived polymers can be produced from 1,4 pentanediol, while MTHF can be used as a solvent and has been identified as a component for the P-series fuel [130, 131]. In general, higher H_2 pressures and temperatures are required to carry out the hydrogenation of the GVL than for LA. Finally, MTHF can be converted into fuels viz. C_4–C_9 alkanes, in the presence of an acid and metal catalysts at high pressure and moderate temperatures [132, 133]. Besides, using GVL as a fuel or hydrogenating it to MTHF, several strategies have been proposed to convert GVL into energy dense drop-in fuels such as “valeric biofuels”, which were successful as fuel additives. These processes normally start with ring-opening of GVL to produce pentanoic acid over a bifunctional metal-acid catalyst.

In the next step, pentanoic acid undergoes esterification to form valeric esters in the presence of alcohols and solid acid catalysts.

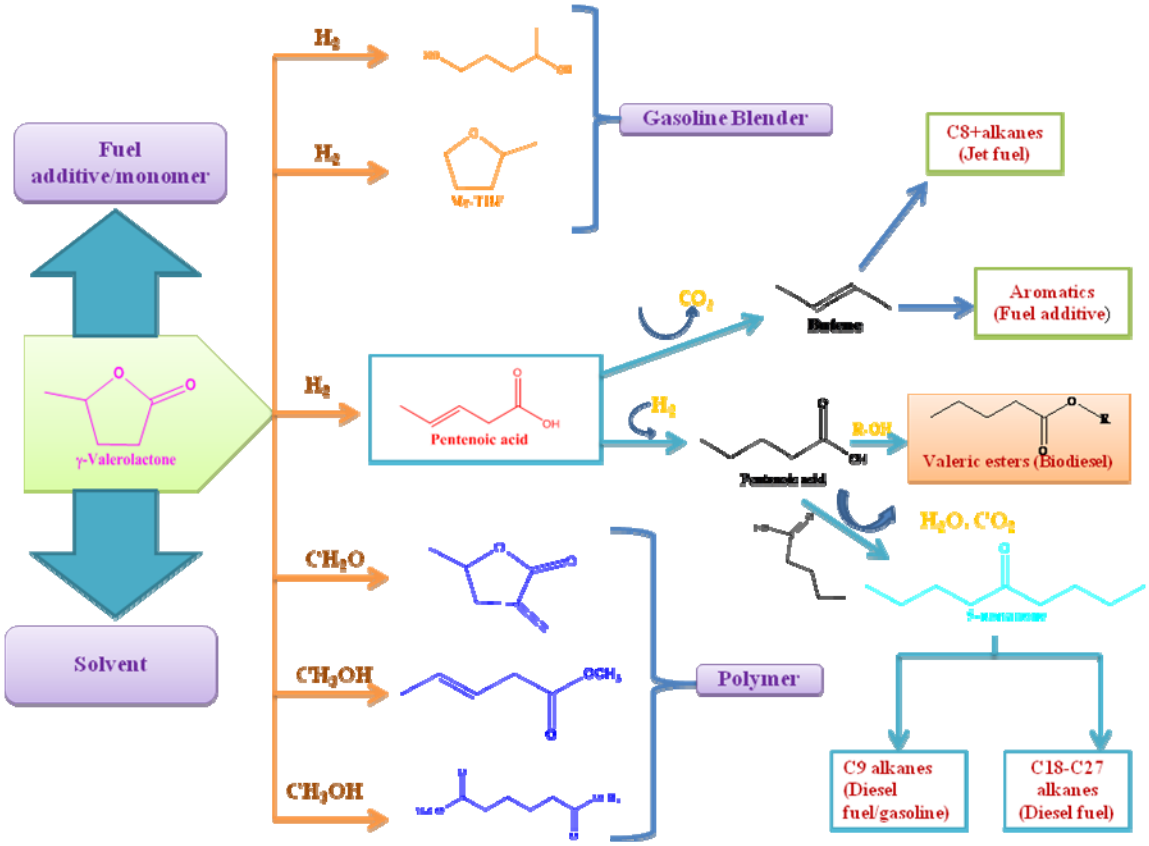

Figure 1.15. Catalytic hydrogenation of levulinic acid and its esters

To upgrade the pentanoic acid into liquid fuels, the molecular weight needs to be increased and the oxygen content decreased. 5-nonanone produced from GVL has many possibilities for upgrading. By successive hydrogenation and dehydration reactions over metal and acid catalysts, 5-nonanone can be converted into nonane while, the shorter ketones produced as by products were converted into C_6–C_7 alkanes that can be removed by evaporation. Nonane can be used as a fuel additive to diesel or converted into gasoline by isomerization and aromatization reactions over zeolites to produce a mixture of branched C_9 alkanes. The 5-nonanone can also be hydrogenated over Ru/C to produce 5-nonanol, which can be dehydrated in the presence of acid catalysts, such as Amberlyst-70, to produce a mixture of C_9 olefins. To increase the molecular weight, C_9 olefins can be oligomerized over an acid catalyst to produce a mixture of C_{18}–C_{27} olefins

that can be used as diesel fuel. In this strategy, other lower molecular weight ketones produced during the process were converted into C_6–C_7 olefins, which also undergo oligomerization producing a mixture of C_6–C_{27} alkanes. Another option to increase the energy density of GVL proceeds through acid-catalyzed decarboxylation to produce butene and CO_2. GVL was converted into pentenoic acid and decarboxylated in the presence of acid catalysts, such as silica-alumina. Even when the GVL was directly decarboxylated to produce butene, the reaction pathway with pentenoic acid as an intermediate was more favorable. GVL can be used to produce, not only fuels, but also interesting monomers such as α-methylene-γ-valerolactone to make polymers similar to those derived from petroleum but with different chemical properties. α-methylene-γ-valerolactone compound has similar properties to methyl methacrylate, and the incorporation of the lactone structure increased the thermal stability of the polymer. Another alternative to produce polymers from GVL was proposed by the production of methyl pentenoate via ring opening of GVL in methanol over acid catalysts. The methyl pentenoate was then converted into nylon precursors such as caprolactone, caprolactam, or adipic acid by hydroformylation, hydrocyanation, or hydroxycarbonylation, respectively [134, 135].

Various other compounds derived from GVL can be used as solvents were identified by Horvath et al. [125] such as alkoxyvalerates are produced by the addition of trialkyl orthofomates in the presence of an acid catalyst, ionic liquids such as tetra-alkylammonium 4-hydroxyvalerate and cholinium 4-hydroxyvalerate were prepared by reacting tetraalkylammonium hydroxides with GVL at room temperature. There are many possibilities of using GVL for different chemicals, solvents, and polymers. GVL acts as a sustainable solvent and its comparative study is carried out with various solvents having fuel properties as shown in Table 1.3. Development of such catalytic processes is an important step that gives the highest commercialization possibility in near future.

Table 1.3. Fuel properties of GVL

Properties	**Methanol**	**Ethanol**	**MTBE**	**ETBE**	**GVL**
MW(g/mol)	32.04	46.07	88.15	102.17	**100.12**
Carbon(w%)	37.5	52.2	66.1	70.63	**60**
Hydrogen(w%)	12.6	13.1	13.7	13.81	**8**
Oxygen(w%)	49.9	34.7	18.2	15.66	**32**
Boiling Point(^{o}C)	65	78	55	72.73	**207.208**
Melting Point(^{o}C)	¬98	¬114	¬109	¬94	**¬31**
Density(^{o}C)	0.7910	0.8	0.74	0.742	**1.05**
Open Cup Flash Point(^{o}C)	16.1	14	-363	-19	**96**
Ld50 oral for rat (mg/kg)	5628	7060	4800	5000	**8800**

1.7.3.2.4. Challenges and catalytic strategies for production of LA and its ester and their hydrogenation to GVL.

Most research pertaining to LA hydrogenation to produce GVL has employed pure, commercial LA or mixtures of commercial compounds that simulate the products that would be obtained from the hydrolysis of cellulose or lignocellulosic biomass (e.g., mixtures of LA and formic acid). Few researchers have considered the presence of mineral acids, such as sulfuric acid (SA) or HCl, which are commonly used in the hydrolysis of lignocellulosic biomass to produce LA. According to the reaction pathway presented in Figure 1.16, GVL production relies heavily on LA production, and several reviews have appeared focusing on LA producing from lignocellulosic feedstocks via Biofine process had success but needs the use of a two reactor system. The formation of insoluble degradation products, known as humins, was an issue in these reactors [136,137].

- ✓ LA produced from biomass was associated with decrease in GVL yields significantly due to impurities and mineral acids present in the feed that deactivate the catalyst.

- ✓ In case of solid acid catalysts, the yield of LA is low and catalyst recovery becomes challenging. The separation/purification of the GVL and the low yields are associated when cellulose was used as a starting material.
- ✓ Active metal deactivation in aqueous phase hydrogenation of LA
- ✓ Requirement of precious noble metal catalysts for conversion of LA and LA: FA to GVL.

As mentioned previously, aqueous-phase processing of lignocellulose allows for the separation of different portions of biomass, i.e. cellulose, hemicellulose and lignin, thereby enabling the separate processing of these different biomass fractions.

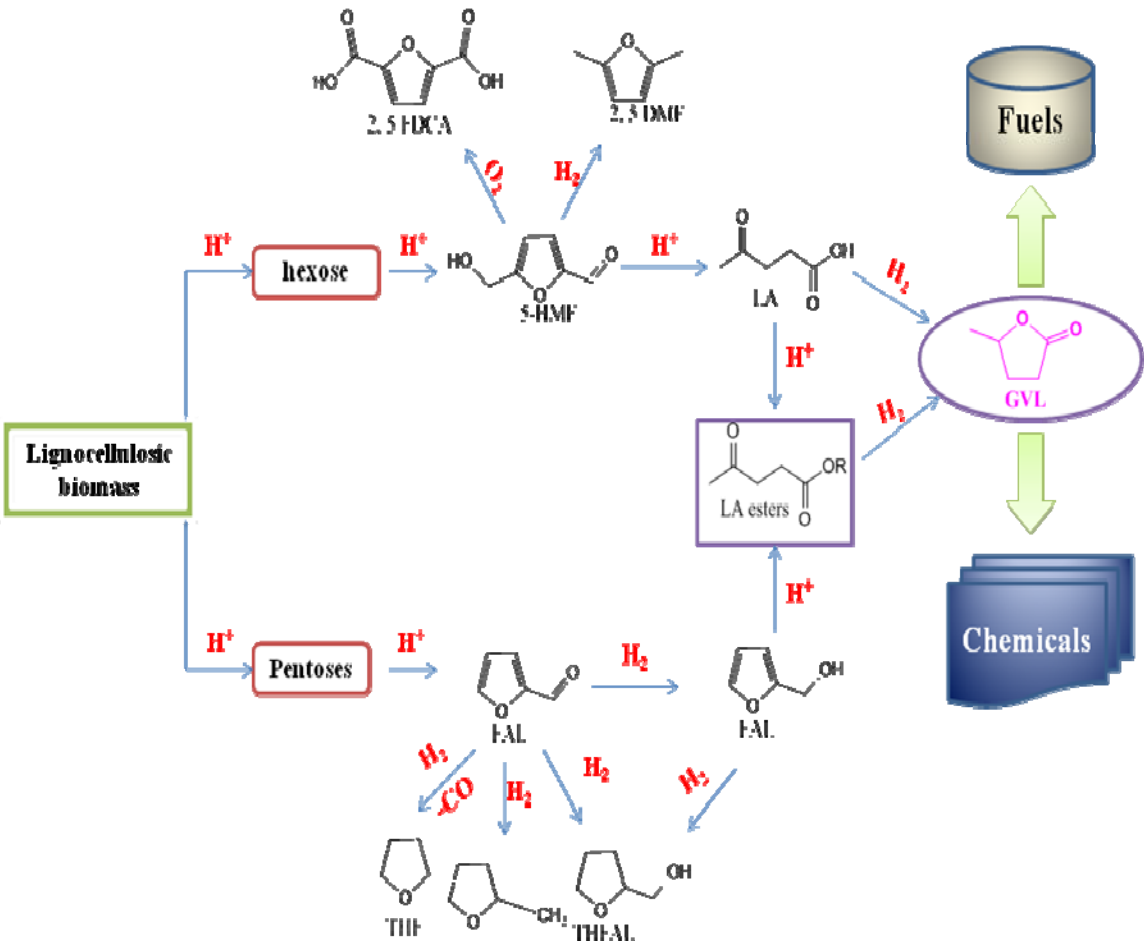

Figure 1.16. Pathways for synthesis of LA and GVL

In this strategy, solid biomass is first subjected to mild pre-treatment in aqueous solution containing dilute acid to solubilize the hemicellulose as xylose. Dilute acid hydrolysis of

hemicellulose leads to high amounts of xylose, with various byproducts and subsequent hydrolysis of xylose to furfural with loss of water molecule. Furfural undergoes hydrogenation giving a variety of platform molecules such as furfuryl alcohol, tetrahydro furfuryl alcohol, 2-methyl furan and THF etc. Among these products, furfuryl alcohol can converted to levulinic acid and ester of LA by using acid catalyzed rehydration. The acid-catalyzed hydrolysis of cellulose typically involves deconstruction of cellulose to glucose followed by its dehydration to 5-HMF and then hydration gives LA:FA mixture. The remaining lignin portion can be used as a source for heat and power generation or can be upgraded to form lignin-derived solvents. For this reason, a useful strategy for the production of GVL from bio-derived LA could be start with controlled oxygen removal reactions to produce functional intermediates. These partially deoxygenated platforms are more stable compared to over functionalized sugar molecules and at the same time, have sufficient functionality to allow for the production of fuels as well as selective production of a wide range of value-added chemicals.

1.8. Literature survey on hydrogenation of levulinic acid

1.8.1. LA hydrogenation with external H_2

In recent years, the study of the preparation of GVL has become a research topic of intense interest. However, GVL is often produced by hydrogenation of levulinic acid in presence of a noble metal catalyst, and the reaction is usually performed in liquid phase in a batch reactor system. Several catalyst systems including both homogeneous and heterogeneous have been reported for this important sustainable process of LA hydrogenation to GVL. A summary of the relevant literature on LA hydrogenation is presented in Table 1.4.

Table 1.4. Literature study of LA hydrogenation to GVL with external H_2

Catalyst	Substrate	Reaction conditions			% conversion	% Product distribution	Reference
		Temp (C)	H_2Press (bar)	Time (h)			
HRuCl(Dpm)3	Carboxylic acids	60					138
Ru/C + TFA,	Glucose/Fructose	180	60	8	--	54 (GVL) Yield	139
$RuCl_2$ (PPh3)2	LA	180	11		100	99	140
$Ru(acac)_3$ + p(n-Oct)3	LA	160	100	4.5	99	99	141
$Ru(acac)_3$ + Bu-DPPDS	LA	140	10	4.5	99	99	142
0.05 mol% $[Ir(COE)2Cl]_2$	LA	100	50	24		98	143
$Ru(acac)_3$ + TPPTS	LA	160	100	18		99	144
PtO_2	LA	r.t.	3	44		87	145
5% Ru/C	LA	265	1	--	100	98 (GVL)	146
5% Pd/C	LA	265	1	--	100	90 (GVL)	146
Pt/TiO_2	LA	200	40	--	--	95	147
Re "black"	LA	106	148		100	71 (GVL)	148
5% Ir/C	LA	150	50		49	97 (GVL)	150
5% Ru/C	LA	130	12		99		149
5% Ru/C	LA	25	50		99	89 (GVL)	149
RuSn (3.6:1)/C	LA	220			98	95	150

RuSn/C	LA	180	35	--	99	99	151
5%Ru/Al_2O_3	LA	150	103	2	99	99.5(GVL)	152
5% Ru/ C	LA	130	35	4	92	99 (GVL)	153
15 RuRe/C	LA	150	35	--	80	99	154
1% Ru/H̃ZSM-5	LA	200	40	4	99	55 (GVL) 45 (PA)	155
Ru(NPs)	LA	130	5	--	99	99	156
5%Ru/C + ILs + n-octanol	LA	100	35	4	99	99	157
5 wt% Ru/C and Amberlyst-70	LA	70	30		100	100 (GVL)	158
5% Ru/Strabon	LA	100	10	2	99	95(4H-LA)	159
5% Ru/C + $H2SO_4$	Cellulose	150/180	35	TOS	45	22	160
5% Ru/C+MCM-41-n-SO_3H	Cellulose	230	870	0.4	99	39	161
2.8%Ru–3.9%Re/C	LA	160	150	0.1		85	162
Raney Ni and Cu-Cr_2O_3	LA	220	202	--	99	41	163
Cu-SiO_2	LA	265	1	TOS	100	94	164
Cu-Fe	LA	200	70	10	99	91	165
Cu-Cr	LA	200	35-70	--	--	90	166

Among homogeneous catalysts, Ru and Rh complexes were commonly used in aqueous solution. For example, Joo et al. demonstrated the use of water-soluble homogeneous ruthenium catalysts for the hydrogenation of oxo and keto acids [138]. Osakada et al. reported that 99% yield of GVL was obtained with [$RuCl_2(PPh_3)_3$] as a catalyst [139]. The use of a pre-formed homogeneous water soluble ruthenium catalysts from $RuCl_3$ and tris(3-sulfonatophenyl) phosphane (TPPTS) in combination with TFA gave quantitative C_6-sugar conversions but a lower GVL yield (23 mol%) compared to the heterogeneous Ru catalyst [140].The recent study showed that biphasic catalysis in a DCM/water mixture using homogeneous Ru-catalyst made in situ from $RuCl_3 \cdot 3H_2O$ and Na_3TPPTS allowed the synthesis of GVL in near quantitative yields at mild conditions

as well as ethyl levulinate was converted into GVL using a Ru-BINAP complex obtained in situ from [Ru- $(acetate)_2$(BINAP)] with 2 equivalent of HCl in ethanol, and a yield of 96% was obtained under 100 bar hydrogen pressure with only 0.1 mol% of catalyst. However, with sodium borohydride as a reductant, LA also could be converted into GVL in presence of hydrogen and methanol [141-144].

The first heterogeneous catalyst reported for LA hydrogenation in 1930 by Sehuette and Thomas was platinum oxide catalyst in organic solvents to give a GVL with an yield of 87% after 44 h under 3 bar hydrogen [145]. LA hydrogenation has been reported mostly over Ru and Pt catalysts owing to their superior catalytic activity [146-149]. Mehdi and coworkers found that LA could be hydrogenated to GVL through the dehydration and lactonization of hydroxypropanioic acid using Pd, Ni, and Pt catalysts [125]. Alonso et al. noted that nearly quantitative GVL yield was achieved in hydrogenation LA under hydrogen pressure of 35 bar over RuSn/C catalyst. They also used the hydrolysis products of cellulose as raw materials for the production of GVL by using H_2SO_4 as a catalyst as well as use of various biphasic systems were reported for easy separation of LA from biomass fractions such as alkyl phenol [150,151]. Other noble metals studied for LA hydrogenation were Pd, Ru, and Re. LA hydrogenation has been also studied in supercritical CO_2 over Ru-alumina and Ru-silica catalysts giving 99% conversion with complete selectivity to GVL under severe conditions of temperature and pressure (200 °C and 200 bar H_2) [152]. Yan et al. have reported liquid-phase hydrogenation of LA to GVL over 5% Ru/C in a batch reactor giving 99% selectivity to GVL at 92% LA conversion. However, activity and stability of Ru/C catalyst was not reproducible in subsequent catalyst recycles due to substantial active metal leaching [153]. Braden et al. reported a combination of two different noble metals (Ru–Re) with very high (15%) metal loading, in spite of which the conversion was restricted to only 15–40% [154]. Later, active Ru in combination with various acidic supports and or homogenous acids such as Amberlyst, MCM-41-SO_3H, H_2SO_4 and starbon were reported for the synthesis of GVL, pentanoic acid from cellulose and bio-derived LA [155-161]. Recently, bimetallic Ru-Re supported on carbon reported for hydrogenation of LA to GVL with quantitative yield of GVL at 160 bar of excess H2 pressure [162]. The LA hydrogenation rate was also found to be greatly improved with increase in hydrogen

pressure. An improved yield of 94% for GVL was reported by Christian et al. who evaluated Raney nickel as well as copper chromite catalyst in the liquid phase hydrogenation of LA. The LA hydrogenation performed at 250 ^{o}C under 202 bar hydrogen resulted in a complex mixtures composed of GVL, 1,4-pentanediol, and MTHF [163]. Copper in combination with toxic chromium were reported for LA hydrogenation with >200 ^{o}C temperature and >50-70 bar H_2 pressure [164-166].

Based on the above discussion, we conclude that noble metals, including Re, Ru, Pd, and Pt, exhibited excellent catalytic activity in GVL production via LA reduction. As we are aware of the fact that the prices of these precious metals are exorbitantly high along with their scarcity which make the process economically unviable on a commercial scale hence, strategies for catalyst development should be focused on either completely non-noble metals or the combination of non-noble metal with the noble metal for effectively reducing the loading of the later. In such efforts, the activity of non-noble metals can be enhanced by using suitable supports. Such developments are based on fundamental knowledge of active species of the catalyst and structure activity correlation which can be investigated by detailed characterization and activity studies. We have focused both these aspects in this work.

1.8.2. LA hydrogenation without external H_2

In order to make GVL synthesis from LA as a completely sustainable process and to eliminate the hazards associated with using external high pressure hydrogen, researchers have been exploring the catalytic transfer hydrogenation of LA. In many earlier studies, formic acid had been used as the hydrogen source rather than hydrogen gas [167-169]. In these reports, noble metals have been shown to give excellent activity for decomposition of formic acid to produce H_2. Formic acid decomposition accompanied with LA as a substrate can become the best alternative for GVL synthesis without external hydrogen. Additionally, the catalytic transfer hydrogenation eliminates the requirement of high pressure equipment which otherwise is a must for hydrogenation with an external H_2 and literature on CTH of LA is summarized in Table 1.5.

Table 1.5. Literature study of LA hydrogenation to GVL without external H_2

Catalyst	Substrate	Reaction conditions	% conversion	% Product distribution	Reference
Ru/C + TPPS + TFA	Glucose/ Fructose	180 ^oC, 16 h, solvent water,	--	23 (GVL)	140
Base+ Pd/Al_2O_3	LA:FA	220 ^oC, 12 h, solvent water		29	170
$RuCl_3.3H_2O$ + PPh_3 + Net_3	LA:FA	150 ^oC, 6h, solvent water	--	95	171
$Ru/P/SiO_2$+Ru/C	LA:FA	150 ^oC, 6 h, solvent water		30	172
Au/ZrO_2-VS	LA	170 ^oC, 6 h, Solvent water	99	99	173
Au/ZrO_2	Butyl LA: butyl formate	170 ^oC, 6 h, Solvent water, butanol	96	94 (GVL)	174
Ir-Complex	LA:FA	25 ^oC, 24 h, Solvent Water		94 (GVL)	175
ZrO_2	LA, Butyl LA, 2 butanol	170 ^oC, 16 h, Solvent, 2 butanol	99	94	176
Raney Ni	LA, 2propanol	170 ^oC, 2 h, Solvent, 2 propanol	99	99	177
ZrO_2-573	LA, ethanol	250 ^oC, 1 h, Supercritical ethanol	95	81	178

Kopetzki and Antonietti demonstrated transfer hydrogenation of LA under hydrothermal conditions catalyzed by bases as well as by simple sodium sulfate [170]. Horvath and coworkers reported Ru complex in water for the transfer hydrogenation of LA with formic acid as hydrogen donor. A method of combined dehydration/(transfer)-hydrogenation was developed for converting C_6 sugars to GVL using a pre-formed homogeneous water soluble Ru-TPPTS catalyst in combination with TFA to give quantitative C_6 sugar conversions with a much lower GVL yield (23 mol%) compared to the heterogeneous counterpart of Ru [140]. Recently Deng et al. reported a new route for converting various biomass-derived oxygenates (cellulose, starch, and sugars) into GVL without using an external H_2 in presence of $RuCl_3/PPh_3$ pyridine catalyst using an aqueous mixture of levulinic acid and formic acid (1:1) [171, 172]. Two-stage

conversion of biomass-derived carbohydrate into GVL studied over Au/ZrO_2 catalyst in presence of formic acid was one of the simple, efficient, ecologically friendly, and robust catalytic systems developed to-date for the selective reductive transformation of biomass-derived compounds [173, 174]. In another catalyst study Deng. et al. reported iridium pincer catalyst for transfer hydrogenation of LA:FA mixture selectively to GVL [75]. Further investigations, levulinic acid and its esters could be converted to GVL over metal oxide catalysts by catalytic transfer hydrogenation. Chia et al. reported liquid phase transfer hydrogenation of levulinic acid and its esters using secondary alcohol over metal oxide but suffers from poor yield (<50%) and very low catalyst substrate ratio (1:1) [176]. Tang et al. showed ethyl levulinate hydrogenation to GVL in presence of supercritical ethanol medium over zirconia catalyst however, the reaction temperature was as high as 250-300 ^{o}C and the catalyst could not be recycled due to its deactivation [177]. Recently, room temperature CTH of ethyl levulinate to GVL is reported over RANEY Ni catalyst in presence of isopropanol [178].

1.8.3. GVL synthesis starting from FAL via esters of LA

Recently, researchers have focused their attention on the alternate route for GVL which involves furfuryl alcohol as a starting material derived from hemicelluloses which becomes more atom economic than that from cellulose derived glucose and the summary is presented in Table 1.6.

Lange et al. have reported ion-exchange resins and zeolites as solid acid catalysts for the conversion of furfuryl alcohol to ethyl levulinate, but with a very low selectivity to ethyl levulinate due to the formation high boiling byproducts [179]. Organo-inorganic hybrid solid acids were proposed by Zhang et al. for the production of butyl levulinate with 93% yield but without showing the catalyst reusability [180]. Some of the other novel approaches include the use of biphasic systems with new solvents such as 2-sec-butylphenol (SBP) and 4-propyl guaiacol (PG) for the recycling of mineral acid in the production of furfural and levulinic acid from the hemicellulose portion of lignocellulose giving a yield of 60–70% [181].

Table 1.6. Literature study on synthesis of levulinic esters

Catalyst	Substrate	Reaction conditions	% Product distribution	Reference
Amberlyst 15	FAL	125 ^{o}C, TOS, solvent ethanol,	85 (MeLA)	179
$[BmimSO_3H]_3PW_{12}O_{40}$	FAL	110 ^{o}C, 12 h, solvent n-butanol	88 (MeLA)	180
H_2SO_4	FAL	125 ^{o}C, 3 h solvent SBP	70	181
[BMIm-SO_3H][HSO_4]	Sucrose/glucose	150 ^{o}C, 6 h, solvent ethanol	30	182
$In(OTf)_3$ + PTSA	Cellulose	180 ^{o}C, 5 h, Solvent methanol	20	183
H_2SO_4	5-HMF	75 ^{o}C, 24 h, Solvent ethanol, n-butanol	16	184
Amberlyst-15	5-HMF	140 ^{o}C, 5 h, Solvent, Ethanol	99	185
$Cs_{2.5}H_{0.5}PW_{12}O_{40}$	Cellulose	300 ^{o}C, 2 h, Solvent, ScMeOH	20	186
SO4 /ZrO_2-TiO_2	Glucose	200 ^{o}C, 2 h, ScMeOH	40	187

The imidazolium and pyridinum based ILs functionalized with (SO_3H, PTSA and $ClSO_3H$) acidic groups studied by Saravanamurugan et al. in the presence of naphthalene as an added solvent showed 70% selectivity to methyl levulinate with hydroxy methyl furfural ether as a byproduct [182]. The direct conversion of the cellulose unit of glucose to methyl levulinate was reported by Tominaga et al. using homogeneous mixed Lewis and Brønsted acid systems resulting in methyl levulinate selectivity in the range of 20–50% from cellulose hydrolysis in methanol medium [183]. Various acid catalysts systems were reported for the synthesis of FAL ethers and levulinic esters from direct cellulose and 5-HMF [184-187]. A tandem approach combining acid hydrolysis and hydrogenation reactions together over heterogeneous (Ru/C) and acid catalysts (mineral acid) has also been proposed for the catalytic conversion of cellulose to platform chemicals.

1.9. Objectives of the thesis

All the three different strategies for GVL production as covered in the literature survey section [1.8] have their respective advantages and are being studied extensively. However, almost all the studies have been done using noble metal catalysts with a major drawback of higher extent of metal leaching under reaction conditions. Hence, we had undertaken a very systematic study on developing the non-noble metal and non leaching catalyst systems for GVL production from LA/esters and FAL with and without using external hydrogen. The objectives and scope of this thesis are given below.

- Preparation of the following catalyst systems:
  - Ru catalysts supported on C, SiO_2 and Al_2O_3 by impregnation method
  - Mixed oxides of Cu with ZrO_2 by co-precipitation method
  - Bimetallic Ag-Ni catalysts
  - Functionalized ionic liquids prepared by ion exchange method.
- Physicochemical characterization of the prepared catalysts by various techniques such as powder X-ray diffraction, SEM, EDAX, BET surface area, Raman, FTIR, Chemisorptions, HRTEM, and XPS.
- Standardization of analytical methods for the model reaction systems using GC and HPLC.
- Activity testing of the prepared catalysts for selective hydrogenation of levulinic acid, methyl levulinate and FAL in high pressure batch and continuous reactors.
- To develop novel catalytic systems for hydrogenation of levulinic acid, esters of LA and 5-methyl FAL without an external source of hydrogen.
- Optimization of reaction parameters such as temperature, pressure, catalyst and substrate loading in order to achieve highest conversion and selectivity, for all the hydrogenation reactions studied in this work.

- To correlate the observed activity and selectivity patterns with the catalyst characterization data for elucidation of catalytic reaction pathways in various systems of GVL synthesis.

1.10. REFRENCES

1. The Roadmap for Biomass Technologies in the U.S., Biomass R&D Technical Advisory Committee, US Department of Energy, Accession No. ADA 436527, (2002).
2. D. A. Simonetti, J. A. Dumesic, ChemSusChem 1 (2008) 725.
3. D. Y. Goswami, F. Kreith, CRC Press/Taylor & Francis 1 (2007) 1.
4. B. P. Stat. Rev. World Energy. White House. http://usgovinfo.about.com/b/2007/01/23/ (2007).
5. Directive Eur. Union Parliam, J. Eur. Union. http://ec.europa.eu/energy/ (2003).
6. J. P. Lange Lignocellulose conversion: an introduction to chemistry, process and economics. Biofuels, Bioprod Biorefin 1 (2007) 39.
7. P. M. Sanders, Macromol. Biosci. 7 (2007) 105.
8. R. D. Perlack, L. L. Wright, A. F. Turhollow, R. L. Graham, B. J. Stokes, D. C. Erbach, Biomass as feedstock for a bioenergy and bioproducts industry: DOE/GO-102005-2135, Oak Ridge National Laboratory. http:// feedstockreview.ornl.gov/pdf/billion_ton_vision.pdf. (2005).
9. D. L. Klass, Biomass for the renewable energy and fuels, Cleveland CJ (ed) Encyclopedia of energy. Elsevier, London 24 (2004).
10. M. Stocker, Angew Chem Int Ed 47 (2008) 9200.
11. P. M. Sanders, Macromol. Biosci. 7 (2007) 105.
12. J. J. Bozell, ACS Symp. Ser. 92 (2006) 1.
13. Y. Chisti, Biotechnol. Adv.25 (2007) 294.
14. A. Aden, M. Ruth, K. Ibsen, J. Jechura, K. Neeves, J. Sheehan, B. Wallace, L. Montague, A. Slayton and J. Lukas, National Renewable Energy Laboratory, Golden, CO, NREL/TP-510-32438 (2002).
15. E. S. Lipinsky, Science 212 (1981) 1465.
16. J. J. Bozell, Clean, Soil Air Water 36 (2008) 641.
17. T. L. Donaldson, O. L. Culberson, Energy 9 (1984) 693.
18. J. P. Kaiser and K. W. Hanselmann, Experientia 38 (1982) 167.
19. J. J. Bozell, J. E. Holladay, D. Johnson, J. F. White, Top Value Added Chemicals

from Biomass. Volume II – Results of Screening for Potential Candidates from Biorefinery Lignin, PNNL-16983 (2007).

20. K. Weissermel, H.J. Arpe, Industrial Organic Chemistry, Wiley VCH Ed. (2003).
21. R. L. Pruett, Science 211 (1981) 11.
22. G. W. Huber, S. Iborra, A. Corma, Chem. Rev.106 (2006) 4044.
23. A. Corma, S. Iborra, A. Velty, Chem. Rev. 107 (2007) 2411.
24. G. W. Huber, A.Corma, Angew. Chem. Int. Ed.46 (2007) 7184.
25. D. Tilman, R. Socolow, J. A. Foley, J. Hill, E. Larson, L. Lynd, S. Pacala, J. Reilly, T. Searchinger, C. Somerville, R. Williams, Science 325 (2009) 270.
26. L. R. Lynd, J. H. Cushman, R. J. Nichols, C. E.Wyman, Science 251 (1991) 1318.
27. N. Mosier, C. E. Wyman, B. E. Dale, R. T. Elander, Y. Y. Lee., M. Holtzapple, M. R. Ladisch, Bioresour. Technol. 96 (2005) 673.
28. F. S. Chakar, A. J. Ragauskas, Ind. Crops Prod. 20 (2004) 131.
29. R. Vanholme, K. Morreel, J. Ralph, W. Boerjan, Curr. Opin. Plant Biol. 11 (2008) 278.
30. C. E. Wyman, B. E. Dale, R. T. Elander, M. Holtzapple, M. R. Ladisch, Y. Y. Lee, Bioresour. Technol. 96 (2005) 2026.
31. T. A. Lloyld, C. E.Wyman, Bioresour. Technol. 96 (2005) 1967.
32. A. R. Aden M. K. Ibsen, J. Jechura, K. Neeves, J. Sheehan, B. Wallace, L. Montague, A. Slayton, J.Lukas, NREL/TP-510-32438, (2002).
33. A. Aden, T. Foust, Cellulose 16 (2009) 535.
34. R. J. A. Gosselink, E. D. Jong, B. Guran, A. Abachelir, Ind. Crops Prod. 20 (2004) 121.
35. R. J. Evans, T. A. Milne, M. N. Soltys, J. Anal. Appl. Pyrolysis 9 (1986) 207.
36. T. R. Carlson, J. Jae, Y.C. Lin, G. A. Tompsett, G. W. Huber, J. Catal. 270 (2010) 110.
37. J. Jae, G. A. Tompsett, Y. Lin, T. R. Carlson, J. Shen, T. Zhang, B. Yang, C. E. Wyman, W. C. Conner, G. W. Huber, Energy Environ. Sci. 3 (2010) 358.
38. C. E. Wyman, S. R. Decker, M. E. Himmel, J. W. Brady, C. E. Skopec, L. Viikari, Polysaccharide (2005) 995.

39. R. Rinaldi, F. Schuth, ChemSusChem 2 (2009) 1096.
40. B. C. Saha, J. Ind. Microbiol. Biotechnol. 30 (2003) 279.
41. J. Zaldivar, J. Nielsen, L. Olsson, Appl. Microbiol. Biotechnol. 56 (2001) 17.
42. E. Iglesia, S. C. Reyes, R. J. Madon, S. L. Soled, Adv. Catal. 39 (1993) 221.
43. P. J. Woolcock, R. C. Brown, Biomass and Bioenergy 52 (2013) 54.
44. M. E. Dry, Catal. Today 71 (2002) 227.
45. D. J. Hayes, Catal. Today 145 (2009) 138.
46. T. R. Carlson, G. A. Tompsett, W. C. Conner, G. W. Huber, Top. Catal. 52 (2009) 241.
47. G. W. Huber, Breaking the Chemical and Engineering Barriers to Lignocellulosic Biofuels: (2007).
48. R. R. Soares, D. A. Simonetti, J. A. Dumesic, Angew. Chem., Int. Ed. 45 (2006) 3982.
49. D. C. Elliott, Energy Fuels 21 (2007) 1792.
50. S. Czernik, A. V. Bridgwater, Energy Fuels 18 (2004) 590.
51. J. P. Diebold, A Review of the Chemical and Physical Mechanisms of the Storage Stability of Fast Pyrolysis Bio-Oil. Report No. NRREL/SR-570-27613, (2000).
52. J. Jae, G. A. Tompsett, Y. Lin, T. R. Carlson, J. Shen, T. Zhang, B. Yang, C. E. Wyman, W. C. Conner, G. W. Huber, Energy Environ. Sci. 3 (2010) 358.
53. M. F. Demirbas, Appl. Energy 86 (2009) 151.
54. D. A. Simonetti, J. A. Dumesic, ChemSusChem, 1 (2008) 725.
55. L. Petrus, M. A. Noordermeer, Green Chem. 8 (2006) 861.
56. D. A. Simonetti, J. Rass-Hansen, E. L. Kunkes, R. R. Soares, J. A. Dumesic, Green Chem. 9 (2007) 1073.
57. K. Klier, Adv. Catal. 31 (1982) 243.
58. D. Mohan, C.U. Pittman, P.H. Steele. Energy Fuels 20 (2006) 848.
59. S. R. A. Kersten, W. P. M. van Swaaij, L. Lefferts, K. Seshan, Catalysis for Renewables: From Feedstock to Energy Production, ed. Weinheim: Wiley-VCH 6 (2007) 119.
60. T. R. Carlson, T. P. Vispute, G. W. Huber. ChemSusChem 1 (2008) 397.

61. R. R. Soares, D. A. Simonetti, J. A. Dumesic, Angew. Chem., Int. Ed. 45 (2006) 3982.
62. P. G. Blommel, G. R. Keenan, R. T. Rozmiarek, R.D. Cortrigth, Int. Sugar J. 110 (2008) 672.
63. G. W. Huber, R. D. Cortright, J. A. Dumesic, Angew. Chem., Int. Ed. 43 (2004) 1549.
64. E. L. Kunkes, D. A. Simonetti, R. M. West, J. C. Serrano- Ruiz, C. A. Gartner, J. A. Dumesic, Science 322 (2008) 417.
65. T. Werpy, G. Petersen, Top Value Added Chemicals From Biomass, Volume I www.eere.energy.gov/biomass/pdfs/35523.pdf, New York (2004).
66. J. J. Bozell, J. E. Holladay, D. Johnson, J. F. White, Top Value Added Chemicals from Biomass. Volume II – PNNL-16983 (2007).
67. K. Weissermel, H. J. Arpe, Industrial Organic Chemistry, 4thedn. Wiley VCH,Weinheim (2003).
68. M. Aden, Ruth, K. Ibsen, J. Jechura, K. Neeves, J. Sheehan, B. Wallace, L. Montague, A. Slayton, J. Lukas, NREL/TP-510-32438 (2002).
69. Jenkins, Biofuels, Bioprod. Biorefin. 2 (2008) 133.
70. J. J. Bozell, G. R. Petersen, Green Chem. 12 (2010) 539.
71. G. W. Huber, Next Generation Hydrocarbon Biorefineries, ed. (2008).
72. B. C. Gates, G. W. Huber, C. L. Marshall, P. N. Ross, J. Sirola, Y. Wang, Mater. Res. Bull. 33 (2008) 429.
73. Catalysis Looks to the Future, Panel on New Directions in Catalytic Science and Technology, Technical Report, National Academy of Sciences National Research Council, DOE/ER/14103-T1, Washington, DC, (1992).
74. C. H. Bartholomew, R. J. Farrauto, in Fundamentals of Industrial Catalytic Processes, Wiley Interscience, Hoboken, NJ, 2nd edn, (2006).
75. D. L. Klass, in Encyclopedia of Energy, ed. C. J. Cleveland, Elsevier, London, 2004, pp. 193–212.
76. F. Kreith, D.Y. Goswami, Handbook of Energy Efficiency and Renewable Energy (2007).
77. H. Fukuda, A. Kondo, H. Noda, J. Biosci. Bioeng. 92 (2001) 405.

78. F. R. Ma, M. A. Hanna, Bioresour. Technol. 70 (1999) 1.
79. R. Rinaldi, F. Schuth, Energy Environ. Sci. 2 (2009) 610.
80. P. Imhof, J. C. vanderwaal, ISBN 978-3-527-33169-7 Wiley-VCH, Weinheim, (2013).
81. C. H. Bartholomew, R. J. Farrauto, in Fundamentals of Industrial Catalytic Processes, Wiley Interscience, Hoboken, NJ, 2nd edn, (2006).
82. G. W. Huber, J. W. Shabaker, J. A. Dumesic, Science 300 (2003) 2075.
83. G. W. Huber, R. D. Cortright, J. A. Dumesic, Angew. Chem. Int. Ed. 43 (2004) 1549.
84. G. W. Huber, J. N. Chheda, C. J. Barrett and J. A. Dumesic, Science 308 (2005) 1446.
85. R. R. Davda, J. W. Shabaker, G. W. Huber, R. D. Cortright and J. A. Dumesic, Appl. Catal., B.56 (2005) 171.
86. G. W. Huber, J. A. Dumesic, Catal. Today 111 (2006) 119.
87. J. Wei, J. C. W. Kuo, Ind. Eng. Chem. Fundam. 8 (1969) 114.
88. S. M. Jacob, B. Gross, S. E. Voltz, V. W. Weekman, AIChE J. 22 (1976) 701.
89. O. Bobleter, Polysaccharides (2005) 893.
90. J. Lecomte, A. Finiels, C. Moreau, Starch 54 (2002) 75.
91. D. Mercadier, L. Rigal, A. Gaset, J. P. Gorrichon, J. Chem. Technol. Biotechnol. 31 (1981) 489.
92. C. Moreau, R. Durand, S. Razigade, J. Duhamet, P. Faugeras, P. Rivalier, P. Ros, G. Avignon, Appl. Catal. A 145 (1996) 211.
93. B. Girisuta, L. P. B. M. Janssen, H. J. Heeres, Green Chem., 2006, 8, 701–709.
94. R. R. Davda, James A. Dumesic, Chem. Commun. (2004) 36.
95. R. B. Mane, A. M. Hengne, A. A. Ghalwadkar, S. Vijayanand, P. H. Mohite, H. S. Potdar, C. V. Rode, Catal. Lett. 135 (2010) 141.
96. C. V. Rode, A. M. Hengne, A. A. Ghalwadkar, R. B. Mane, P. H. Mohite, H. S. Potdar, WO 2011/138643 A2 (2012).
97. M. Besson, P. Gallezot, Catal. Today 81 (2003) 547.
98. R. A. Sheldon, M. Wallau, I. W. C. E. Arends, U. Schuchardt, Acc. Chem. Res.,

31 (1998) 485.

99. K. Tanabe, W. F. Holderich, Appl. Catal. A: Gen. 181 (1999) 399.
100. R. Glaser, J. Weitkamp, in Handbook of Porous Materials, ed.1 (2002) 395.
101. Y. Ogihara, R. L. Smith Jr., H. Inomata, K. Ara, Cellulose 12 (2005) 595.
102. T. Okuhara, Chem. Rev. 102 (2002) 3641.
103. A. Bruggink, R. Schoevaart, T. Kieboom, Org. Process Res. Dev. 7 (2003) 622.
104. H. Carothers, G. L. Dorough, F. J. Van Natta, J. Am. Chem. Soc. 54 (1932) 761.
105. R. Datta, In Kirk-Othmer Encyclopedia of Chemical Technology, ed., 14 (2004) 114.
106. J. C. Serrano-Ruiz, J. A Dumesic, Green Chem. 11 (2009) 1101.
107. I. Bechthold, K. Bretz, S. Kabasci, R. Kopitzky, A. Springer, Chem. Eng. Technol. 31 (2008) 647.
108. N. Nghiem, B. H. Davison, M. I. Donnelly, S.P. Tsai, J.G. Frye, ACS Symp. Ser. 784 (2001) 160.
109. J. G. Zeikus, M. K. Jain, P. Elankovan, Appl. Microbiol. Biotechnol. 51 (1999) 545.
110. G. J. Mulder, J. Prakt. Chem. 21 (1840) 219.
111. Kitano, Chem. Econo. Engine. Rev. (1975) 25.
112. R. H. Leonard, Ind. Eng. Chem. (1956) 1331.
113. B. Girisuta, L. Janssen, H. J. Heeres, Chem. Eng. Res. Des. 84 (2006) 339.
114. B. Girisuta, L. Janssen, H. J. Heeres, Ind. Eng. Chem. Res. 46 (2007) 1696.
115. S. W. Fitzpatrick, ACS Symp. Ser. 921 (2006) 271.
116. S. W. Fitzpatrick, US Pat, 4897497 (1990).
117. S. W. Fitzpatrick, US Pat, 5608105 (1997).
118. H. Mehdi, V. Fabos, R. Tuba, A. Bodor, L. T. Mika, I. T. Horvath, Top. Catal. 48 (2008) 49.
119. H. Uslu, S. I. Kirbaslar, K. L. Wasewar, J. Chem. Eng. Data 54 (2009) 712.
120. C. Chang, P. L. Cen, X. J. Ma, Bioresour. Technol. 98 (2007) 1448.
121. B. Girisuta, B. Danon, R. Manurung, L. Janssen, H. J. Heeres, Bioresour. Technol. 99 (2008) 8367.
122. J. Horvat, B. Klaic, B. Metelko, V. Sunjic, Tetrahedron Lett. 26 (1985) 2111.

123. J. J. Bozell, L. Moens, D. C. Elliott, Y.Wang, G.G. Neuenscwander, S. W. Fitzpatrick, R. J. Bilski, J. L. Jarnefeld, Resour., Conserv. Recycl. 28 (2000) 227.
124. Biometics Inc., Munipal Solid Waste Conversion Project, Final Report, Contract No: 4204-ERTER-ER-96., Biometics Inc., Boston, Ma, (1996).
125. I. T. Horvath, H. Mehdi, V. Fabos, L. Boda, L. T. Mika, Green Chem. 10 (2008) 238.
126. D. J. Hayes, S. Fitzpatrick, M. H. B. Hayes, WILEY-VCH, Weinheim, 1 (2006) 139.
127. B. V. Timokhin, V. A. Baransky, G. D. Eliseeva, Russ. Chem. Rev. 68 (1999) 73.
128. H. Heeres, R. Handana, D. Chunai, C. B. Rasrendra, B. Girisuta, Green Chem. 11 (2009) 1247.
129. L. E. Manzer, Appl. Catal. A: Gen. 272 (2004) 249.
130. M. Balat, Energy Sources 27 (2005) 569.
131. Y. Kar, H. Deveci, Energy Sources 28 (2006) 909.
132. S. W. Fitzpatrick, J. J. Bozell, M. K. Patel, Renewable for the Production of Chemicals and Materials. 921 (2006) 271.
133. S. W. Fitzpatrick, WO, 1996040609, (1995).
134. G. Dayma, F. Halter, F. Foucher, C. Togbé, C. Mounaim-Rousselle, P. Dagaut, Energy Fuels 26 (2012) 4735.
135. W. H. Luo, U. Deka, A. M. Beale, E. R. H. van Eck, P. C. A. Bruijnincx, B. M. Weckhuysen, J. Catal. 301 (2013) 175.
136. S. K. R. Patil, C. R. F. Lund, Energy Fuels 25 (2011) 4745.
137. S. K. R. Patil, J. Heltzel and C. R. F. Lund, Energy Fuels 26 (2012) 5281.
138. F. Joo, M. T. Beck, React. Kinet. Catal. Lett. 2 (1975) 257.
139. K. Osakada, T. Ikariya, S. Yoshikawa, J. Organomet. Chem. 231 (1982) 79.
140. H. Heeres, R. Handana, D. Chunai, C. B. Rasrendra, B. Girisuta and H. J. Heeres, Green Chem. 11 (2009) 1247.
141. F. M. A. Geilen, B. Engendahl, A. Harwardt, W. Marquardt, J.Klankermayer, W. Leitner, Angew. Chem., Int. Ed. 49 (2010) 5510.
142. J. M. Tukacs, D. Király, A. Strádi, G. Novodarszki, Z. Eke, G. Dibó, T. Kéglb,

L. T. Mika, Green Chem. 14 (2012) 2057.

143. W. Li, J.H. Xie, H. Lin, Q.L. Zhou, Green Chem. 14 (2012) 2388.
144. F. M. A. Geilen, B. Engendahl, M. Hölscher, J. Klankermayer, W. Leitner, J. Am. Chem. Soc. 133 (2011) 14349.
145. H. A. Schuette, R. W. Thomas, J. Am. Chem. Soc. 52 (1930) 3010.
146. P. P. Upare, J. M. Lee, D. W. Hwang, S. B. Halligudi, Y. K. Hwang, J. S. Chang, J. Ind. Eng. Chem. 17 (2011) 287.
147. J. P. Lange, R. Price, P. M. Ayoub, J. Louis, L. Petrus, L. Clarke, H. Gosselink, Angew. Chem. Int. Ed. 49 (2010) 4479.
148. H. S. Broadbent, G. C. Campbell, W. J. Bartley, J. H. Johnson, J. Org. Chem. 24 (1959) 1847.
149. M. G. Al-Shaal, W. R. H. Wright, R. Palkovits, Green Chem. 14 (2012) 1260.
150. D. M. Alonso, S. G. Wettstein,. J. Q. Bond, T. W. Root, J. A. Dumesic, ChemSusChem 4 (2011) 1078.
151. S. G. Wettsteina, J. Q. Bonda, D. M. Alonsoa, H. N. Phamb, A. K. Datyeb, J. A. Dumesic, Appl. Catal. B: Environ. 117 (2012) 321.
152. R. A. Bourne, J. G. Stevens, J. Ke, M. Poliakoff, Chem. Commun. 44 (2007) 4632.
153. Z. P. Yan, L. Lin, S. Liu, Energy Fuels 23 (2009) 3853.
154. D. J. Braden, C. A. Henao, J. Heltzel, C. C. Maravelias, J. A. Dumesic, Green Chem. 13 (2011) 1755.
155. W. Luo, U. Deka, A. M. Beale, E. R.H. van Eck, P. C.A. Bruijnincx , B. M. Weckhuysen, J. Catal. 301 (2013) 175.
156. C. Ortiz-Cervantes, J. J. Garcia, Inorganica Chimica Acta 397 (2013) 124.
157. M. Selva, M. Gottardo, A. Perosa, Acs Sustainable Chemistry & Engineering Volume: 1 (2013) 180.
158. A. M. R. Galletti, C. Antonetti, V. De Luise, M. Martinelli, Green Chem. 14 (2012) 688.
159. R. Luque, J. H. Clark, Catal. Commun. 11 (2010) 928.
160. E. I. Gürbüz, D. M. Alonso, J. Q. Bond, J. A. Dumesic, ChemSusChem 4 (2011) 357.

161. Z. Wu, S. Ge, C. Ren, M. Zhang, A. Yip, C. Xu, Green Chem. 14 (2012) 3336.
162. L. C. Demailly, B. K. Ly, D. P. Minh, B. Tapin, C. Especel, F. Epron, A. Cabiac, E. Guillon, M. Besson, C. Pinel, ChemSusChem DOI: 10.1002/cssc.201300608.
163. R.V. Christian J. H. Brown, R. M. Hixon, J. Am. Chem. Soc. 69 (1947) 1961.
164. P. P. Upare , J. M. Lee, Y. K. Hwang , D. W. Hwang, J.-H. Lee, S. B. Halligudi, J. S. Hwang, J. S. Chang, ChemSusChem 4 (2011) 1749.
165. K. Yan, A. Chen, Fuel 115 (2014) 101.
166. K. Yan, A. Chen, Energy 58 (2013) 357.
167. B. Loges, A. Boddien, H. Junge, M. Beller, Angew. Chem. Int. Ed. 120 (2008) 4026.
168. C. Fellay, P. J. Dyson, G. Laurenczy, Angew. Chem. Int. Ed. 120 (2008) 4030.
169. Y. Himeda, Green Chem. 11 (2009) 2018.
170. D. Kopetzki, M. Antonietti Green Chem. 12 (2010) 656.
171. L. Deng, J. Li, D.-M. Lai, Y. Fu, Q.-X. Guo, Angew. Chem. Int. Ed. 48 (2009) 6529.
172. L. Deng, Y. Zhao, J. Li, Y. Fu, B. Liao, Q.-X. Guo, ChemSusChem 3 (2010) 1172.
173. X. L. Du, L. He, S. Zhao, Y.M. Liu, Y. Cao, H. Y. He, K. N. Fan, Angew. Chem. Int. Ed. 50 (2011) 7815.
174. X. L. Du, Q. Y. Bi, Y. M. Liu, Y. Cao, K.-N. Fan, ChemSusChem 4 (2011) 1838.
175. J. Deng, Y. Wang, T. Pan, Q. Xu, Q. X. Guo, Y. Fu, ChemSusChem 6 (2013) 1163.
176. M. Chia, J. A. Dumesic, Chem. Commun.47 (2011) 12233.
177. X. Tang, L. Hu, Y. Sun, G. Zhao, W. Hao, L. Lin, RSC Advance 3 (2013) 10277.
178. Z. Yang, Y. B. Huang, Q. X. Guo, Y. Fu, Chem. Commun. 49 (2013) 5328.
179. J. P. Lange, D. Wouter, V. D. Graaf, R. J. Haan, ChemsusChem, 2 (2009) 437.
180. Z. Zhang, K. Dong, Z. Zhao, ChemSusChem 4 (2011) 112.
181. E. I. Grbz, S. G. Wettstein, J. A. Dumesic, ChemSusChem 5 (2012) 383.

182. K. Tominaga, A. Mori, Y. Fukushima, S. Shimada, K. Sato, Green Chem. 13 (2011) 810.

183. S. Saravanamurugan, O. N. V. Bu, A. Riisager, ChemSusChem 4 (2011) 723.

184. M. Balakrishnan, E. R. Sacia, A. T. Bell, Green Chem. 14 (2012) 1626.

185. P. Lanzafame, D.M. Temi, S. Perathoner, G. Centi, A. Macario, A. Aloise, G. Giordano, Catal. Today 175 (2011) 435.

186. F. Rataboul, N. Essayem, Ind. Eng. Chem. Res. 50 (2011) 799.

187. L. Penga, J. Zhuanga, L. Lin, J. Nat. Gas Chem. 21 (2012) 138.

Chapter 2

Experimental and characterization techniques

2.1. Materials

Levulinic acid (99%), γ-valerolactone (GVL, 98%), methyl levulinate (99%), ethyl levulinate (99%), butyl levulinate (99%), furfuryl alcohol (99%), 1-methyl imidazole and 1, 4 butane sultone, formic acid (FA, 97%) and [$(RuCl_3).3H_2O$] were purchased from Sigma-Aldrich, Banglore, India. Methanol, ethanol and isopropanol were purchased from Rankem, India. γ-Alumina, fumed silica, copper nitrate, silver nitrate, aluminum nitrate, zinc nitrate, barium nitrate, zirconium nitrate and iron(II) sulphate, nickel(II) sulphate, sodium borohydride, montmornlite (MMT) [$(Na,Ca)_{0.33}(Al,Mg)_2(Si_4O_{10})(OH)_2 \cdot H_2O$] were purchased from Loba Chemie, Mumbai, India. Distilled water was deionized by using Millipore (Mili-Q) water system. High purity grade nitrogen and hydrogen gases were procured from M/s. Inox Ltd. Mumbai, India.

2.2. Catalyst preparation

Various catalysts were used for hydrogenation reactions and the details of catalyst preparation are given below. A scheme of the experimental setup used for the catalyst preparation is shown in Figure 2.1.

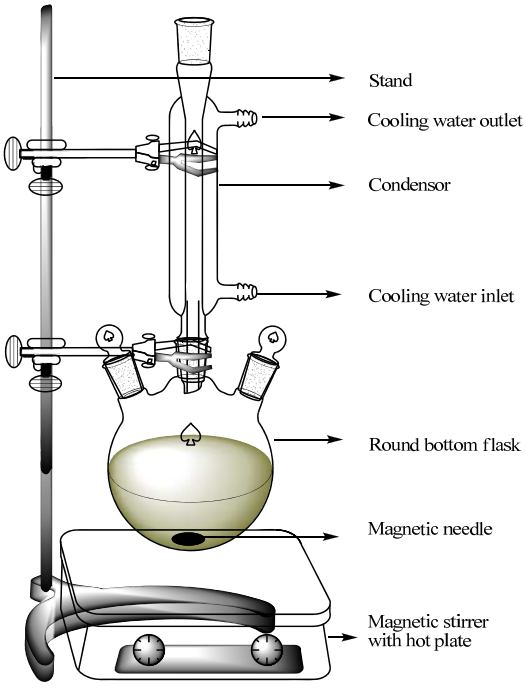

Figure 2.1. General setup for catalyst preparation

2.2.1. Supported noble metal catalysts

Supported Ru, Pd, Pt catalysts were prepared by impregnation method as shown in Figure 2.2. The synthesis was performed by suspending 2 g of support in an aqueous medium using calculated amount of the respective metal precursors and then suspension was stirred for 1 h. It was then subsequently reduced using 5 mL of $NaBH_4$ (1 mol) as a reducing agent. The catalyst was filtered and dried at 110 ^oC for 12 h.

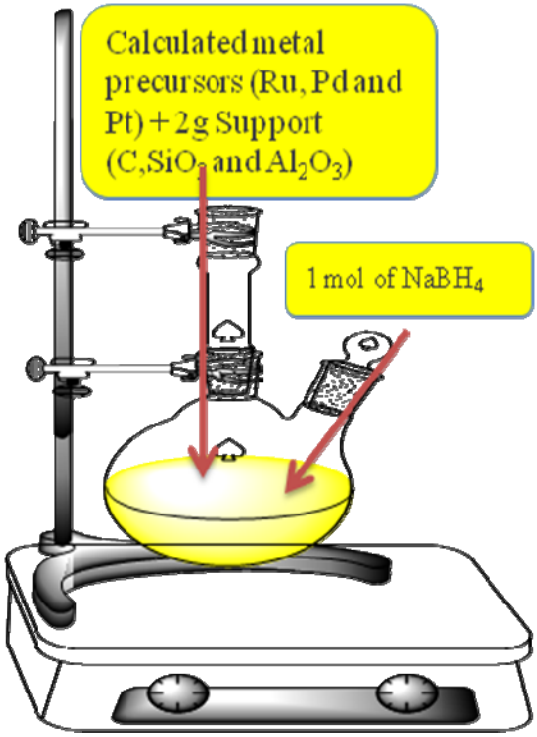

Figure 2.2. Setup for supported catalysts preparation by impregnation method

2.2.2. Cu-ZrO_2

The zirconia supported bimetallic silver nickel (Ag-Ni-ZrO_2) and copper–zirconia (Cu–ZrO_2) catalysts were prepared by using co-precipitation method as shown in Figure 2.3.

In typical procedure, 0.05 M aqueous solutions of Cu $(NO_3)_2 \cdot 3H_2O$ and $Zr(NO_3)_3 \cdot 3H_2O$ were taken and precipitated using 0.2 M aqueous potassium carbonate at room temperature. The precipitate was aged further for 6 h at room temperature. Then the precipitate was separated by filtration and washed with deionized water to remove the traces of potassium. The precipitate thus obtained, was dried in static air oven at 100 ^oC

for 8 h and calcined at 400 ^{o}C for 4 h. Prior to the reaction, the calcined catalyst was reduced in H_2 pressure.

All other copper catalysts tested in this work (Cu–Al_2O_3, Cu– BaO, Cu–Cr_2O_3, Cu–Cr_2O_3–Al_2O_3, Cu–BaO–Al_2O_3) were prepared by using a co-precipitation method. In a typical preparation, 0.5 M of each of Cu $(NO_3)_2 \cdot 3H_2O$ and the other metal nitrate in case of two component system, while 0.4 M of each of Cu $(NO_3)_2$ nitrate precursors of the respective metals (Al, Cr and Ba) in case of tricomponents, were dissolved in deionized water and precipitated using 0.2 M aqueous potassium carbonate at room temperature. The precipitate was aged further for 6 h at room temperature. Then the precipitate was separated by filtration and washed with deionized water to remove the traces of potassium. The precipitate thus obtained was dried in static air oven at 373 K for 8 h and calcined at 673 K for 4 h. Prior to the reaction, the calcined catalyst was reduced in H_2 flow.

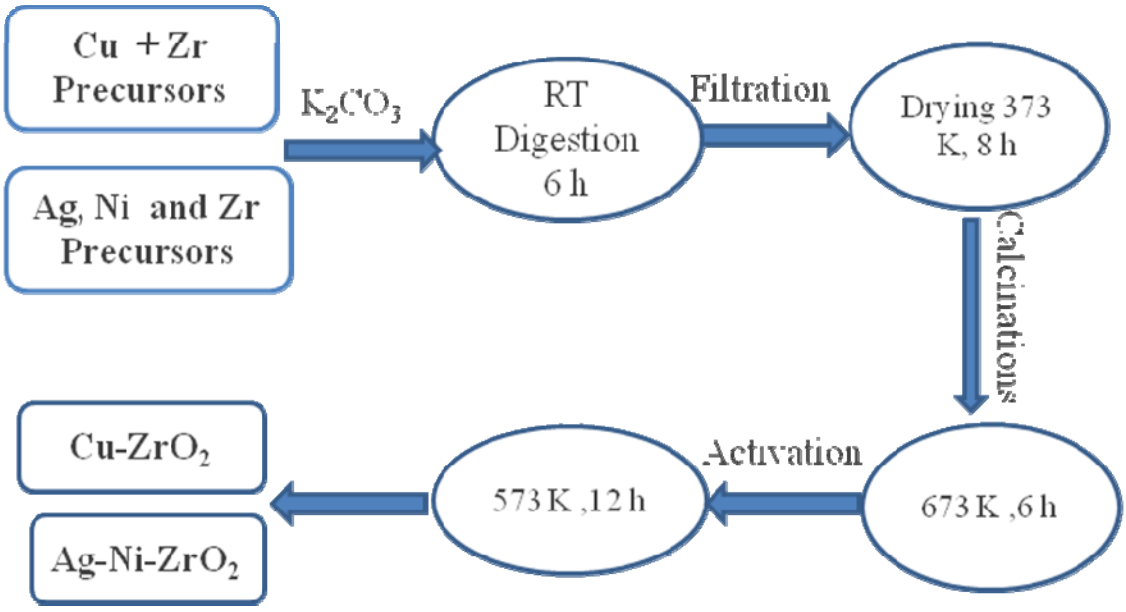

Figure 2.3. Setup for preparation of copper catalysts co-precipitation method

2.2.2.1. Ag-Ni-ZrO_2

Ag-Ni-ZrO_2 catalyst was prepared by the co-precipitation method in which 0.05M aqueous solutions of each Ag $(NO_3)_2$, $Ni(NO_3)_3.6H_2O$ and Zr $(NO_3)_3.3H_2O$ were taken and precipitated using 0.2 M aqueous potassium carbonate at room temperature. The precipitate was aged further for 6 h at room temperature. Then the precipitate was separated by filtration and washed with deionized water to remove the traces of potassium. The precipitate thus obtained was dried in static air oven at 373 K for 8 h and calcined at 673 K for 4 h. Prior to the reaction, the calcined catalyst was reduced in H_2 pressure.

All other catalysts tested (ZrO_2, Ag-ZrO_2, Ni-ZrO_2 and Ru-ZrO_2) were prepared by co-precipitation and impregnation methods. The required amounts of each Ag, Ni and Zr nitrate precursors were dissolved in deionized water and precipitated using 0.2 M aqueous potassium carbonate at room temperature. The precipitate was aged further for 6 h at room temperature. Then the precipitate was separated by filtration and washed with deionized water to remove the traces of potassium. The precipitate thus obtained was dried in static air oven at 373 K for 8 h and calcined at 673 K for 4 h. Prior to the reaction the calcined catalyst was reduced in H_2 flow.

Supported Ru/ZrO_2 catalyst was prepared by impregnation method. The synthesis was performed by suspending 2 g of prepared zirconia in aqueous medium using calculated amount of the metal precursor ($RuCl_3.3H_2O$) and then suspension was stirred for 1 h. It was then subsequently reduced using 5 mL of $NaBH_4$ (1 mol) as a reducing agent. The catalyst was filtered and dried at 110 ^oC for 12 h.

2.2.3. Supported Ni catalysts

2.2.3.1. 50% Ni-MMT-*insitu*

6.0 g of MMT was dispersed in 300 mL 1 N NaCl, stirred for 1 h at 6000 rpm on mechanical stirrer and the suspension was left to stand overnight at 250 rpm at room temperature. The slurry was centrifuged at 3000 rpm and the solid was dried in oven at 378 K for 4 h. The powder obtained was ground to 200 mesh size and used for preparation of nanocomposites.

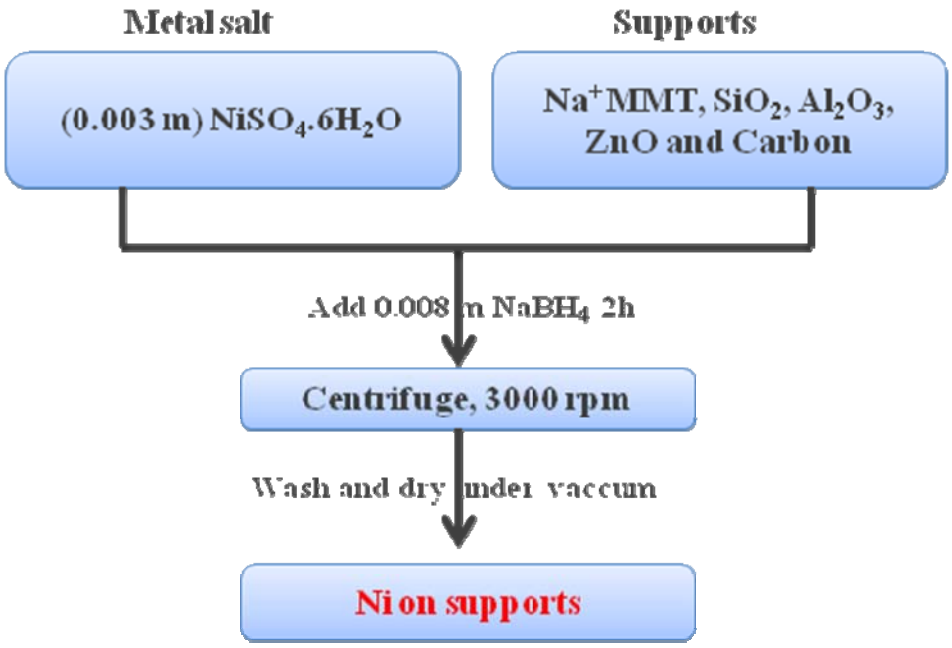

Figure 2.4. Preparation of supported Ni catalysts by co-precipitation method

To a suspension of 1 g of pretreated MMT in 50 mL of deionized water, aqueous solution of 0.003 M $NiSO_4.6H_2O$ in 200 mL of Milli-Q water was added with constant stirring under N_2 atmosphere. The whole mixture was stirred for 30 min followed by drop wise addition of 0.008 M $NaBH_4$ over a period of 2 hrs under nitrogen atmosphere. The whole mixture was centrifuged at 3000 rpm, washed with acetone and dried under vacuum.

All other Al_2O_3, SiO_2, ZrO_2, ZnO and C supported Ni catalysts were prepared as follows: To a suspension of 1g of support in 50 mL of deionized water, aqueous solution of 0.003 moles $NiSO_4.6H_2O$ dissolved in 200 mL of Milli-Q water was added with constant stirring under N_2 atmosphere. The whole mixture was stirred for 30 min followed by drop wise addition of 0.008 M $NaBH_4$ over a period of 2 h under nitrogen atmosphere which was then centrifuged at 3000 rpm, washed with acetone and dried under vacuum.

2.2.4. Acidic ILs and Supported Metal Catalysts

2.2.4.1. Acidic ILs

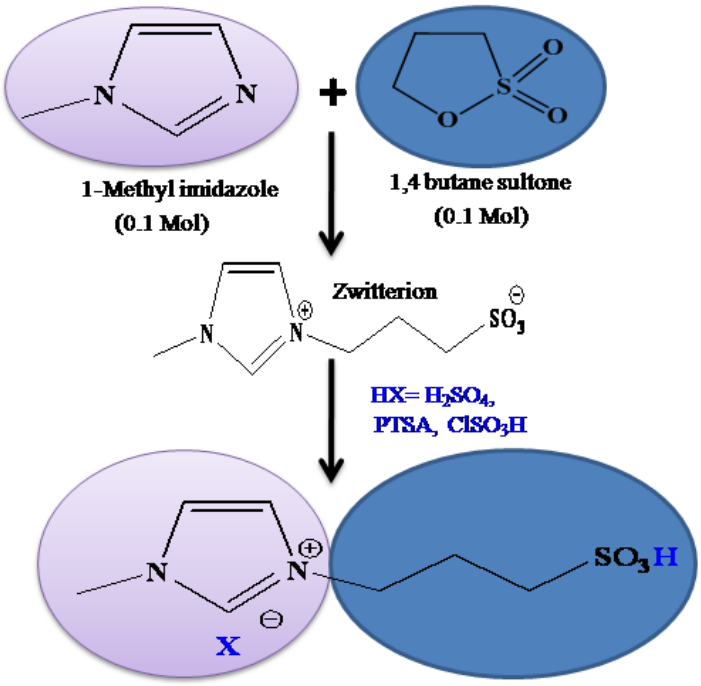

Figure 2.5. Synthesis of acidic ILs by quaternization method

Flow chart of the catalyst preparation is shown in Figure 2.5. Accordingly, 1-methlyimidazole and 1,4 butanesultone (0.2 M) were charged in to 100 mL round bottom flask and the mixture was then stirred at 40-80 ^{o}C for 1h. The solid zwitterion was recovered by filtration and washed with diethyl ether to completely remove the unreacted reactants and then dried under vacuum, overnight. A stoichiometric amount of respective sulfonic acid was subsequently added drop wise to the respective zwitterion and the mixture was again stirred at 80 ^{o}C for 6 h. The viscous liquid thus obtained was washed with diethyl ether and dried under vacuum, overnight.

2.2.4.2. Carbon supported catalysts

Carbon supported Ru, Pd, Re, Pd and Ag catalysts were prepared by the impregnation method. In a typical procedure, 2 g of activated carbon was suspended in an aqueous medium containing calculated amount of the respective metal precursor under stirring for 1 h. It was then subsequently reduced using 5 mL of $NaBH_4$ (1 M). The catalyst was then filtered and dried at 110 ^{o}C, for 12 h.

2.3. Performance criteria of a catalyst

Three major criteria usually considered to assess the performance of a catalyst are given below [33].

2.3.1. Activity

Catalyst efficiency can be evaluated by the turn over frequency (TOF).

Turn over frequency (time^{-1}):

It is the ratio of moles of reactant per mole of catalyst per unit time.

$$TOF = \frac{\text{Converted moles of substrate}}{\text{moles of catalyst used } x \text{ time}} \qquad \text{.....1.1}$$

2.3.2. Selectivity

Selectivity (S) is expressed by the ratio of the amount of desired product (P) formed to the amount of substrate consumed during the reaction. It also gives information about the possible reaction pathway. In addition to the desired reaction, parallel and sequential reactions can also take place (Figure 2.6). A high selectivity is essential for more economical as well as ecological processes.

$$\text{Selectivity} = \frac{\text{moles of desired product}}{\text{converted moles of the reactant}} \qquad \text{.....1.2}$$

Sequential reactions **Parallel reactions**

$A \rightarrow P \rightarrow P_1$

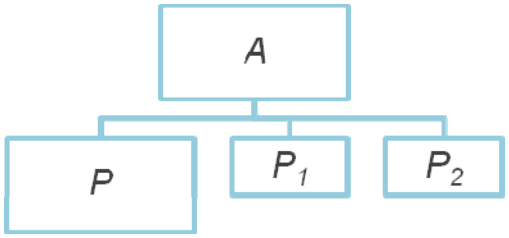

Figure 2.6. Sequential and parallel reactions

Where *A* is reaction starting material

P is desired product

P_1 and P_2 side products

Selectivity in catalysis is one of the most important factors that can be controlled in several ways such as by structural, chemical, electronic, kinetic and energy consideration [34].

2.3.3. Stability

Stability of a catalyst is very important issue in catalytic reaction. Chemical, thermal and mechanical stability of the catalyst determines lifetime of the catalyst. Number of factors including decomposition, coking and poisoning can affect the stability of a catalyst.

Turn over number:

Catalyst stability can be calculated in terms of turn over number and defined as the ratio of moles of reactant reacted per moles of catalyst.

$$\text{TON} = \frac{\text{Converted moles of substrate}}{\text{moles of catalysts used}} \qquad \text{…..1.3}$$

The TON term specifies the maximum use that can be made of a catalyst for a reaction under defined conditions by a number of molecular reactions or reaction cycles up to the decay of activity

Suitability of a catalyst can be decided considering the following order of priority.

Selectivity > Stability > Activity

2.4. Physiochemical characterization of catalyst

The prepared catalyst samples were characterized by various physico-chemical methods such as BET surface area analyzer, X-ray diffraction analysis, Raman spectroscopy, infrared spectroscopy, SEM, TEM, XPS and H_2 pulse titration. This section of chapter 2 gives a brief account of the theory and principles of various characterization techniques used for the current study. The procedure for each experimental technique is described. Characterization results are discussed in the relevant chapters.

2.4.1. Surface area measurement

The Brunauer-Emmett-Teller (BET) is the most widely acceptable method for analyzing multilayer physisorption isotherms of inert gases to determine the surface area of solids and the distribution of mesopore size in these solids as shown in Figure 2.7 [1].

Surface area is calculated by comparing the integrator count due to desorption with that from the calibration signal of the mass, (W adsorbed is given by equation) (2.1)

$$W = \frac{A}{A_{cal}} V_{cal} \frac{P_a M}{RT} \qquad \text{.....2.1}$$

Where,

W	mass of adsorbate adsorbed on the sample, g
V_{cal}	calibration volume (cm^3)
A	sample integrator counts
A_{cal}	calibration integrator counts
P_a	ambient pressure
M	adsorbate molecular weight (28 for N_2)
T	temperature in K
R	gas constant (82.06 $cm^3.atm.K^{-1}.mol^{-1}$)

BET equation (2.2) yields a straight line when $1/W(P_0/P-1))$ is plotted versus P/P_0. The slope,$(C-1)/W_mC$, and the intercept, $1/W_mC$, are used to determine the weight adsorbed at the monolayer.

$$\frac{1}{W(P_o/P-1)} = \frac{C-1}{W_m C}\frac{P}{P_o} + \frac{1}{W_m C} \qquad \text{.....2.2}$$

Where,

W	weight of adsorbate adsorbed at relative pressure P/Po
P	Partial pressure of adsorbate
P_0	saturated vapor pressure of adsorbate
Wm	weight of adsorbate adsorbed at a coverage of one monolayer

C a constant which is a function of the adsorbate heats of condensation and adsorption

The value of the slope *S* and the y-intercept *i* of the line are used to calculate the monolayer adsorbed gas quantity W*m* and the BET constant *C*, using the following equation.

$$W_m = \frac{1}{s+i} \quad \text{…..2.3}$$

The total surface are of the sample, S_t, is determined from equation

$$S_t = \frac{W_m N A_{cs}}{M_a} \quad \text{…..2.4}$$

Where,

M_a adsorbate molecular weight

W_m weight of adsorbate adsorbed at a coverage of one monolayer

N Avogadro's number = 6.023×10^{23}

A_{cs} cross sectional area of adsorbate molecule for N_2 gas 16.2×10^{-20} m^2

$$S_{BET} = \frac{S_t}{\text{weight of sample}} \quad \text{…..2.5}$$

BET surface areas of the specimen have been measured by using of N_2 adsorption at 77 K preformed on a Chemisoft TPx (Micromeritics-2720) instrument.

2.4.2. Temperature programmed reduction (TPR) method

Temperature programmed reduction method is a technique in which a chemical reaction is monitored between metal particles and hydrogen gas while the temperature increases linearly with time. This method is used to find the most efficient reduction conditions for the catalyst. Catalyst precursor is subjected to a programmed temperature technique method while a reducing gas mixture (H_2:N_2) is flown over it.

TPR experiments of the prepared copper catalysts were also performed on a Chemisoft TPx (Micromertics-2720). In the TPR experiment, U-tube (quartz tube) was filled with solid catalyst. This sample holder was positioned in a furnace equipped with a temperature control. A thermocouple was placed in the solid for temperature measurement. Equal quantity of fresh vacuum dried catalyst was taken in the U-tube. Initially, flow of inert gas (argon) was passed through U-tube to remove the air present in the lines, and heated in Ar atmosphere with a flow rate of 25 mL min^{-1} to 200 °C for 30 min to remove the moisture and surface impurities present on the sample and then it was cooled to room temperature. Ar was replaced by a mixture of 5% H_2 in Ar gas for the TPR experiment with a heating rate of 10 °C min^{-1} starting from the room temperature to 700 °C and a thermal conductivity detector (TCD) measured the hydrogen uptake.

2.4.3. NH_3-Temperature programmed desorption

NH_3-TPD experiments were carried out on a Chemisoft TPx (Micromeritics-2720) instrument. In order to evaluate acidity of the catalysts, ammonia TPD measurements were carried out by: (i) pre-treating the samples from room temperature to 300 ^{0}C under helium flow rate of 25 mL/min. (ii) adsorption of ammonia at 50 ^{0}C (iii) desorption of ammonia with a heating rate of 10 ^{o}C min^{-1} starting from the adsorption temperature to 700 ^{o}C.

2.4.4. Py-IR

Py-IR spectra were recorded on Shimadzu FTIR 8000 attached with SSU (Second sampling unit) using 20 mg catalyst sample. Sample was filled in a sample cup, 20 mL of pyridine were injected in N_2 flow. FTIR spectra were recorded on a Perkin-Elmer instrument. The pellets for analysis were prepared by mixing 2mg of the catalyst with 150 mg of KBr. FTIR spectra were recorded between 400 to 4000 cm^{-1} with accumulation of 20 scans and 4 cm^{-1} resolution.

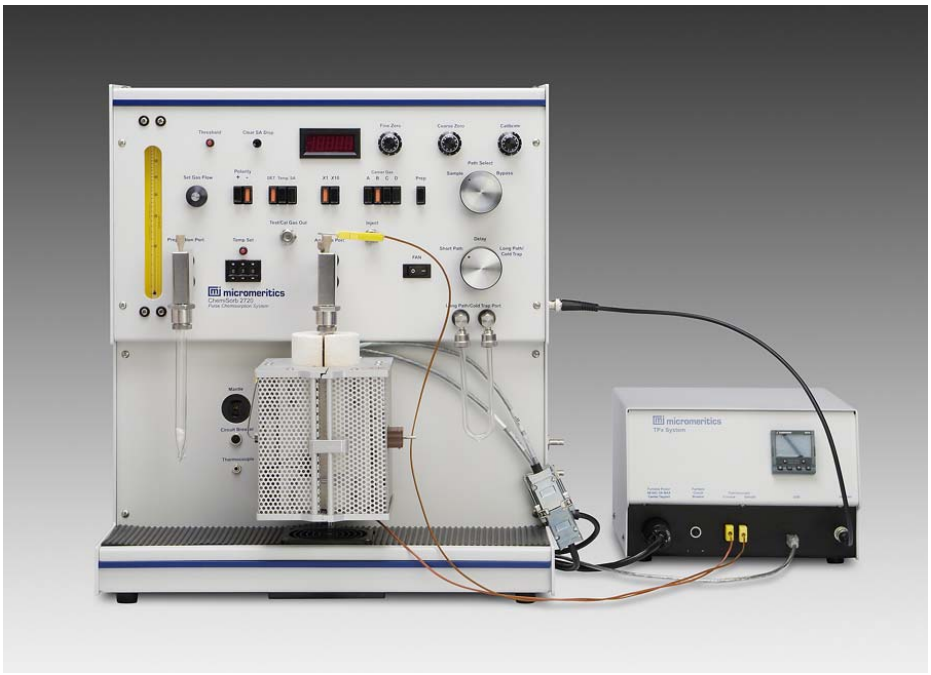

Figure 2.7. Chemisoft TPx (Micromeritics-2720) instrument

2.4.5. X-ray diffraction

Powder X-ray diffraction method is widely used for material characterization especially qualitative identification of crystalline phases. It provides the information about the identification of crystalline phases, lattice parameters, crystallite size measurement. It can detect crystalline materials having crystallites of greater than 3-5 nm and up to 100 nm. The X-ray diffraction patterns were obtained by measurement of the angels by which an X-ray beam is diffracted by the sample. Bragg's equation relates the distance between two hkl planes (d) and the angle of diffraction (2θ) as given in equation 2.6 [2].

$$n\lambda = 2d\sin\theta \quad \text{…..2.6}$$

Where,

λ	wavelength of the X-ray
n	integer called order of the reflection
d	distance between two lattice place
θ	angle of incidence plane

The average crystalline size of the metal particle can be estimated by Debey-Scherrer equation 2.7 [3].

$$< L >= \frac{K\lambda}{\beta \cos\theta} \quad \text{…..2.7}$$

In which,

<L> is a measure for the dimension of the particle in the direction perpendicular to the reflecting plane

λ is the X-ray wavelength

β is the peak width

θ is the angle between the beam and the normal on the reflecting plane

K is a constant i.e. (0.9)

For calculation of peak width

$$\beta = \sqrt{B_1^2 - B_2^2} \quad \text{…..2.8}$$

Where,

B_1 is the FWHM (full width half maxima)

B_2 is the instrument broadening (0.15)

X-ray powder diffraction patterns have been recorded on a PAnalytical PXRD Model X-Pert PRO-1712, using Ni filtered Cu Kα radiation (λ=0.154 nm) as a source (current intensity, 30 mA; voltage, 40 kV) and a X-celerator detector. The samples were scanned in the 2θ range of 5-80°. The species present on the surface were identified by their characteristic 2θ values of the relevant crystalline phase.

2.4.6. X-ray photoelectron spectroscopy

The X-ray photo electron spectroscopy [4-7] is based on the photoelectric effect, which involves the bombardment of a sample surface with X-ray and measurement of the concomitant photoemitted electrons. The photoemitted electrons have discrete kinetic energies that are characteristic of the emitting atoms and their bonding states. The shifts

in core-level energies give information on the surface elemental composition, the oxidation state of the elements and chemical analysis [8].

The kinetic energy, E_k, of these photoelectrons is determined by the energy of the X-ray radiation, hv, and the electron binding energy E_b as given by,

$$E_k = hv - E_b \quad \text{…..2.9}$$

The experimentally measured energies of the photoelectrons are given by

$$E_k = hv - E_b - \psi \quad \text{…..2.10}$$

Where,

E_k	is the kinetic energy of the photoelectron
h	is Plank's constant
v	is the frequency of the exciting radiation
E_b	is the binding energy of the photoelectron with respect to the Fermi level of the sample
ψ	is the work function of the spectrometer

The shape of each peak and the binding energy can be slightly altered by the chemical state of the emitting atom. Hence, XPS can provide information on chemical bonding. The number of catalytic properties such as oxidation state of active species, interaction of a metal with a support, change in oxidation state upon activation of the catalyst, nature surface impurities, can be studied by using this characterization technique. XPS measures the intensity of photoelectrons as a function of their kinetic energy.

X-ray Photoelectron spectra were acquired on a VG Microtech Multilab ESCA 3000 spectrometer using a non-monochromatized MgKα X-ray source (hv= 1253.6 eV). Base pressure in the analysis chamber was 4×10^{-10} Torr. The errors in all the B.E. values

were within ± 0.1 eV. The binding energy correction was performed using the C_{1S} peak of carbon at 284.6 eV as the reference.

2.4.7. Fourier-transform infrared spectroscopy (FTIR)

In FTIR spectroscopy, the incident electromagnetic wave is absorbed by a molecule upon excitation of molecular vibration modes. Application of FTIR spectroscopy in catalysis is to identity adsorbed species and the way in which these species are chemisorbed on the surface of the catalyst [9]**.** The frequency of these vibrations depends upon the nature and binding of the molecules.

FTIR spectroscopy in the frame work region (400-4000 cm^{-1}) provides additional information to identify the adsorbed species and adsorbed reaction intermediates and their structures on catalyst surfaces [10].

FTIR spectra was recorded on a Perkin-Elmer make instrument. The pellets for analysis were prepared by mixing 3 mg of the catalyst with 50 mg of KBr. FTIR spectra were recorded between 450 to 4000 cm^{-1} with accumulation of 20 scan and 4 cm^{-1} resolution

2.4.8. High resolution transmission electron microscopy (HRTEM)

Transmission electron microscopy technique involves a primary electron beam of high energy and high intensity passing through a condenser to produce parallel rays, which impinge on the sample. As the attenuation of the beam depends on the density and the thickness, the transmitted electrons form a two-dimensional projection of the sample mass, which is subsequently magnified by the electron optics to produce a so-called bright field image. The dark field image is obtained from the diffracted electron beams, which are slightly off angle from the transmitted beam [11-16].

This technique allows the size distribution, external morphology, chemical composition and shape of metal particles in supported and unsupported catalyst to be characterized down to the level of atomic resolution better than 0.5 nm [10].

Operating conditions of a TEM instrument are 100-200 keV electrons, 10^{-6} mbar vacuum, 0.5 nm resolution and a magnification of 3 x 10^5 to 10^6. TEM analysis was performed on a Jeol Moeld JEM 1200 electron microscope operated at an accelerating voltage of 120 kV. A small amount of the solid sample was sonicated in methanol for 1 min. A drop of

prepared suspension was deposited on a Cu grid coated with carbon layer and grid was dried at room temperature before analysis.

2.4.9. Raman spectroscopy

Raman spectroscopy is based on the inelastic scattering of photons, which loses energy by exciting vibrations in the sample [17]. Raman spectroscopy is generally used for characterizing the materials to find the crystallographic orientation of a sample, chemical structure of molecules. It allows studying surface metal oxide species on typical oxide support materials. It offers to study the molecular vibrations below 1100 cm^{-1} [17]. The radial breathing mode is commonly used technique to evaluate the diameter of sample and used to understand the structure of the composition.

The Raman spectra of sample were recorded on a Horiba JY LabRAM HR800 micro-Raman spectrometer with 17 mW 632.8 nm laser excitation.

2.5. Catalyst activity measurement

2.5.1. Batch reactor set up

All the batch hydrogenation experiments were carried out in a 300 mL capacity stirred autoclave supplied by Parr Instruments Co. USA, which was equipped with heating arrangement, overhead stirrer, thermo well, internal cooling coil, gas inlet and outlet, liquid sampling valve, safety rupture disc, pressure gauge as well as transducer for digital pressure display, separate automatic controller to control the temperature, agitation speed, solenoid valve and high temperature cutoff module. Water circulation through the internal cooling loop equipped with automatic cut-off arrangement controlled the temperature inside the reactor with an accuracy of ±1 °C. A schematic of the batch slurry reactor set-up is shown in Figure 2.8.

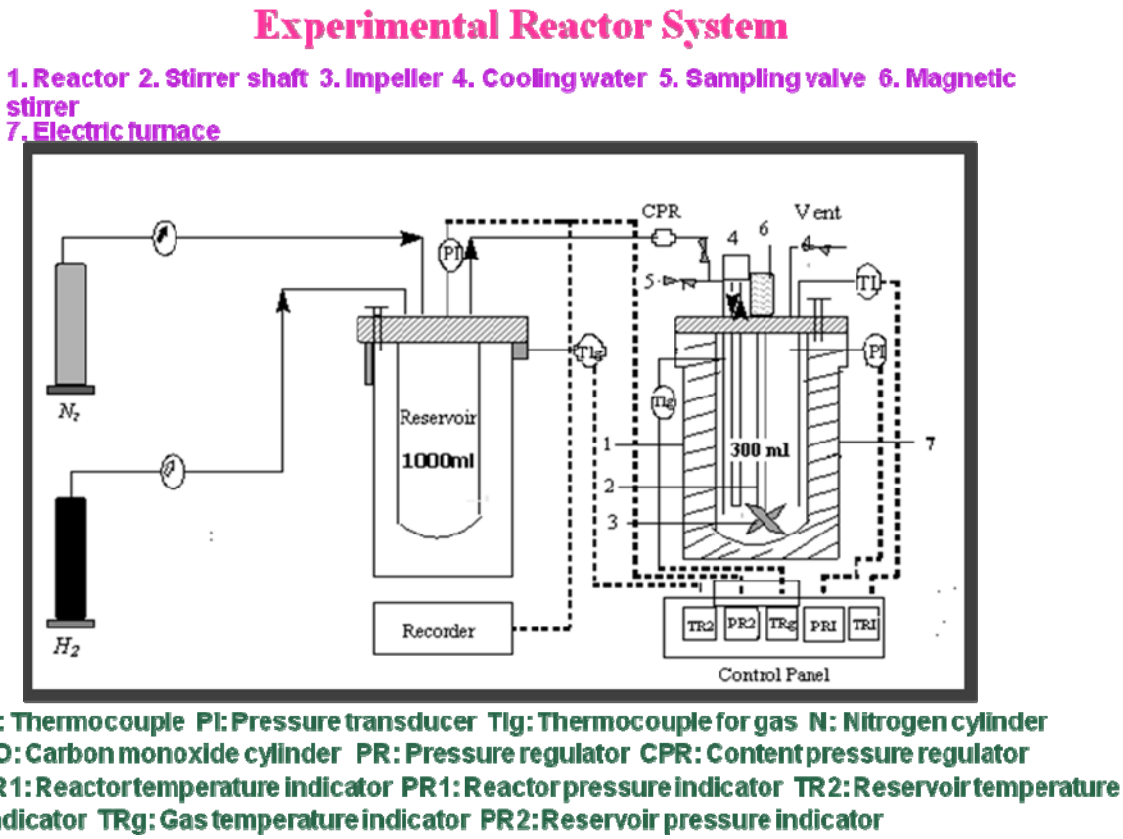

Figure 2.8. Parr reactor setup

In a typical hydrogenation experiment, required amount of substrate was charged into the reactor. Total volume of the liquid phase was always kept to 100 mL by adding appropriate solvent and the required amount of slurry of catalyst was charged in an autoclave carefully and reactor vessel was closed. The contents were first flushed 2-3 times with N_2 gas for the removal of trapped air and then flushed with H_2. Then the temperature was ramped to the required temperature. After attaining the desired temperature, the system was pressurized with H_2 gas to the desired pressure. Initial liquid sample was withdrawn before starting the reaction, by switching the stirrer on and the progress of the reaction was monitored by observing the pressure drop in the reservoir as a function of time. When the reaction was over, as indicated by a constant H_2 pressure on the pressure display, the reactor was cooled to room temperature and excess H_2 gas was vented out safely and the reactor contents were discharged. Samples were withdrawn at regular time intervals for the analysis using gas and liquid chromatography.

2.5.2. Continuous high pressure reactor setup

Bench scale continuous hydrogenation experiments were carried out in a high-pressure, fixed-bed reactor supplied by M/s. Geomechanique, France. A schematic of the reactor setup is shown in Figure 2.9. It consisted of stainless steel tube of 0.35 m length and 1.5 x 10^{-2} m inner diameter that was heated by two tubular furnaces whose zones (TIC1 and TIC2) were independently controlled at the desired bed temperature. The reactor was provided with two thermocouples [Chromel-Alume thermocouples (type K)] to measure the temperature at two different points. The reactor was equipped with mass flow controllers, pressure indicator, and controller (PIC) devices. A storage tank was connected to the metering pump through a volumetric burette to measure the liquid flow rate. The pump had a maximum capacity of 3 x 10^{-4} m^3/h under a pressure of 10 MPa. The gas outlet line was equipped with a backpressure controller, which maintained a constant pressure in the unit by continuous pressure release. The other end of the reactor was connected to a gas-liquid separator through a condenser. The experiments were carried out over 10 and 20 g of catalyst in the form of pellets having 4 mm diameter. The section 5 cm and 5 cm below the catalyst bed was packed with inert packing (carborundum), thus providing the catalyst bed depth of ~25 cm. The reactor was flushed thoroughly with H_2 at room temperature before the start of the actual experiment. After attaining the desired temperature, the reactor was pressurized with H_2. The liquid feed was "switched on" after the reactor has reached the operating pressure and kept there for 1 h to obtain the constant liquid flow rate. Liquid samples were withdrawn at regular intervals of time and were analyzed by gas chromatography.

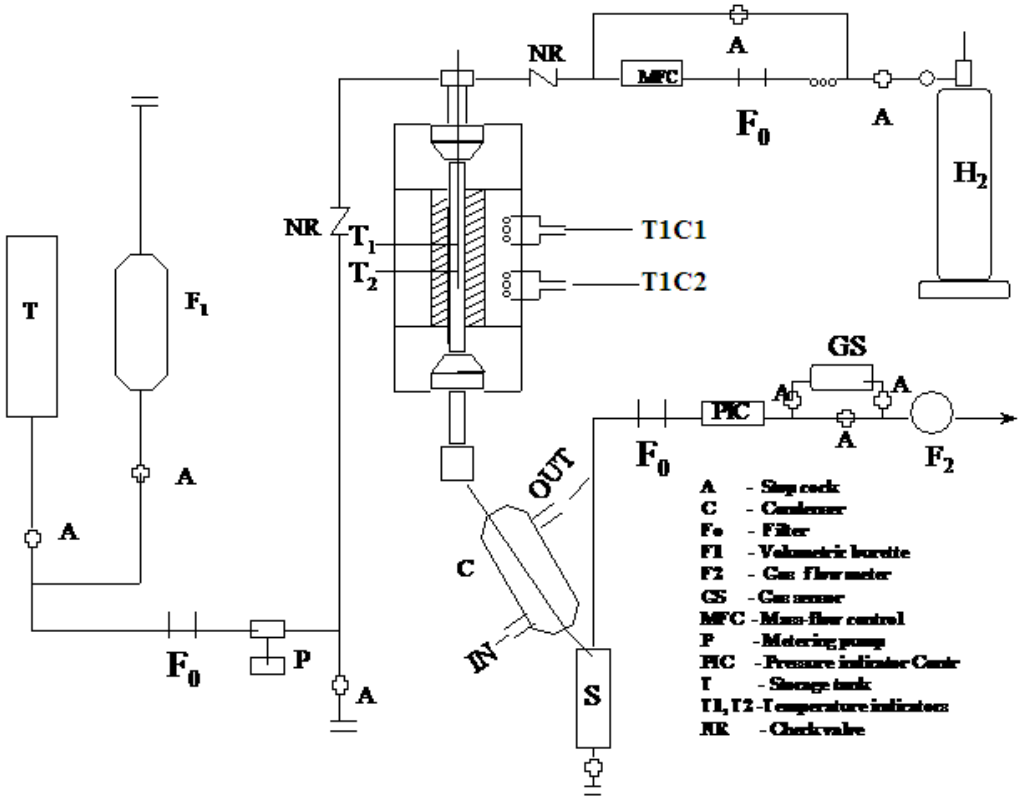

Figure 2.9. Continuous reactor setup

(1) Reactor (2) stirrer shaft (3) impeller (4) cooling water (5) sampling valve (6) magnetic stirrer (7) electric furnace

TI: Thermocouple **PI**: Pressure transducer **TIg**: Thermocouple for gas **N**: Nitrogen cylinder **H_2**: Hydrogen gas cylinder **PR**: Pressure regulator **CPR**: Content pressure regulator **TR1**: Reactor temperature indicator **PR1**: Reactor pressure indicator **TR2**: Reservoir temperature Indicator **TRg**: Gas temperature indicator **PR2**: Reservoir pressure indicator

2.6. Analytical methods

Chromatography

Chromatography is a separation process that is achieved by distributing the components of a mixture between two mutually immiscible phases, one phase is stationary and other is mobile. A sample component introduced in a mobile phase carried along with a column containing a distributed stationary phase. The species of sample undergo repeated interactions between the mobile phase and stationary phase. Those components held preferentially in the stationary phase are retained longer in the system than those that are distributed selectively in the mobile phase. Separation can be achieved by selection of both phases, and the sample component gradually separated in bands in the mobile phase. As a consequence, solutes are eluted from the system as local concentrations in the mobile phase in the order of their increasing distribution coefficients with respect to the stationary phase: the least retarded component emerges first; the most strongly retained component elute last [18, 19]**.**

Applications:

Depending on mobile phase the chromatographic techniques are divided in to two parts

- Gas chromatography
- Liquid chromatography

2.6.1. Gas chromatography

In gas chromatography, inert gas used as a mobile phase e.g. He, H_2, N_2 and analysis sample must be thermally stable and volatile that of organic/inorganic compounds. Colum is heart of chromatography where actual separation is take place. The detail of stationary phases used for the quantitative and qualitative analysis is shown in Table. 2.1

Table 2.1. Selected stationary phase used for gas-liquid chromatography analysis.

Column trade name & Column details	Stationary phase	Operating range /limit	Compounds analyzed in this work
HP-FFAP, **(Free Fatty acid phase column) 30 m x 0.53 mm x 1.0 µm***	5% methylpolysiloxane + polyethylene glycol (Nitroterephthalic acid modified polyethylene glycol) High polarity	60 - 250^{o}C	Glycerol, levulinic acid, 5-methyl furfural, 5-HMF
HP-5 **30 m x 0.32 mm x 1 µm***	(5%-Phenyl)-methylpolysiloxane, Non-polar	60 - 325^{o}C	Levulinic acid, Methyl levulinate, Furfural, Furfuryl alcohol, γ-valerolactone

* Column length x column ID x film thickness

Gas chromatography Hewlett- Packard model and Thermo-Trace-700 having an HP-5 column with a FID detector were employed for the analysis of the samples. Major advantages of FID include a detection limit that is approximately two to three orders of magnitude smaller than that for a thermal conductivity and helium gas used as a carrier. On basis of plot of response Vs time, the qualitative and quantitative analyses were performed.

2.6.2. High performance liquid chromatography

HPLC (Iris32, Chemito instruments pvt. Ltd) system consisting of aminex column and a refractive index detector. H_2SO_4 (0.5 M) was used as the mobile phase at a flow rate of 1 mL min^{-1}. Both column the detector temperatures were 40 ^{o}C. Samples of 10 µL were injected into the column using an auto sampler.

2.6.3. Gas Analysis

The gaseous products were analyzed by a gas chromatography (GC) analyzer equipped with a PORAPAK-Q column and a thermal conductivity detector (TCD) detector. The carrier gas is argon.

2.6.4. Calculation for response factor, % conversion and % selectivity

$$Rf = \frac{\text{Concentration in moles}}{\text{area under the respective peak}} \quad \text{.....2.11}$$

$$\%, \text{Conversion} = \frac{\text{Intial moles of substrate} - \text{Final moles of substrate}}{\text{Initial moles of substrate}} \times 100 \quad \text{.....2.12}$$

$$\%, \text{Selectivity} = \frac{\text{moles of product formed}}{\text{moles of substrate consumed}} \times 100 \quad \text{.....2.13}$$

2.7. References

1. S. Brunauer, P. H. Emmett, E. Teller J. Am. Chem. Soc. 60 (1938) 309.
2. I. Chorkendorff, J. W. Niemantsverdriet in Concepts of modern catalysis and kinetics, Wiley-VCH, Weinheim, (2003) pp 131.
3. A. L. Petterson Phy. Rev. 56 (1939) 978.
4. P. K. Ghosh in Introduction to photoelectron spectroscopy, Wiley, New York, (1983).
5. J. F. Watts in Introduction to surface analysis by XPS and AES, Wiley, New York, (2003).
6. D. Briggs, M. P. Seah (Eds.) in Practical surface analysis; Auger and X-ray photo electron spectroscopy, Vol. 1, 2nd edition, Wiley, New York (1990).
7. S. Hüfner in Photoelectron spectroscopy, Springer-Verlag, Berlin, (1995).
8. W. M. Deglass, G. L. Haller, R. Kellerman, J. H. Lunsford in Spectroscopy in heterogeneous catalysis, Acadamic press, New York, (1979)
9. I. Chorkendorff, J. M. Niemantsverdriet in Concepts of modern catalysis and kinetics, Wiely-VCH, Weinheim (2003) 155.
10. J. Hagen in Industrial catalysis, 2nd edition, Wiley-VCH, Germany, (2006) pp 215.
11. G. Lawes in Scanning Electron microscopy and X-ray microanalysis, John Wiley and Sons Ltd., Chichester (1987).
12. J. R. Fryer in Chemical applications of transmission electron microscopy, Acadamic press, San Diego, (1979).
13. J. M. Thomas, O. Terasaki, P. L. Gai, W, Zhou, J. Gonzalez-Callbet Acc. Chem. Res. 34 (2001) 583.
14. A. Alfredsson, M. Keung, A. Monnier, G. D. Stucky, K. K. Unger, F. Schuth *J.* Chem. Soc. Chem. Comm. (1994) 921.
15. J. I. Goldstein, H. Yakowitz (Eds.) in Practical scanning electron microscopy, Plenum press, New York, (1975).
16. G. Lawes in Scanning electron microscopy and X-ray microanalysis, John Wiley and Sons Ltd., Chichester, (1987).
17. J. M. Niemantsverdriet in Spectroscopy in catalysis, 3rd edition, Wiley-VCH, Weinheim, (2007) pp 238.

18. P. W. Raymond in Principles and practice of chromatography, Book I, Chrom-Ed Book Series, (2003) pp.2.
19. H. H. Willard, L. L. Merritt, J. A. Dean, F. A. Settle in Instrumental methods of analysis, 7th edition, CBS Publishers, New Delhi (2007) pp 247.

Chapter 3

Supported noble metal catalysts for hydrogenation of methyl levulinate

Several supported noble metal catalysts were screened for the hydrogenation of methyl levulinate (MeLA) to γ-valerolactone (GVL). Among these catalysts, 5% Ru/C showed the highest conversion of 95% of MeLA with 91% selectivity to GVL. A detailed characterization was carried out using TPR, XRD, XPS and BET techniques. XPS studies revealed that higher extent of Ru^0 species in case of carbon supported Ru was responsible for its higher hydrogenation activity as compared to Ru on other supports. Effect of process parameters such as temperature, H_2 pressure, catalyst and substrate concentration and metal loading on MeLA conversion and selectivity to GVL also has been studied. 5% Ru/C catalyst was found to be stable up to five reuses.

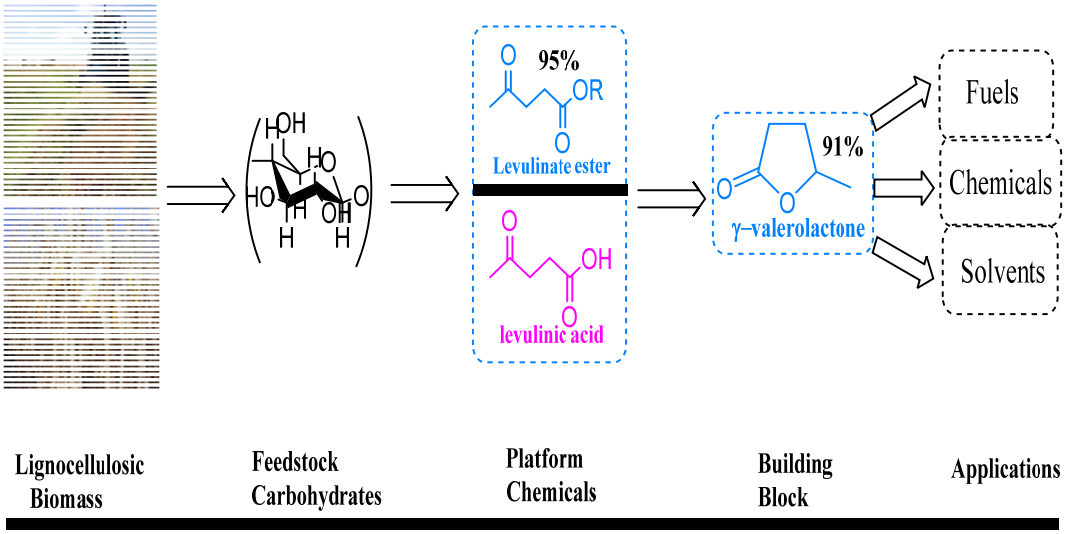

***Catal. Lett.* 142 (2012)779-787**

3.1. Introduction

As highlighted in chapter 1, cellulosic biomass constitutes a huge and renewable resource that can be converted into a wide variety chemical and fuel products [1-2]. In this context, γ-valerolactone (GVL) has drawn increasing attention because of its benign properties and versatility with which it can be converted to downstream applications for the next generation fuel and fuel additives [3-5]. Horvath *et al.* has already demonstrated that GVL after hydrogenation gives pentanoic acid that is a starting compound for several other fuel/fuel additives [6-9]. The low yields of levulinic acid due to polymeric humin formation during thermal decomposition of lignocellulosic biomass in aqueous acid medium alone can be significantly improved in presence of alcohols directly giving the corresponding levulinic esters [10-13]. The subsequent catalytic hydrogenation of levulinic esters to GVL (Scheme 3.1.) thus offers greater commercial potential due to (i) suppression of active metal leaching of hydrogenation catalyst caused by free carboxyl of levulinic acid and (ii) recyclability of alcohol formed during hydrogenation.

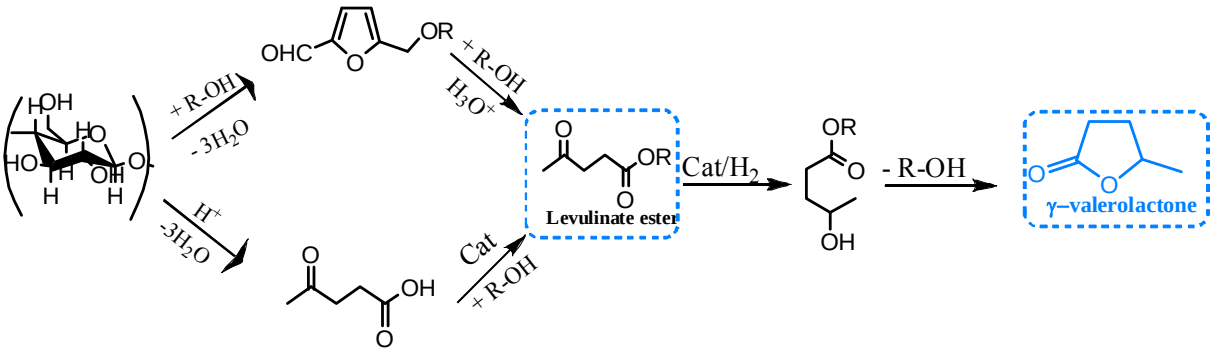

Scheme 3.1. Hydrogenation of methyl levulinate to GVL

The limited literature published so far, on conversion of LA esters or LA to GVL includes mainly the homogeneous catalyst systems having major drawbacks of catalyst separation and subsequent reuse, as well as poor selectivity to GVL. While in case of heterogeneous catalyst systems, leaching of active metal was observed with LA as a substrate [14-18].

Since in the literature Ru catalyst is reported for LA hydrogenation, we decided to carry out a systematic study on catalyst screening using other noble metals such as Pt and Pd and the results were compared with Ru catalyst. Our study also includes the influence of various supports such as carbon, silica and alumina on the activity for MeLA hydrogenation. Among several catalysts studied in this work, 5% Ru/C was found to be the best for selective catalytic hydrogenation of methyl levulinate giving 95% conversion and 91% selectivity to GVL. Further, the effect of various reaction parameters such as temperature, H_2 pressure, catalyst and substrate concentrations on methyl levulinate conversion and GVL selectivity was also studied over 5% Ru/C catalyst.

3.2. Experimental

Ru, Pd and Pt supported on C, SiO_2 and Al_2O_3 catalysts were prepared by wet impregnation method and the detailed experimental procedure of their preparation has been described in chapter 2 (section 2.2.1). The catalysts were characterized by various techniques according to the procedures described in section 2.4. Activity of the prepared catalysts was evaluated for the hydrogenation of levulinic acid to GVL and a typical experimental procedure is described in section 2.5.1.

3.3. Results and Discussion

Among the various catalysts screened (discussed in section 3.4.1), 5% Ru/C showed the highest activity and selectivity. Hence, detailed characterization of 5% Ru on various supports was carried out and the results are discussed below.

3.3.1. Catalyst Characterization

3.3.1.1. BET surface area

The specific BET surface areas of carbon, silica and alumina supported Ru catalysts are shown in Table 3.1. The highest surface area of 139 m^2/g was observed for 5% Ru/C while several order of magnitude lower surface area namely, 64 and 1.7 m^2/g were obtained for Ru on silica and alumina respectively. Least surface area for alumina supported catalyst is due to the higher extent of aggregation while, ruthenium encapsulation by silica is reported for Ru on silica [20].

Table 3.1. BET surface area for various supported Ru catalysts

Sr.No	Catalysts	Surface area (m^2/g)
1	5% Ru/C	139
2	5% Ru/SiO_2	64
3	5% Ru/Al_2O_3	1.7

3.3.1.2. X-ray diffraction

XRD patterns of the 5% Ru supported on carbon, silica and alumina are shown in Figure 3.1. For both Ru on carbon and silica samples, broad peaks were observed indicating highly amorphous nature of the material. In case of Ru/C catalyst, diffraction peak at 2θ = 43.3° was attributed to graphitic carbon phase (002) while the peak at 2θ = 25.7° for Ru/SiO_2 could be attributed to silica phase.

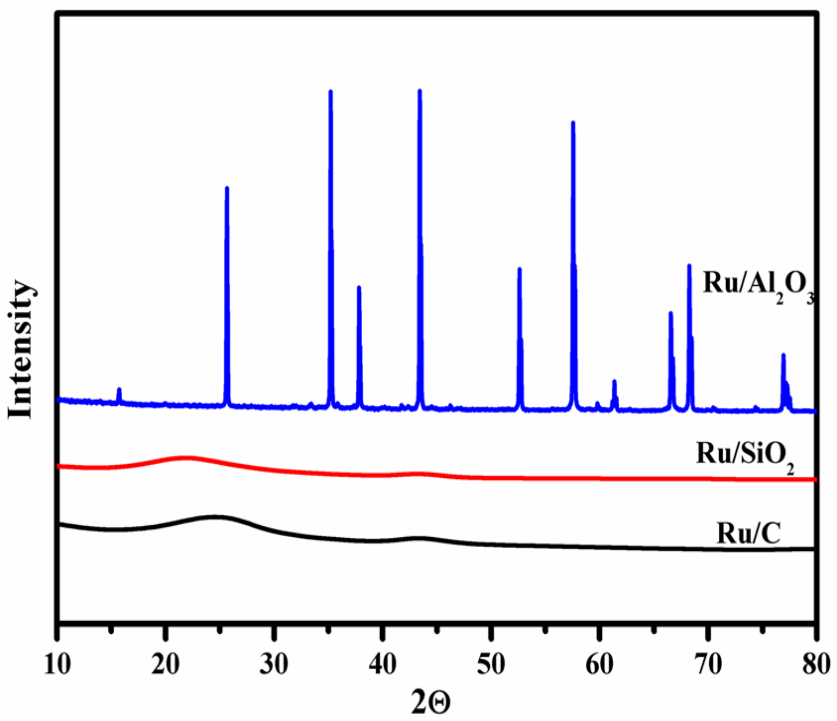

Figure 3.1. XRD pattern for 5% Ru/C, 5% Ru/Al_2O_3 and 5%Ru/SiO_2

While in case of alumina supported Ru catalyst, sharp diffraction peaks at 2θ = 25.3°, 37.1°, 43.48° and 57.21° with higher intensities attributed to γ-alumina phases were observed due to highly crystalline nature of the sample. In all the samples no characteristic peaks of Ru were observed indicating either very high dispersion of Ru and/or Ru being diffused in the bulk matrix of the support [19].

3.3.1.3. H_2 –TPR

Figure 3.2 shows temperature programmed reduction (TPR) profiles in the range of 50-250^{0}C for Ru supported on C, SiO_2 and Al_2O_3.

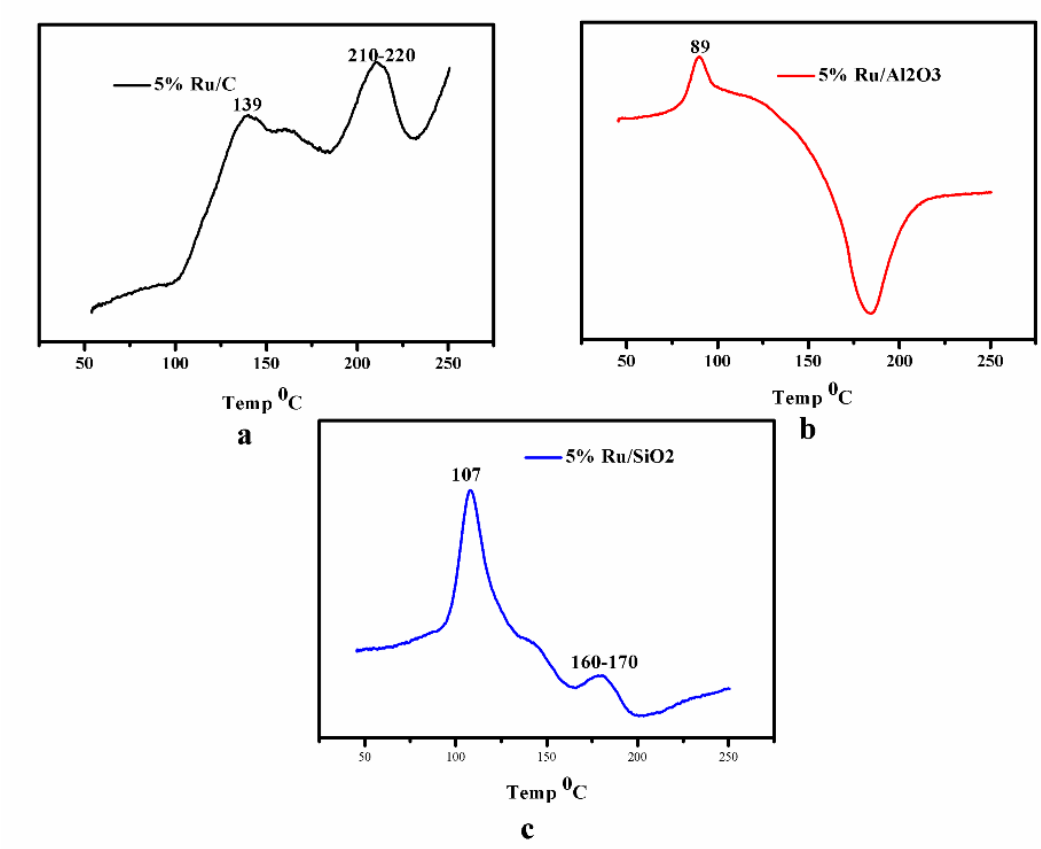

Figure 3.2. H_2 TPR profiles for (a) 5% Ru/C (b) 5% Ru/Al_2O_3 (c) 5%Ru/SiO_2

As shown in Figure 3.2, TPR profiles of Ru/C catalysts showed a major reduction peak extending from 200-220 °C which correspond to the reduction of Ru (III) to metallic Ru [21]. Silica supported Ru catalyst showed a peak at 107^{0}C indicating only partial

reduction of Ru (III) to Ru (II) while another small peak at 160-170^{0}C could be due to second step reduction of Ru (II) to Ru (I) however, the possibility of Ru (II) to Ru^0 can not be ruled out. The lower temperature of reduction to Ru^0 was due to the fact that ruthenium sites were encapsulated by silica, which partially dissolved during the ion-exchange under alkaline conditions and then precipitated on top of the exchanged surface during filtering/washing forming some other superficial ruthenium species [20-23]. 5% Ru/Al_2O_3 TPR profile showed a single peak at 90-100^{0}C which corresponds to the reduction of metallic precursor or ruthenate $(RuOH)_3$ [24]. Among all these samples, only 5%Ru/C showed maximum reduction which was also in accordance with its high activity towards hydrogenation of methyl MeLA.

3.3.1.4. XPS

Figure 3.3 (A) presents the XPS of Ru $3d_{5/2}$-$3d_{3/2}$ in Ru/C sample. After deconvolution, the most intense doublet at 279.9 and 283 eV ($\delta = 4.1$ eV) was due to metallic Ru [22]. The second set of doublet at 284.3 and 286.9 eV ($\delta = 4.1$ eV) could be assigned to Ru (VI) state as RuO_3. Figure 3.3 (B) shows XPS of O1s for Ru/C sample. After deconvolution an intense peak at 529.7 eV corresponds to (O^{2-}) indicating formation RuO_3 [24-25]. The percentage of the Ru species calculated after deconvolution suggests that 40 % of the Ru was present in the metallic state Ru^0 while remaining 60% of Ru is present in the oxide form of ruthenium. It should be noted that the catalysts were prepared using sodium borohydride as a reducing agent having mole ratio of Ru:B is (5:1). XPS study revealed that no boron species was found hence possibility of Ru:B alloy formation was completely eliminated. Figure 3.4 (A) shows XPS of Ru $3d_{5/2}$-$3d_{3/2}$ states in 5% Ru supported on mesoporous silica. A less intense doublet at 279.9 and 284 eV ($\delta = 4.1$ eV) suggests Ru^0 state. Another doublet at 283.3 and 287.4 eV ($\delta = 4.1$eV) suggests Ru (VI) state in accordance with O1s peak at 532.8eV as shown in Figure 3.4 (B)[20]. Figure 3.5 (A) shows XPS of Ru $3d_{5/2}$ -$3d_{3/2}$ for alumina supported ruthenium catalyst. An intense doublet at 280.3 and 285.4 eV ($\delta = 5.1$ eV) corresponds to Ru (II) state in RuO_2. The second set of doublet at 283.3 and 287.4 eV ($\delta = 4.1$ eV) could be assigned to the Ru (VI) state in RuO_3. Figure 3.5 (B) shows XPS of O1s of Ru on

alumina catalyst. Two intense peaks at 530.9 and 532.2 eV could be assigned to oxide and hydroxide (OH^-) species of Ru, respectively [25].

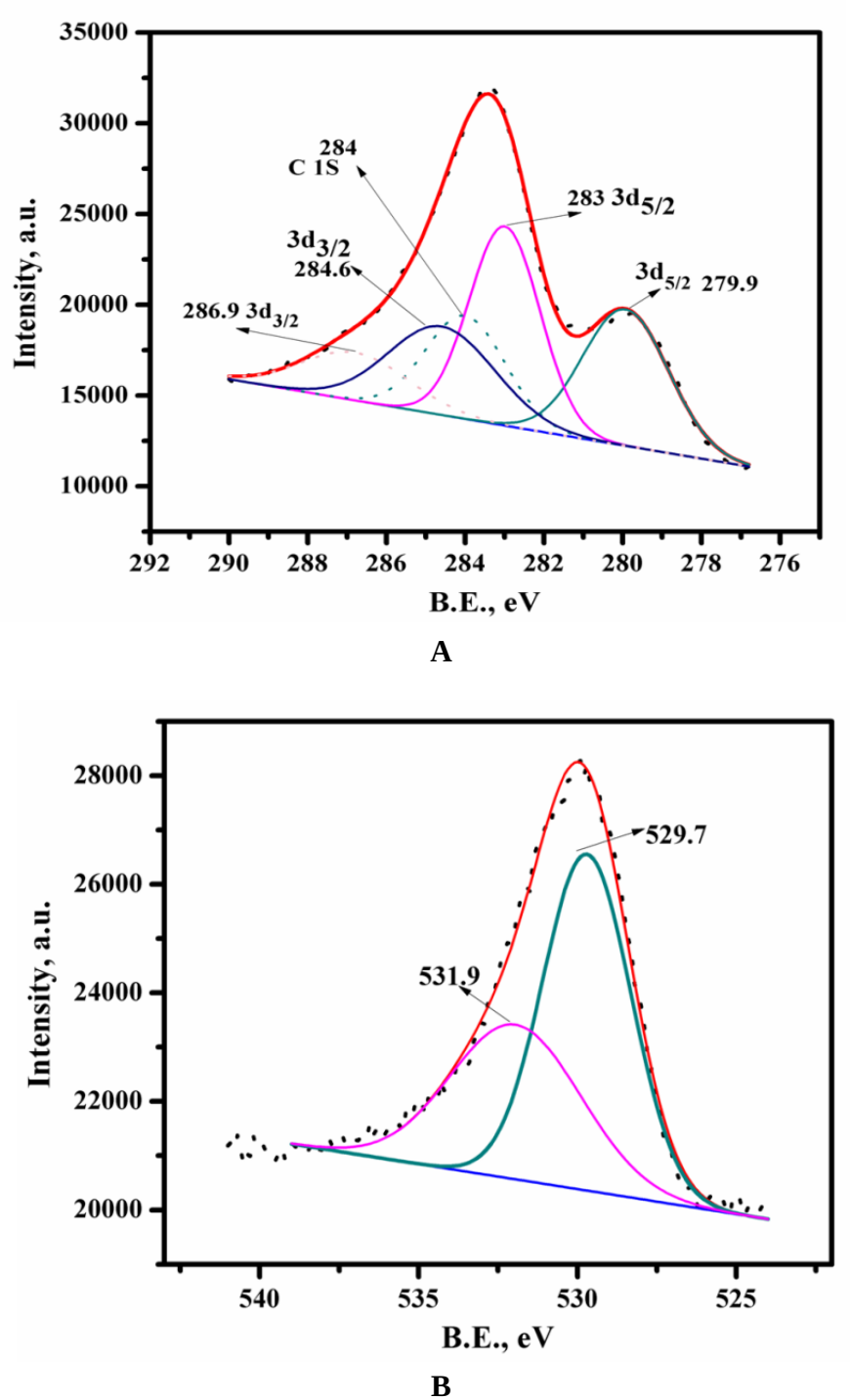

Figure 3.3. XPS spectra for carbon supported Ru catalysts. (A) Ru and carbon (B) O1s

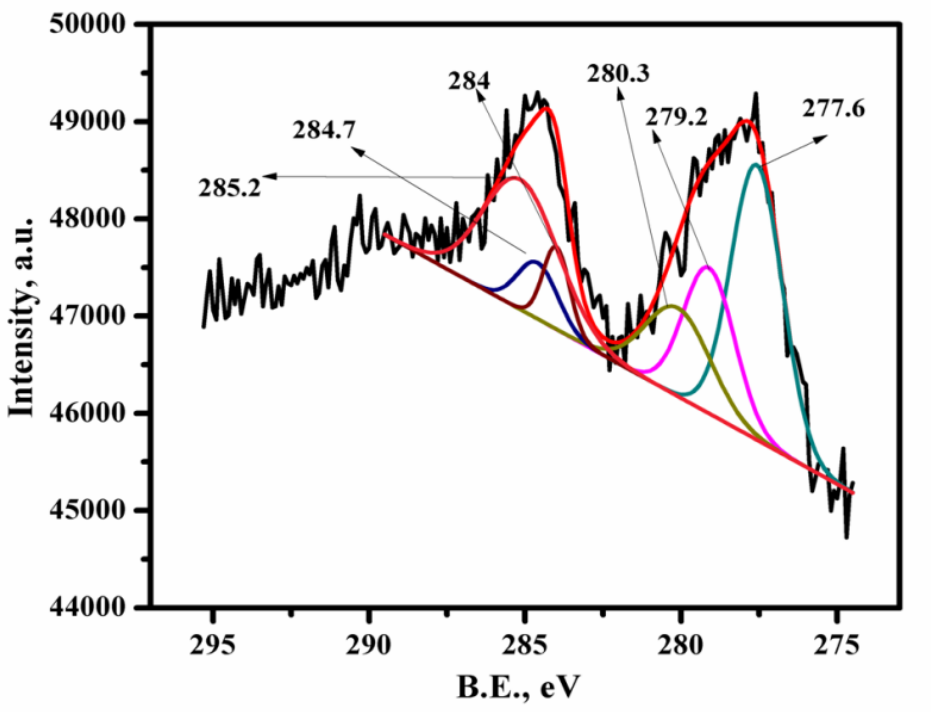

A

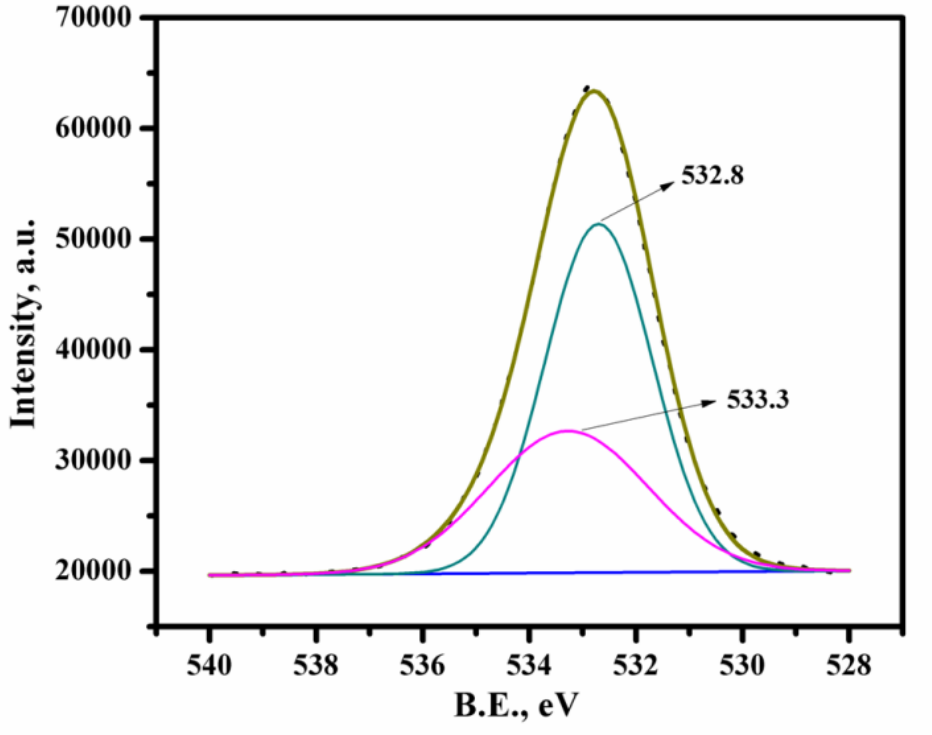

B

Figure 3.4. XPS spectra for silica supported Ru catalysts. (A) Ru and silica (B) O1s

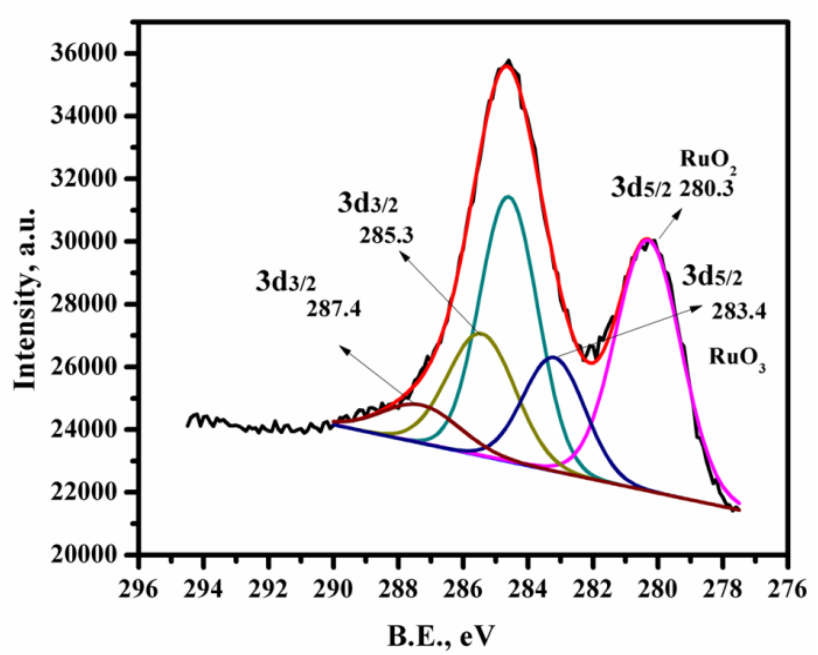

A

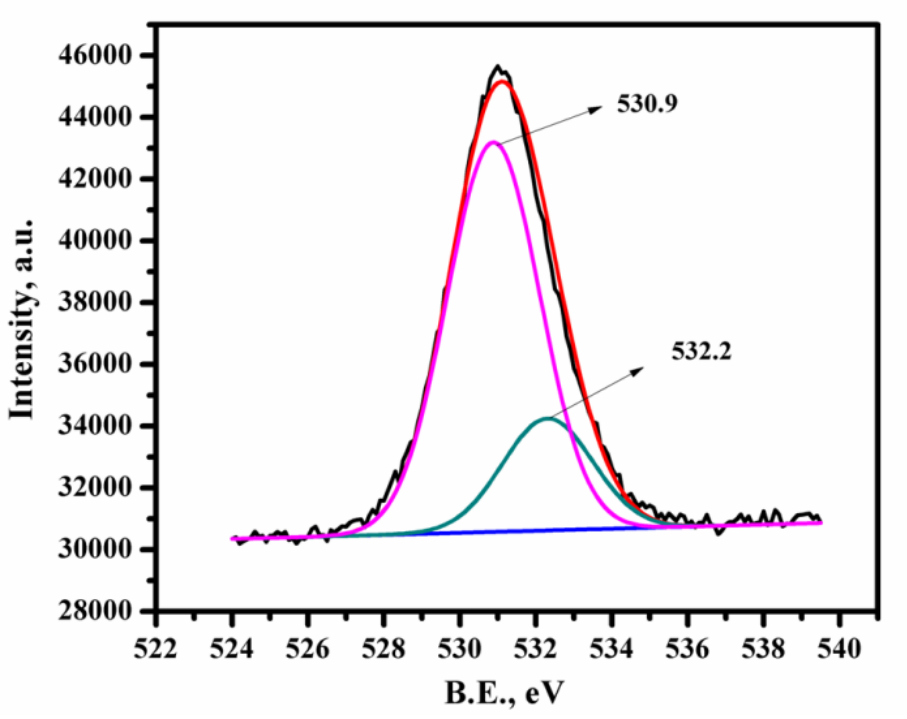

B

Figure 3.5. XPS spectra for alumina supported Ru catalysts. (A) Ru and alumina (B) O1s

3.3.2 Activity testing

3.3.2.1. Catalyst screening

Series of supported noble metal catalysts were screened for the hydrogenation of methyl levulinate and their activity results are shown in Table 3.2.

Table 3.2. Catalyst screening for methyl levulinate hydrogenation

Sr. No.	Catalysts	Conversion (%)	Selectivity (%)		
			Gamma-valerolactone	Methyl 4-hydroxypentanoate	Others
1	5% Ru/C	95	91	09	<0.01
2	5% Pt/C	18	47	20	33
3	5% Pd/C	14	65	15	20
4	5% Ru/SiO_2	15	89	11	<0.01
5	5% Ru/Al_2O_3	7	47	28	25

Reaction conditions : Methyl levulinate, 5% (w/w); Solvent, MeOH (95ml); H_2 pressure, 500 psi; temperature, 130 ^oC; reaction time, 2 h.

Although Pd and Pt showed some activity for hydrogenation of methyl levulinate, substantial amount of byproducts were also formed due to further hydrogenation of GVL. As ruthenium is known for hydrogenation of aliphatic carbonyl group, we evaluated ruthenium on various supports for the hydrogenation of methyl levulinate [23]. Among the three supports, carbon supported ruthenium catalyst showed the highest conversion of 95 % which was about 5–13 times higher than the ruthenium on silica and alumina, respectively. The activity of these catalysts was in the following order: Ru/C>Ru/SiO_2>Ru/Al_2O_3. Selectivity to GVL was also found to be highest (91 %) for 5 % Ru/C catalyst. Although the order of catalytic activity is same as the order of surface areas of these catalysts, the order of magnitude difference in activities cannot be explained only on the basis of surface area difference. For example, the difference of surface areas of 5 % Ru/C and 5 % Ru/SiO_2 was about two fold but the activity difference between these catalysts was about six folds. As seen from the TPR characterization, 5 % Ru/C showed the presence of Ru^0 which is responsible for catalyzing the hydrogenation reaction. This

is also in accordance with XPS studies which revealed the presence of Ru^0 species in 5 % Ru/C catalyst. On the contrary, 5 % Ru/SiO_2 showed very less Ru^0 species in both TPR and XPS analysis (Figures 3.2 c, 3.4). In case of 5 % Ru/SiO_2, the major species present were Ru (IV) and Ru (VI). The incomplete reduction of 5 % Ru/SiO_2 was due to the encapsulation of Ru by silica leading to its lower hydrogenation activity [20–23]. 5 % Ru/Al_2O_3 catalyst did not show presence of any Ru^0 species. This catalyst mainly contained ruthenium in the form of its oxide and hydroxide as revealed by its TPR and XPS characterizations (Figures 3.2 b, 3.5). Ruthenium hydroxide formation on alumina support could be due to Al–O–Al bridged species [20]. Since, we used $NaBH_4$ reduction method, complete reduction of ruthenium precursors did not take place particularly, in case of silica and alumina supports where more stable other ruthenium species were formed [26].

Since, 5 % Ru/C showed the highest activity and selectivity, further studies on effect of reaction conditions on methyl levulinate hydrogenation was carried out using this catalyst and the results are discussed below.

3.3.3. Effect of parameters

3.3.3.1. Effect of hydrogen pressure

Figure 3.6 shows the results of effect of hydrogen pressure on methyl levulinate hydrogenation at 130 ^oC. The conversion of methyl levulinate increased by a factor of two (45 to 95%) with increase in hydrogen pressure from 100 to 500 psi. the selectivity to GVL also increased from 78 to 91% with increase in hydrogen pressure. Increase in activity with increase in hydrogen pressure is obviously due to higher dissolved concentration of hydrogen according to Henry's law [18].

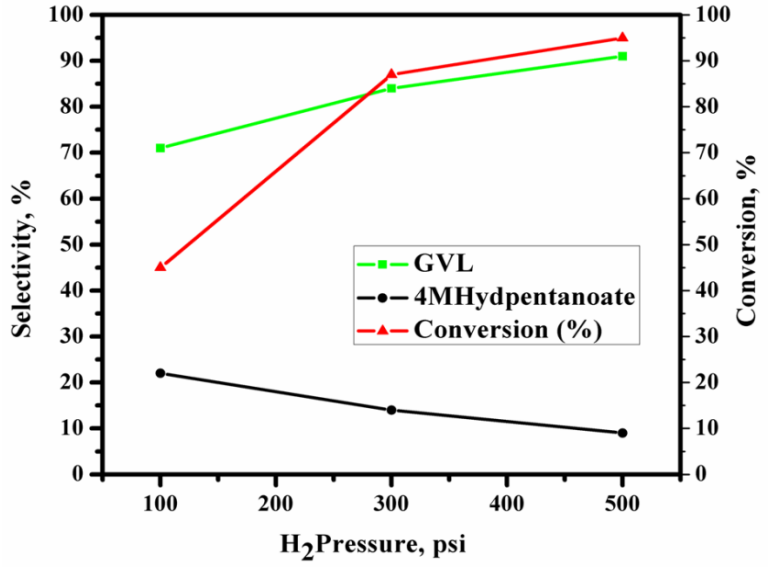

Figure 3.6. Effect of hydrogen pressure on hydrogenation of MeLA

Reaction conditions: Methyl levulinate, 5% (w/w); solvent, MeOH (95 ml); H_2-Pressure, 100-500 psi; temperature, 130 ^oC; catalyst, 0.5 g (5% Ru/C); reaction time, 2h.

3.3.3.2. Effect of reaction temperature

Figure 3.7 shows influence of reaction temperature on conversion and selectivity pattern in methyl levulinate hydrogenation over 5% Ru/C catalyst.

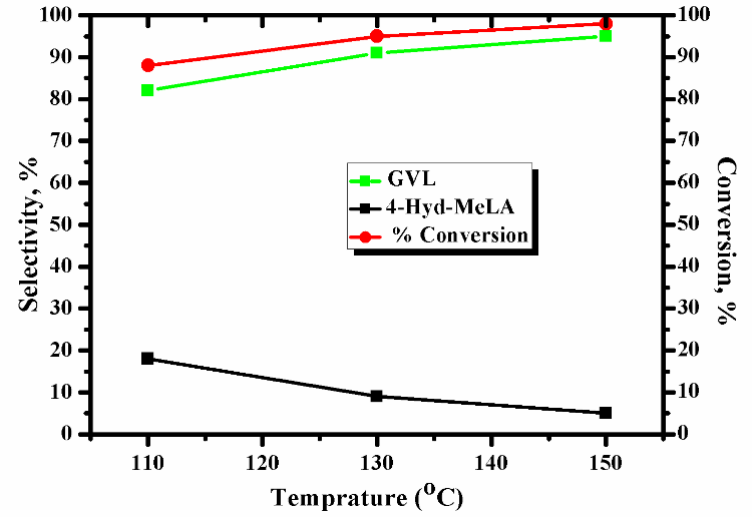

Figure 3.7. Effect of temperature on hydrogenation of MeLA

Reaction conditions: Methyl levulinate, 5% (w/w); solvent, MeOH (95 ml); H_2 pressure, 500 psi; temperature, 110-130 ^oC ;catalyst, 0.5 g (5% Ru/C); reaction time, 2 h.

Methyl LA conversion increased from 88 to 98% with increase in temperature from 110 to 150 ^{o}C. GVL selectivity progressively increased from 79 to 83% with increase in temperature from 110-150 ^{o}C as the hydrogenation of the intermediate, 4-hydroxyl methyl levulinate also picked up with increase in temperature.

3.3.3.3. Effect of substrate concentration

The effect of methyl LA concentrations on hydrogenation reactions was studied in the range of 5-20 wt % methyl LA and the results are shown in Figure 3.8.

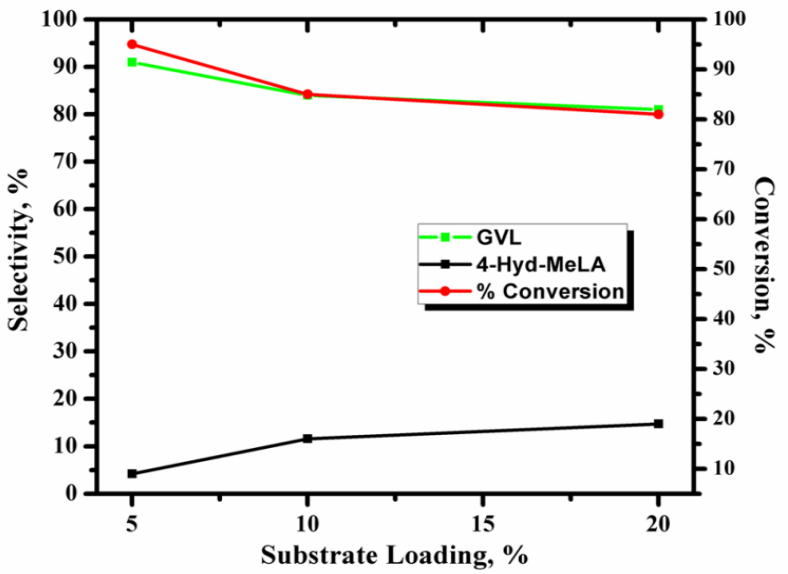

Figure 3.8. Effect of substrate concentration on hydrogenation of MeLA

Reaction conditions: Solvent, MeOH (74-95 ml); H_2 pressure, 500 psi; temperature, 130 ^{o} C; catalyst, 0.5 g (5% Ru/C); reaction time, 2 h.

The conversion of methyl LA decreased marginally from 95 to 81% as the concentration of methyl LA increased from 5-20 wt %. The decrease in methyl LA conversion was due to the limiting number of catalytic sites at high methyl LA concentration because the catalyst amount was constant. The decrease in conversion at higher concentration (20%) of methyl levulinate was also associated with increase in selectivity to 4-hydroxyl methyl pentanoate upto 19% at the cost of GVL selectivity.

3.3.3.4. Effect of catalyst concentration

Figure 3.9 shows the effect of catalyst concentration on the conversion of methyl levulinate and selectivity was also studied in the range of 0.250 to 0.750 g at 130 ^{o}C.

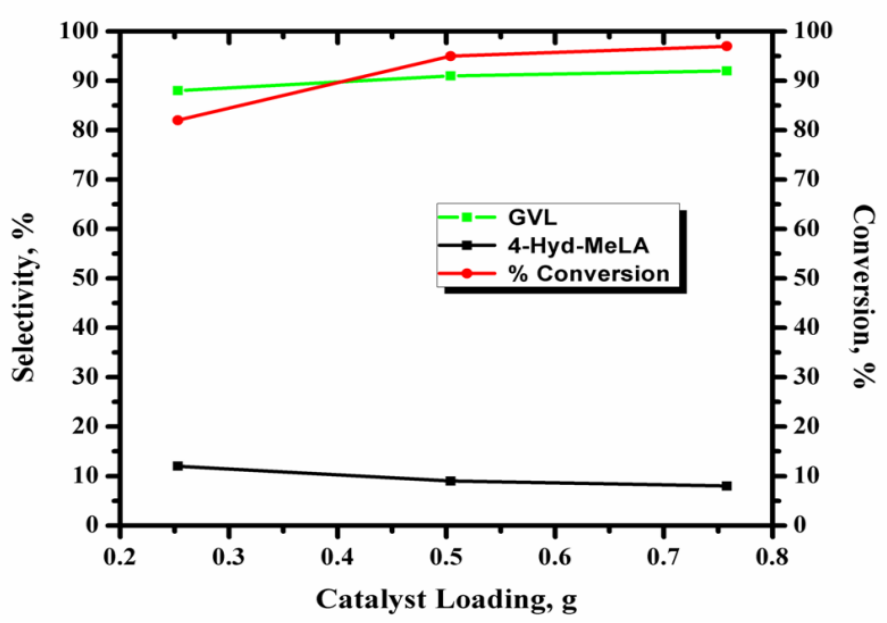

Figure 3.9. Effect of catalyst concentration on hydrogenation of MeLA

Reaction conditions: Methyl levulinate, 5% (w/w); solvent, MeOH (95 ml); H_2 pressure, 500 psi; temperature, 130 ^{o}C; catalyst, 0.25-0.75 g (5% Ru/C); reaction time, 2 h.

It was found that the conversion of methyl levulinate increased from 82 to 97% with increase in the catalyst concentration from 0.250 to 0.750 g. The increase in methyl LA conversion was mainly because of higher availability of active catalytic sites with increasing the catalyst concentration. There was no variation in selectivity with increase in catalyst concentration indicating neither further hydrogenation of GVL took place nor the possibility of any reversible reaction.

3.3.3.5. Effect of metal loading

Effect of active metal loading on carbon in range of 1-5% on conversion and selectivity of methyl LA hydrogenation is shown in Figure 3.10. The conversion of methyl LA

increased linearly by 5 times from 18 to 95% with increase in active metal loading from 1 to 5% on the carbon support.

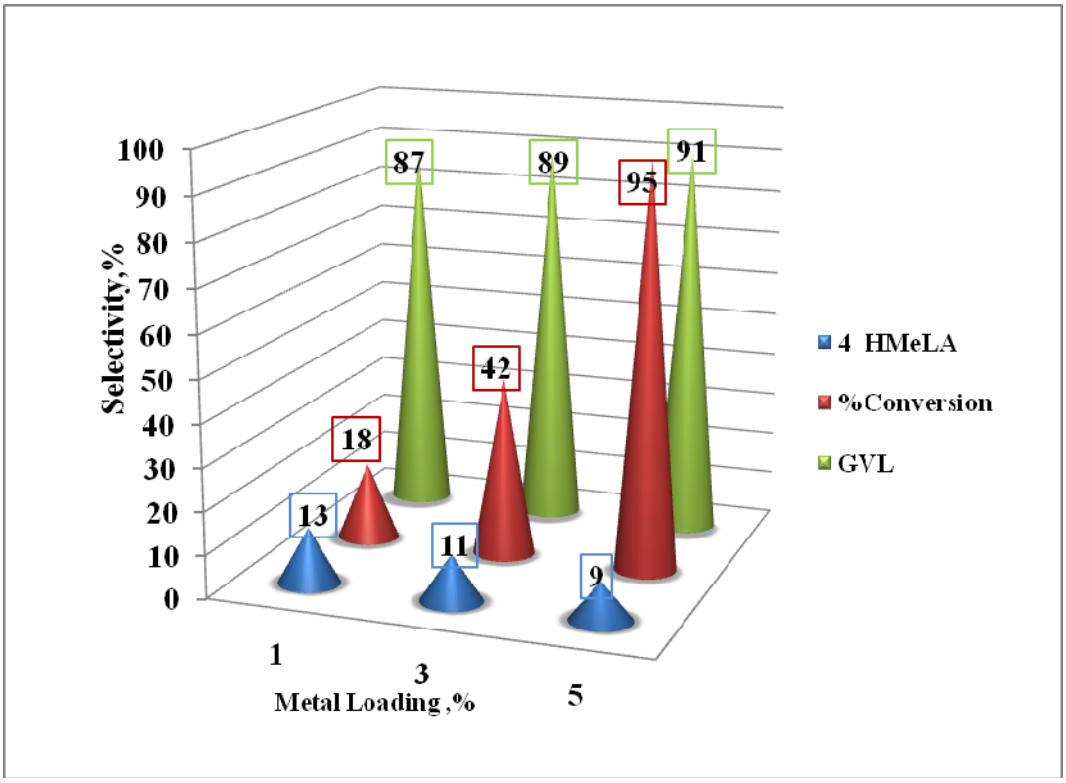

Figure 3.10. Effect of metal loading on hydrogenation of MeLA

Reaction conditions: Methyl levulinate, 5% (w/w); solvent, MeOH (95 ml); metal loading, 1-5% Ru/C; H_2 pressure, 500 psi; temperature, 130 ^oC; catalyst, 0.5 g; reaction time, 2 h.

However, selectivity of GVL was slightly affected (87%) for the lowest metal loading of 1% due to the less availability of active component for the hydrogenation of carbonyl group of methyl LA.

3.3.3.6. Effect of substrate screening

In order to verify the versatility of 5% Ru/C catalyst few other derivatives of levulinic acid esters were also tested for hydrogenation and the results are shown in Figure 3.11. Although conversion remained the same, selectivity to the corresponding substituted

GVL decreased from 91-60% with increase in chain length from methyl to butyl substituent as methyl is a better leaving group than butyl.

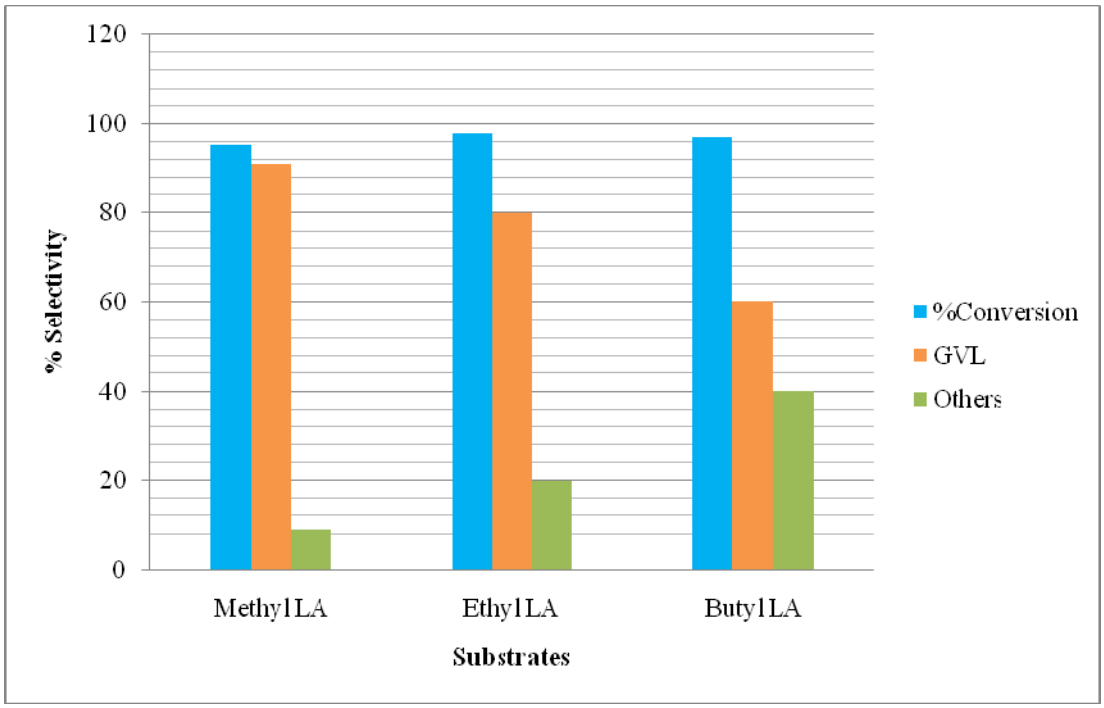

Figure 3.11. Substrate screening for GVL synthesis

Reaction conditions: Substrate concentration 5% (w/w); solvent, (MeOH, EtOH, ButOH) (95 ml); H_2 pressure, 500 psi; temperature, 130 ^oC; catalyst (5% Ru/C), 0.5 g; reaction time, 2 h.

3.3.4 Catalyst recyclability

The catalyst reusability studies for 5% Ru/C catalyst was carried out as follows. After the first hydrogenation experiment, the reaction crude was allowed to settle down and the supernatant clear product mixture was separated out. To the catalyst left in the reactor, fresh charge was added and the subsequent hydrogenation was continued. This procedure was followed for four subsequent runs and the results are shown in Figure 3. 12. Our 5% Ru/C catalyst showed almost the same activity as that of the fresh catalyst even after 4th

reuse. A slight decrease in conversion from 95 to 83% could be due physical losses during sampling of the reaction crude from time to time.

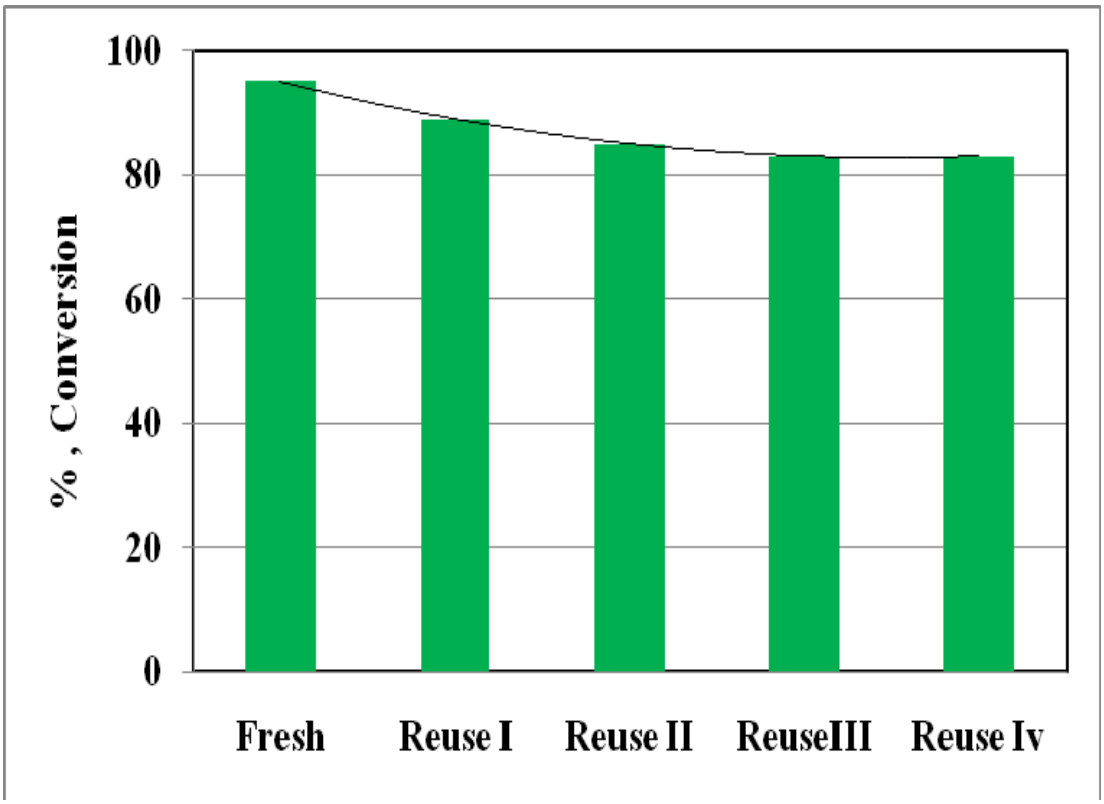

Figure 3.12. Catalyst recycle study for hydrogenation of methyl levulinate

Reaction conditions: Methyl levulinate, 5 % (w/w); solvent, MeOH (95 ml); H_2 pressure, 500 psi; temperature, 403 K; catalyst, 0.5 g (5 % Ru/C); reaction time, 2 h

3.3.4. 1. Catalyst stability

In order to confirm the marginal drop in activity during catalyst recycle study was only due to the handling losses, a standard leaching test was also carried out [27, 28]. As can be seen from Figure 3.13, the hot reaction crude filtrate after the catalyst separation at partial levulinate conversion did not show any activity.

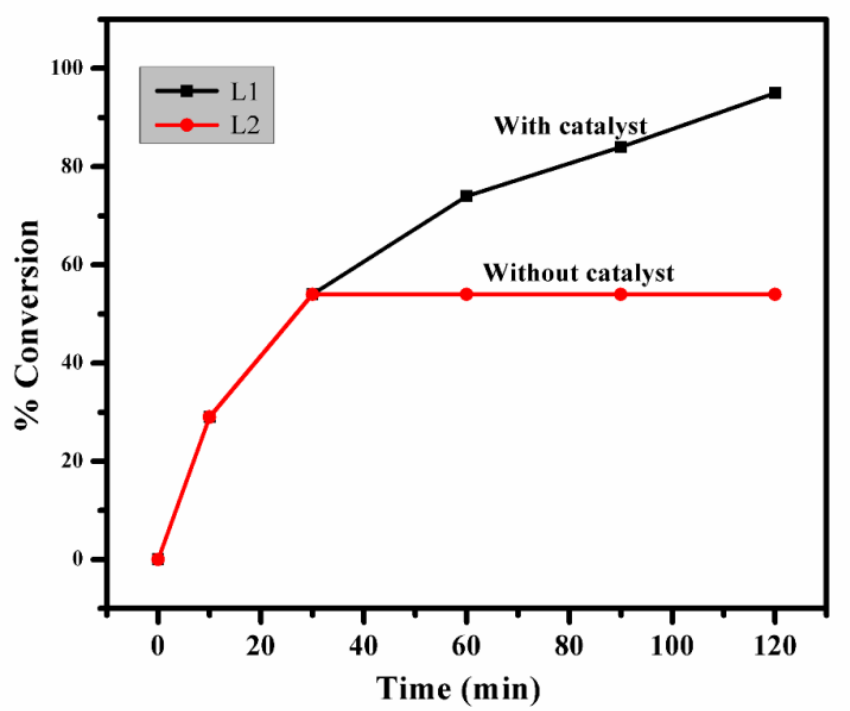

Figure 3.13 Catalyst stability study for hydrogenation of methyl levulinate

Reaction conditions: Methyl levulinate, 5% (w/w); solvent, MeOH (95 ml); H_2 pressure, 500 psi; temperature, 403K; catalyst, 0.5 g (5% Ru/C); reaction time, 2 h. **L_1** -With catalyst under the reaction conditions same as above. **L_2**- Without catalyst after ½ hr under reaction conditions same as above.

3.4. Conclusion

Among Pd, Pt and Ru supported catalysts, Ru/C catalyst showed the highest conversion and selectivity to GVL in methyl LA hydrogenation. As compared to C support, SiO_2 and Al_2O_3 supports showed several folds lower hydrogenation activity for Ru catalyst. TPR and XPS studies revealed that Ru^O species were in less concentration or absent in case of Ru/SiO_2 and Ru/Al_2O_3 catalyst, due to either encapsulation of Ru with silica or due to some other stable species such as $Ru(OH)_3$ formed on the surface.

3.5. References

1. D. L Klass, Fuels and chemicals, Academic Press, London (1998).
2. E. I. Grbz, D. M. Alonso, J. Q. Bond, J. A Dumesic, ChemSusChem 4 (2011) 357.
3. J. J. Bozell, L. Moens, D. C. Elliott, Y. Wang, G. G. Neuenschwander, S. W. Fitzpatrick, R. J. Bilski, J. L. Jarnefeld, Resour. Conserv. Recycl. 28 (2000) 227.
4. R. A. Bourne, J. G. Stevens, J. Ke, M. Poliakoff, Chem. Commun. (2007) 4632.
5. J. C. Serrano-Ruiz, D. Wang, J. A. Dumesic, Green Chem. 12 (2010) 574.
6. I. T. Horvath, H. Mehdi, V. Fabos, L. Boda, L. T. Mika Green Chem. 10 (2008) 238.
7. H. Mehdi, V. Fabos, R. Tuba, A. Bodor, L. T. Mika, I. T. Horvath, Top Catal. 48 (2008) 49.
8. E. Manzer, Appl. Catal. A: Gen. 272 (2004) 249.
9. J. P. Lange, J. Z. Vestering, R. J. Haan, Chem. Commun. (2007) 3488.
10. B. C. Windom, T. M. Lovestead, M. Mascal, E. B. Nikitin, T. J. Bruno, Energy Fuels. 25 (2011) 1878.
11. B. Kim, J. Jeong, S. Shin, D. Lee, S. Kim, H. Yoon, J. K. Cho, ChemSusChem 3 (2010) 1273.
12. X. Hu, C. Z. Li, Green Chem. 13 (2011) 1676.
13. P. Lincai, L. Lu, J. Zhanga, S. Jianbin, L. Shijie, Appl. Catal. A: Gen. 397 (2011) 259.
14. J. P. Lange, R. Price, P. M. Ayoub, J. Louis, L. Petrus, L. Clarke, H. Gosselink, Angew. Chem. Int. Ed. 49 (2010) 1.
15. F. Joo, M. T. Beck, React. Kinet. Catal. Lett. 2 (1975) 257.

16. J. P. Lange, L. Petrus, WO Pat. 2007099111(2007).
17. H. A. Schutte, R. W. Thomas, J. Am. Chem. Soc. 52 (1930) 3010.
18. Z. P. Yan, L. Lin, S. Liu, Energy Fuels 23 (2009) 3853.
19. Y. Zhao, J. Zhou, J. Zhang, S. Wang, Catal. Lett. 131(2009) 597
20. G. C. Bond, R. Rajaram, R. Burch, Appl. Catal. A: Gen. 27 (1986) 379.
21. M. Reinikainen, M. K. Niemela, N. Kakuta, S. Suhonen, Appl. Catal. A: Gen. 174 (1998) 61.
22. A. Guerrero-Ruiz, P. Badenes, I. Rodro A guez-Ramos, Appl. Catal. A: Gen. 173 (1998) 313.
23. W. Zou, R. D. Gonzales, J. Catal. 133 (1992) 202.
24. R. C. Lederhos, A. C. L. Pablo, C. P. Fernando, N. S. F. Goli, Catal. Lett. 110 (2006) 23.
25. A. Z. Foelske, O. Barbieri, M. Hahn, R. Kotz, Electrochem. Solid-State Lett. 9 (2006) 268.
26. Y. Pouilloux, F. Autin, C. Guimon, J. Catal. 176 (1998) 215.
27. I. W. C. E. Arends, R. A. Sheldon, Appl. Catal. A: Gen. 212 (2001) 175.
28. R. A. Sheldon, M. Wallau, I. W. C. E. Arends, U. Schuchardt, Acc. Chem. Res. 31 (1998) 485.

Chapter 4

Copper catalyzed hydrogenation of levulinic acid and its methyl ester

For developing non-noble metal catalyst systems for LA hydrogenation, several copper based catalysts were prepared, characterized and evaluated for their activity. Among these, nanocomposites of Cu-ZrO_2 and Cu-Al_2O_3 quantitatively catalyzed the hydrogenation of levulinic acid and its methyl ester to give 90-100% selectivity to γ-valerolactone in methanol and water respectively. Both Cu-ZrO_2 and Cu-Al_2O_3 nanocomposites were prepared by co-precipitation method using mixed precursors under controlled conditions. XRD results showed that the main active phase of the reduced Cu-ZrO_2 catalyst was metallic copper and particle size was found to be of 10-14 nm by HRTEM. The active metal leaching was maximum for Cu-Al_2O_3 catalyst in water medium due to formation of a blue color copper-carboxylate complex. Surprisingly, copper leaching was completely suppressed in case Cu-ZrO_2 catalyst in methanol in spite of the substrate loading was increased from 5 to 20% w/w. The excellent recyclability of Cu-ZrO_2 catalyst with complete LA conversion and >90% GVL selectivity makes it a sustainable process having a commercial potential.

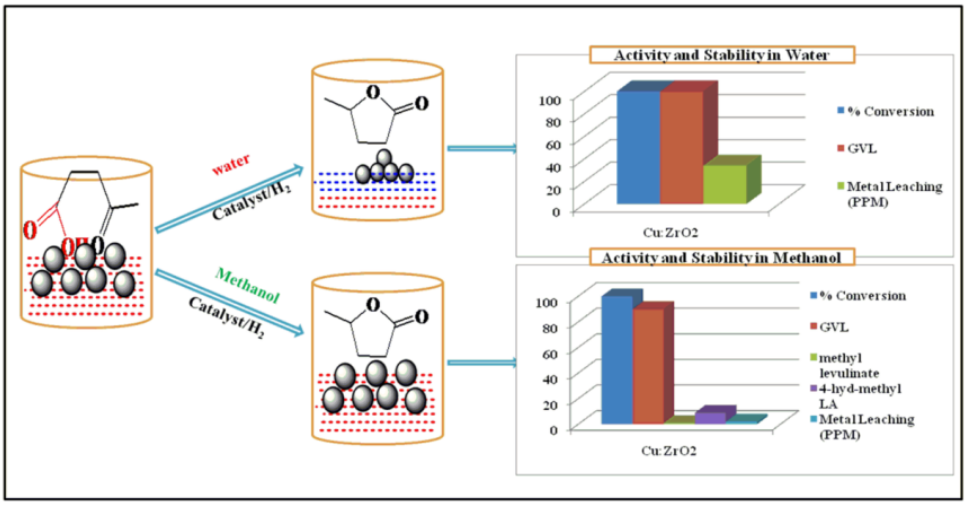

***Green Chem.*, 14 (2012) 1064–1072**

4.1. Introduction

A tremendous impetus worldwide has been laid on 'Biorefinery' concept with the aim for developing new catalytic routes for the conversion of several biobased platform molecules into fuels and multiple commodity products [1, 2]. The major challenge in this endeavor is the selective hydro-deoxygenation with minimum number of processing steps by designing appropriate catalyst systems and at the same time would require less number of processing steps as compared to as compared to the fossil derived hydrocarbons [3, 4]. As mentioned previously (chapters 1 and 3), downstream processing of LA gives several useful molecules and one of these is γ- valerolactone (GVL) obtained by the catalytic hydrogenation of LA. GVL is a sustainable commodity chemical having great commercial importance due to its applications as a solvent in lacquers, as a food additive and can be converted to a variety of monomers. It is also considered as a potential fuel additive for replacing ethanol in gasoline-ethanol blends [3-5].

As shown in Scheme 4.1, GVL synthesis from LA involves the first step of hydrogenation to give an intermediate, 4-hydroxy levulinic acid followed by its subsequent cyclization either by homogeneous or heterogeneous catalysts. Recently, a process for GVL from LA with high yield was reported using noble metal homogeneous catalysts systems [6, 7]. Homogeneous catalyst systems obviously have serious drawbacks of catalyst recovery and its recycle in addition to multistep synthesis of ligands, thus far from the commercial application. Heterogeneous catalyst systems, reported for the hydrogenation of LA include supported Ru, Pt, Pd and Re as well as chromium containing copper catalysts [8-16]. Similar studies were carried out using homogeneous as well as heterogeneous Ru based catalysts however, substantial leaching of the precious noble metals was observed [17].

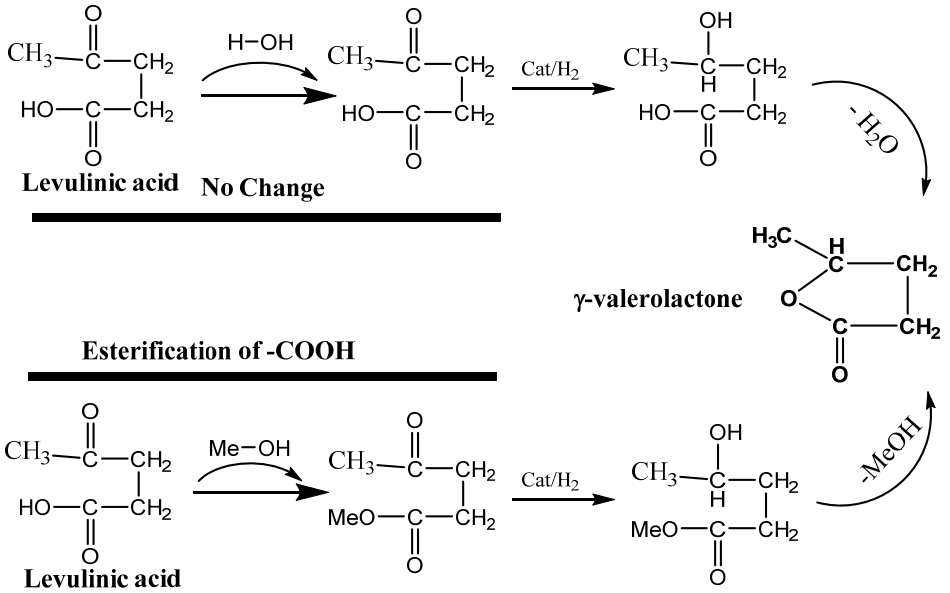

Scheme 4.1. Reaction pathway for hydrogenation of levulinic acid

The potential commercial application of LA hydrogenation to GVL process can thus be possible by developing a two way strategy viz. (i) a route which eliminates/minimizes the active metal leaching; and (ii) developing a non noble metal catalyst for an improved process economics. In the present chapter we demonstrate for the first time, the efficiency of a non noble Cu-ZrO_2 and Cu-Al catalysts for the hydrogenation of LA to GVL. Between the two catalysts, metal leaching was also drastically reduced for Cu-ZrO_2 catalyst (34 ppm) as compared to Cu-Al_2O_3 (174 ppm) in water medium due to stable tetragonal phase formation of ZrO_2 which strongly binds to the active Cu. The extent of metal leaching was further reduced to almost nil (2 ppm) with *in situ* formation of methyl levulinate in methanol solvent, followed by its subsequent hydrogenation to GVL. Hence, the catalyst reusability was also possible for three times unlike Ru based catalysts [11]. Our copper based catalyst will thus have a significant potential of commercial development since the lignocellulose decomposition is increasingly carried out in presence of alcohol to enhance overall yield of LA ester as compared to LA, due to substantial reduction in humin formation [18].

4.2. Experimental

All copper catalysts tested in this work (Cu–ZrO_2, Cu–Al_2O_3, Cu– BaO, Cu–Cr_2O_3, Cu–Cr_2O_3–Al_2O_3, Cu–BaO–Al_2O_3) were prepared by using a co-precipitation method and the detailed experimental procedure of their preparation has been described in chapter 2 (section 2.2.2). The catalysts were characterized by various techniques according to the procedure described in section 2.4. Activity of the prepared catalysts was evaluated for the hydrogenation of levulinic acid to γ-valerolactone and a typical experimental procedure is described in section 2.5.1. The quantitative analysis of liquid samples was carried out by gas chromatography method using FID detector, HP-5 capillary column and helium as a carrier gas. Other details of temperature programming method (60-190 ^{0} C) etc. are described in chapter II, section 2.5.

4.3. Results and discussion

4.3.1. Catalyst characterization

As Cu-ZrO_2 catalyst showed the highest performance and stability for the hydrogenation of LA and its methyl ester, a detailed characterization of Cu-ZrO_2 was carried out and the results were also compared with those of other Cu based catalysts studied in this work.

4.3.1.1. BET surface area and isotherms

BET surface area of Cu-ZrO_2 was found to be 22.1 m^2/g with pore volume of 0.06 cc/g and pore size of 2.7 nm (Table 4.1). The microporous nature of the material was confirmed by type I adsorption isotherm as shown in Figure 4.1. The characteristic feature of a Type I isotherm is a long horizontal plateau, which extends up to relatively high P/P_0. Such sorption isotherms can be described by the Langmuir equation which was developed on the assumption that adsorption, was limited to at the most one monolayer. Any factor that can limit the quantity adsorbed to a few monolayer which is relevant to a type I isotherm prevailing for micropores, where the small pore width prevents multilayer adsorption and limits the amount adsorbed as shown in Figure 4.1.

Table 4.1. Textural properties of Cu-ZrO_2 catalyst

Catalyst	Surface Area m^2/g	Pore Volume cc/g	Pore Size (nm)
Cu-Zr (1:1)	22.1	0.061	2.7

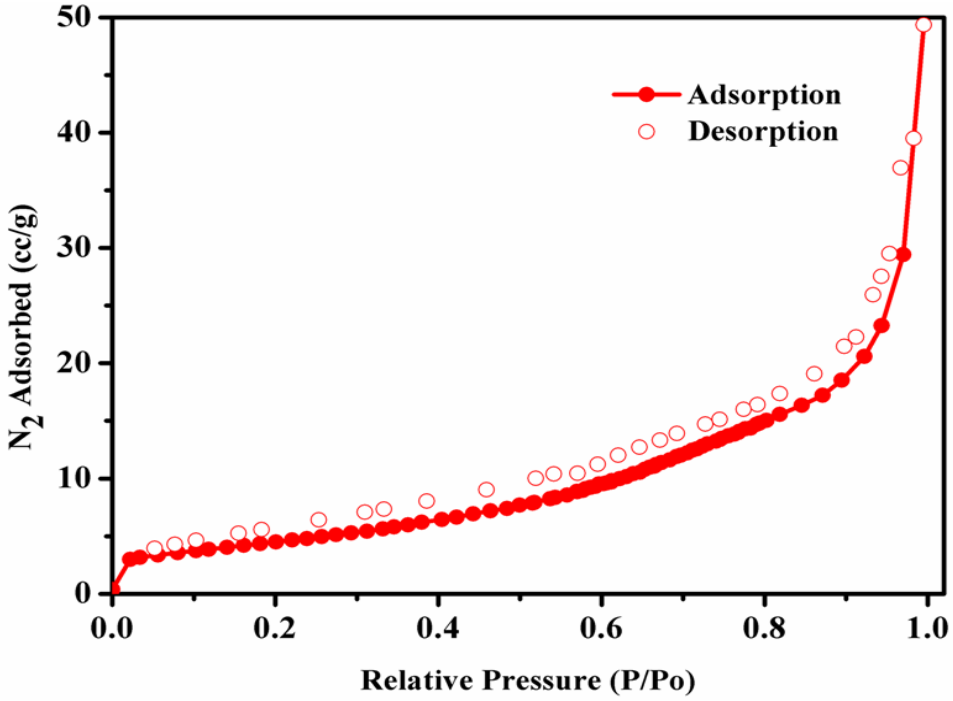

Figure 4.1. Adsorption isotherm of Cu-ZrO_2 catalyst

4.3.1.2. X-ray diffraction

XRD patterns of activated and used Cu-ZrO_2 catalyst samples are shown in Figure 4.2. The appearance of indexed diffraction lines at $2\theta = 43.5^o$ (111), 50.6^o (200), 60.2^o (202) and 74.3^o (220) indicate the presence of the crystalline phases of metallic Cu in all the samples [19]. The particle size evaluated from Scherrer equation using the peak at $2\theta = 43.5^o$ having maximum intensity was found to be 13.5 nm, that matched very well with the HRTEM results (discussed later). XRD results showed that the main active phase of the reduced Cu-ZrO_2 catalyst was metallic copper and a peak at $2\theta = 30.5^o$ (particle size = 8 nm) indicated the tetragonal phase of zirconia [19-20]. While, the sample recovered

after the reaction carried out in water, showed that metallic copper phase remained intact as evidenced by a peak at $2\theta = 43.5^{o}$, however appearance of a new peak at $2\theta = 36.5^{o}$ indicated the formation of Cu_2O as shown in Figure 4.2 (c). The increased sharpness of the peak at $2\theta = 30.5^{o}$ in the used sample, could be due to the increase in crystallite size (from 8 to 11 nm) of ZrO_2. In contrast to this, XRD of Cu-ZrO_2 recovered from the methanol medium (Figure 4.3) showed the presence of metallic copper phase without any characteristic peak of Cu_2O.

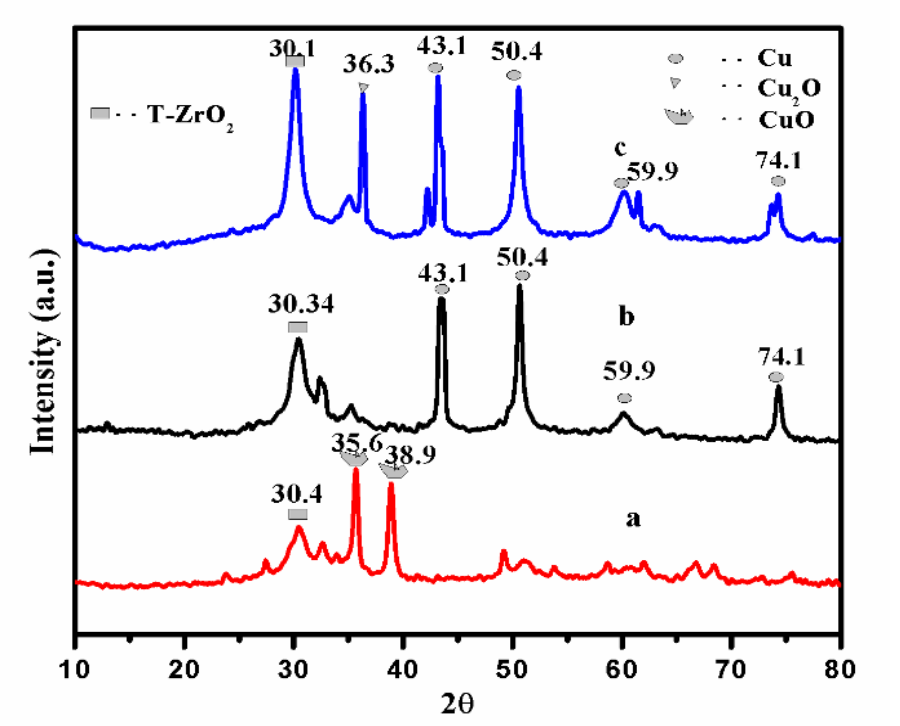

Figure 4.2. XRD patterns for nano Cu-ZrO_2 catalyst (a) calcined Cu-ZrO_2 (b) activated Cu-ZrO_2 (c) used Cu-ZrO_2 in water.

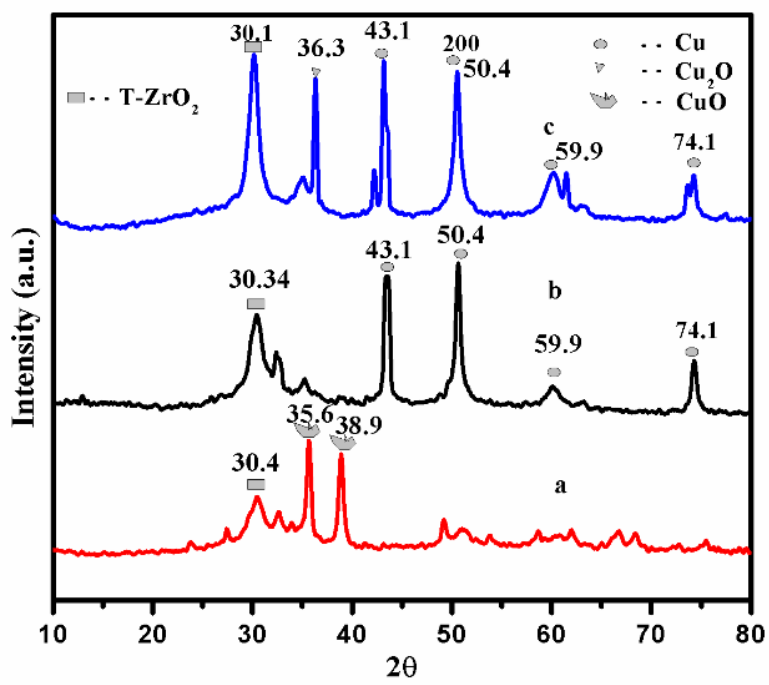

Figure 4.3. XRD patterns for nano Cu-ZrO_2 catalyst (a) calcined Cu-ZrO_2 (b) activated Cu-ZrO_2 (c) used Cu-ZrO_2 in methanol.

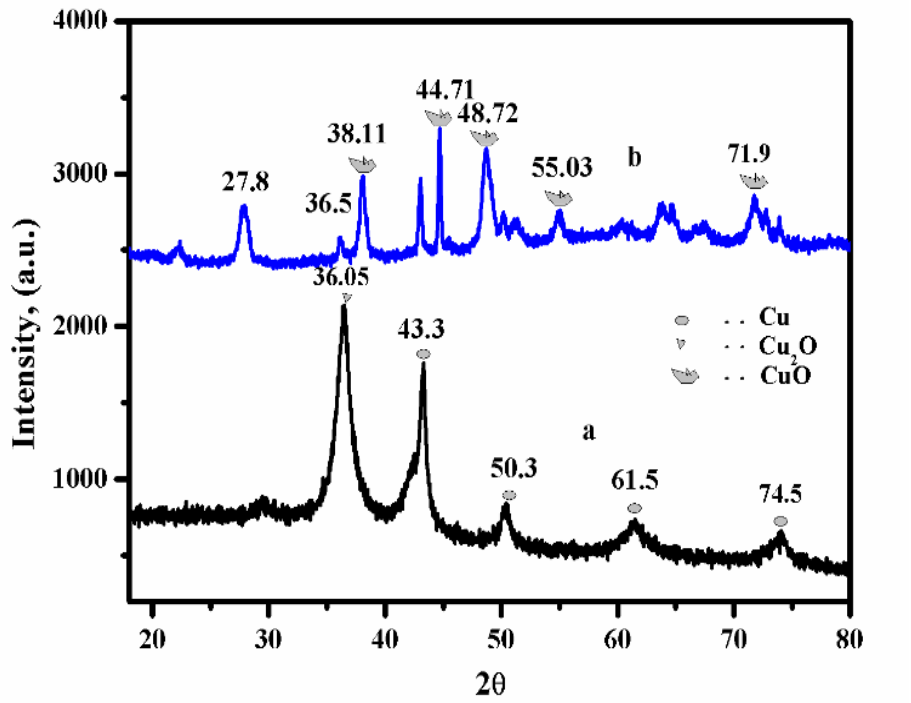

Figure 4.4. XRD patterns for nano Cu-Al_2O_3 catalyst (a) Activated Cu-Al_2O_3 (b) Used Cu-Al_2O_3 in water.

Although XRD pattern of activated Cu-Al_2O_3 catalyst in Figure 4.4 showed metallic copper and Cu_2O phases at $2\theta = 43.5^o$ (111) and $2\theta = 36.5^o$ respectively, in contrast to Cu-ZrO_2 both these phases disappeared and appearance of peaks at $2\theta = 38.1^o$, 44.7^o, 48.72^o and 71.9^o and another peak at $2\theta = 27.8^o$ indicate the presence of CuO and alumina phases, respectively.

4.3.1.3. XPS

In order to evaluate the extent of various copper species formed, XPS of Cu-ZrO_2 was also studied and XPS spectrum is shown in Figure 4.5. The Cu 2p XPS of the activated Cu-ZrO_2 catalyst sample showed a broad peak in the range of 932–935 eV, which was ascribed to the presence of various Cu species. The wide Cu $2p_{3/2}$ signals showed the presence of two peaks of different binding energies namely, 932.4 eV and 933.08 eV corresponding to metallic Cu and Cu^+ in Cu_2O, respectively. The extent of Cu metal and Cu^+ was evaluated as 67 % and 33%, respectively.

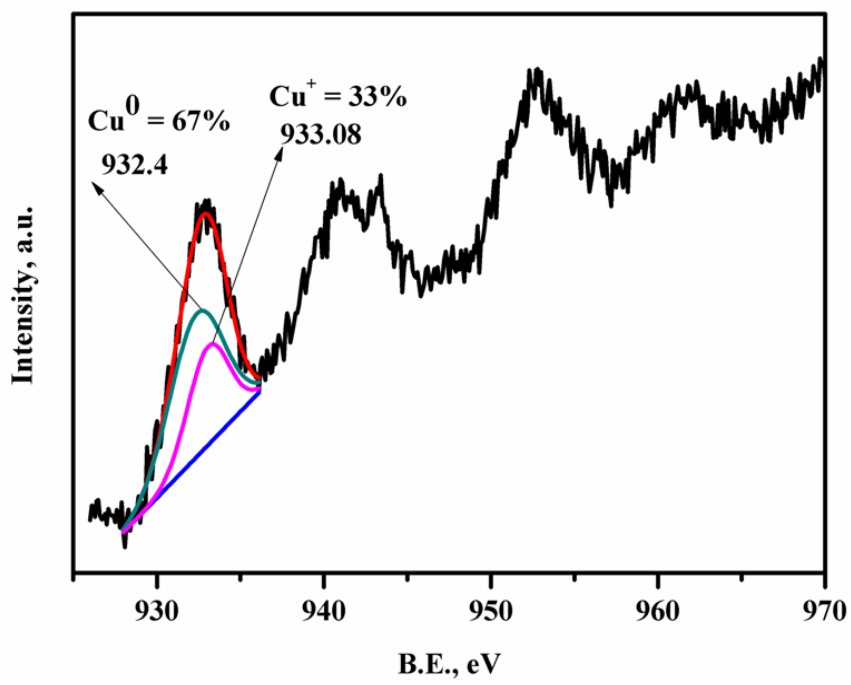

Figure 4.5. XPS of used Cu-ZrO_2 catalyst

4.3.1.4. Raman study

In Raman spectra of freshly activated (Figure 4.6, a) and recovered (Figure 4.6, b) Cu-ZrO_2 catalyst samples, weak and strong bands at 144, 436 and 627cm^{-1} could be assigned to tetragonal ZrO_2, which was in accordance with the XRD results. In addition, the bands at 248 and 308 cm^{-1} were of surface CuO due to the exposure of the sample to air.[20] Although these bands in the recovered sample shifted to new values nevertheless, these are characteristics of tetragonal ZrO_2 phase which is in good agreement with the XRD results. Also, the absence of sharp bands in the spectra after the reaction indicates the semi crystalline nature due to exposure under reaction conditions [20].

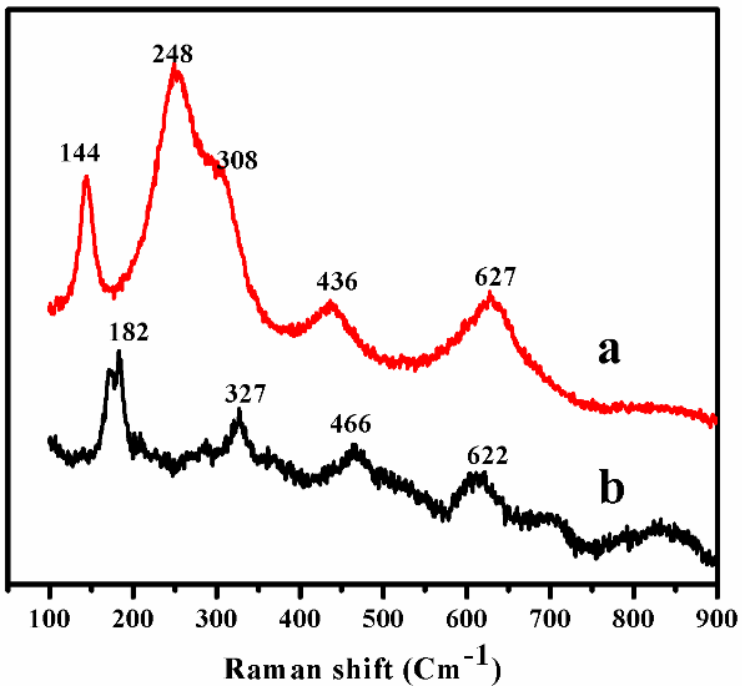

Figure 4.6. Raman study of nano Cu-ZrO_2 catalyst (a) activated Cu-ZrO_2 (b) used Cu-ZrO_2 in water.

4.3.1.5. NH_3-Temprature programmed desorption

Figures 4.7 (A) and (B) show NH_3-TPD profiles and Py-IR respectively, for various copper catalysts. Among these catalysts, Cu-Al_2O_3 and Cu-ZrO_2 showed broad peaks of NH_3 desorption in a high temperature region of 500-700 ^oC, indicating the presence of

strong acid sites, while other two catalysts (Cu-Cr_2O_3 and Cu-BaO) did not show any NH_3 desorption peaks indicating the absence of detectable acid sites.

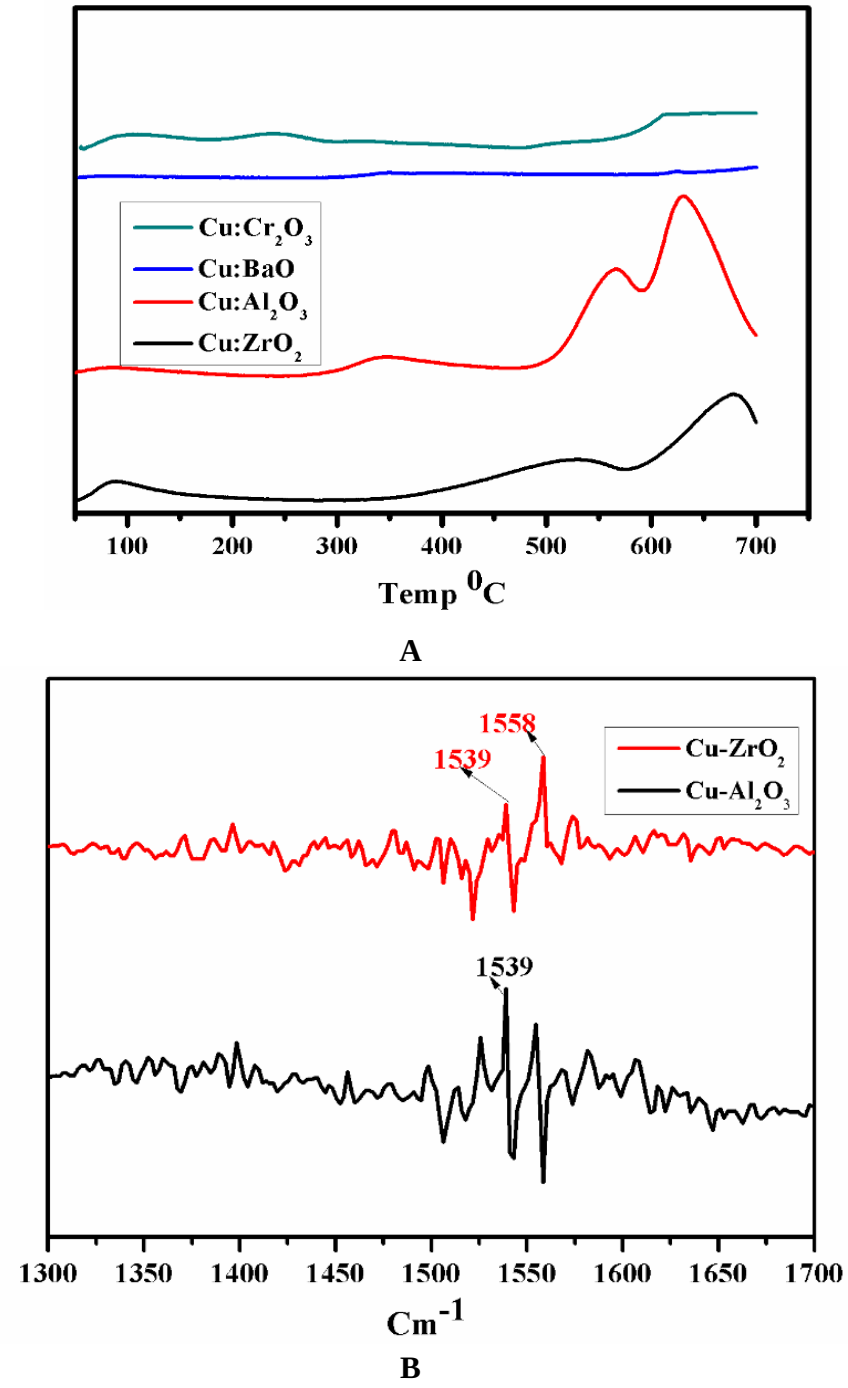

Figure 4.7. NH_3 TPD and Py-IR profiles of copper based catalysts (A) NH_3 TPD profiles of copper catalysts (B) Pyridine IR of copper with Al and Zr catalysts.

In order to distinguish between the acid sites, Py-IR of both Cu-ZrO_2 and Cu-Al_2O_3 samples were also studied which showed distinct peaks at 1539 and 1558 cm^{-1} due to mixed Lewis-Brønsted and only Brønsted acid sites respectively. The strong acidity of Cu-ZrO_2 evidenced by NH_3 TPD and Py-IR, resulted into its higher activity for acid catalyzed esterification of LA in methanol as discussed later [19-21].

4.3.1.6. TG-DTA

Catalyst stability was studied by TG-DTA and the results are shown in Figures 4.8 (A) and (B). TG profiles of Cu-Cr_2O_3 and Cu-BaO showed the decomposition of these catalysts after 400 ^oC and 600 ^oC, respectively. On the other hand, both Cu-ZrO_2 and Cu-Al_2O_3 showed excellent stability upto 700 ^oC. DTA of TG profiles of all the samples in Figure 4.8, (B) showed 8-9% weight loss around 100-120 ^oC, due to the loss of water molecules.

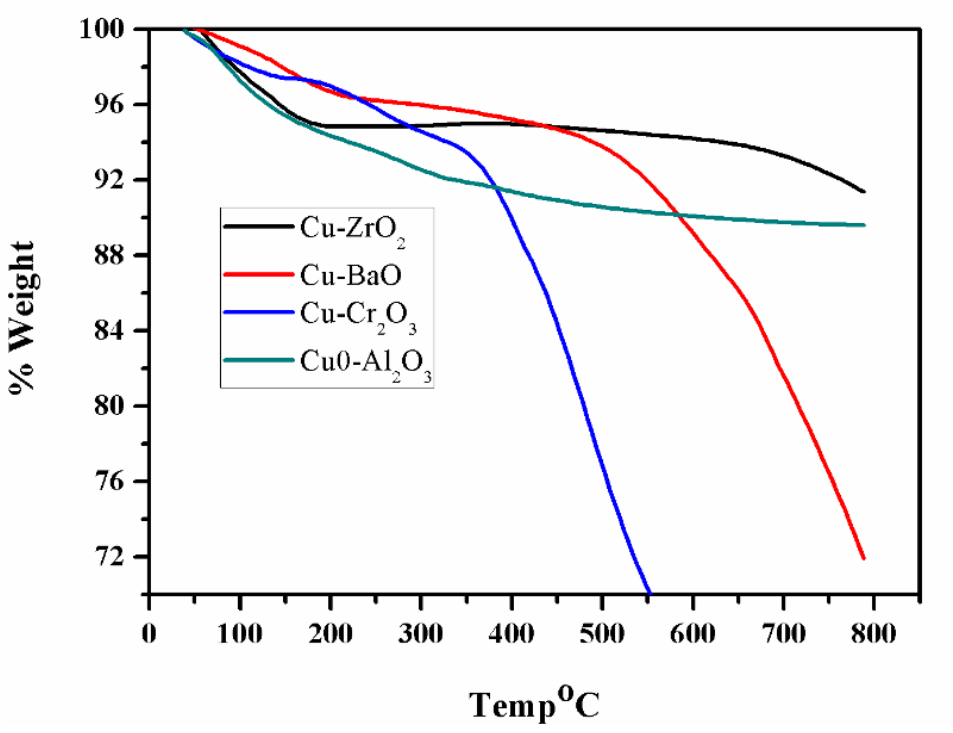

A

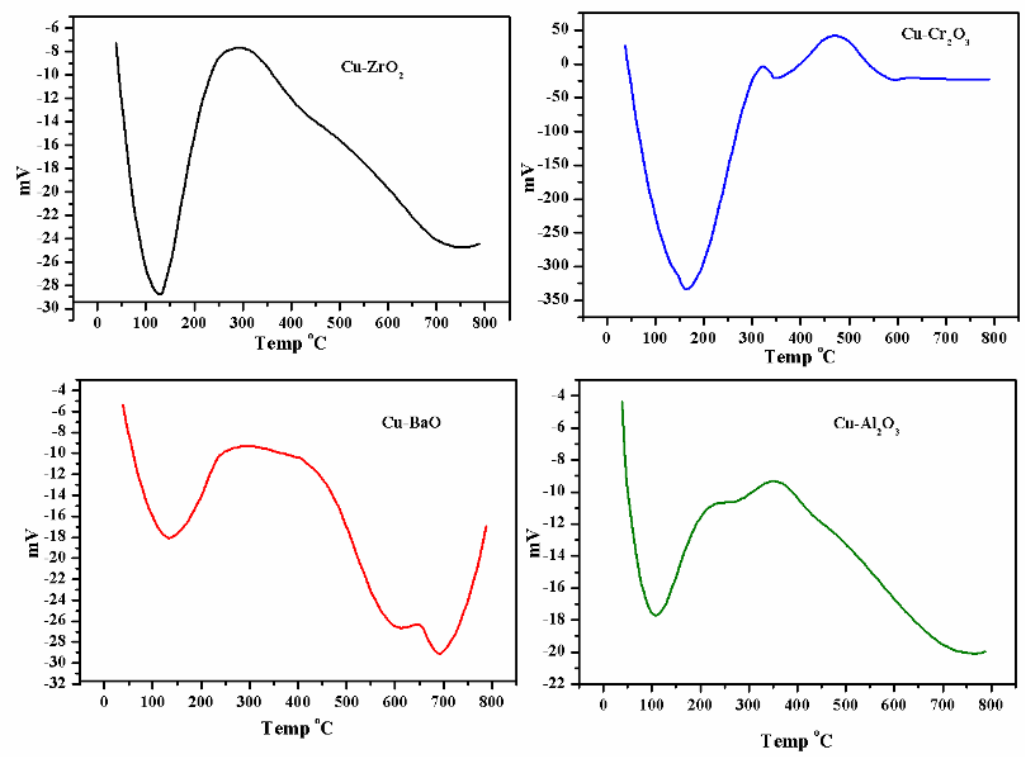

B

Figure 4.8. TG/DTA profiles of copper based catalysts (A) TG analysis of copper catalysts (B) DTA of Copper catalysts the broad exothermic peaks for Cu-Cr_2O_3 and Cu-BaO

The broad exothermic peaks for Cu-Cr_2O_3 and Cu-BaO catalysts could be due to the loss of Cu in the form of CuO, to the extent of 30% which was much higher than that observed for Cu-ZrO_2 and Cu-Al_2O_3 (8-9%) catalysts [22-23]. This confirms the higher stability of Cu-ZrO_2 catalyst as well as retention of active Cu for higher hydrogenation activity than that of other Cu catalysts.

4.3.1.7. H_2-TPR

Figure 4.9 shows the H_2 TPR of all the copper catalysts studied in this work. All the samples exhibited a broad band of H_2 consumption in the range of 180–356 °C. The shape of the H_2 consumption peak was asymmetric with a shoulder or a tail, as a result of a complex overlapping of several elemental reduction processes such as sequential reduction of CuO to Cu^0 via Cu_2O [24-25]. The highest reduction temperature (359 °C) of

Cu-ZrO_2 sample confirms the strong interaction of Cu and ZrO_2, contributing to its greater stability under reaction conditions.

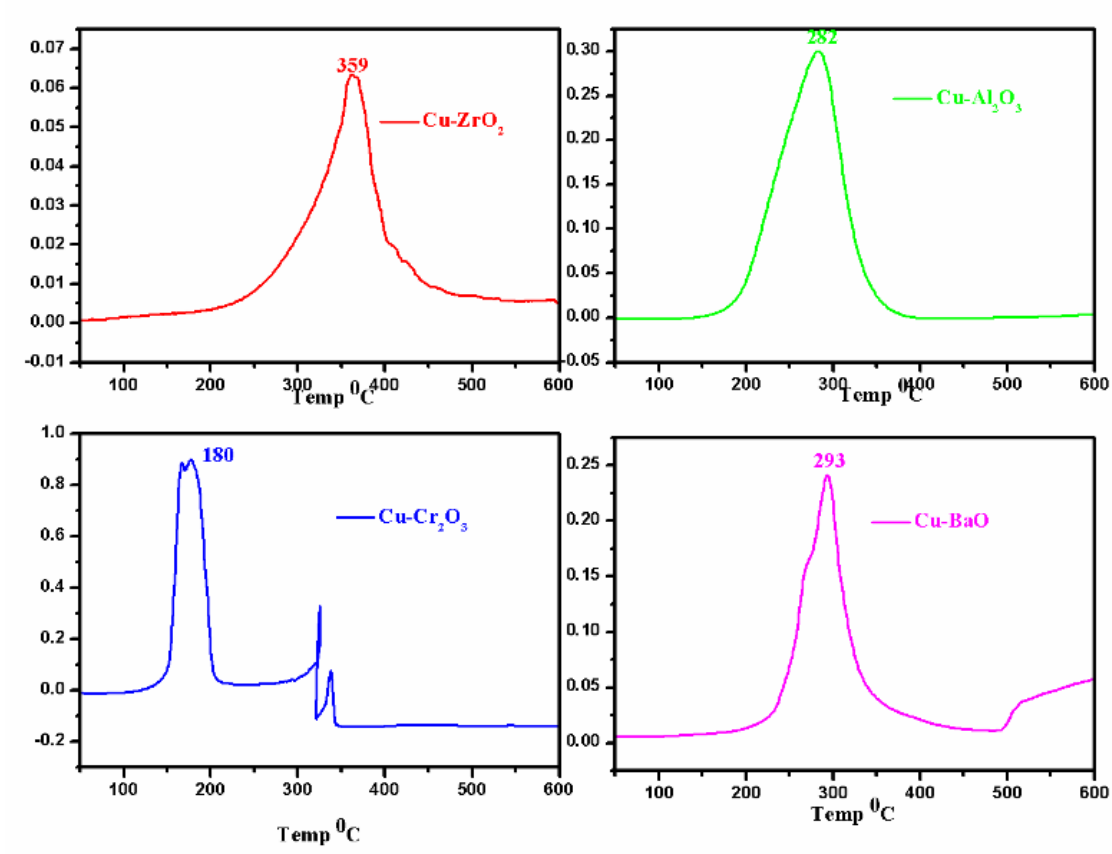

Figure 4.9. H_2 TPR profiles of copper based catalysts.

4.3.1.8. HRTEM

Figure 4.10 (A) and (B) shows HRTEM images of Cu–ZrO_2 before and after reaction in the water medium respectively. The TEM image (Figure 4.10, A) shows the well dispersed nature of the Cu nanoparticles on the zirconia surface with particle sizes in the range of 10–14 nm which is close to the particle size estimated from XRD (13–14 nm) [26]. HRTEM of the used Cu–ZrO_2 sample (Figure 4.10, B) showed minor agglomeration of Cu particles giving the particle size of 13–15 nm.

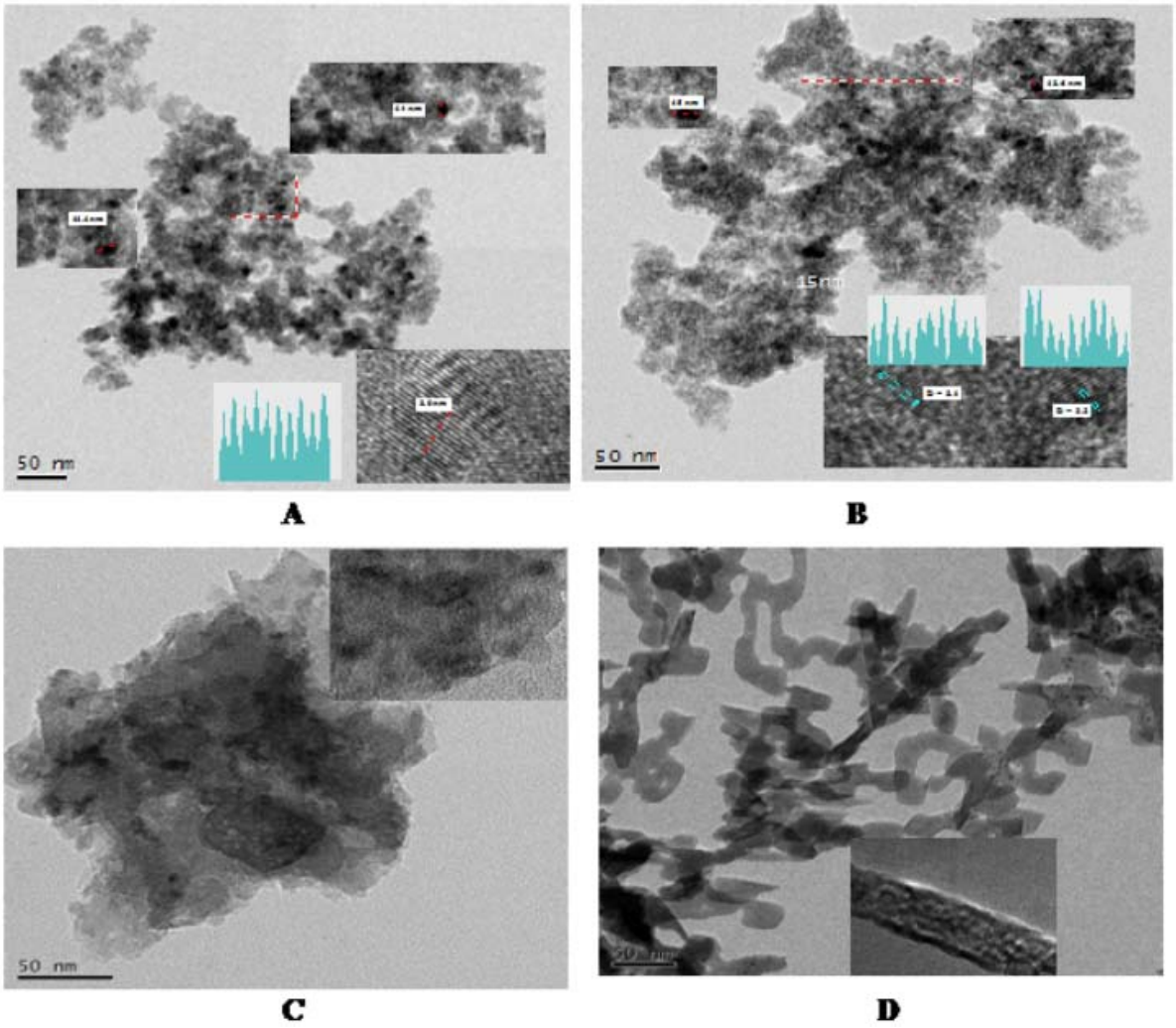

Figure 4.10. HR-TEM images of nano catalyst (A) activated Cu-ZrO_2 catalyst (B) used Cu-ZrO_2 catalyst in water (C) activated Cu-Al_2O_3 catalyst (D) used Cu-Al_2O_3 catalyst in water.

The 'd' spacing of the used catalyst determined form the pattern of fringes (inset right bottom, Figure 4.10, B) was found to be 3.2 Å which was also close to that obtained by XRD (2.9 Å) for 2θ = 43.5° (111) plane of metallic copper. On the contrary, fresh Cu–Al_2O_3 (Figure 4.10, C) showed agglomeration of the particles and did not allow to specify the fringes pattern. In case of recovered Cu–Al_2O_3 (Fig. 4.10, D) the particles got oriented into a distinct rod like structure without any fringes. This could be due to substantial leaching of Cu, as discussed in detail later (Table 4.3).

4.3.2. Catalyst activity measurement

4.3.2.1. Catalyst screening

The preliminary results on hydrogenation of LA to GVL using various copper catalysts in both water and methanol solvents are presented in Table 4.2. The desired product GVL was identified by H^1NMR, ^{13}C-NMR, DEPT and the respective spectra are given in Figures 4.11-4.13.

Table 4.2. Catalyst screening for hydrogenation of LA in water and methanol

Sr. No.	Catalysts	Water		Methanol			
		Conversion, %	Selectivity, %	Conversion, %	Selectivity, %		
			GVL		GVL	4-HMeLA	MeLA
1	**Cu-ZrO_2 (1:1)**	**100**	**100**	**100**	**90**	**9**	**1**
2	Cu- Al_2O_3 (1:1)	100	100	100	86	10	4
3	Cu-Cr_2O_3 (1:1)	9	100	72	45	20	35
4	Cu-BaO (1:1)	12	100	78	41	9	50
5	Cu-Cr_2O_3-Al_2O_3 (4:4:2)	40	100	89	82	14	2
6	Cu-BaO-Al_2O_3 (4:4:2)	45	100	92	86	8	6

Reaction conditions: : Levulinic acid, 5% (w/w); solvent, water and MeOH (95 ml); temp, 200 ^oC; H_2 pressure, 500 psi; catalyst, 0.5 g; reaction time, 5h.

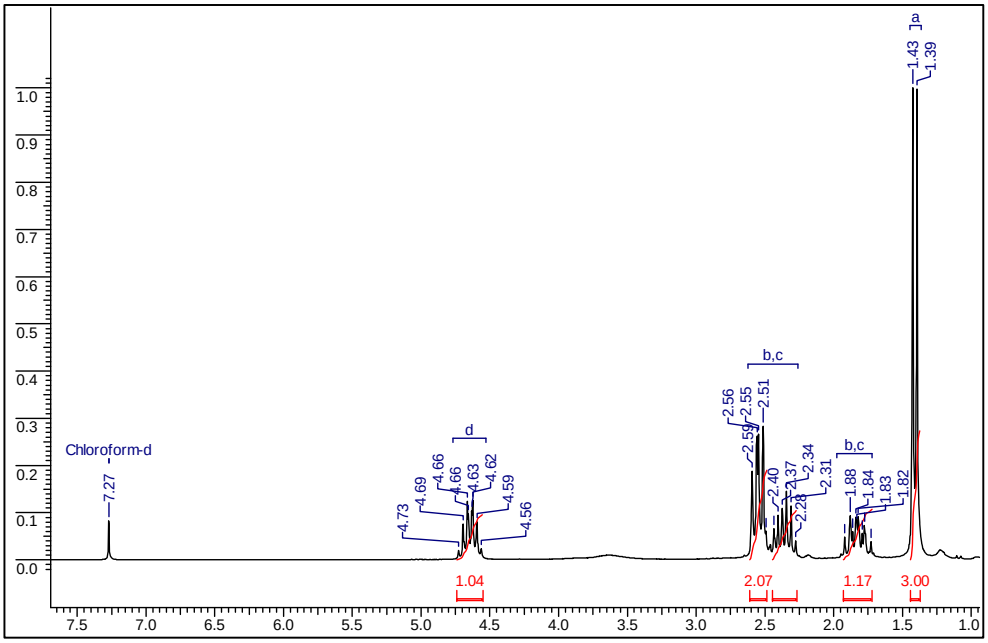

Figure 4.11. NMR spectra of γ- valerolactone

^{1}H-NMR ($CDCl_3$ 200MHz) : δ□1.39-1.43 (d, 3H), 1.73-1.93 (m, 1H), 2.28-2.43 (m, 1H), 2.51-2.59 (m, 2H), □4.56-4.73 (m, 1H).

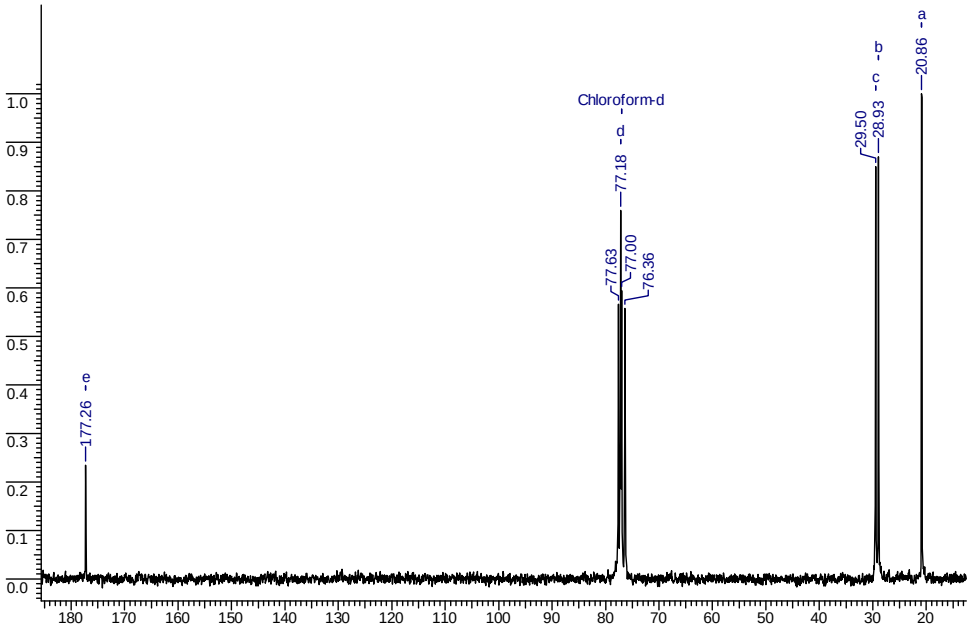

Figure 4.12. C^{13} NMR spectra of γ- valerolactone

^{13}C NMR ($CDCl_3$, 50MHz) : δ 20.86, 28.93, 29.50, 77.18, 177.26.

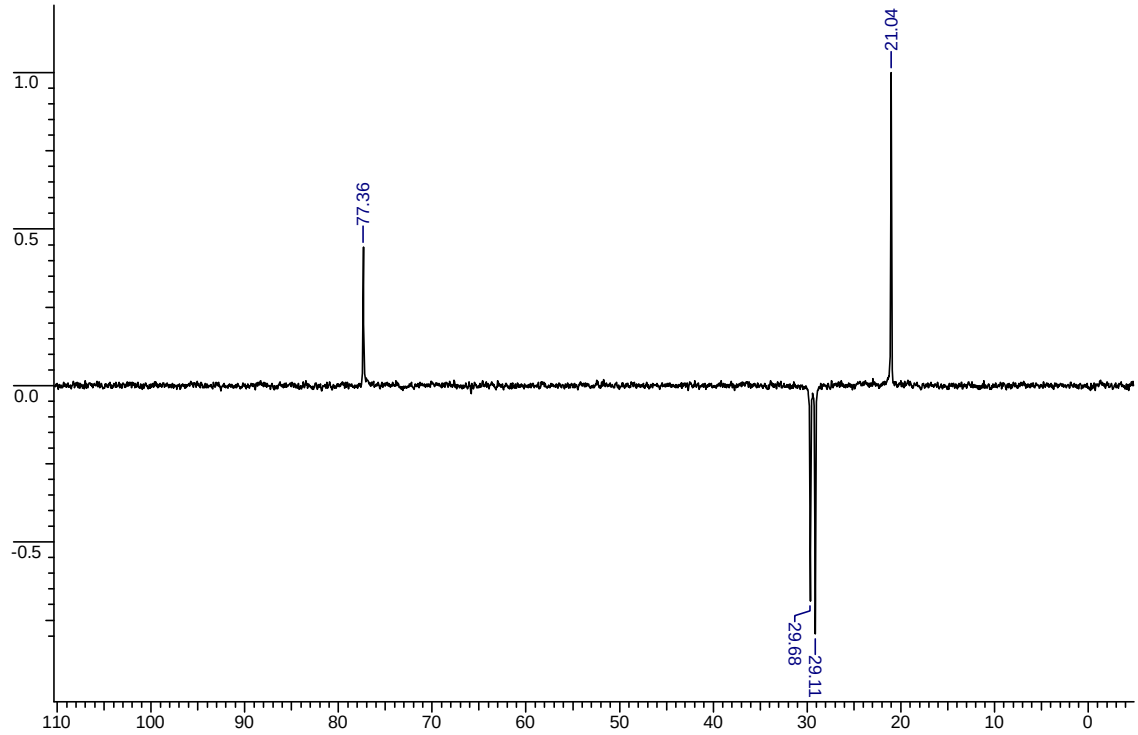

Figure 4.13. DEPT C^{13} NMR spectra of γ- valerolactone

It is interesting to note that copper in combination with Zr and Al showed complete LA conversion in water while, copper with other metals showed very poor LA conversion in the range of 4–45%, although complete GVL selectivity was obtained in all the cases. On the other hand, in methanol solvent, a maximum GVL selectivity of up to 90% was achieved only in the case of Cu–ZrO_2 and Cu–Al_2O_3 catalysts. Copper, in combination with other metals, gave LA conversion of <90% with GVL selectivity ranging from 45–86%. The lowering of the GVL selectivity was due to unconverted 4-HMeLA and MeLA (Scheme 4.1). The poor surface acidity of the Cu catalysts with metals other than Zr and Al, as evidenced by NH_3-TPD, was responsible for the slower rate of esterification Figure 4.7. This also affected the further steps of Cu catalyzed hydrogenation and acid catalyzed cyclization to GVL leading to accumulation of 4-HMeLA and MeLA. The marginal lower selectivity to GVL in methanol over Cu–ZrO_2 catalyst was due to less facile cyclization of 4-hydroxyl methyl levulinate having a bulkier methyl group as compared to that of 4-hydroxyl levulinic acid. The excellent catalytic performance of our copper–zirconia catalyst could be due to (i) its strong surface acidity that catalyzes cyclization of

the intermediate hydroxyl levulinic acid–ester due to the protonation of hydroxyl group, [27] (ii) the microporous nature of Cu–ZrO_2 as evidenced by the type I isotherm (Figure 4.1, Table 4.1), [28] (iii) ZrO_2 also plays a role in the first step of hydrogenation in which hydrogen adsorbs dissociatively on ZrO_2, [29] (iv) among the dopent oxides of other metals such as barium, chromium and aluminium, ZrO_2 is the most stable to "decoking" conditions during repeated catalyst regeneration cycles, and (v) ZrO_2 shows much higher stability against its leaching in aqueous LA solution in high temperature reaction conditions, as proven by the catalyst recycles studies described later [12, 13].

4.3.2.2. Stability of the catalyst

As stability is critical for the efficient use of any catalyst, Cu metal leaching was studied for the Cu–ZrO_2 and Cu–Al_2O_3 catalysts since almost complete conversion of LA with similar selectivities to GVL were obtained for both catalysts. The extent of Cu metal leaching was dramatically affected by change in the reaction medium. As can be seen from Table 4.3, the active metal leaching was maximum (174 ppm) for the Cu–Al_2O_3 catalyst while, it was only 34 ppm in case of the Cu–ZrO_2 catalyst in the water medium. Even in methanol solvent, metal leaching up to 31 ppm was observed for Cu–Al_2O_3 while, it was almost completely suppressed in the case of the Cu–ZrO_2 catalyst. However for the Cu–ZrO_2 catalyst, no metal leaching was observed when methyl levulinate was used as a substrate in spite of the substrate loading being increased from 5 to 20% w/w. Copper metal leaching was evident visibly by observing the blue colour of the crude reaction in the case of the Cu–Al_2O_3 catalyzed reaction, as shown in Figure 4.14. The blue colour of the solution was due to the formation of a soluble metal carboxylate complex with levulinic acid [30].

Table 4.3. Catalytic activity and stability for synthesis of GVL

Catalysts	Substrate	Solvent	Conversion, %	Selectivity, %			Metal Leaching (ppm)
				GVL	Me-LA	4-hydroxy Me- LA	
Cu-ZrO_2	Levulinic Acid	Water	100	>99.9	0.01	0.01	34
	Levulinic acid	Methanol	100	90	2	8	2
	Methyl levulinate	Methanol	95	92	SM	8	ND
	*Methyl levulinate	Methanol	81	79	SM	21	ND
Cu-Al_2O_3	Levulinic Acid	Water	100	>99.9	0.01	0.01	174
	Levulinic acid	Methanol	100	86	4	10	31
	Methyl levulinate	Methanol	93	88	SM	12	ND

Reaction conditions: : LA, *MeLA, (5%, 20% w/w); temp, 200 ^{o}C; H_2 pressure, 500 psi; catalyst, 0.5 g; reaction time, 5 h.

Figure 4.14. Final reaction sample of LA hydrogenation in water and methanol (A) final reaction sample of LA in water with Cu-Al_2O_3 catalyst (B) final reaction sample of MeLA in methanol with Cu- ZrO_2 catalyst.

Reaction Conditions: Levulinic acid, 5% (w/w); solvent, water, methanol (95 mL); temp, 200 ^oC; catalyst, 0.5 g; (Cu–Al_2O_3, Cu–ZrO_2) reaction time, 5 h.

This was also confirmed by FT-IR (Figures 4.15 A and B) in which the frequency of the carbonyl group of levulinic acid shifted from 1702 cm^{-1} to 1565 cm^{-1}, while no change was observed for methyl levulinate as a substrate [30]. Thus metal leaching could be avoided at least in the case of Cu–ZrO_2 in the presence of methanol, where the carboxyl group undergoes trans-esterification thus rendering the free carboxylic group unavailable, so cannot form a soluble copper complex [30].

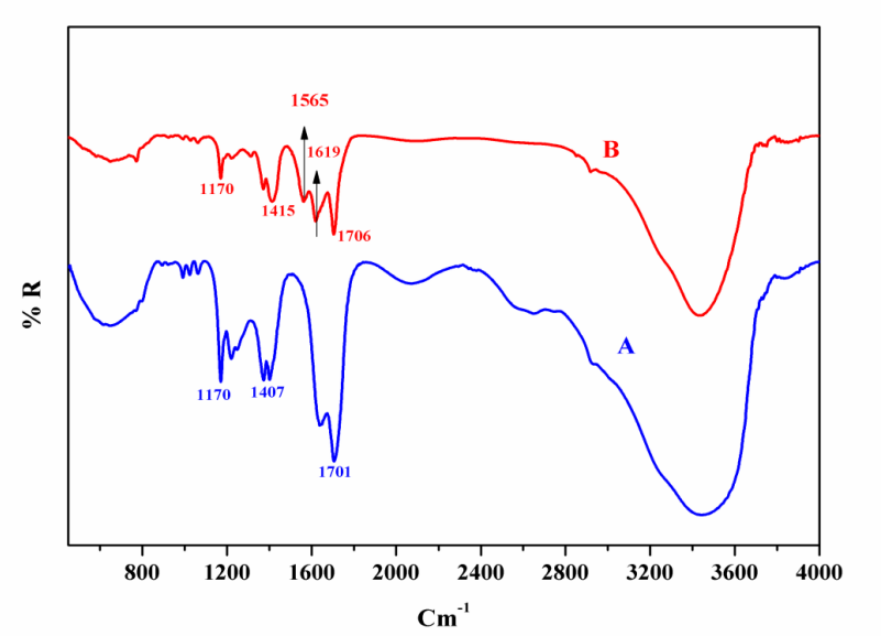

A

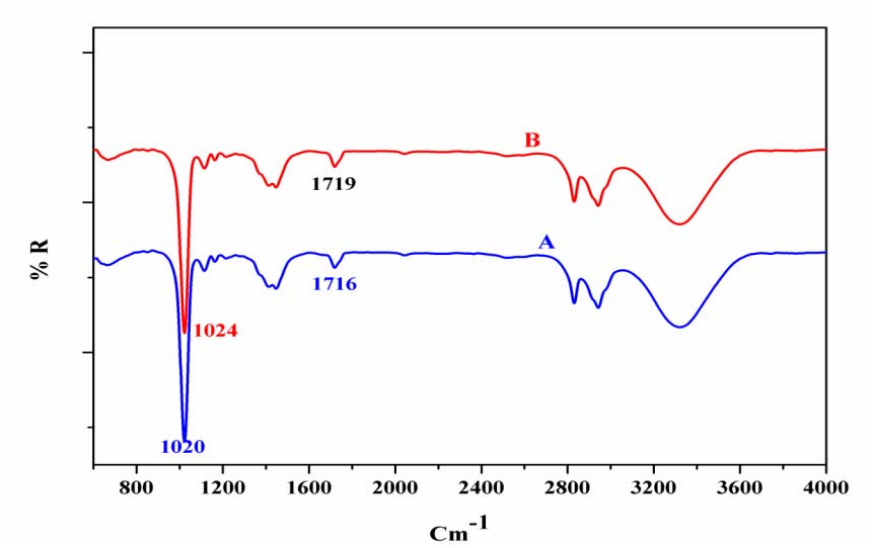

B

Figure 4.15. FTIR study LA hydrogenation (A) LA hydrogenation in water (B) Methyl LA hydrogenation in methanol

Reaction Conditions: Levulinic acid, Methyl Levulinate 5% (w/w); solvent, water, methanol (95 ml); Temp, 200 ^{o}C; catalyst, 0.5 g; (Cu-Al, Cu-Zr) reaction time, 5h.

The proposed reaction mechanism as shown in Scheme 4.1, is believed to proceed differently in methanol than in water. In presence of methanol, the first step of esterification of the carboxyl group forms methyl levulinate and its subsequent hydrogenation to GVL involves the elimination of methanol, which can be recycled. On the other hand, in water the first step is the direct hydrogenation of the keto group to give 4-hydroxy levulinic acid followed by its dehydration to give cyclic GVL.

4.3.2.3. Concentration Vs time activity

The role of acidity of Cu–ZrO_2 and Cu–Al_2O_3 catalyst was further studied by the kinetics of the first step esterification reaction. Figure 4.16 shows selectivity vs. time pattern for conversion of LA to methyl levulinate over various copper based catalysts in methanol. Copper with Zr and Al gave complete formation of methyl levulinate within first 30 min of the reaction while, other metals like Ba and Cr showed lower activity for the esterification step.

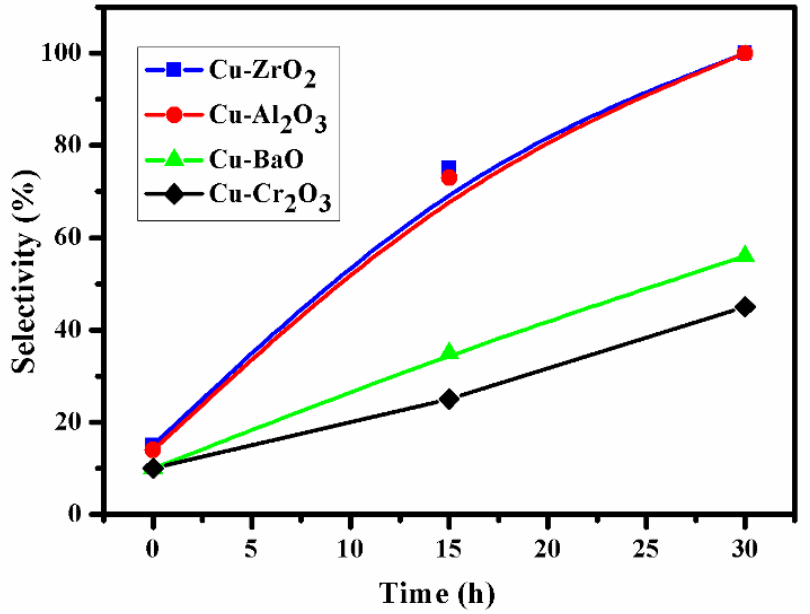

Figure 4.16. Selectivity profile for methyl levulinate formation

Reaction Conditions: Levulinic acid, 5% (w/w); solvent, water, methanol (95 mL); temp, 200 ^{o}C; catalyst, 0.5 g; reaction time, 5 h.

It is also interesting to note that the hydrogenation of methyl levulinate begins only after the complete formation of methyl levulinate, indicating the competitive adsorption of LA and methyl levulinate (Figures 4.17, A and B).

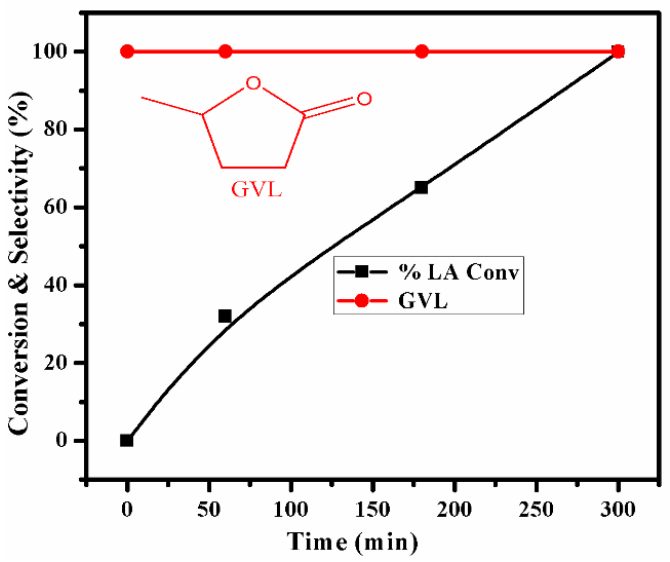

A

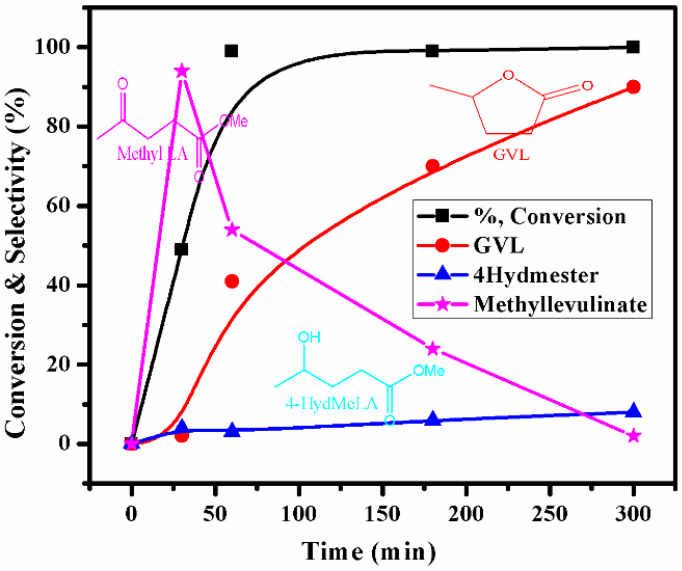

B

Figure 4.17. Conversion selectivity pattern of LA Hydrogenation in (A) water (B) methanol

Reaction Conditions: Levulinic acid, 5% (w/w); solvent, water, methanol (95 mL); temp, 200 ^{o}C; catalyst, 0.5 g; reaction time, 5 h.

4.3.3. Catalyst recycle study

The catalyst reuse studies for Cu–ZrO_2 catalyst were carried out as follows. After the first hydrogenation was complete, the reaction crude was allowed to settle down and supernatant clear product mixture was removed from the reactor. A fresh charge of reactants was added to the catalyst residue retained in the reactor and the subsequent run was continued. This procedure was followed for three subsequent runs and the results are shown in Figure 4.18 and Figure 4.19. Our copper zirconia catalyst showed almost the same activity with slight decrease in selectivity for LA hydrogenation in methanol even after the third recycle. A marginal decrease in selectivity from 90 to 80% could be due to sintering of the active sites of metal particles. Figure 4.19 (b) shows reuse of copper zirconia catalyst with a lower catalyst loading of 0.15 g which gave consistent activity as indicated by complete conversion after the third recycle. The catalyst activity dropped down to 70% in an aqueous medium due to copper leaching in the reaction crude (Table 4.3).

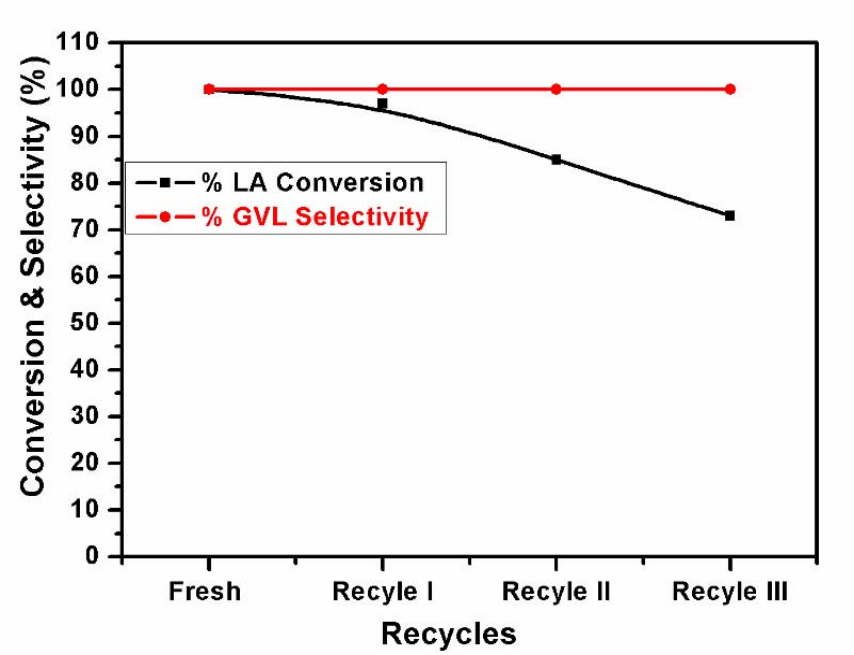

Figure 4.18. Recycle study of LA hydrogenation in water

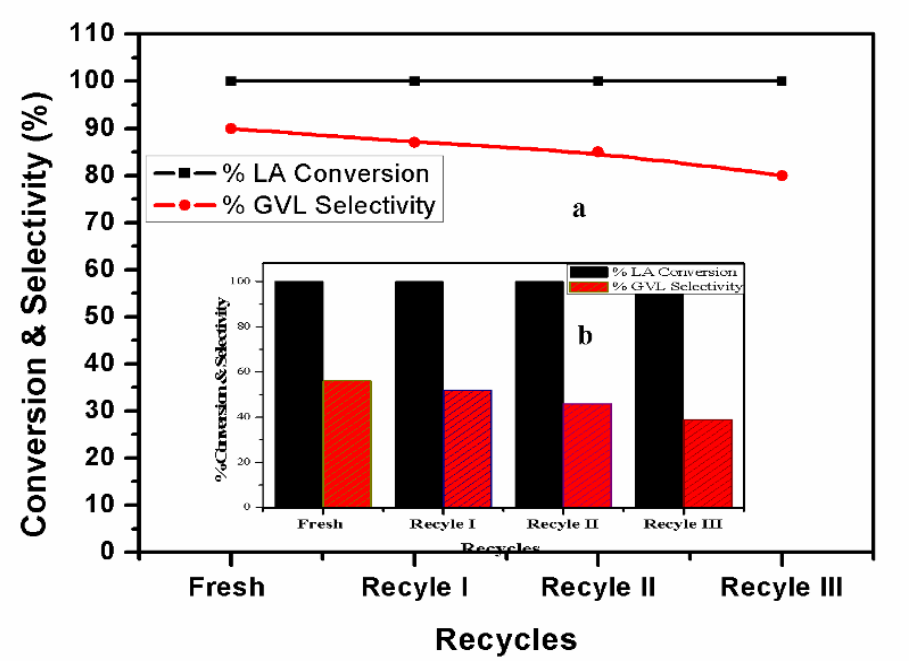

Figure 4.19. Recycle study of LA hydrogenation in methanol (a) 0.500 mg catalyst loading (b) 0.150 mg catalyst loading

4.3.4. Continuous hydrogenation of levulinic acid and its methyl ester to GVL

Since Cu on zirconia was established as the best non noble metal catalyst in batch reactor studies for LA hydrogenation to GVL, its time on stream activity was also studied. For this purpose, continuous hydrogenation of methyl levulinate and levulinic acid was studied over a fixed bed of catalyst (4 g) packed in a single tube reactor. Figure 4.20 shows a consistent conversion of 80 to 85 % was obtained for both the substrates, methyl LA and levulinic acid over a total period of 100 h. the selectivity to GVL achieved was >90%. This time on stream study confirms the suitability of the catalyst and process from scale up point of view.

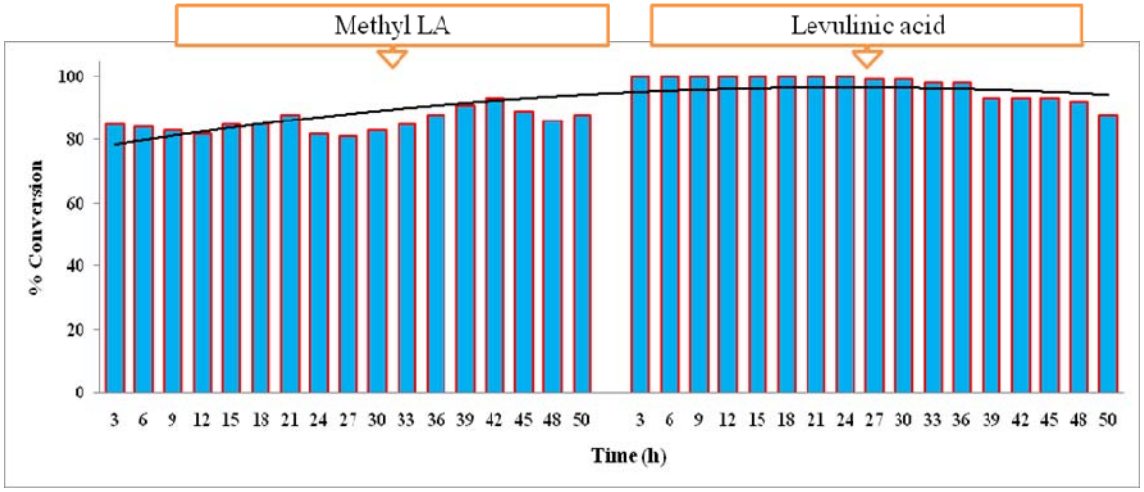

Figure 4.20. TOS of Cu-ZrO_2 catalyst for the hydrogenation of MeLA and LA

Reaction Conditions: Catalyst, 4 gm palletized (Cu: Zr); LA & MeLA Concentration, 5% (w/ w); Solvent, Methanol; Reaction Temperature, 200 °C; Feed Flow Rate, 0.5 ml/min; Hydrogen pressure, 500 psi; Reaction time,100 h.

4.4. Conclusion

Non-noble metal nanocomposite catalysts were developed for the first time by incorporating Zr and Al with copper, for selective hydrogenation of levulinic acid and its methyl ester to GVL. HRTEM revealed the particle size of copper in a range of 10–14 nm. Both XRD and Raman spectroscopy confirmed the formation of the Cu–ZrO_2 nanocomposite and also the presence of mixed oxide phases along with Cu^0. Both the catalysts showed complete conversion of LA and its ester with >90% selectivity to GVL. Interestingly, for LA hydrogenation in methanol only Cu–ZrO_2 could be recycled efficiently four times, with almost no leaching of the active metal. In methanol, the hydrogenation was found to proceed via the first step of the trans-esterification to the corresponding ester followed by its *in situ* hydrogenation to GVL.

4.5. References

1. M. J. Climent, A. Corma and S. Iborra, Green Chem. 13 (2011) 520.
2. J. J. Bozell, G. R. Petersen, Green Chem. 12 (2010) 539.
3. I. T. Horvath, H. Mehdi, V. Fabos, L. Boda, L. T. Mika, Green Chem. 10 (2008) 238.
4. G. W. Huber, S. Iborra, A. Corma, Chem. Rev. 106 (2006) 4044.
5. E. Manzer, Appl. Catal. A, 272 (2004) 249.
6. J. P. Lange, J. Z. Vestering, R. J. Haan, Chem. Commun. (2007) 3488.
7. C. V. Bylandtlaan, WO, 099111, (2007).
8. R. W. Christian, H. D. Brown, R. M. Hixon, J. Am. Chem. Soc. 69 (1947) 1961.
9. H. A. Schutte, R. W. Thomas, J. Am. Chem. Soc. 52 (1930) 3010.
10. R. A. Bourne, J. G. Stevens, J. Ke and M. Poliakoff, Chem. Commun. (2007) 4632.
11. Z. P. Yan, L. Lin and S. J. Liu, Energy Fuels 23 (2009) 3853.
12. J. P. Lange, R. Price, P. M. Ayoub, J. Louis, L. Petrus, L. Clarke, H. Gosslink, Angew. Chem. Int. Ed. 49 (2010) 4479.
13. R. J. Hann, J. P. Lange, US 0046399 (2011).
14. D. J. Braden, C. A. Henao, J. Heltzel, C. C. Maravelias, J. A. Dumesic, Green Chem. 13 (2011) 1755.
15. L. Deng, Y. Zhao, J. Li, Y. Fu, B. Liao, Q. X. Guo, ChemSusChem 3 (2010) 1172.
16. X. L. Du, L. He, S. Zhao, Y. M. Liu, H. Y. He, K. N. Fan, Angew. Chem. Int. Ed. 50 (2011) 7815.
17. D. J. Li, D. M. Lai, Y. Fu, Q. X. Guo, Angew. Chem. Int. Ed. 48 (2009) 6529.
18. X. Hu, C. Z. Li, Green Chem. 13 (2011) 1676.

19. L. Wang, W. Zhu, D. Zheng, X. Yu, J. Cui, M. Jia, W. Zhang, Z. Wang, React. Kinet. Mech. Catal. 101 (2010) 365.

20. L. C. Wang, Q. Liu, M. Chen, Y. M. Liu, Y. Cao, H. Y. He, K. N. Fan, J. Phys. Chem. C 111 (2007) 16549.

21. K. V. R. Chary, K. K. Seela, D. Naresh, P. Ramakanth, Catal. Commun. 9 (2008) 75.

22. Y. Wang, R. A. Caruso, J. Mater. Chem. 12 (2002) 1442.

23. M. K. Dongare, A. M. Dongare, V. B. Tare, E. Kemnitz, Solid State Ionics 152 (2002) 455.

24. C. Z. Yao, L. C. Wang, Y. M. Liu, G. S. Wu, Y. Cao, W. L. Dai, H. Y. He, K. N. Fan, Appl. Catal. A, 297 (2006) 151.

25. Z. HY, Z. YL, H. L, Z. ZY, W. HJ, L. YW, Catal. Commun. 9 (2008) 342.

26. X. Guo, D. Mao, G. Lu, S. Wang, G. Wu, Catal. Commun. 12 (2011) 1095.

27. K. Arata, Green Chem. 11(2009) 1719.

28. S. Xie, E. Iglesia, A. T. Bell, Chem. Mater. 12 (2000) 2442.

29. J. Wambach, A. Baikerb, A. Wokaun, Phys. Chem. Chem. Phys. 1 (1999) 5071.

30. L. Chen, H. Meng, L. Jiang, S. Wang, Chem.–Asian J. 6 (2011) 1757.

Chapter 5

Catalytic transfer hydrogenation of LA and its esters

In order to develop alternate route to GVL without using external hydrogen, catalytic transfer hydrogenation of LA to GVL was successfully demonstrated using isopropanol and formic acid as hydrogen donors over rationally designed montmorillonite (MMT) supported Ni and Ag-Ni/ZrO_2 catalysts, respectively. Ni-MMT catalyst using IPA showed the highest conversion of levulinic acid >99% with highest selectivity of >99% to GVL within 1h and it could be also efficiently recycled up to five times with consistent activity and selectivity. In this unique approach, the acidic MMT support catalyzed the LA esterification in the presence of secondary alcohol, which is also an efficient H_2 donor for CTH. In an alternate approach, Ag-Ni/ZrO_2 catalyst was developed for aqueous LA: FA, CTH system. The synergism of Ag and Ni was responsible for efficient FA decomposition and subsequent hydrogenation of LA. The magnetic nature of the catalyst offers its easy recovery for efficient recyclability. This approach is standardized for hydrogenation of several C_3-C_6 platform molecules in an aqueous medium.

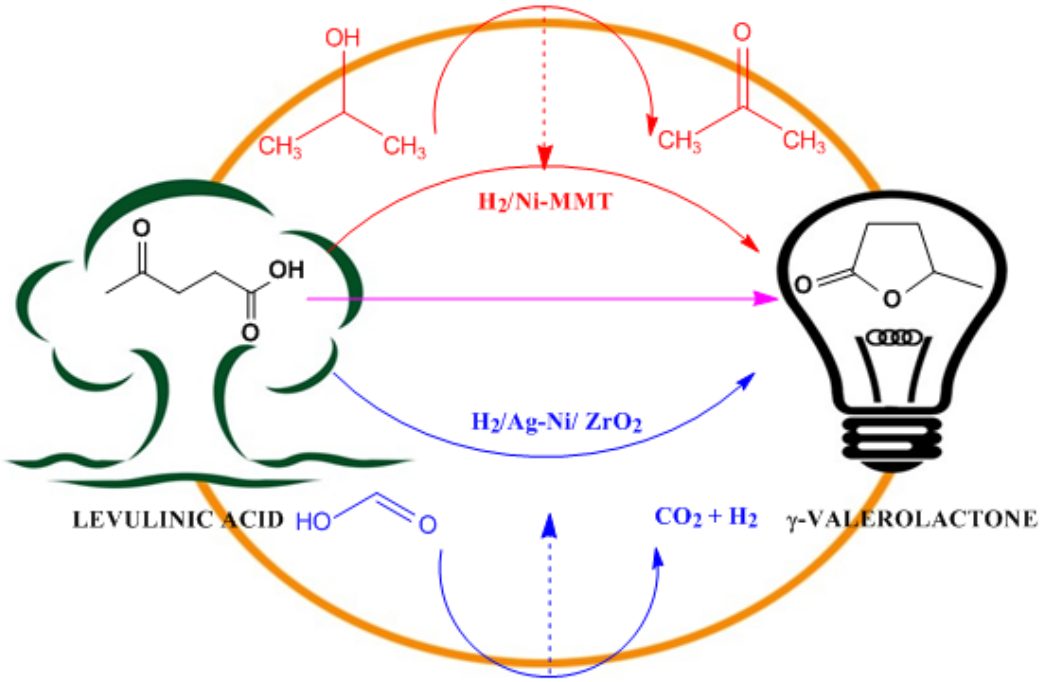

RSC Advances, RA-ART-09-2013-045384 [Revision]

Appl. Catal. B: Environmental [Communicated]

5.1. Introduction

The first generation biofuels are produced from sugars, starch, and vegetable oils. Although instrumental in developing the initial market for biofuels, these were not likely to fulfill the large volume demand of the transport sector as they were directly competing with the food products. A more promising feedstock is the lignocellulosic material, which is more abundant, has a lower cost, and is potentially more sustainable. Hence, strategies for the utilization of renewable sources which could replace petroleum based refinery, recently focused on the conversion of lignocellulosic biomass to the platform molecules. Since these bio-derived platform molecules include oxygen-rich functionality, the current refinery processes are inapplicable directly hence, it is necessary to design and develop new catalysts and novel strategies [1-4]. The production of γ-valerolactone (GVL) by hydrogenation of levulinic acid is a vital step in the developmental efforts on conversion of biomass to primary sources of platform molecules and their subsequent downstream valorization to commodity, fine chemicals, fuel and fuel additives [5,6]. Hydrolysis of lignocellulosic biomass to hexose sugars followed by their selective dehydration and rehydration to levulinic acid demonstrates the viability of chemo catalytic transformations from basic biomass feedstock for the production of chemicals for transportation fuels [7-10]. γ-valerolactone (GVL) has tremendous potential applications due to its energy density and allied chemical properties comparable to the conventional fuel [11-15] GVL obtained as a hydrogenation product of LA, is a versatile bio-fuel platform chemical, as it can be converted to valeric acid and directly into pentyl-valerate which is a renewable diesel additive. Valeric acid esterification with EG, 1,2 PDO or glycols gives di-valerates and tri-valerates with higher energy density [16-18]. GVL decarboxylation to butenes followed by oligomerisation gives liquid alkenes of > C8 for fuel application [19]. Both noble and non-noble metals (Ru, Pd, Pt, Ir and Cu, Ni) are active for the hydrogenation of levulinic acid using molecular hydrogen. However, the use of precious metal catalysts proposed for all these catalytic transformations makes the overall process economy unfavorable and at the same time, non-noble catalysts do not show stability in aqueous LA medium [20-27]. Also, majority of the studies on LA hydrogenation to GVL are on use of external high pressure H_2, which has a serious

drawback due to its hazardous nature. Moreover, use of an alternative H_2 source can make the process more environmental benign. In this regard, the best option to avoid the use of external H_2 is catalytic transfer hydrogenation (CTH) using either secondary alcohol or formic acid as H_2 donors [28-30]. For example, Deng et al. reported homogenous Ru salt along with homogenous base for LA hydrogenation [31,32] while Du et al. studied zirconia supported Au catalyst for transfer hydrogenation of butyl levulinate using butyl formate as a source of hydrogen [33]. Chia et al. reported liquid phase transfer hydrogenation of levulinic acid and its esters using secondary alcohol over metal oxide but suffers from poor yield (<50%) and very low catalyst substrate ratio (1:1) [34]. Tang et al. showed ethyl levulinate hydrogenation to GVL in presence of supercritical ethanol medium over zirconia catalyst. Due to higher reaction temperature of 250-300 ^{o}C the catalyst was deactivated and could not be recycled efficiently [35]. Recently, room temperature hydrogenation of ethyl levulinate to GVL is reported over Raney Ni catalyst in presence of isopropanol for CTH [36].

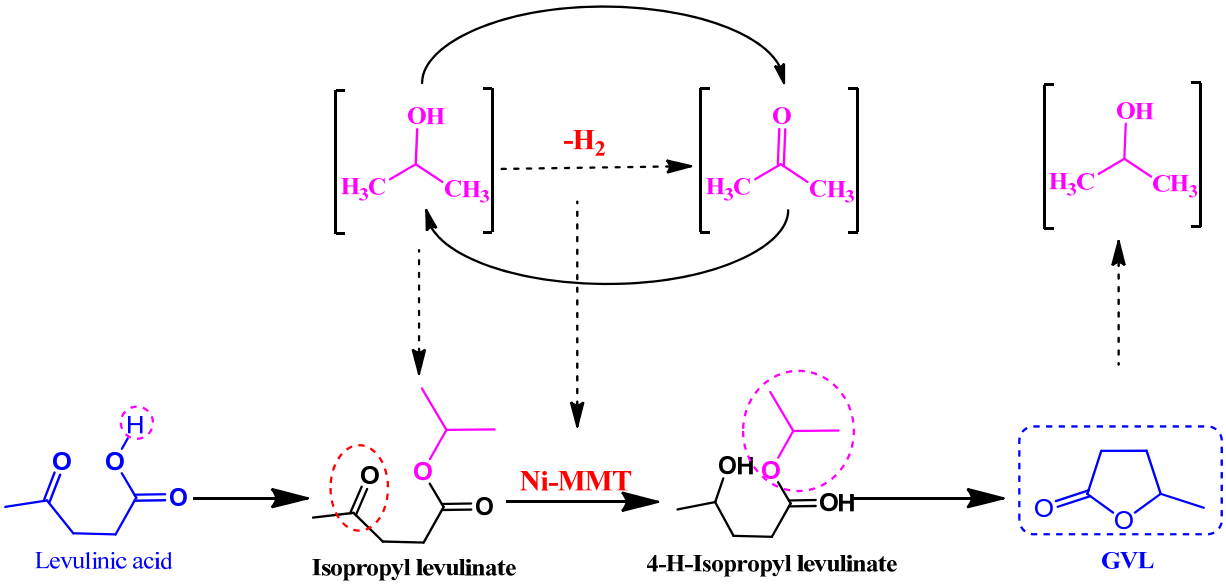

Scheme 5.1. Transfer hydrogenation of levulinic acid over Ni-MMT catalyst

Non-noble metals or their oxides such as bare Ni metal catalyst or metal oxides ZrO_2, MgO alone studied for CTH of levulinic esters to GVL are reported to give low yield of GVL (20-30%) inspite of high catalyst to substrate ratio (2:1, 3:1) over longer reaction

times (9, 16h). Non precious metal oxides reported for CTH involving Meerwein-Ponndorf-Verley reduction also did not show recyclability of the corresponding hydrogen donor. So, a bifunctional catalyst by combining the non-noble metal function with a suitable support would contribute to the efficient catalytic activity and stability for catalytic transfer hydrogenation reactions.

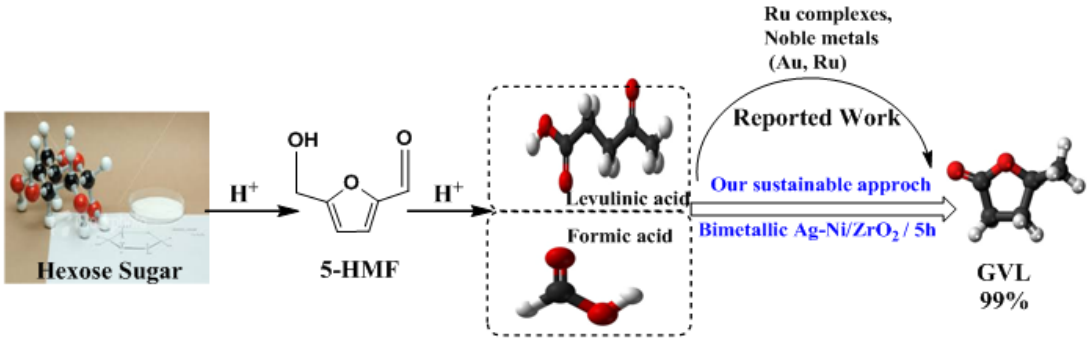

Scheme 5.2. Transfer hydrogenation of levulinic acid over Ag-Ni-ZrO_2 catalyst

Use of FA as a H_2 donor in particular, has an added advantage that the production of levulinic acid (LA) from cellulose is typically carried out using dilute mineral acid solutions which also produces equimolar amounts of formic acid (FA), via glucose and hydroxymethylfurfural (HMF) as intermediates. However, LA isolation and purification becomes complicated by the presence of intractable materials and use of external hydrogen for further hydrogenation to produce GVL. From this perspective, equimolar aqueous mixture of LA:FA as it is, can be converted to γ-valerolactone (GVL) via in-situ hydrogenation over recyclable and selective catalysts. This would lead to the most economical and sustainable process for GVL. However, hydrogen generations via dehydrogenation of FA as well as hydrogenation of LA are separately catalyzed by metal complexes dissolved in organic solvents [37-41] and supported noble metals. Since, all the reported heterogeneous catalysts until now consist of only noble metals having a high cost and scarce availability, the process is far from its large-scale practical applications. Hence, use of transition metals from the first row e.g. nickel nanoparticles (NPs) have been widely investigated as the catalysts for dehydrogenation as well as hydrogenation reactions [42-47]. Recently, bimetallic NPs have been investigated extensively as they were found to be more active than their single component counterparts for the

dehydrogenation of FA as well as for hydrogenation of levulinic acid. Some of these include Ag-Pd, Au-Pd, Au-ZrO_2 and Ag-pd-Co/C which either have high noble metal loading (>15%) or high catalyst loading (>1.5g) in the reaction [48]. The cost effectiveness without sacrificing the performance can be harnessed by an appropriate combination of a noble metal with a non-noble metal. The activity and selectivity of such catalysts will depend on the synergetic effect, metal composition, and particle size because FA decomposition to generate hydrogen has several unresolved issues, such as the need of precious metals (e.g., Pd, Rh), homogeneous base, metal complexes and severe reaction conditions [49].

We report here two different catalyst systems, supported Ni and Ag-Ni/$ZrO_2$for two different CTH routes to GVL from LA and its esters using IPA and formic acid, respectively. Among several combinations studied for CTH using IPA, MMT supported Ni showed the highest conversion of levulinic acid of >99% with highest selectivity of >99% to GVL within 1h, as shown in Scheme 5.1. Our catalyst could be also efficiently recycled up to five times with consistent activity and selectivity for catalytic transfer hydrogenation. The strong acidic nature and strength of MMT support enables to facilitate the esterification of LA as well as cyclization step while, Ni is responsible for hydrogenation of the carbonyl group. The metal leaching usually taking place in aqueous LA hydrogenation is easily avoided in our unique approach involving LA ester formation over the acidic MMT support in presence of the secondary alcohol which is also an efficient H_2 donor for CTH.

For GVL synthesis from aqueous mixture of LA:FA in which FA acts as a hydrogen donor, we developed a magnetically separable Ag-Ni-ZrO_2 which gave the complete conversion of LA and selectivity to GVL as shown in Scheme 5.2. More importantly, this hydrogenation process can be accomplished in presence of formic acid that is produced in the original acidic dehydration step. The success of this catalytic system will not only improve the atom economy of the process, but also will avoid the energy-intensive separation of LA from the mixture of LA and formic acid from the aqueous solution.

5.2. Experimental

All the catalysts (Ag-Ni-ZrO_2, ZrO_2, Ag-ZrO_2, Ni-ZrO_2 and Ru-ZrO_2) tested were prepared by using co-precipitation method and the detailed experimental procedure of their preparation have been described in chapter 2 (section 2.2.2.1). The catalysts were characterized by various techniques according to the procedure described in section 2.4. Activity of the prepared catalysts was evaluated for the hydrogenation of levulinic acid to γ-valerolactone and a typical experimental procedure is described in section 2.5.1. The quantitative analysis of liquid samples was carried out by gas chromatography method using FID detector, HP-5 capillary column and helium as a carrier gas. Other details of temperature programming method (60-190 ^oC) etc. are described in chapter II, section 2.6.

5.3. Results and discussion

5.3.1. CTH using IPA as a H_2 donor

Monometallic Ni catalysts on various supports were prepared for the purpose of CTH of LA using IPA as a solvent and as H_2 donor. In order to explain the variation in their performance, a systematic structural characterization was done, the results of which are discussed below.

5.3.1.1. Catalyst Characterization

5.3.1.1.1. BET surface area

The surface areas, pore volumes and average pore diameter of Ni catalysts on various supports along with bare Ni are presented in table 5.1. Among all the catalysts, bare Ni showed the least values while, the order varied for others catalysts as follows: Ni-Al_2O_3<Ni-ZrO_2<Ni-MMT<Ni-SiO_2<Ni-C. it is interesting to note that the activity (as discussed later, section 5.3.1.3.) of these catalysts did not vary according to their order of variation in the surface area and other physico-chemical properties e.g. Ni-MMT having the surface area much less (more than one third) than that of Ni-C (maximum surface area) showed the highest activity. Hence, the activity, selectivity trends need to be explained based on additional factors such as acidity, oxidation states etc. Since Ni-MMT catalyst showed the best activity for CTH of LA in IPA, its physico-chemical properties

were also compared with those of MMT support alone. It was observed that the reduction in surface area of parent MMT after Ni loading was due to the fact that Ni NPs occupied the inter lattice spaces which was also confirmed by the XRD studies as discussed below.

Table.5.1. Physico-chemical characterization of supported Ni catalysts

Sr.No	Catalyst	Surface Area (m^2/gm)	Pore volume (cc/g)	Average Pore diameter (A^0)
1	50% Ni-MMT	34	0.074	43
2	50% Ni-Al_2O_3	18	0.059	29
3	50% Ni-SiO_2	60	0.099	34
4	50% Ni-ZrO_2	20	0.084	78
5	50% Ni-C	145	0.129	13
6	Na-MMT	98	0.104	51
7	Bare Ni	12	0.012	11

Since, Ni-MMT catalyst showed the highest activity for CTH of LA, the detailed characterization of this catalyst was carried out, which is discussed below.

5.3.1.1.2. XRD

XRD patterns of support MMT, bare Ni and Ni-MMT before and after reduction are shown in Figure 5.1. The appearance of indexed diffraction peak of montmorillonite at 2θ =26.2^o, belongs to quartz phase of silica along with a peak at 2θ = 20.05^o (211) which almost disappeared after insertion of Ni NPs in its lattice structure Although, bare Ni and activated Ni-MMT catalysts showed a broad hump at 2θ =43.5^o corresponding to metallic Ni, the recovered sample (Figure 5.1, d) showed XRD peaks at 2θ = 43.5^o (111), 51.1^o (200) and 78.3^o (220) which could be attributed to face centered cubic structure of metallic Ni, due to *in situ* reduction of Ni species under reaction condition. The average crystallite size evaluated from Scherer equation was found to be 30–40 nm [50, 51].

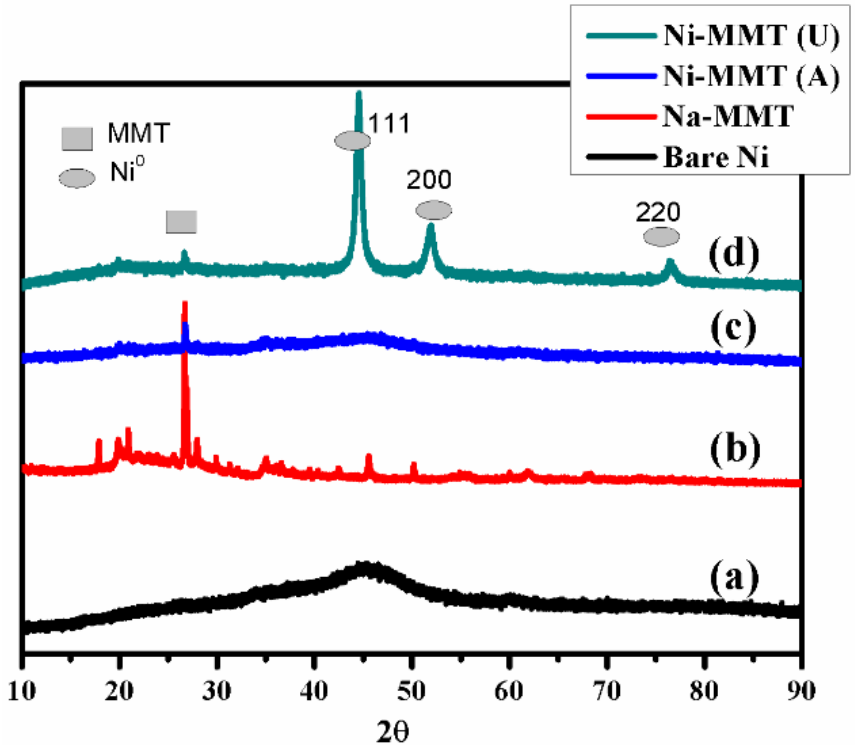

Figure 5. 1. XRD patterns of Ni-MMT catalyst (a) Bare Ni (b) Na^{+}- MMT (c) Activated Ni-MMT (d)Used Ni-MMT.

5.3.1.1.3. HRTEM

The high resolution transmission electron microscopy (HRTEM) images as shown in Figure 5.2 revealed an average particle size of Ni nanoparticles to be in the range of 20–40 nm. The morphology of Ni-MMT nanocomposite was found to be spherical in the form of chains of beads of metal particles. The selected area of the image indicates the Ni nanoparticles incorporated with chain beads of MMT support [52].

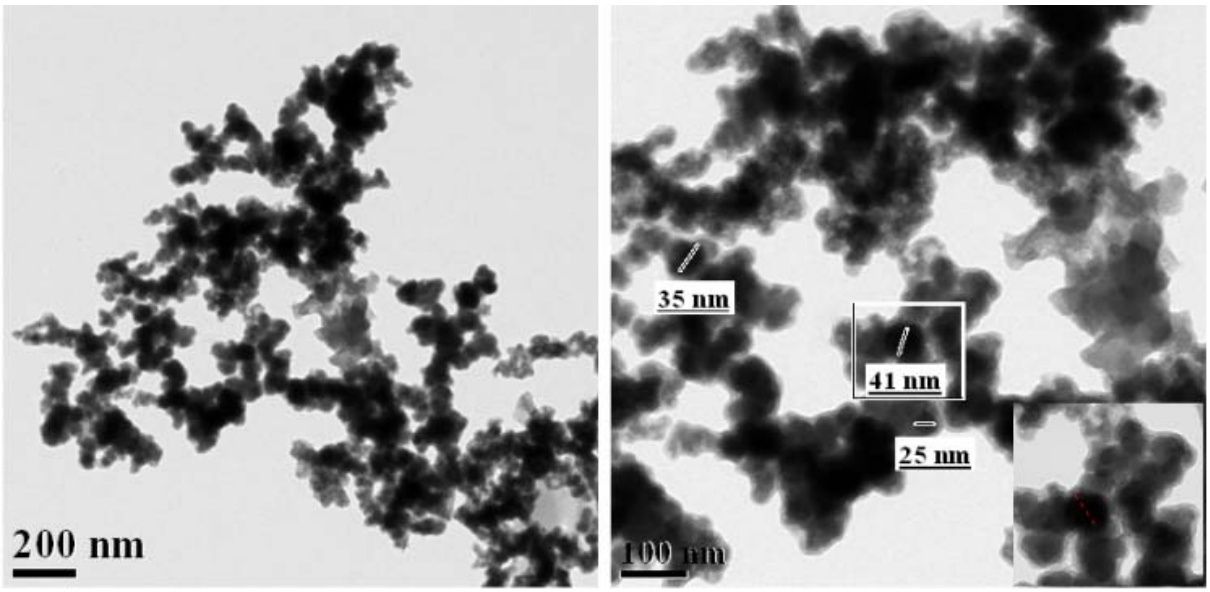

Figure 5.2. HR-TEM images of activated Ni-MMT catalysts

5.3.1.1.4. XPS

Figure 5.3(A) presents the XPS of Ni $2p_{3/2}$ of activated Ni-MMT sample. The intense doublet at 855.7 and 856.6 eV represents Ni oxide phase in the form of NiO and $(NiOH)_2$, respectively. The satellite peak was observed at 862.2 eV which could be assigned to hydroxide and oxide species of Ni such as NiO and $Ni(OH)_2$ and a small peak at 852.4 eV was attributed to metallic nickel (Ni^o). Figure 5.4 shows, the binding energies at 530.1 and 531.3 eV of O1s indicating oxygen was present in the form of NiO and hydroxide $Ni(OH)_2$. Figure 5.3(B) shows the Ni 2p XPS of bare Ni-MMT sample, in which the peaks at 852.1, 854.2 and 855.4 eV represents to Ni in the form of Ni^o and NiO respectively. Similarly, the O1s spectra of sample shows two peaks at 529 and 529.9 eV which was corresponds to oxygen present in environment of NiO as shown in Figure 5.4 (B). While, in case of used Ni-MMT catalyst as shown in Fig 5.3(C), XPS peaks in the range of 852 to 856.8 eV were assigned to the Ni present in the form of metallic Ni, NiO and $(NiOH)_2$ which was in accordance with the O1s spectra showing peaks at binding energies of 530.1, 532.2 and 533.2 eV respectively, as shown in Figure 5.4 (C) [53, 54]. Table 5.2 shows the extent of Ni metal, NiO and Ni $(OH)_2$ evaluated for fresh Ni-MMT and was found to be 10%, 64% and 26%, respectively. However, the increase in the

concentration of metallic species by two and four times in both bare Ni and used Ni-MMT sample as compared to the activated Ni-MMT, matched very well with the XRD results. The higher extent of metallic Ni, in the used sample was obvious due to the *in situ* reduction of non-zero Ni species under reduction conditions.

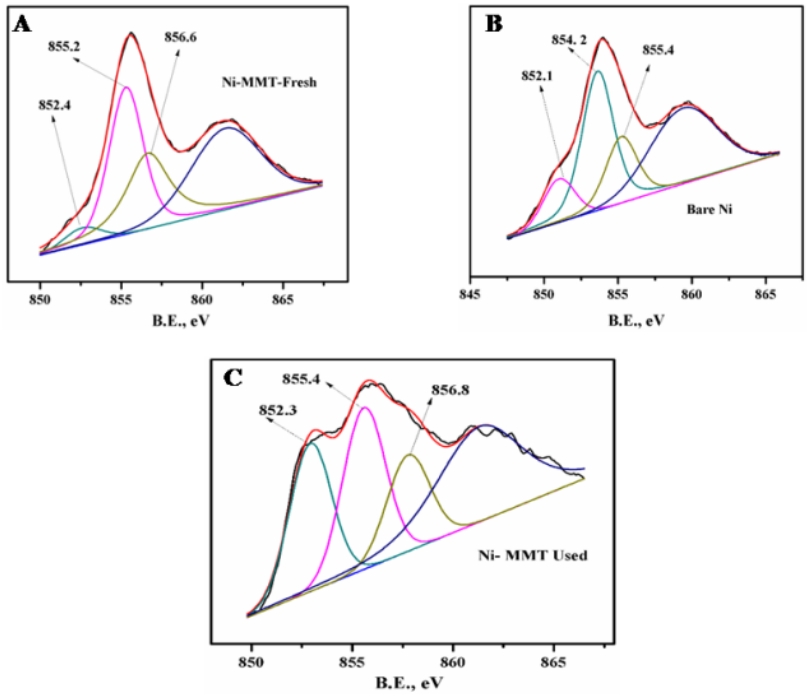

Figure 5.3. XPS study of nickel (2p) (A) Fresh Ni-MMT (B) Bare Ni (C) Used Ni-MMT

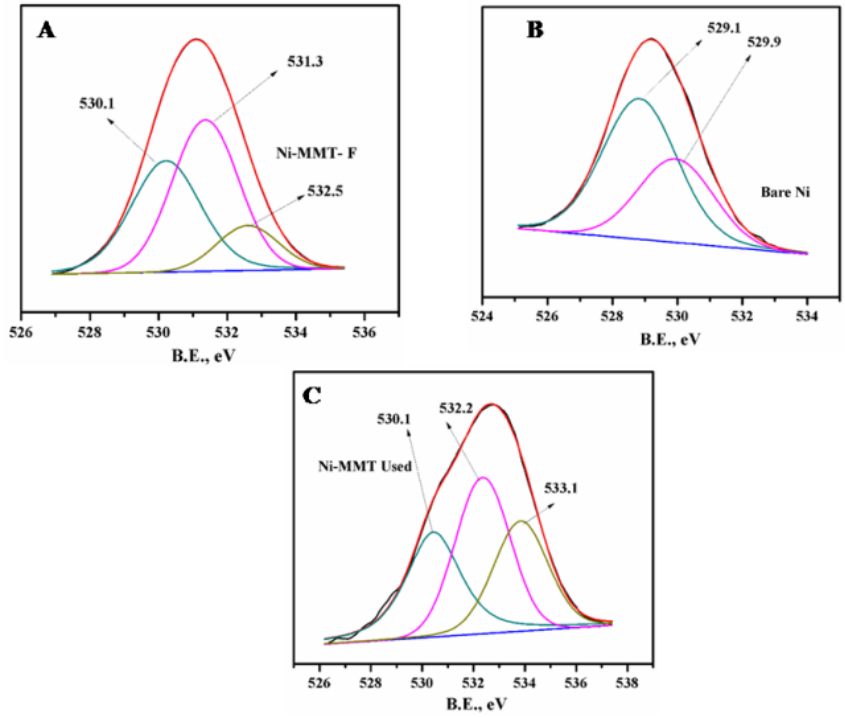

Figure 5.4. XPS study of O1s (A) Activated Ni-MMT (B) Bare Ni (C) Used Ni-MMT.

Table 5.2. XPS study of Ni catalysts

Sample	**Species**		
Fresh 50%-Ni-MMT	**Ni^0**	**NiO**	$Ni(OH)_2$
BE	852.4	855.2	856.6
%	**9.31**	**64.37**	**26.31**
Bare Ni NP's	**Ni^0**	**NiO**	$Ni(OH)_2$
BE	852.1	854.2	855.4
%	**18.5**	**54.17**	**27.29**
Used 50%-Ni-MMT	**Ni^0**	**NiO**	$Ni(OH)_2$
BE	852.9	855.4	856.8
%	**35.99**	**40.05**	**23.94**

5.3.1.1.5. FTIR

Figure 5.5 shows FTIR of MMT which is helpful in estimating the degree of dissolution of layered structure. The parent MMT exhibited intense absorption band at ~1034 cm^{-1} for Si–O stretching vibrations of tetrahedral layer while the bands at 522 and 460 cm^{-1} were due to Si–O–Al and Si–O–Si bending vibrations, respectively. Another band near 800 cm^{-1} was characteristic of amorphous silica which was ascribed to after pretreatment

of MMT as well as the absorption bands at 3633 and 1645 cm^{-1} were due to stretching and bending vibrations of -OH groups of Al–OH, respectively. Ni-MMT sample showed a shift in band from ~1034 cm^{-1} to ~1003 cm^{-1}, indicating the changes in bonding environment in a tetrahedral layer of MMT. As expected, bare Ni did not show any prominent peaks of IR stretching [55, 56].

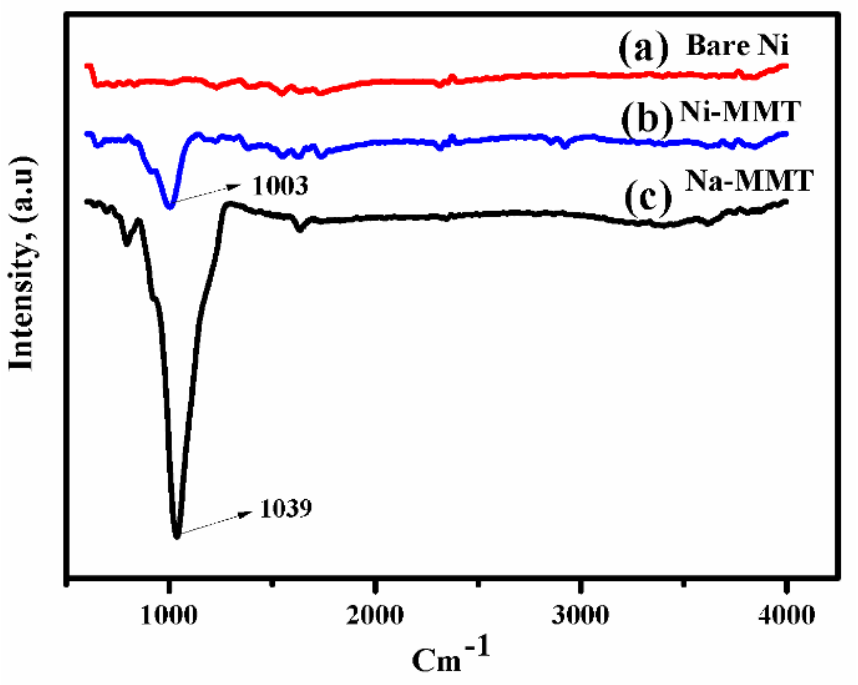

Figure 5.5. FTIR study of Ni catalysts (a) Bare Ni (b) Activated Ni-MMT (c) Na-MMT

5.3.1.1.6. DR-UV

DR-UV study of Ni^{+2}-MMT, Ni-MMT and bare Ni are shown in Figure 5.6. It was observed that as prepared sample of Ni-MMT before reduction showed broad surface plasmon resonance (SPR) absorption band in the range of 300-700 nm which could be ascribed to NiO. However, both reduced Ni-MMT and bare Ni did not show any prominent peaks of absorption bands of NiO, confirming the formation of metallic nanoparticles of Ni after reduction by $NaBH_4$ [57].

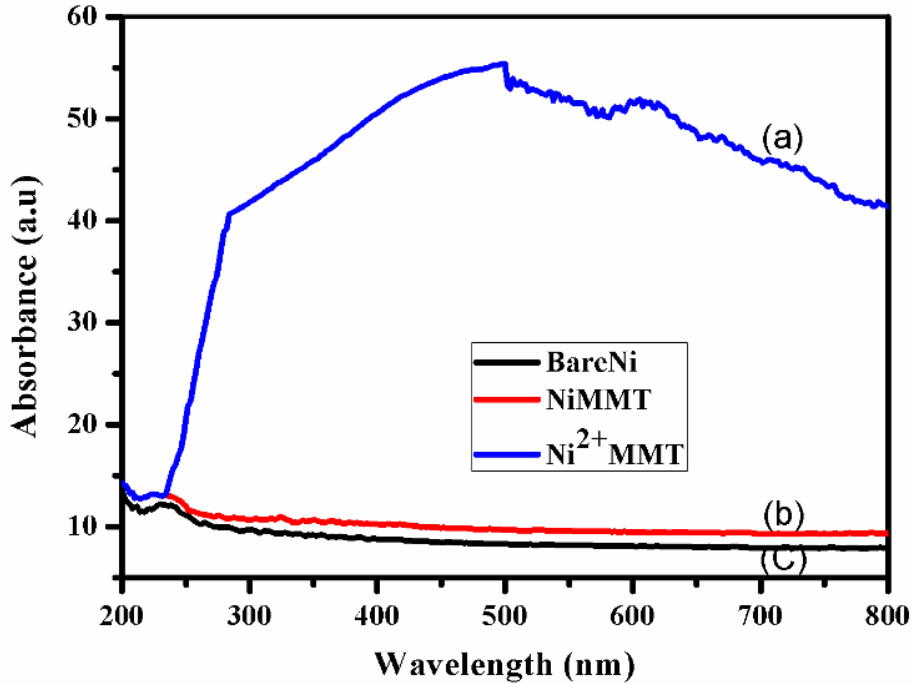

Figure 5.6. DR-UV study of Ni catalysts (a) Ni^{+2}-MMT (b) Activated Ni-MMT (c) Bare Ni

5.3.1.1.7. NH_3-TPD

Figures 5.7 and 5.8 show NH_3-TPD profiles and Py-IR for various supported nickel catalysts, respectively. Among these catalysts, Ni-MMT showed broad peaks of NH_3 desorption in a high temperature region of 550–650 °C, indicating the presence of strong acid sites. Other two catalysts (Ni-ZnO and Ni-C) showed NH_3 desorption peaks in the temperature region from 300-400 ^oC and 100-200 ^oC respectively, while Ni-Al_2O_3 catalyst showed broad NH_3 consumption peak in the range of 300-400 ^oC. This study confirmed the strongest acid strength of Ni-MMT catalyst which was favorable for LA esterification and cyclization of 4-hydroxy IPA-LA to GVL.

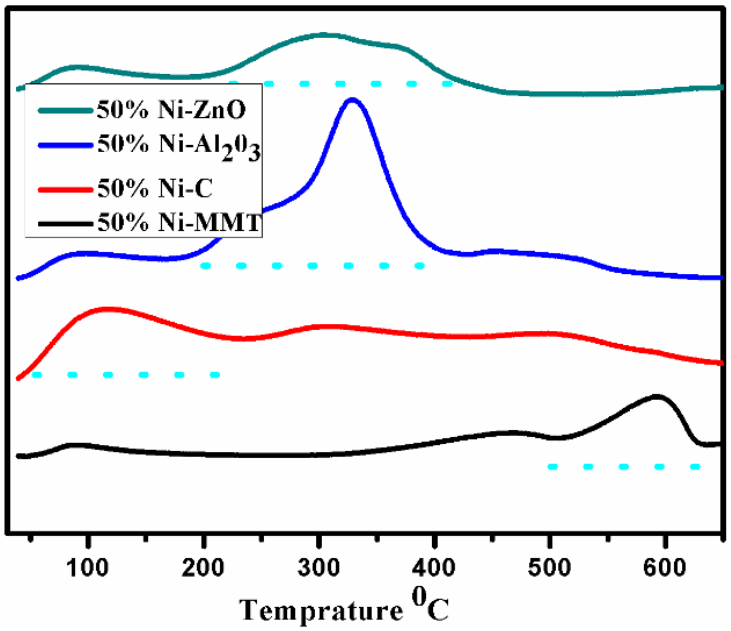

Figure 5.7. NH_3-TPD study of Ni catalysts

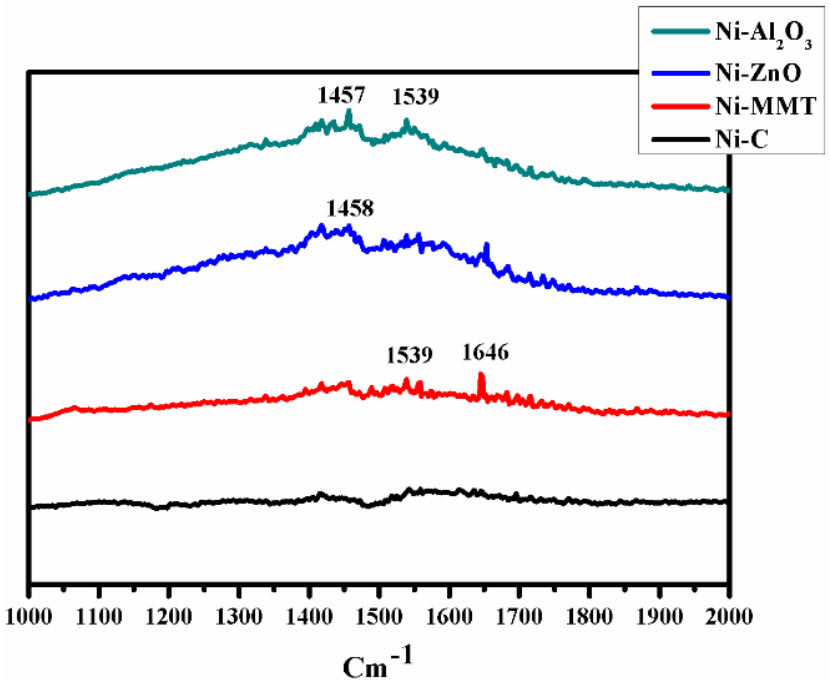

Figure 5.8. Py-IR study of supported Ni catalysts

In order to distinguish between the acid sites, Py-IR of various supported Ni samples were also studied and the results are presented Figure 5.7. Ni-MMT catalyst showed distinct peaks at 1539 and 1642 cm^{-1} due to Brønsted acid sites while Ni-ZnO and Ni-Al_2O_3 showed preferably the presence of Lewis acid sites as evidenced by the peaks at 1457-1458 cm^{-1}. The carbon supported Ni catalyst did not show any characteristics peaks of acidic nature. This study clearly suggests that high acidic strength and Brønsted acidic nature of MMT supported Ni play an important role in release of hydrogen from secondary alcohol by selective β-H elimination as well as esterification and cyclization involved in levulinic acid hydrogenation pathway to form GVL [58].

5.3.1.1.8. H_2-TPR

Figure 5.9 (A-E) shows the H_2 TPR of all the nickel catalysts studied in this work. All the samples exhibited a broad band of H_2 consumption in the range of 400–700 °C. The shape of the H_2 consumption peak was asymmetric with a shoulder or a tail, as a result of a complex overlapping of several elemental reduction processes such as sequential reduction from NiO to Ni^0. The peak at highest temperature of >600 ^oC for both Ni-ZrO_2 and Ni-Al_2O_3 samples requires more H_2 for reduction to the metallic form of Ni while, the easy reducibility of Ni-MMT as indicated by a peak at lower temperature 534 ^oC contributed to its greater activity for catalytic transfer hydrogenation reaction [59].

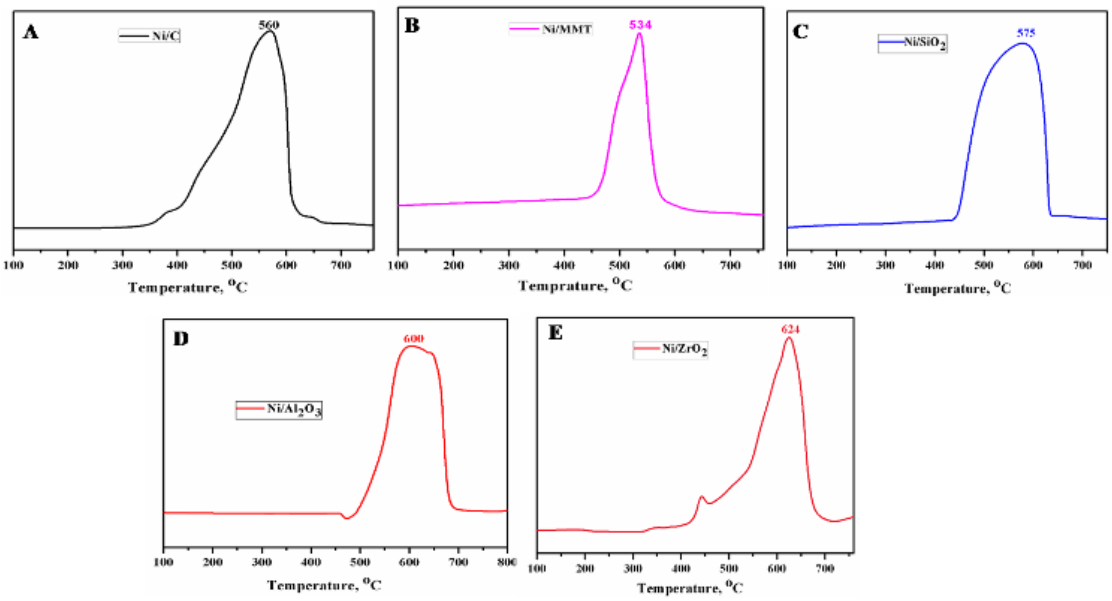

Figure 5.9. H_2-TPR study of supported Ni catalysts

5.3.1.2 Activity testing

5.3.1.2.1. Catalyst screening in a batch operation

The performance of various catalysts for transfer hydrogenation of levulinic acid to GVL using isopropanol (IPA) as a hydrogen donor is shown in Table 5.3. The MMT support alone was not effective for dehydrogenation of IPA as well as hydrogenation of LA efficiently, as confirmed by only 2% selectivity to the desired GVL with 58% conversion of LA (entry 1, Table 5.3). On the other hand, bare Ni showed 69 % conversion with 52 % selectivity to GVL. However, in combination of with the support MMT, Ni efficiently catalyzed LA hydrogenation with complete conversion and >99% selectivity to GVL which is two to five times higher than bare Ni and the support. All other supported (Al_2O_3, SiO_2, ZnO, ZrO_2 and C) Ni catalysts gave conversion ≤ 90% for LA hydrogenation with GVL selectivity in the range of 35-90%. The lowering of GVL selectivity was due to the unconverted intermediates, isopropyl LA and 4-hydroxy IPA-LA (Scheme 5.1). The highest activity of Ni/MMT catalyst could be explained by its highest acidity and the presence of both Brønsted/Lewis acid sites as evaluated by NH_3-TPD and Py-IR. As reported, LA hydrogenation to GVL is a facile reaction with highest activity and selectivity to GVL over the catalyst systems containing metal combined with

Brønsted acid sites. For example, Amberlyst-70 with 5% Ru/C catalyst was active for LA hydrogenation with 99% selectivity to GVL under mild operating conditions [60]. A plausible reaction pathway could be proposed involving first esterification of levulinic acid in presence of isopropanol to give isopropyl levulinate with simultaneous of isopropanol to release hydrogen by β-H elimination giving 4-hydroxy IPALA followed by its cyclization to GVL with isopropanol as a byproduct.

Table 5.3. Catalytic screening of LA hydrogenation in IPA

Entry	Catalyst	Conversion (%)	Selectivity (%)		
			GVL	IPA-levulinate	4-H-IPA-levulinate
1	50% Ni-MMT	99	99	0.01	**1**
2	50 % Ni/Al_2O_3	99	90	0.01	**10**
3	50 %Ni/SiO_2	95	40	58	**2**
4	50%$Ni-ZrO_2$	97	89	10	**2**
5	50%Ni-C	88	69	28	**3**
6	50% Ni-ZnO	92	35	64	**1**
7	Na-MMT	58	2	97	**1**
8	Bare Ni	69	52	40	8

Reaction conditions: Levulinic acid, 5% (w/w); solvent, IPA (95 mL); metal loading, 50%; temperature, 200 ^oC ; N_2 atm; catalyst, 0.5 g; reaction time, 1h.

Use of isopropanol for CTH is highly beneficial, as it serves (i) a protecting group for levulinic acid thus, preventing metal leaching due to free carboxylic acid, (ii) efficient hydrogen donor for hydrogenation and forming acetone which could be recycled over metal surface to regenerate isopropanol. For selective dehydrogenation of IPA followed by hydrogenation of LA to GVL requires strong metal support interaction while, acidic strength of the support plays an important role to enhance the activity for LA esterification as well as for the cyclization step and metallic sites are involved in selective hydrogenation of LA ester to GVL.

5.3.1.3. Effect of reaction parameters

5.3.1.3.1. Solvent Screening

The choice of a suitable solvent as a H_2 donor is very important in CTH reaction. Hence, various C_1-C_4 alcohols were screened for the CTH of LA to GVL over the best catalyst, Ni-MMT and the results are shown in Table 5.4. The use of primary alcohols (methanol to n-butanol) for transfer hydrogenation of levulinic acid did not show complete conversion and the selectivity to GVL was in the range of only 1-7%, due to unconverted respective esters of levulinic acid as well as the primary alcohols were poor hydrogen donors for CTH processes. This is due to the fact that primary alcohols eliminate H atom to form alkoxy group which causes poisoning of the catalysts responsible for poor activity towards the transfer hydrogenation of LA.

Table 5.4. Solvent screening for CTH of LA to GVL over Ni-MMT catalyts

Solvent	% Conversion	Levulinic esters	GVL	Others
Methanol	99	99	1	<0.01
Ethanol	99	98	2	<0.01
n-Propanol	99	95	4	1
n-Butanol	99	90	7	3
Isoproanol	99	<0.01	99	1
Isobutanol	99	<0.01	99	1

Reaction conditions: Levulinic acid, 5% (w/w); solvent, (MeOH, EtOH, n-PrOH, n-BuOH, isoPrOH and isoBuOH) (95 mL); Metal loading, 50%; temperature, 200 ^oC; N_2 atm; catalyst, 0.5 g; reaction time, 1h.

As against this, the use of secondary alcohols (isopropanol, isobutanol) as a hydrogen donor for transfer hydrogenation gave complete conversion of levulinic acid with 99% selectivity to the desired product GVL. It clearly suggests that in the catalytic transfer hydrogenation through Meerwein–Ponndorf–Verley (MPV) reaction, the hydrogen donor plays an important role in the release of H-atoms required for the reduction step [34, 36].

5.3.1.3.2. Effect of metal loading

Figure 5.10 shows the effect of metal loading on conversion and selectivity for hydrogenation of levulinic acid at 200 ^{o}C. It was found that selectivity to GVL decreased from 99 to 61% with decrease in active metal loading of Ni from 50 to 10%. The conversion of levulinic acid slightly decreased at lower metal loading due to the formation of esterification product. The decrease in selectivity with decrease in metal loading could be due to less availability of the active sites on the catalyst surface for the hydrogenation of an intermediate isopropyl levulinate to 4-hydroxy Isopropyl levulinate followed by its cyclization to GVL.

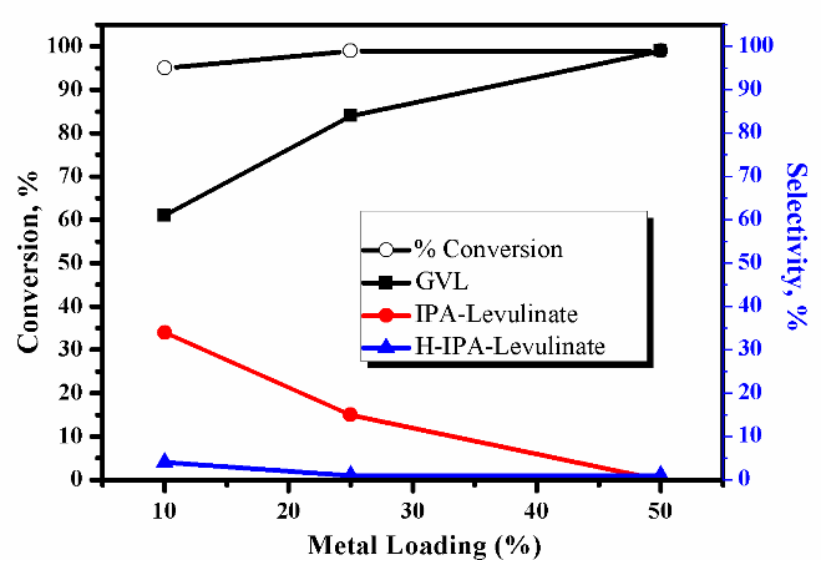

Figure 5.10. Effect of metal loading on CTH of LA

Reaction conditions: Levulinic acid, 5% (w/w); solvent, IPA (95 mL); temperature,200 ^{o}C; N_2 atm; catalyst, 0.5 g; Metal loading, 10 – 50%; reaction time, 1h.

5.3.1.3.3. Effect of substrate loading

Further study on effect of concentration of levulinic acid on conversion and selectivity was performed for transfer hydrogenation of levulinic acid to achieve the maximum productivity of GVL. Figure 5.11 shows that the conversion of LA decreased from 99 to 79% with increase in levulinic acid concentration from 5 to 20%. However, the selectivity to GVL lowered by two and half times (39%) with increasing concentration of

LA upto four times because the limiting number active sites of catalyst were available with higher substrate concentration. Another reason of dropdown of activity and selectivity in hydrogenation reaction with increase in substrate loading was the accumulation of unconverted IPA-LA and 4-hydroxy IPA-LA.

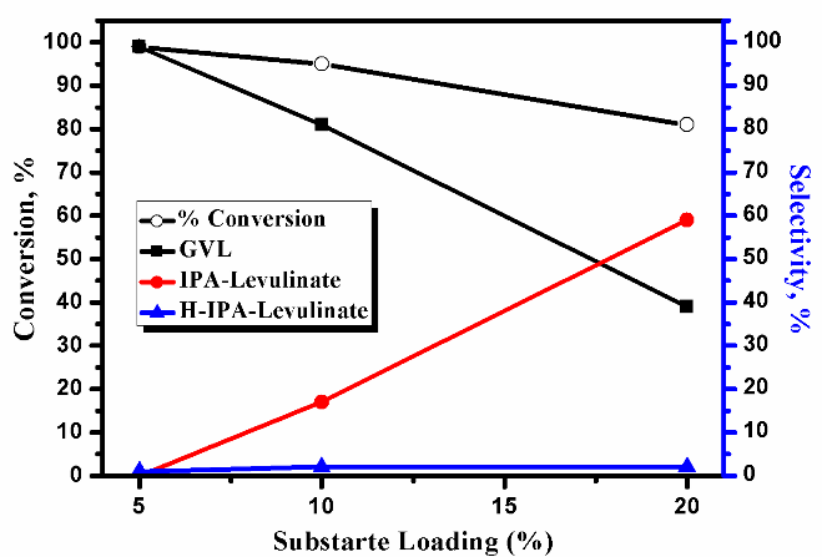

Figure 5.11. Effect of substrate concentration on CTH of LA

Reaction conditions: Levulinic acid, 5% (w/w); solvent, IPA (95 mL); Metal loading, 50% ; temperature, 200 ^{o}C; N_2 atm; catalyst, 0.5 g; reaction time, 1h.

5.3.1.3.4. Effect of solvent ratio

To check the stability of catalyst for transfer hydrogenation as well as to assess the requirement of minimum concentration of hydrogen donor for transfer hydrogenation, a mixture of isopropanol with water with their varying compositions was used. Figure 5.12 shows that the conversion of levulinic acid decreased from 99 to 79% with increase in molar ratio of water to isopropanol from 10:90 to 50:50. While, the selectivity to GVL decreased substantially from 99 to 39% with increase in water ratio upto 50:50 due to deactivation of the metal sites in an aqueous medium. Nevertheless, the rate of esterification was almost constant as evident from unconverted isopropyl levulinate and 4-hydroxy IPALA remaining upto 60%. In order to study the influence of oxidized form of hydrogen donor for competitive adsorption on active surface of catalyst, CTH

experiments with increase in molar ratio of acetone to IPA from 10:90 to 50:50 were also carried out. As can be seen from Figure 5.13, a consistent conversion 99% of LA with 99% selectivity to GVL was achieved for all the molar ratios of acetone to IPA studied in this work. It clearly confirmed that no adverse effect of recycled hydrogen donor was observed on activity and selectivity for catalytic transfer hydrogenation of levulinic acid to GVL.

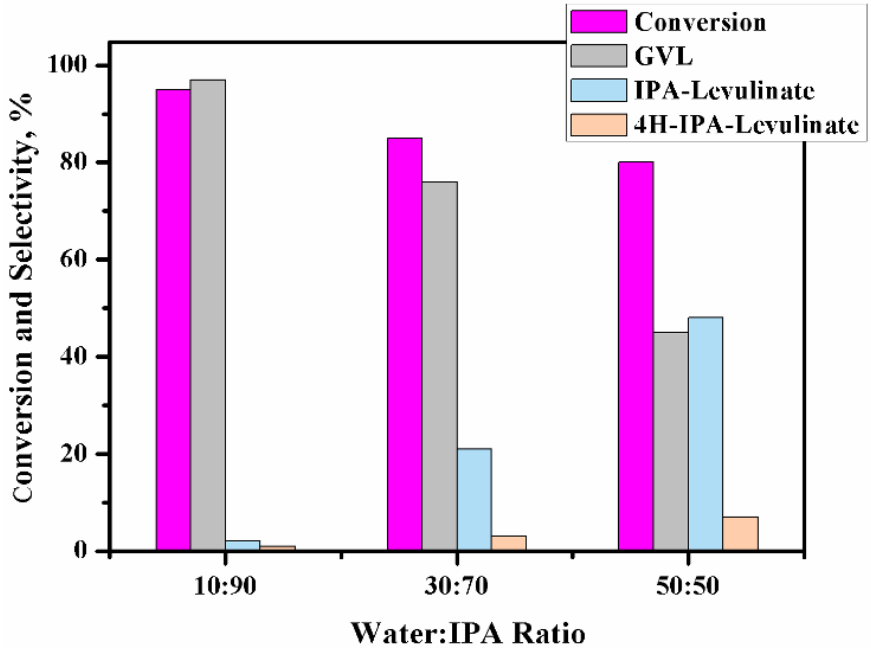

Figure 5.12. Effect of water & IPA ratio on CTH of LA

Reaction conditions: Levulinic acid, 5% (w/w); solvent, IPA (95 mL); temperature, 200 ^{o}C; N_2 atm; catalyst, 0.5 g; reaction time, 1h.

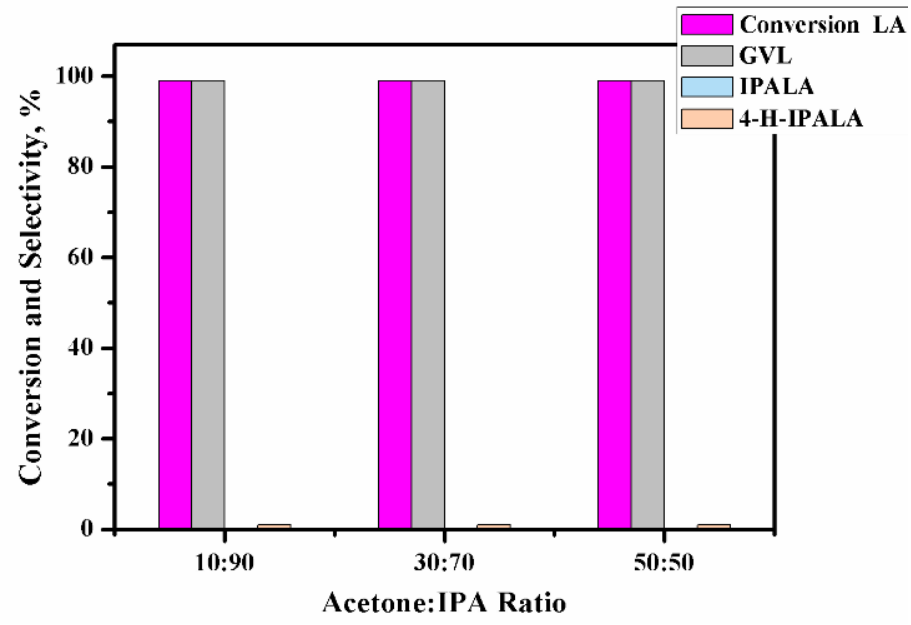

Figure 5.13. Effect of Acetone & IPA ratio on CTH of LA

Reaction conditions: levulinic acid, 5% (w/w); solvent, IPA (95 mL); Metal loading, 50%; temperature, 200 ^{o}C; N_2 atm; catalyst, 0.5 g; reaction time, 1h.

5.3.2. Catalyst Recycle study

The recycle study for Ni-MMT catalyst was carried out as follows [27, 63]. After the first hydrogenation run was complete, the reaction crude was allowed to settle down and supernatant clear product mixture was removed from the reactor. A fresh charge of reactants was added to the catalyst residue retained in the reactor and the subsequent run was continued. This procedure was followed for four subsequent runs and the results are shown in Figure 5.14. The catalyst could be efficiently reused up to five times without any drop in the activity and selectivity for transfer hydrogenation of levulinic acid to GVL in isopropanol as a solvent and as a hydrogen donor. A slight decrease in selectivity from 99 to 95% could be due to loss of catalyst during sampling from time to time.

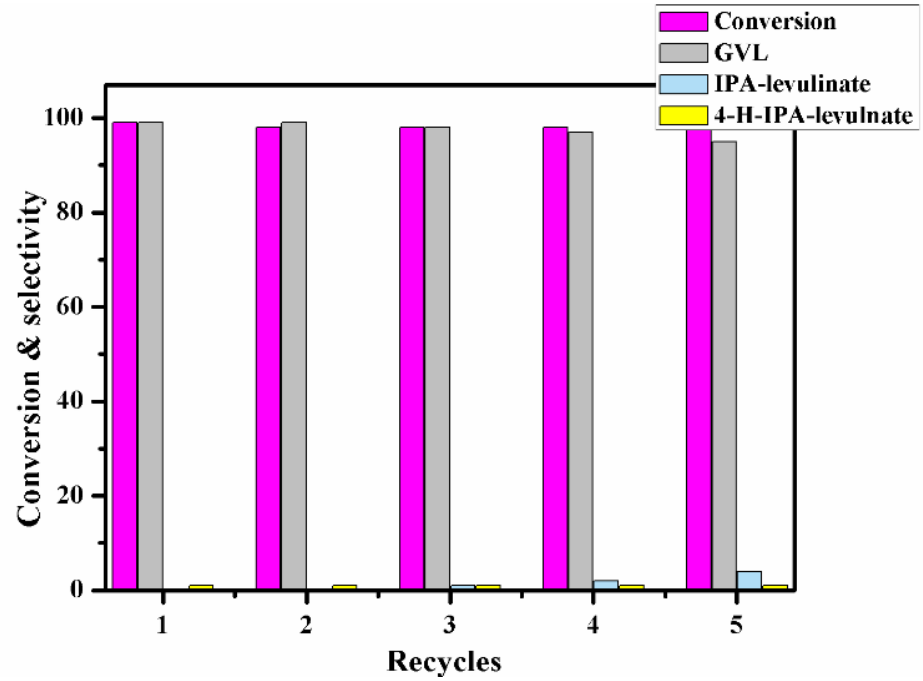

Figure 5.14. Recycle study of catalytic transfer hydrogenation of LA

Reaction conditions: levulinic acid, 5% (w/w); solvent, IPA (95 mL); Metal loading, 50%; temperature, 200 ^{o}C; N_2 atm; catalyst, 0.5 g; reaction time, 1h.

5.3.3. CTH using FA as H_2 donor

Several zirconia supported mono and bimetallic Ag-Ni catalysts were evaluated for CTH of LA to GVL in an aqueous LA:FA mixture in which, FA acts as the hydrogen source. Among these, Ag-Ni-ZrO_2 catalyst showed the best performance hence it was thoroughly characterized to understand the active species catalyzing both FA decomposition and LA hydrogenation and these results are discussed in details below.

5.3.3.1. Catalyst Characterization

5.3.3.1.1. X-ray diffraction

The typical X-ray diffraction (XRD) patterns of ZrO_2, Ag-ZrO_2, Ni-ZrO_2 and Ag-Ni-ZrO_2 catalysts are presented in Figure 5.15. All these samples exhibit broad peaks at 2θ = 28.5^{o}, 30.1^{o} (111), attributed to the mixed tetragonal and monoclinic phases of zirconia. In Ag-ZrO_2, the peaks at 2θ= 38.1^{o}, 44.4^{o}, 64.71^{o} and 77.4^{o} (JCPDS-4784) correspond to the reflections of the (111), (200), (220), and (311) crystalline planes of cubic Ag, which confirmed the reduction of Ag^{+} to Ag^{o} in Ag-ZrO_2 [61].

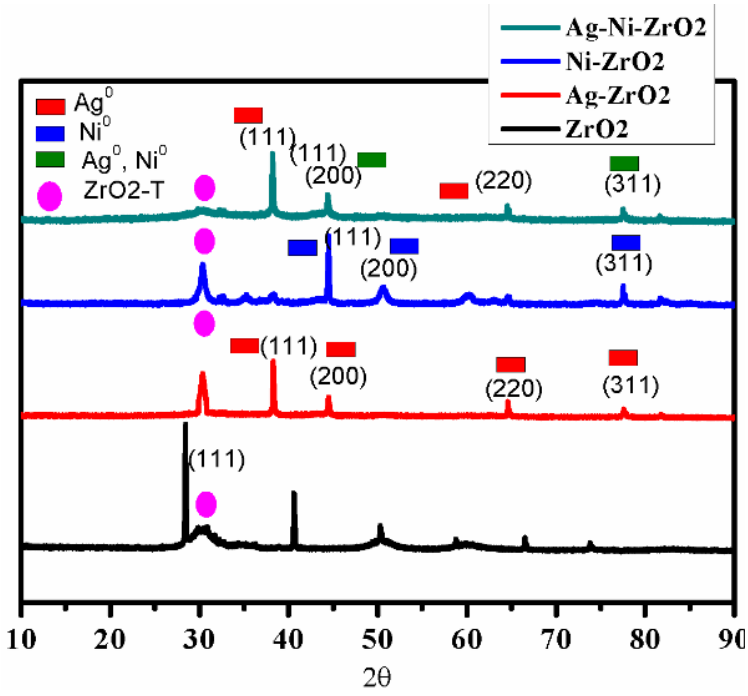

Figure 5.15. XRD patterns of ZrO_2, Ag/ZrO_2, $Ni\text{-}ZrO_2$ and $Ag\text{-}Ni\text{-}ZrO_2$

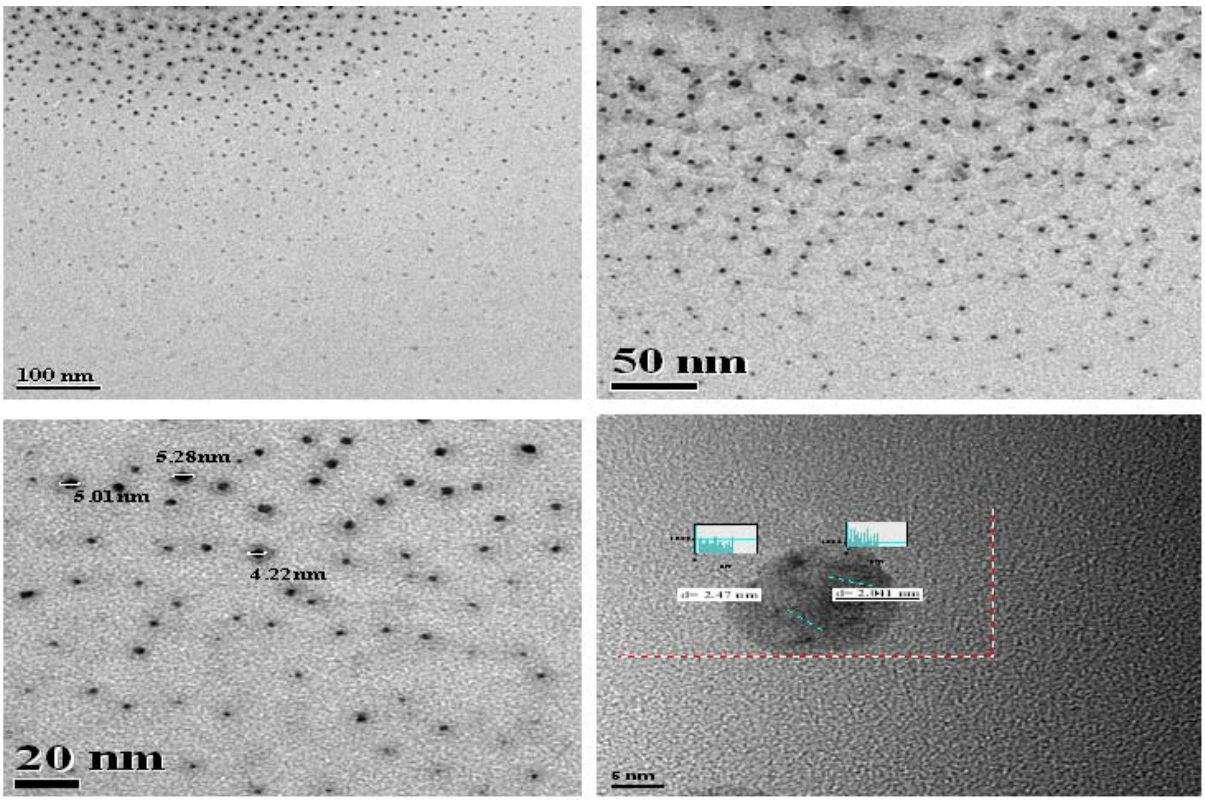

Figure 5.16. HR- TEM images of $Ag\text{-}Ni\text{-}ZrO_2$

Similarly, in Ni-ZrO_2 sample, the peaks at 2θ = 44.51°, 51.80° and 78.1° correspond to the reflections due to (111), (200) and (220) planes of the face center cubic structure of the metallic Ni. However, in case of Ag-Ni supported on zirconia, peaks observed at 2θ = 38.1°, 44.4°, 64.71° and 77.2° were attributed to both metallic Ag and Ni, with a slight shift due to bimetallic nature of the nanocomposite [62] . The particle size estimated by Scherer equation for the planes (111) of Ag and (111) of Ni was found to be in the range of 8-10 nm which was in accordance with HRTEM results as shown in Figure 5.16.

5.3.3.1.2. HR-TEM

The high resolution transmission electron microscopy (HRTEM) images of ZrO_2 supported Ag, Ni and Ag-Ni catalysts in Figure 5.17 shows that these nanoparticles had a spherical morphology along with average particle size in the range of 5-10 nm.

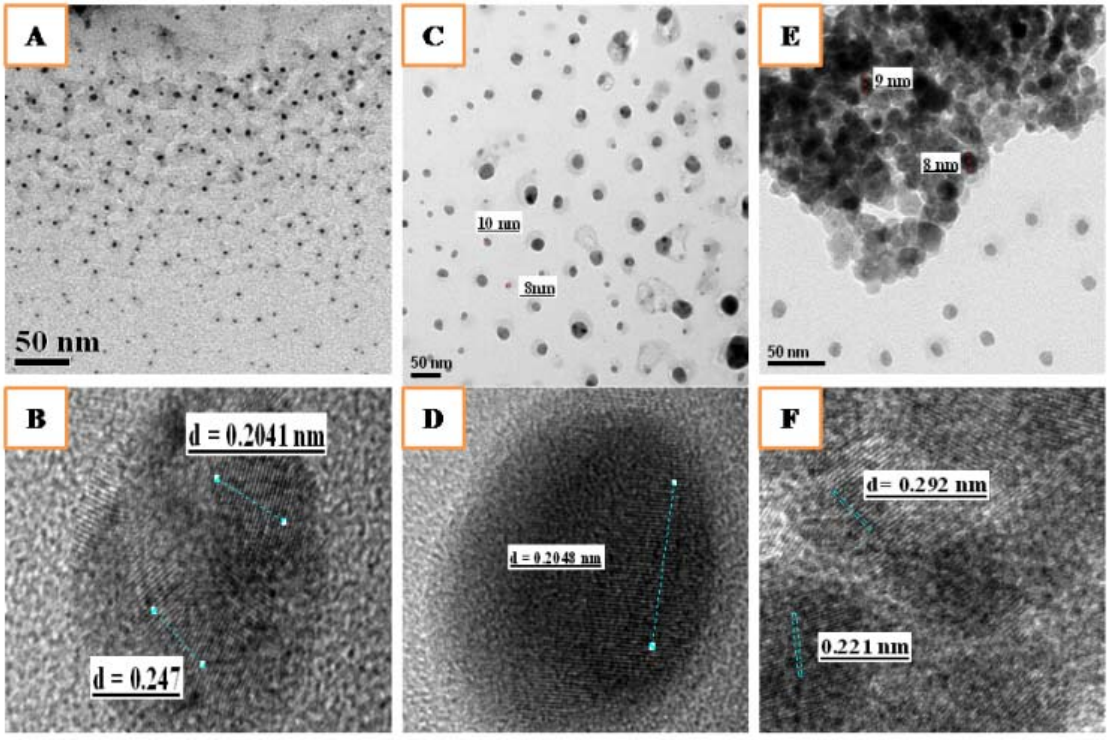

Figure 5.17. HR-TEM images of A) Ag-Ni-ZrO_2 B) Fringe pattern of Ag-Ni-ZrO_2 C) Ni-ZrO_2 D) Fringe pattern of Ni-ZrO_2 E) Ag- ZrO_2 F) Fringe pattern of Ag- ZrO_2

The presence of both Ni and Ag was confirmed by the high resolution images of individual Ag and Ni NP Figure 5.17 (B). Monometallic Ag and Ni catalysts showed

spherical morphology with slight increase in the particle size in the range of 10-12 nm due to some agglomeration (Figures 5.17 C and E). Fringe pattern of Ag-Ni-ZrO_2 showed lattice fringe distance of 0.247 nm corresponding to (111) of fcc metallic Ag (0.24 nm). The lattice fringes with 'd' spacing of 0.207 nm was also observed in the edge region, which could be ascribed to the (111) planes of metallic Ni. [63] This study clearly suggests that dispersion of both the metallic species over zirconia support consist of nanoparticles having particle size <5 nm which resembled with the XRD results.

5.3.3.1.3. H_2 TPR

The TPR patterns of the zirconia supported Ag, Ni and Ag-Ni samples are shown in Figure 5.18. The monometallic Ag/ZrO_2 showed broad H_2 consumption peak in the range of 450-650 ^oC which could be assigned to the reduction of Ag^+ to metallic silver. The high reduction temperature required for Ag/ZrO_2 indicates the strong metal/support interactions [64]. For Ni/ZrO_2 catalysts, a broad H_2 consumption peak with tailing was observed in the region of 270 to 520 ^oC. This response could be attributed to the sequential reduction of Ni^{2+} to Ni^o. However, the TPR profile of Ag−Ni/ZrO_2 exhibited a low intensity H_2 consumption peak with two maxima at 265 and 485 ^oC.

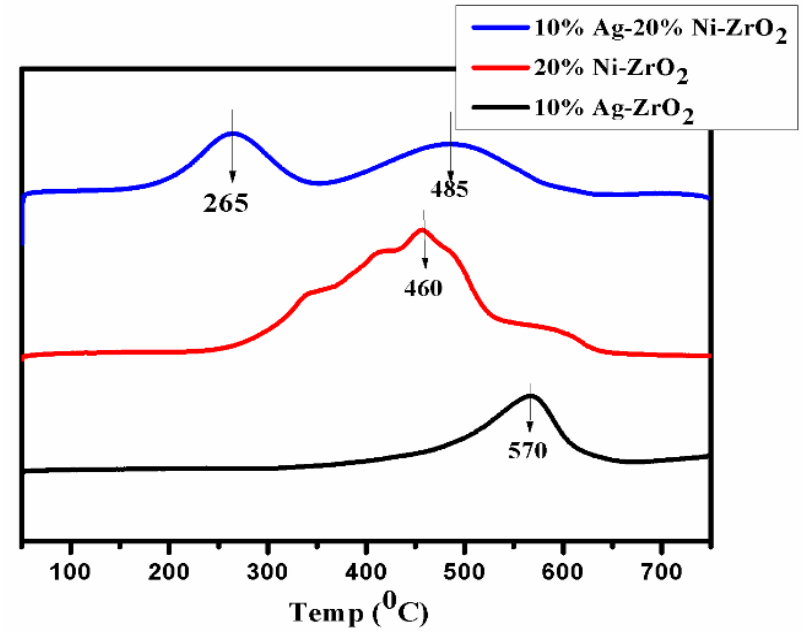

Figure 5.18. H_2-TPR profile of Ag, Ni and Ag-Ni-ZrO_2

The occurrence of two reduction peaks in TPR at low temperature could be ascribed to the reduction of silver and nickel oxide species due to synergetic effect of Ag and Ni responsible for the efficient activity for dehydrogenation as well as hydrogenation reactions [65, 66].

5.3.3.1.4. DR-UV study

The nature of Ag-Ni formation was also explained by comparing the DR-UV spectra of individual Ag-ZrO_2, Ni-ZrO_2 and Ag-Ni-ZrO_2 samples shown in Figure 5.19. The monometallic Ag/ZrO_2 showed Surface Plasmon Resonance (SPR) band at ≈334 nm which could be assigned to silver cluster ($Ag^{\delta+}$). In all the three samples, a band was observed at 230 nm which was due to charge transfer of O^- to Zr^{4+} of zirconia present in tetragonal and monoclinic phases. The spectral features of Ni-ZrO_2 sample showed no distinct absorption bands except the zirconia band. The absence of peaks of SPR bands of Ag-Ni/ZrO_2 sample was similar to that observed for Ni-ZrO_2 sample which indicates either complete reduction of metal ions or very small particle size of metallic species [67]. This clearly suggests the bimetallic Ag-Ni nanoparticles formation in zirconia matrix which also resembles with XRD and HR-TEM studies.

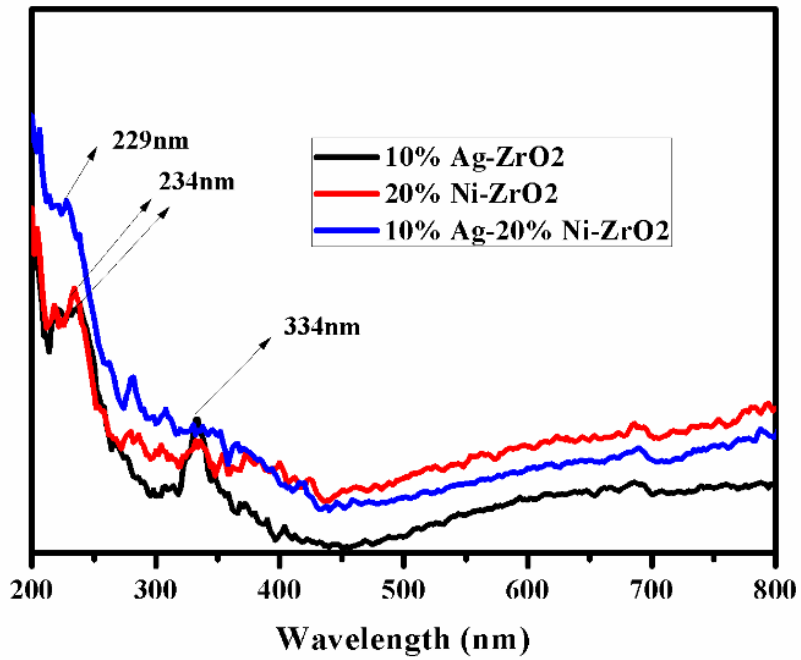

Figure 5.19. DR-UV study of Ag, Ni and Ag-Ni-ZrO_2 catalysts

5.3.3.1.5. XPS

The XPS patterns of Ag, Ni and Ag-Ni supported on ZrO_2 catalysts are shown in Figure 5.20. The binding energy of Ag 3d core levels for Ag Ni NPs shifted towards lower binding energy values suggesting the existence of metallic silver. The spectrum was fitted in terms of two different chemical species with Ag $3d_{5/2}$ binding energies at 368.1 and 366.6 eV, assigned to metallic silver (Ag^0) and silver ions in Ag_2O (Ag^+), respectively.

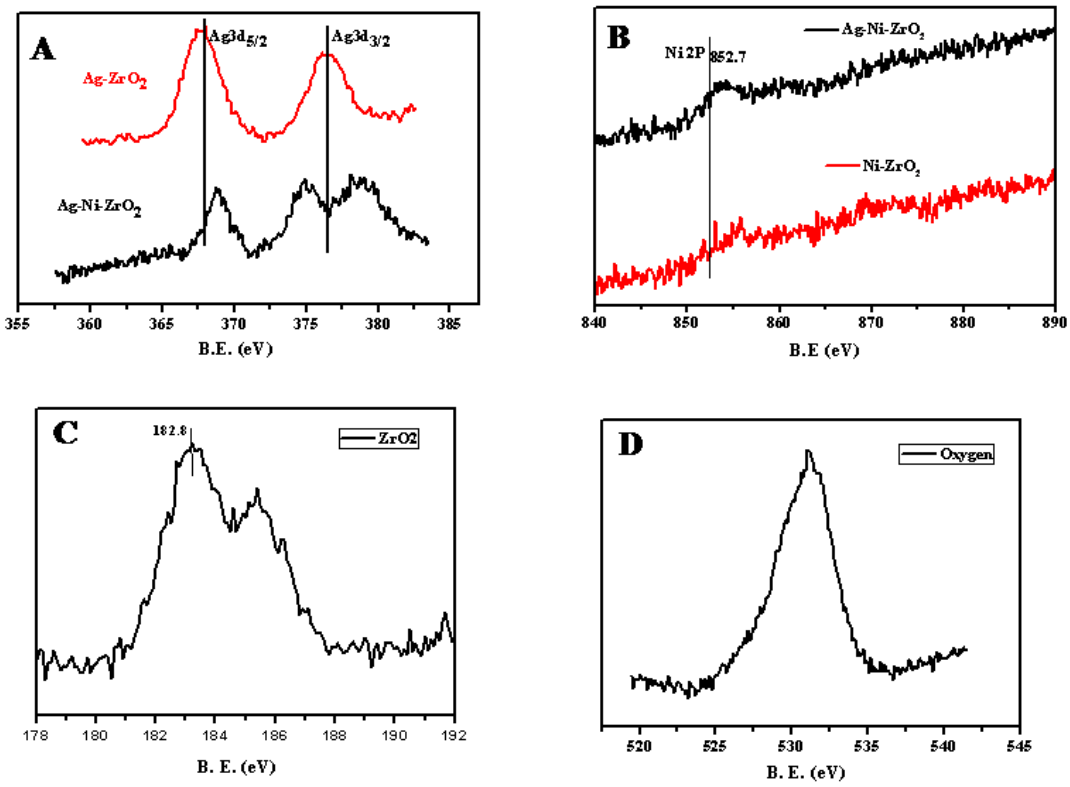

Figure 5.20. XPS study of Ag, Ni, Zr and O in a) Ag in Ag-ZrO_2 and Ag-Ni-ZrO_2 b) Ni in Ni-ZrO_2 and Ag-Ni-ZrO_2 c) Zr in Ag-Ni-ZrO_2 d) Oxygen in Ag-Ni-ZrO_2

While, the XPS spectra of Ni $2p_{3/2}$ showed a peak at 852.5 eV corresponding to metallic Ni^o. The characteristic peaks of Ni do not show any indications for the presence of nickel oxides. From these results, it could be concluded that the Ni NPs are indeed coated or bounded by a thin layer of silver which was in accordance with XRD and HRTEM studies [68].

5.3.4. Activity testing

5.3.4.1. Batch study

The performance of several zirconia supported catalysts was evaluated for CTH of aqueous mixture of levulinic acid and formic acid and the results are shown in Table 5.5. Although, all the catalysts screened in this work gave complete selectivity to hydrogenation product GVL, the yield varied depending on the catalyst, compositions of the two metals and reaction conditions. Both monometallic Ag and Ni on zirconia catalysts gave very low yields of 22 and 34%, respectively, towards GVL while bi-metallic Ag-Ni on zirconia showed more than three times higher yield to GVL than that of monometallic catalysts. Hence, subsequent studies on effect of reaction parameters were carried out over active Ag-Ni/ZrO_2 catalyst. Lowering of reaction temperature from 220 ^oC to 150 ^oC, caused lowering of the yield of GVL to 21% (entry 5, Table 5.5.). Similar trend was also observed for lowering in reaction time (entry 6, Table 1) to 1 h which also caused lowering the yield of GVL from 99 to 34%. Increase in substrate concentration from 5 to 10% slightly decreased the yield of GVL from 99 to 78%. The most important parameter was the effect of Ag-Ni composition on GVL yield. Lowering of Ag loading from 10 to 5% keeping Ni constant substantially decreased the GVL yield, due to low availability of active metal sites either for FA dehydrogenation or LA hydrogenation reactions (entry 7, Table 5.5). Similarly, lowering Ni loading from 20 to 10% (keeping Ag constant at 10%) decreased the GVL yield to 60%. Although, ruthenium is well known active catalyst for aliphatic carbonyl group hydrogenation, zirconia supported Ru catalyst showed very poor activity (<5% GVL yield) for CTH of aqueous mixture of LA: FA, indicating its inability for hydrogen formation through formic acid dehydrogenation (entry 10, Table 5.5). Only ZrO_2 without any metal function showed almost nil (<1%) activity confirming that both formic acid dehydrogenation followed by LA hydrogenation are mediated by active metal catalysts. Thus, the excellent performance of bimetallic nanoparticles Ag-Ni/ZrO_2 towards transfer hydrogenation of LA to GVL using sole hydrogen from formic acid was due to (i) very small particle size of metal particles (5 nm), (ii) synergetic effect due to addition of a co-metal such as Ag for low temperature reduction with minimal hydrogen uptake.

Table 5.5. Catalytic screening for transfer hydrogenation levulinic acid to GVL by using formic acid

Entry	Catalyst	Time (h)	Temp (^oC)	Selectivity (%)	Yield (%)
				GVL	
1	10% Ag/ZrO_2	5	220	100	22
2	20% Ni/ZrO_2	5	220	100	34
3	10% Ag-20% Ni/ZrO_2	5	220	100	99
4	10% Ag-20% Ni/ZrO_2	7	200	100	88
5	10% Ag-20% Ni/ZrO_2	7	150	100	21
6	10% Ag-20% Ni/ZrO_2	1	220	100	34
7	5% Ag-20% Ni/ZrO_2	5	220	100	52
8	10% Ag-10% Ni/ZrO_2	5	220	100	60
9	10% Ag-20% Ni/ZrO_2*	5	220	100	78
10	5% Ru/ZrO_2	5	220	100	5
11	ZrO_2	5	220	<1	<1

Reaction conditions: levulinic acid (43 mmol, *86 mmol): formic acid (43 mmol); solvent, water (93 mL); N_2 atm; catalyst, 0.5 g; catalyst:substarte ratio, (1:10); temperature, 220 ^oC; reaction time,5 h.

In our tandem approach, the role of co-metal for decomposition of formic acid is a very crucial step for the availability of nascent hydrogen without CO formation. In a control experiment, formic acid decomposition was studied separately over different catalysts as shown in Figure 5.21.

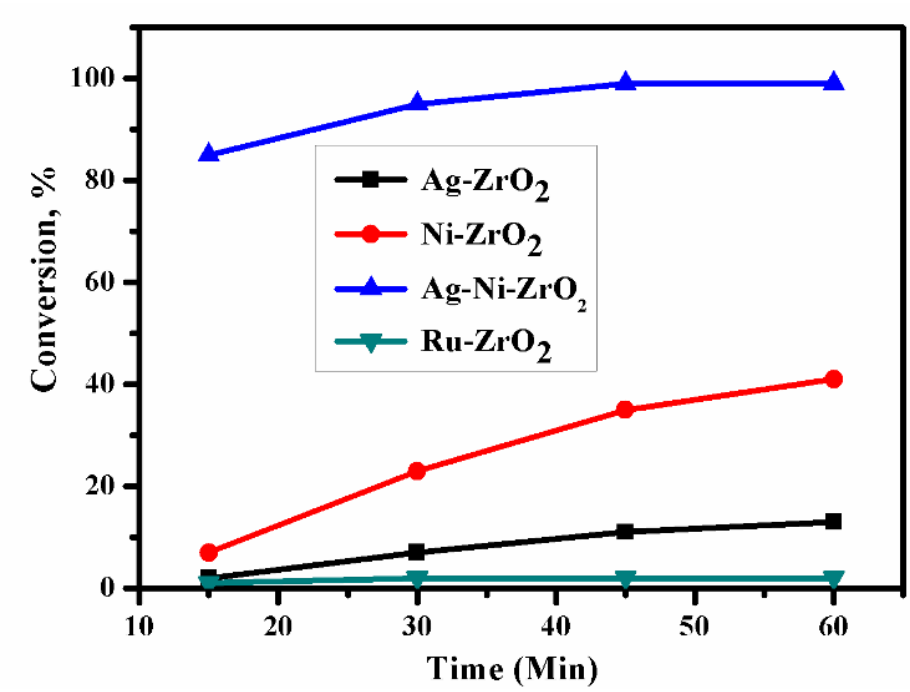

Figure 5.21. Formic acid decomposition profile Ag, Ni, Ag-Ni and Ru-ZrO_2

Reaction conditions: formic acid (43 mmol); solvent, water (95 mL); temperature, 220 ^{o}C; N_2 atm; catalyst, 0.5 g; catalyst:substarte ratio, (1:10) reaction time,5 h.

Ru in combination with zirconia did not show any prominent decomposition of formic acid to produce H_2 and CO_2 while monometallic Ag and Ni on zirconia showed low conversion in the range of 10- 40% as well as selectivity to CO was only (5%) (Figure 5.22 A & B). The synergetic effect of Ag and Ni in Ag-Ni-ZrO_2, immediately boosted the formic acid conversion up to 80% within first 15 min and taking it to completion within 1h. The catalytic decomposition of FA was also evident from increase in reactor pressure from 50 psi to 650 psi within 30 min, the analysis of which showed formation of H_2 + CO_2 mixture without CO selectivity Figure 5.23.

Analysis Date & Time : 20-12-2012 17:53:55
User Name : Admin
Vial# : 1
Sample Name : lah96_3h_r2
Sample ID : lah96_3h_r2
Sample Type : Unknown
Injection Volume :
ISTD Amount :

Data Name : C:\GCsolution\Data\Project1\19 dec\lah96_3h_r3.gcd
Method Name : C:\GCsolution\Data\Project1\Method\Tushar\STD_Met_H2_co2_ch4.gcm
[Description]
@60 for 10 min with Ar gas_50mA

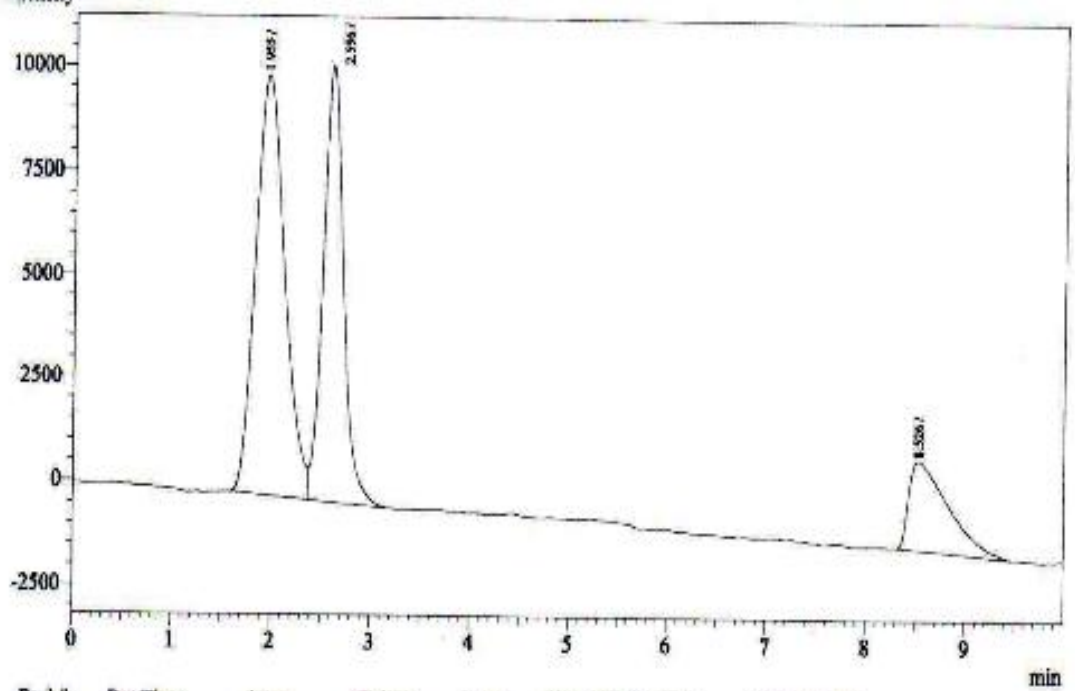

Peak#	Ret.Time	Area	Height	Conc.	Unit	Mark	ID#	Cmpd Name
1	1.955	205138	10131	49.580				
2	2.596	148819	10532	35.968		V		
3	8.526	59797	2142	14.452				
Total		413754	22805					

A

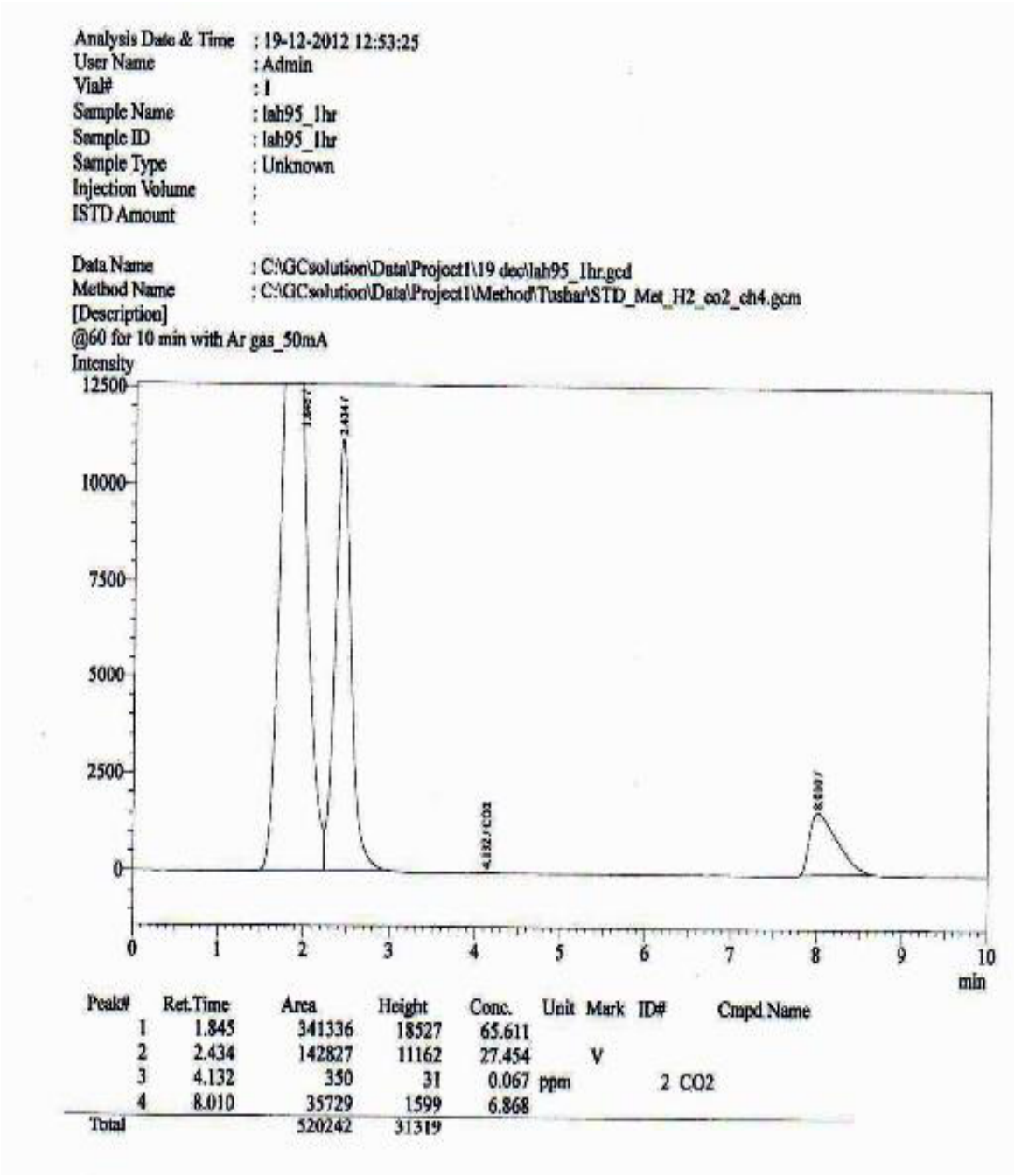

B

Figure 5.22. Gas analysis over (A) Ag-Ni-ZrO_2 catalyst (B) Ni-ZrO_2

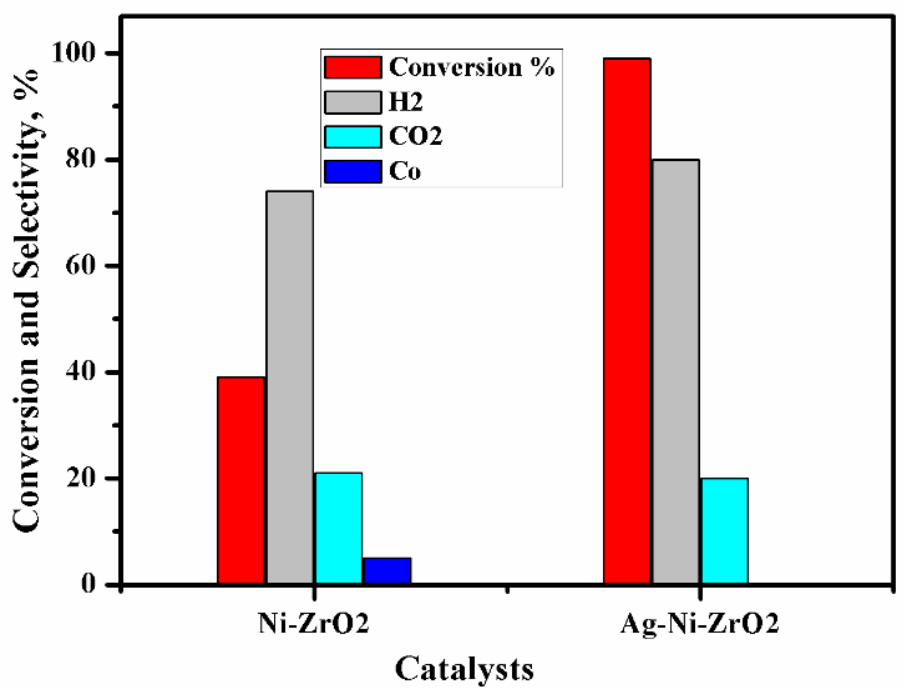

Figure 5.23. Conversion and selectivity pattern for decomposition of formic acid over Ni-ZrO_2 and Ag-Ni-ZrO_2

Reaction conditions: Formic acid (43 mmol); solvent, water (95 mL); temperature, 220 ^oC; N_2 atm; catalyst, 0.5 g; catalyst:substarte ratio, (1:10) reaction time,5 h.

5.3.4.2. Substrate screening

The versatility of our active catalyst was demonstrated by carrying out in-situ hydrogenation of several bio-derived platform molecules ranging from C_3 to C_6 components to the corresponding value added hydrogenated products as presented in Table 5.6. Thus, our bimetallic nanocomposite Ag-Ni-ZrO_2 played a significant role in dehydrogenation of formic acid to release nascent hydrogen and also subsequently catalyzing hydrogenation of levulinic acid to GVL with 99% yield. Among C_3 molecules, lactic acid, glycerol and acetol showed excellent conversion of 87- 99% with a selectivity of 81-95% to 1, 2 PDO as shown in Figure 5.24. The reaction also proceeded successfully (99% conversion) for the hydrogenation methyl and ethyl esters of LA giving complete selectivity to γ-valerolactone (entries 4, 5; Table 2).

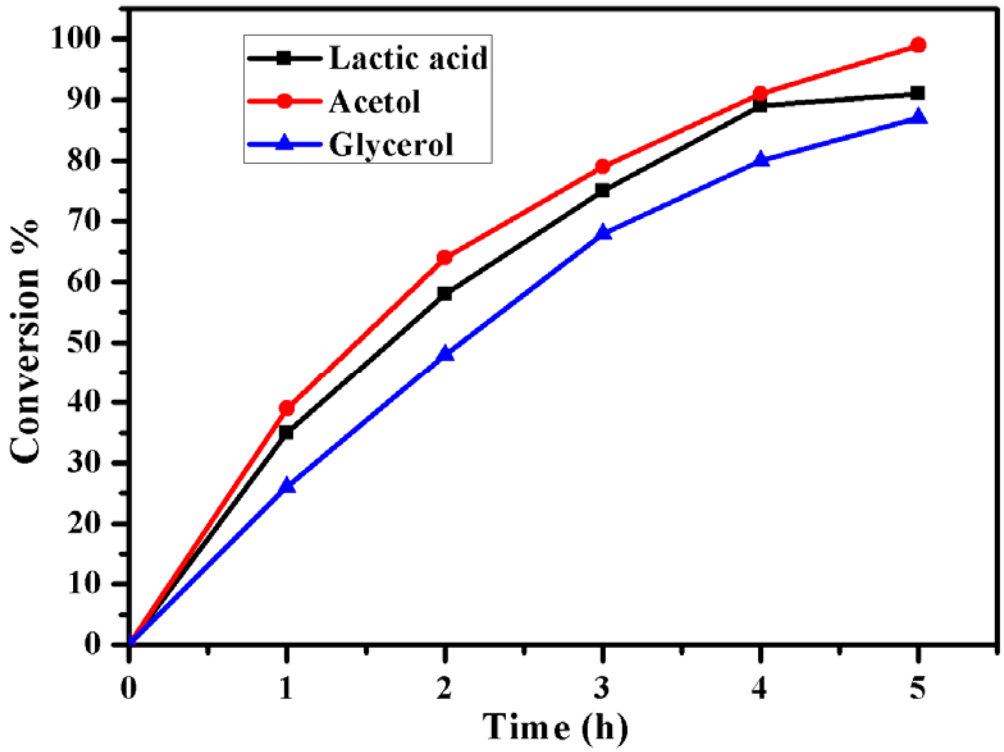

Figure 5.24. Conversion Vs Time profile of lactic acid, Acetol and glycerol over Ag-Ni-ZrO_2 catalyst

Reaction conditions: C_3 substrates (Lactic acid, Acetol and glycerol) (43 mmol), formic acid; (43 mmol); solvent, water (90 mL); temperature, 220 ^oC; N_2 atm; catalyst, 0.5 g; catalyst:substarte ratio, (1:10) reaction time,5 h.

This result is of vital significance as it will lead to the most sustainable process for GVL since, already direct and efficient production of levulinic acid esters from biomass (glucose, fructose and cellulose) is envisaged commercially. The interesting aspect here is selective carbonyl group hydrogenated with selective product formation. In addition, the usefulness of *in situ* hydrogenation over Ag-Ni/ZrO_2 was also demonstrated for conversion of furan based carbonyl group. As expected, 5-methyl furfural (5-methyl FUR) was readily hydrogenated into (bis-hydroxymethyl)- furan (BHMF) with complete conversion and 79% selectivity to BHMF (entry 6, Table 2).

Table 5.6. Transformations of various bio-derived platform molecules over Ag-Ni-ZrO_2 catalyst

Entry	Substrate	Conversion (%)	Product	Selectivity (%)
1	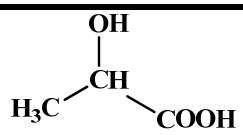 Lactic acid	**91**	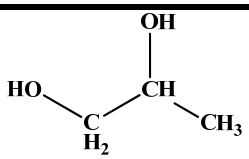 **1, 2 PDO**	**81**
2	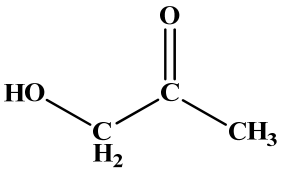 **Acetol**	**99**	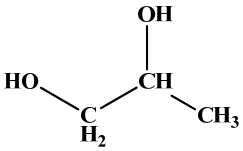 **1, 2 PDO**	**95**
3	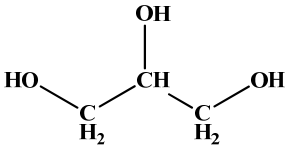 Glycerol	**87**	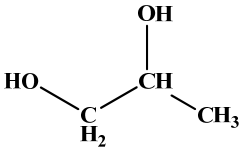 **1, 2 PDO**	**85**
4	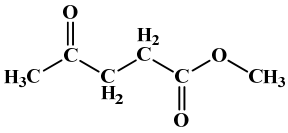 Methyl LA	**99**	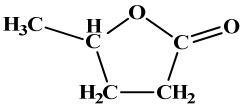 **GVL**	**99**
5	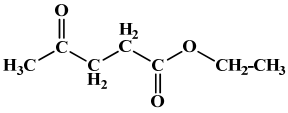 Ethyl LA	**99**	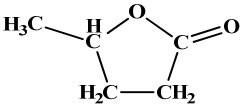 **GVL**	**98**
6	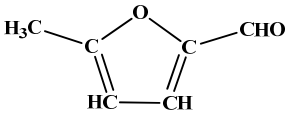 5-Methyl FUR	**99**	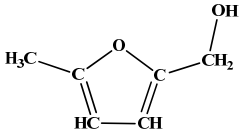 5-Methyl FAL	**79**

Reaction conditions: Substrate (1-6) (43 mmol): formic acid (43 mmol); solvent, water (93 mL); temperature, 220 ^{o}C; N_2 atm; catalyst, 0.5 g; catalyst: substrate ratio, (1:10) reaction time,5 h.

5.3.4.3. Catalyst recycle study

The stability of Ag-Ni-ZrO_2 was also established by its reuse studies for the in-situ hydrogenation of levulinic acid. Ag-Ni/ZrO_2 catalyst was easily recovered by applying magnetic field after each run and used for subsequent runs showing consistent activity (99% conversion) without decrease in selectivity to GVL up to five times Figure 5.25. A slight decrease in catalyst amount from (0.501 to 0.439 g) was due to sampling losses from time to time. ICP analysis confirmed that no detectable metal leaching was observed. Hence, marginal decrease in activity for transfer hydrogenation could be due to less availability metallic sites. This indicated that our catalyst was active, recyclable and stable catalyst under aqueous phase hydrogenation of bio-derived platform molecules.

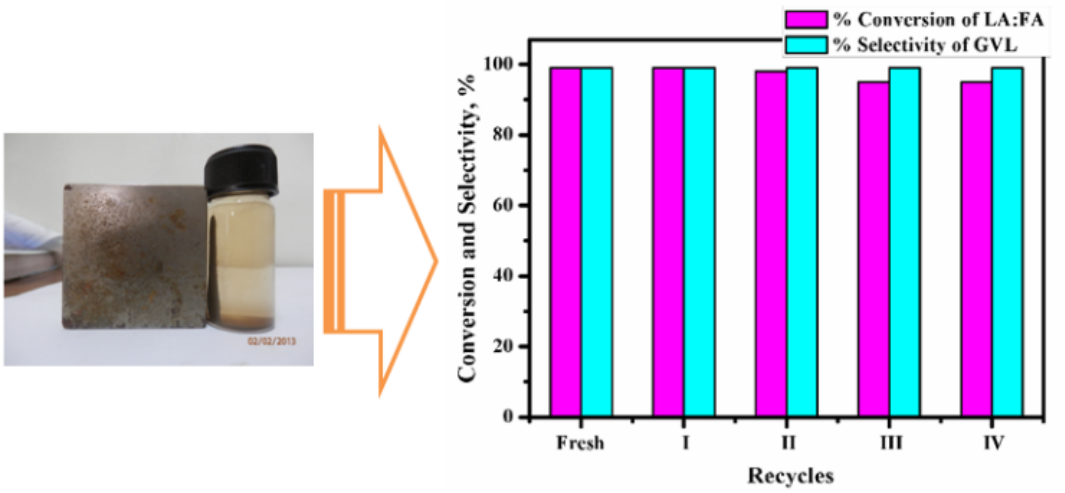

Figure 5.25. Catalyst recovery and its recyclability

Reaction conditions: Levulinic acid (43 mmol): formic acid (43 mmol); solvent, water (90 mL); temperature, 220 ^{o}C; N_2 atm; catalyst, 0.5 g; catalyst:substrate ratio, (1:10) reaction time,5 h.

5.4. Conclusion

In summary, we have successfully developed two different catalyst systems for CTH of LA using IPA and FA as H_2 donors. The fact that both the systems required two different catalysts indicates that different pathways being operated involving the role of different active species. In case of Ni-MMT catalyst using IPA as a hydrogen donor, the acidic MMT support catalyzes the LA esterification in presence of the secondary alcohol which is also an efficient H_2 donor for CTH while, the hydrogenation is being catalyzing metallic Ni sites.

In another CTH case of aqueous LA:FA mixture, bimetallic and magnetically separable Ag-Ni/ZrO_2 catalyst was found to be highly efficient due to the synergism of both the metals. This involves H_2 generation from formic acid and also the in-situ hydrogenation of LA. For both LA and its esters, hydrogenation proceeded smoothly to GVL, confirming the bi-functional role of the catalyst in cyclization of 4-hydroxy LA esters. The generality of this catalyst was well demonstrated for one pot hydrogenation of biomass derived C_3 to C_6 molecules to a variety of useful molecules with almost complete conversion and > 80% selectivity. Due to its magnetic nature, the recovery of the catalyst was very easy and could be recycled up to five times showing neither the loss of activity nor any metal leaching.

5.5. References

1. J. Q. Bond, D. M. Alonso, D. Wang, R. M. West, J. A. Dumesic, Science 327 (2010) 1110.
2. J. P. Lange, R. Price, P. M. Ayoub, J. Louis, L. Petrus, L. Clarke, H. Gosselink, Angew. Chem. Int. Ed. 49 (2010) 4479.
3. J. Q. Bond, D. M. Alonso, R. M. West, J. A. Dumesic, Langmuir 26 (2010) 16291.
4. J. Q. Bond, D. Wang, D. M. Alonso, J. A. Dumesic, J. Catal. 281 (2011) 290.
5. J. M. Tukacs, D. Király, A. Strádi, G. Novodarszki, Z. Eke, G. Dibó, T. Kéglb, L. T. Mika, Green Chem. 14 (2012) 2057.
6. T. N. Pham, D. Shi, D. E. Resasco, Appl. Catal. B: Environ. 145 (2014) 10.
7. H. Heeres, R. Handana, D. Chunai, C. B. Rasrendra, B. Girisuta, H. J. Heeres, Green Chem. 11 (2009) 1247.
8. Y. R. Leshkov, J. N. Chheda, J. A. Dumesic, Science 312 (2006) 1933.
9. H. B. Zhao, J. E. Holladay, H. Brown, Z. C. Zhang, Science 316 (2007) 1597.
10. R. Palkovits, Angew. Chem. Int. Ed. 49 (2010) 4336.
11. M. J. Climent, A. Corma, S. Iborra, Green Chem. 13 (2011) 520.
12. I. T. Horvath, H. Mehdi, V. Fabos, L. Boda, L. T. Mika, Green Chem. 10 (2008) 238.
13. A. P. Dunlop, J. W. Madden, US Patent, 2786852 (1957).
14. S. G. Wettstein, J. Q. Bond, D. M. Alonso, H. N. Pham, A. K. Datye, J. A. Dumesic, Appl. Catal. B: Environ. 117 (2012) 321.
15. S. W. Fitzpatrick, R. J. Bilski, J. L. Jarnefeld, Resour. Conserv. Recycl. 28 (2000) 227.
16. J. C. Serrano-Ruiz, D. J. Braden, R. M. West, J. A. Dumesic, Appl. Catal. B: Environ. 100 (2010) 184.
17. C. E. Chan-Thaw, M. Marelli, R. Psaro, N. Ravasio, F. Zaccheria, RSC Adv. 3 (2013) 1302.
18. T. Pan, J. Deng, Q. Xu, Y. Xu, Q. X. Guo, Y. Fu, Green Chem. 15 (2013) 2967.

19. D. J. Braden, C. A. Henao, J. Heltzel, C. C. Maravelias, J. A. Dumesic, Green Chem. 13 (2011) 1755.
20. L. E. Manzer, Appl. Catal. A 272 (2004) 249.
21. C. Delhomme, L. A. Schaper, M. Zhang-Pree, G. Raudaschl-Sieber, D. Weuster-Botz, F. E. Kühn, J. Organomet. Chem. 724 (2013) 297.
22. W. Li, J-H. Xie, H. Lin, Q-L. Zhou, Green Chem. 14 (2012) 2388.
23. J. P. Lange, J. Z. Vestering, R. J. Haan, Chem. Commun. (2007) 3488.
24. R. A. Bourne, J.G. Stevens, J. Ke, M. Poliakoff, Chem. Commun. (2007) 4632.
25. M. G. Al-Shaal, W. R. H. Wright, R. Palkovits, Green Chem. 14 (2012) 1260.
26. P. P. Upare, J. M. Lee, Y. K. Hwang, D. W. Hwang, J. H. Lee, S. B. Halligudi, J. S. Hwang, J. S. Chang, ChemSusChem 4 (2011) 1749.
27. A. M. Hengne, N. S. Biradar, C. V. Rode, Catal. Lett. 142 (2012) 779.
28. H. Kobayashi, H. Matsuhashi, T. Komanoya, K. Hara, A. Fukuoka, Chem. Commun. 47 (2011) 2366.
29. T. Thananatthanachon, T. B. Rauchfuss, Angew. Chem. Int. Ed. 122 (2010) 6766.
30. J. Jae, W. Zheng, R. F. Lobo, D. G. Vlachos, ChemSusChem 6 (2013) 1158.
31. L. Deng, J. Li, D. M. Lai, Y. Fu, Q. X. Guo, Angew. Chem. Int. Ed. 121 (2009) 6651.
32. L. Deng, Y. Zhao, J. Li, Y. Fu, B. Liao, Q. X. Guo, ChemSusChem, 3 (2010) 1172.
33. X. L. Du, L. He, S. Zhao, Y. M. Liu, Y. Cao, H. Y. He, K. N. Fan, Angew. Chem. Int. Ed. 50 (2011) 7815.
34. M. Chia, J. A. Dumesic, Chem. Commun. 47 (2011) 12233.
35. X. Tang, L. Hu, Y. Sun, G. Zhao, W. Hao, L. Lin, RSC Adv. 3 (2013) 10277.
36. Z. Yang, Y-B. Huang, Q. X. Guo, Y. Fu, Chem. Commun. 49 (2013) 5328.
37. C. Fellay, P. J. Dyson, G. Laurenczy, Angew. Chem. Int. Ed. 120 (2008) 4030.
38. Y. Himeda, Green Chem. 11 (2009) 2018.
39. M. Grasemann, G. Laurency, Energy Environ. Sci. 5 (2012) 8171.
40. L. Deng, J. Li, D. M. Lai, Y. Fu, Q. X. Guo, Angew. Chem. Int. Ed. 48 (2009) 6529.

41. X. Gu, Z. H. Lu, H.L. Jiang, T. Akita, Q. Xu, J. Am. Chem. Soc. 133 (2011) 11822.
42. Y. Huang, X. Zhou, M. Yin, C. Liu, W. Xing, Chem. Mater. 22 (2010) 5122.
43. A. Gazsi, T. Bansagi, F. Solymosi, J. Phys. Chem. C 115 (2011) 15459.
44. S. Zhang, O. Metin, D. Su, S. Sun, Angew. Chem. Int. Ed. 52 (2013) 3681.
45. L. He, Y. Huang, A. Wang, X. Wang, X. Chen, J. J. Delgado, T. Zhang, Angew. Chem. Int. Ed. 51 (2012) 6191.
46. W. F. Chen, K. Sasaki, C. Ma, A. I. Frenkel, N. Marinkovic, J. T. Muckerman, Y. Zhu, R. R. Adzic, Angew. Chem. Int. Ed. 51 (2012) 6131.
47. Z. L. Wang, J. M. Yan, Y. Ping, H. L.Wang, W. T. Zheng, Q. Jiang, Angew. Chem. Int. Ed. 52 (2013) 1.
48. R. He, X. Qian, J. Yin, Z. Zhu, J. Mater. Chem. 12 (2007) 3783.
49. R. He, X. Qian, J. Yin, Z. Zhu, J. Mater. Chem. 12 (2007) 3783.
50. L. Wang, A. Lu, C. Wang, X. Zheng, D. Zhao, R. Liu, J. Colloid Interf. Sci. 295 (2006) 436.
51. P. Sharma, S. K. Bhorodwaj, D. K. Dutta, J. Sci. Conf. Proc. 1 (2009) 40.
52. B. S. Kadu, Y. D. Sathe, A. B. Ingle, R. C. Chikate, K. R. Patil, C. V. Rode, Appl. Catal. B: Environ. 104 (2011) 407.
53. D. Dutta, B. J. Borah, L. Saikia, M. G. Pathak, P. Sengupta, D. K. Dutta, Appl. Clay Sci. 53 (2011) 650.
54. F. Alonso, P. Riente, J. A. Sirvent, M. Yus, Appl. Catal. A: Gen. 378 (2010) 42.
55. V. S. Kshirsagar, A. C. Garade, R. B. Mane, K. R. Patil, A. Yamaguchi, M. Shirai, C. V. Rode, Appl. Catal. A: Gen. 370 (2009) 16.
56. P. Komadel, J. Madejova, F. Bergaya, B. K. G. Theng, G. Lagaly (Eds.), Handbook of Clay Science: Elsevier, Amsterdam, 1 (2006) 263.
57. A. Dhakshinamoorthy, K. Pitchumani, Tetrahedron Lett. 49 (2008) 1818.
58. C. R. Reddy, Y. S. Bhat, G. Nagendrappa, B. S. J. Prakash, Catal. Today 141 (2009) 157.
59. R. P. Hernandez, G. M. Galicia, A. A. Maravilla, J. Palacios, Phys. Chem. Chem. Phys 15 (2013) 12702.

60. A. M. R. Galletti, C. Antonetti, V. D. Luise, M. Martinelli, Green Chem. 14 (2012) 688.
61. H. Guo, Y. Chen, X. Chen, R. Wen, G. H. Yue, D. L. Peng, Nanotechnology 22 (2011) 195604.
62. Z. Zhang, T. M. Nenoff, K. Leung, S. R. Ferreira, J. Y. Huang, D. T. Berry, P. P. Provencio, R. Stumpf, J. Phys. Chem. C 114 (2010) 14309.
63. F. C. Lizana, S. G. Quero, G. Jacobs, Y. Ji, B. H. Davis, L. Kiwi-Minsker, M. A. Keane, J. Phys. Chem. C 116 (2012) 11166.
64. V. Nichelea, M. Signorettoa, F. Menegazzoa, A. Gallob, V. D. Santoc, G. Crucianid, G. Cerratoe, Appl. Catal. B: Environ. 111 (2012) 225.
65. K. A. Bethke, H. H. Kung, J. Catal. 172 (1997) 93.
66. M. Tsuji, M. Hashimoto, T. Tsuji, Chem. Lett. 31 (2002) 1232.
67. T. Bala, S. D. Bhame, P. A. Joy, B. L. V. Prasad, M. J. Sastry, Mater. Chem. 14 (2004) 2941.
68. D. Zhao, B. Q. Xu, Angew. Chem. Int. Ed. 45 (2006) 4955.

Chapter 6

Dehydration/hydrogenation of furfuryl alcohol to GVL via LA esters

Functionalized ionic liquids with various acidic anions were designed as novel heterogeneous solid acid catalysts for alcoholysis of furfuryl alcohol (FAL) in presence of methanol, ethanol, n-butanol and isopropyl alcohol (IPA) to the corresponding levulinic acid esters under mild temperature (90–130 °C) conditions. The extended alkyl chain length of 1-methyl imidazole [MIm] using 1,4-butane sultone enhanced the Brønsted acidity of [BMIm-SH][HSO_4] catalyst resulting into the highest selectivity of >95% to Me-LA with > 99 % conversion of FAL. Using a combination of ionic liquid, [BMIm-SH][HSO_4] and 5% Ru/C catalyst, single-pot transformation of FAL to γ-valerolactone (GVL) is shown successfully for the first time with complete FAL conversion the selectivity as high as 68% to GVL. Our catalyst system could be efficiently recycled five times retaining the original activity and selectivity levels.

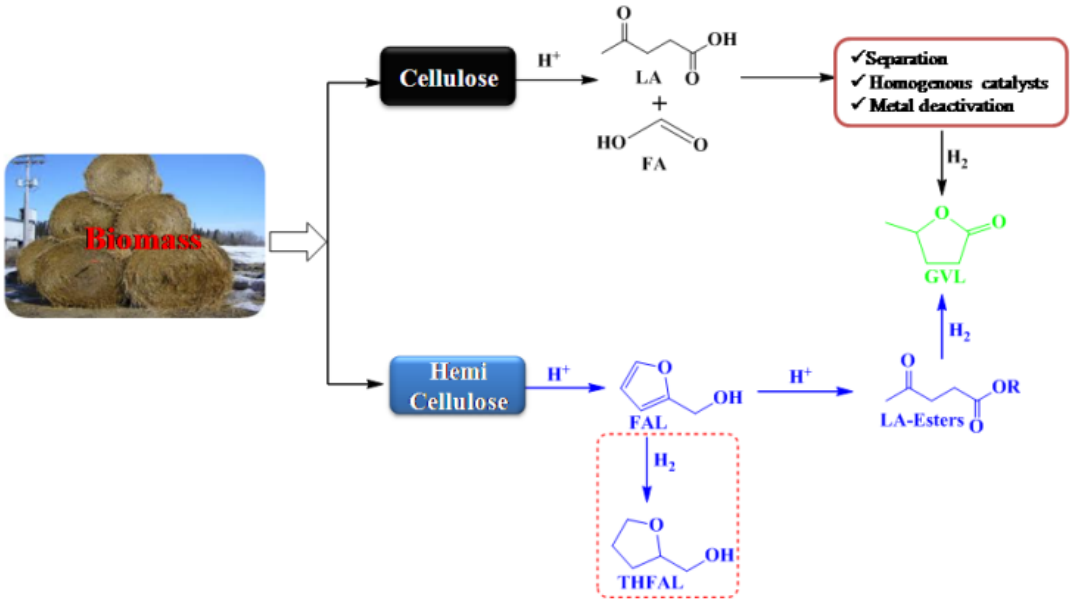

***Green Chem.* 15 (2013) 2540–2547**

6.1. Introduction

The exploitation of bio-based fuels and fuel additives is imperative due to its role in effective remediation of greenhouse gas levels in the atmosphere and to mitigate the economic consequences of the depleting fossil resources [1, 2]. First-generation biofuels (i.e. ethanol and biodiesel) are presently produced from sugars, starch and vegetable oils creating important compatibility and energy density issues. One promising alternative to overcome these limitations of oxygenated fuels is to use more abundant, cheaper and potentially more sustainable non-edible lignocellulosic biomass [3, 4]. We report here the most promising route to achieve this transformation by developing the selective and versatile catalyst system involving acid and metal functions together for alcoholysis and hydrogenation reactions respectively, in a single step. These two are the primary unit processes for conversion of the monomeric carbohydrate building blocks, i.e., mainly C_5 sugars, such as xylose and arabinose, and C_6 sugars in the form of glucose and their respective secondary products, furfural and levulinic acid into the potential fuel additives [5,6]. Furfural produced by the hydrolysis and dehydration of xylan contained in lignocellulose can be easily hydrogenated to furfuryl alcohol. Hence, direct conversion of furfuryl alcohol to levulinic esters followed by its *in-situ* hydrogenation to γ–valerolactone (GVL) becomes a new alternative route for the production of biofuels [7]. Levulinic esters (LA) are mainly obtained by a series of reactions involving first, acid catalyzed esterification of levulinic acid produced from hexose sugars. LA is then hydrogenated to give 4-hydroxy LA followed by its ring cyclization to GVL [8-10]. GVL along with levulinic esters which can be also used as diesel additives, form sustainable liquid transportation fuels replacing ethanol in a gasoline ethanol blend [11, 12]. In addition, another product of single step catalytic hydrogenation of levulinic acid is methyl tetrahydrofuran (MTHF) which has been also approved by US-DOE as a component of P-Series type fuel [13,14]. The formation of levulinic acid and its esters from cellulose and hemicelluloses is possible by two different routes i) hexose triple dehydration to 5-hydroxymethylfurfural (5-HMF) and its rehydration with two water molecules to produce levulinic and formic acids, and ii) hydrolysis of pentose sugars to produce a mixture of C_5 monomers, mainly furfural which is then reduced to furfuryl alcohol followed by its rehydration to produce levulinic acid/ester [15-18].

A commercial Biofine process for the production of levulinic acid requires 3.5 tons of 3.5 wt% sulfuric acid, thus creating a serious environmental pollution and involving tedious work up for the recovery of pure LA [19, 20]. Attempts are being made to overcome such drawbacks by developing heterogeneous catalysts. Several catalytic systems were reported for production of esters of levulinic acid and GVL from biomass and its derivative 5-HMF and FAL [21-26].

In the present chapter, we report a single pot catalytic conversion of furfuryl alcohol to levulinic acid ester and GVL via alcoholysis/hydrogenation sequence using sulfonic acid-functionalized ionic liquids (SO_3H-ILs) and carbon supported Ru, Re, Ir and Ag catalysts. Our novel approach of direct conversion of furfuryl alcohol to GVL has several advantages: (i) yield of methyl levulinate is higher than that for hydrolysis of C_6 sugars due to humin elimination in alcohol medium, (ii) no separation step required for downstream conversion of levulinic acid/esters (iii) complete atom efficiency in the conversion of FAL to GVL (iv) elimination of metal leaching and deactivation of catalysts used for LA hydrogenation to GVL. To the best of our knowledge, this approach of direct conversion of C_5 furfuryl alcohol to C_5 GVL has not been reported so far. We found that 5%Ru/C + [BMIm-SH][HSO_4] showed complete alcoholysis of furfuryl alcohol with 95% selectivity to methyl levulinate followed by its hydrogenation with the highest selectivity of 94% to GVL in a batch reactor.

6.2. Experimental

All acid functionalized ILs were prepared by using a ion exchange method while, supported Ru, Pd, Re, Pd and Ag catalysts were prepared by the impregnation method and the detailed experimental procedures of their preparation have been described in chapter 2, section 2.2.4. The catalysts were characterized by various techniques according to the procedure described in section 2.4. The activity of the prepared catalysts was evaluated for the hydrogenation of levulinic acid to γ-valerolactone and a typical experimental procedure is described in section 2.5.1. The quantitative analysis of liquid samples was carried out by gas chromatography method using FID detector, HP-5 capillary column and helium as a carrier gas. Other details of temperature programming method (60-190 ^oC) etc. are described in chapter II, section 2.6.

6.3. Results and discussion

6.3.1. Alcoholysis of furfuryl alcohol to esters of levulinic acid

6.3.1.1. Activity testing

Two major objectives of the present work were (i) to design a novel, environmentally benign acid catalyst for efficient alcoholysis of furfuryl alcohol to levulinic esters and (ii) to develop a tandem approach to synthesize GVL directly from furfuryl alcohol. For the first stage of this work, we prepared several acid functionalized ILs and their performance evaluation results are shown in Table 6.1.

Table 6.1. Catalyst screening for alcoholysis of furfuryl alcohol to methyl levulinate

Entry	Catalyst	Conversion %	% Selectivity		
			Methyl LA	Methoxy FAL	Other
1	No Catalyst	2	<0.01	81	19
2	$[H_2SO_4]$	68	74	16	10
3	Amberlyst-15	99	40	51	9
4	SO_4-ZrO_2	99	74	19	7
5	20% DTP-SiO_2	69	25	61	14
6	20% DTP-MMT	73	24	63	13
7	[MIm] $[HSO_4]$	96	65	21	14
8	[MIm][TFA]	10	1	95	4
9	[NMP] $[HSO_4]$	99	98	1	1
10	[NMP] [TFA]	11	2	94	4
11	[BMIm-SH][$ClSO_3H$]	98	90	4	6
12	[BMIm-SH][PTSA]	95	76	11	13
13	[BMIm-SH]$[HSO_4]$	99	95	2	3

Reaction conditions: Furfuryl alcohol, 5% (w/w); solvent, MeOH (95 mL); temperature, 130 ^oC; N_2 atm; catalyst, 0.3 g; reaction time, 2 h.

The initial control experiment without any catalyst (entry 1, Table 6.1) showed that furfuryl alcohol conversion was <2% confirming that the alcoholysis of furfuryl alcohol was a catalytic reaction. Among the various solid acid catalysts, almost complete conversion was obtained with Amberlyst-15 and SO_4-ZrO_2 but the selectivity to MeLA was only 40 and 74%, respectively, with the remaining FAL ethers (entries 3, 4 Table 6.1). With other two solid acid catalysts, conversion achieved was less than 75% with a very poor selectivity of 25% to Me-LA. Thus, the simultaneous high activity and

selectivity for furfuryl alcoholysis to Me-LA was not possible using any of the solid acid catalysts screened in this work (entries 5, 6, Table 6.1). This fact is also evident from the reported literature [10, 22, 26]. Therefore, we explored the use of ILs having Brønsted acidity which was systematically varied with anions such as $ClSO_3H$, SO_3H, PTSA and TFA with the same cation MIm. It was observed that furfuryl alcohol conversion of >95% was achieved with cations such as HSO_4 and $Cl\text{-}SO_3H$ (entries 7, 11 Table 6.1) and 10% conversion was obtained with TFA anion (entry 8, Table 6.1). However, with only HSO_4 anion, the selectivity to methyl levulinate was the highest, 98% (entry 9, Table 6.1). As can be seen from Table 6.1, the choice of anion was critical, because with TFA both the cations MIm and NMP exhibited very poor activities in terms of furfuryl alcohol conversion in the range of only 10-11 %. HSO_4 with both the cations, MIm and NMP showed very high conversion (>95%) while the selectivity to methyl levulinate was only 65% in case of [MIm][HSO_4]. Hence this catalyst was further modified by extending its alkyl chain length with 1, 4-butane sultone so that the resulting IL (BMIm-SH) would be more stable and also acquires the enhanced Brønsted acidity. To our expectation, this was actually observed as the [BMIm-SH][HSO_4] catalyst gave dramatic increase in selectivity of methyl levulinate up to 95% [entry 13, Table 6.1]. The appropriate combination of anion and the cation is emphasized by the fact that incomplete alcoholysis gave appreciable formation of intermediate FAL ethers (Scheme 6.1) in case of [MIm][HSO_4] and [BMIm-SH][PTSA] catalysts (entries 7,12 Table 6.1].

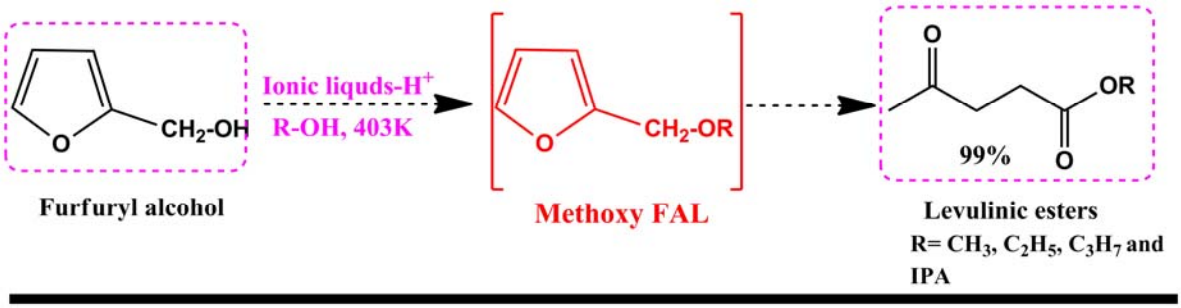

Scheme 6.1. Alcoholysis of furfuryl alcohol to methyl-levulinate

A typical gas-chromatogram of the reaction mixture is shown in Figure 6.1 while, the intermediate, methoxy FAL and the final product methyl levulinate formed in this

alcoholysis reaction were identified by GC-MS as shown in Figures 6.2.and 6.3. Using HSO_4 as the anion, NMP showed almost complete conversion of furfuryl alcohol and selectivity to methyl levulinate [entry 9, Table 6.1].

NATIONAL CHEMICAL LABORATORY PUNE
Dr.Homi Babha Road Pune
Chemical Engg & process Dev

Method filename:	E:\solvent\LA\CONT7.mth
Method name:	Amol
Analysed:	05/21/2013 15:08
Printed:	5/21/2013 15:27
Chromatogram filename:	E:\solvent\LA\1§LAH (MS) 3 20 min.dat

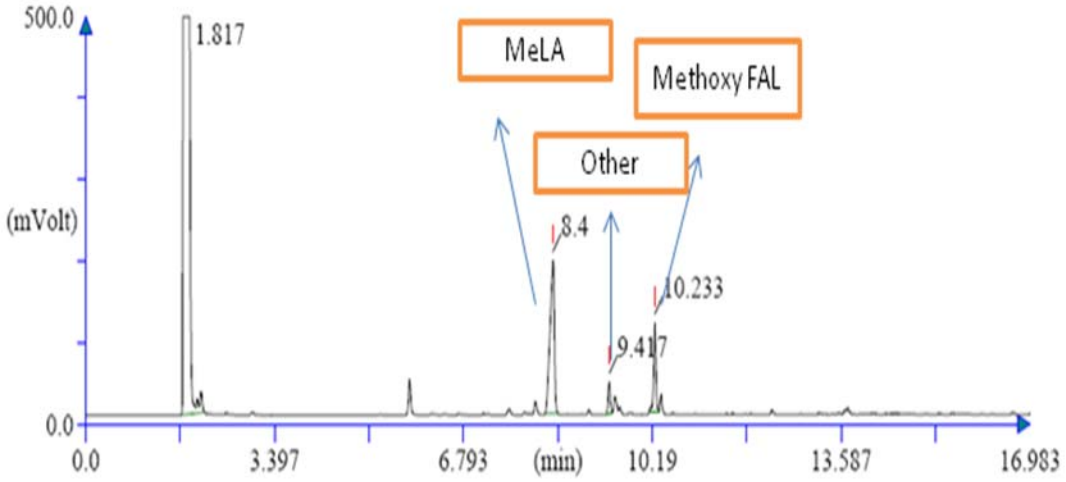

Figure 6.1. GC spectra of furfuryl alcohol alcoholysis

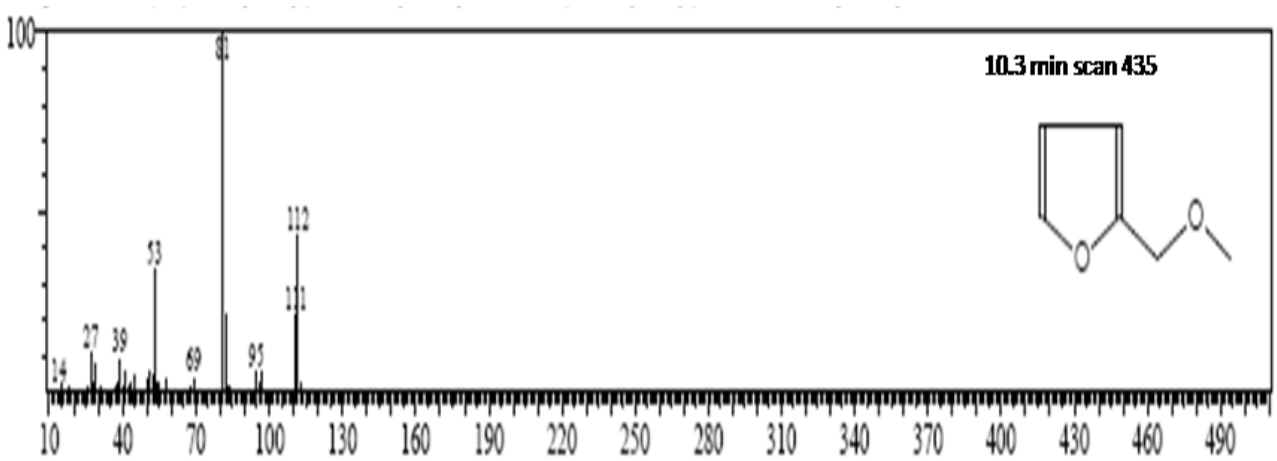

Figure 6.2. Mass spectra of methoxy FAL

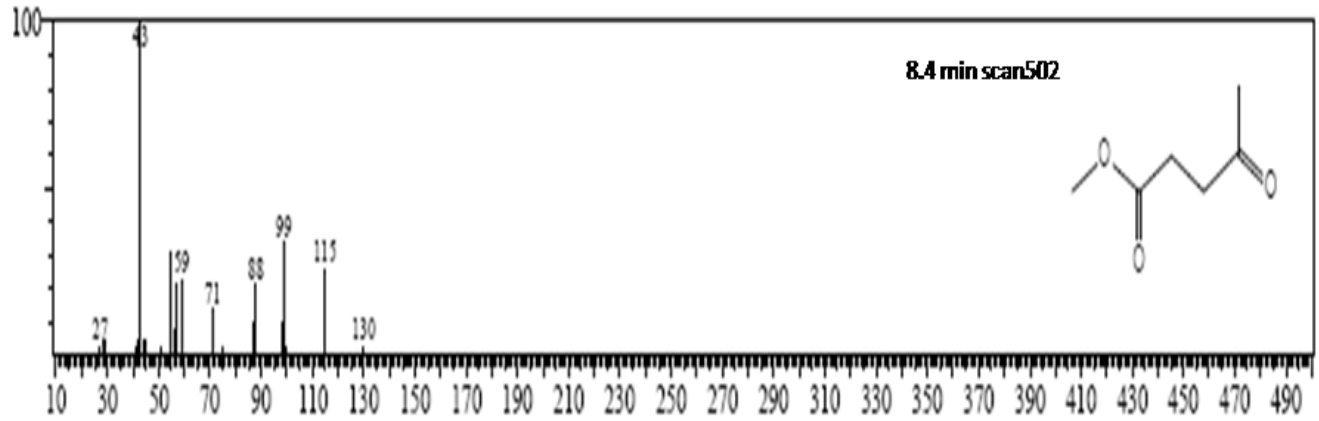

Figure 6.3. Mass spectra of methyl levulinate

However, this catalyst when recovered and was attempted to recycle, its activity dropped down by 50% as shown in Figure 6.4 as against the successful complete recyclability of [BMIm-SH] [HSO_4] catalyst for several times (discussed later). Hence, further study on effect of parameters was carried out using [BMIm-SH] [HSO_4] catalyst.

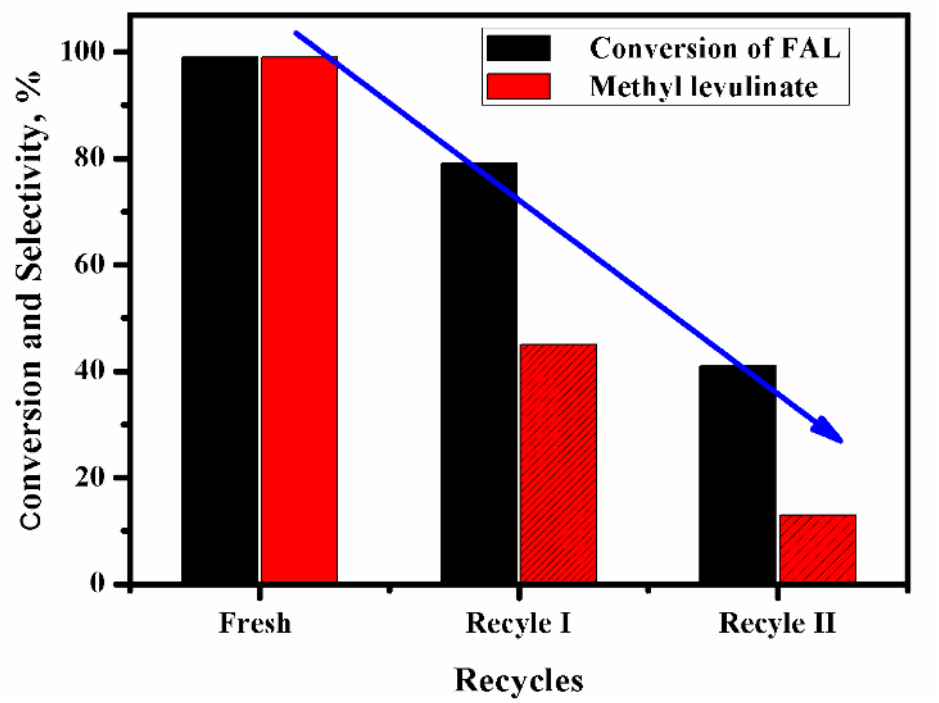

Figure 6.4. Recycle study of NMP[HSO_4] catalyst for FAL to methyl levulinate

Reaction conditions: Furfuryl alcohol, 5% (w/w); solvent, MeOH (95 mL); temperature, 130 ^oC; N_2 atm, catalyst, 0.3 g; reaction time, 2 h.

Along with the catalyst, equally important was choice of the reaction medium as the selectivity to levulinic acid dropped down to 31% in an aqueous medium over the same active catalyst [BMIm-SH][HSO_4], obviously due to the humin formation [27]. The humin formation also makes separation of catalyst and product very much tedious. Hence, direct alcoholysis of furfuryl alcohol in presence of methanol without formation of levulinic acid is the most advantageous strategy from process point of view [8, 28].

6.3.2. Reaction parameters study for FAL alcoholysis

6.3.2.1. Solvent Screening

The efficiency of our [BMIm-SH] [HSO_4] catalyst was further established for the synthesis of a variety of alkyl levulinates, by carrying out the alcoholysis of furfuryl alcohol in presence of different alcohols. Figure 6.5 shows that a consistent activity (99% conversion) was achieved for all the alcohols studied in this work. However, alkyl levulinate selectivity was found to decrease from 99 to 85% with increase in alcohol

chain length from ethanol to n-butanol. The decrease in Me-LA selectivity was associated with the formation of respective ethers of FAL depending on the alcohols used (shown as blue and green bars in Figure 6.5). In case of a branched alcohol like isopropanol, corresponding ester (IPA-LA) selectivity decreased to the extent of 68%. This indicates that the steric factor played an important role in the alcoholysis of furfuryl alcohol.

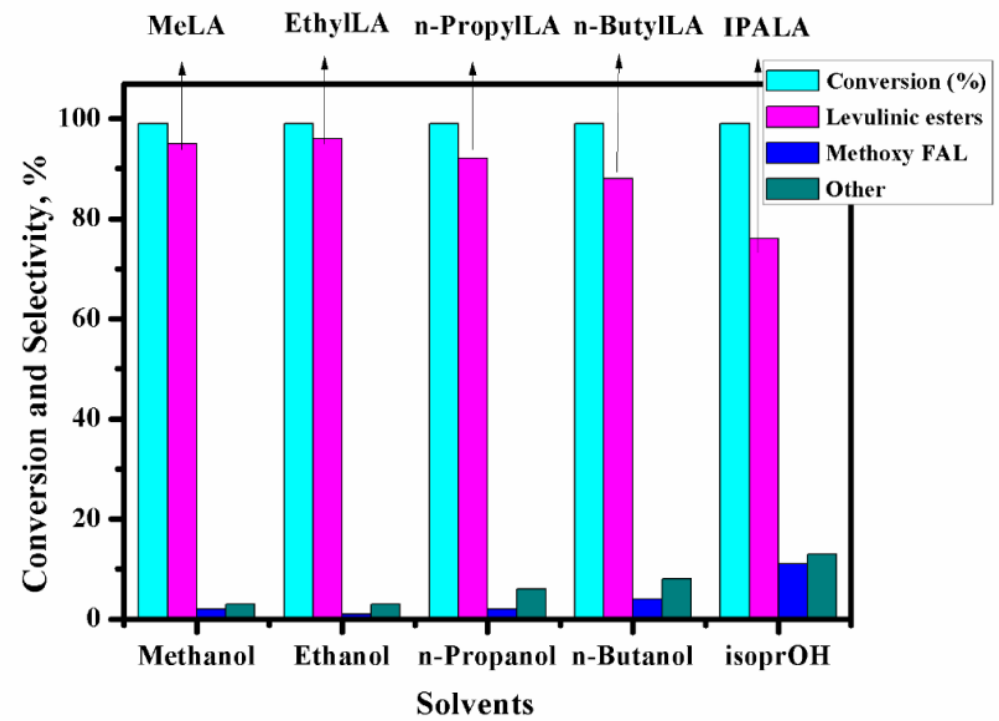

Figure 6.5. Screening of solvent for alcoholysis of furfuryl alcohol

Reaction conditions: Furfuryl alcohol, 5% (w/w); solvent, MeOH, EtOH, n-PrOH, n-BuOH and IsoPrOH (95 mL); temperature, 130 ^{o}C; N_2 atm, catalyst (Acidic IL), 0.3 g; reaction time, 2 h

6.3.2.2. Effect of temperature

The influence of temperature on the alcoholysis of furfuryl alcohol was studied in a range from 100 to 150 ^{o}C keeping other parameters constant and the results are shown in Figure 6.6. Almost complete conversion could be achieved as the temperature increased from 100 to 130 ^{o}C, and remained constant beyond 130 ^{o}C up to 150 ^{o}C. Similarly, the selectivity to Me-LA also increased linearly from 65 to 95% with increase in temperature from 100 to 130 ^{o}C.

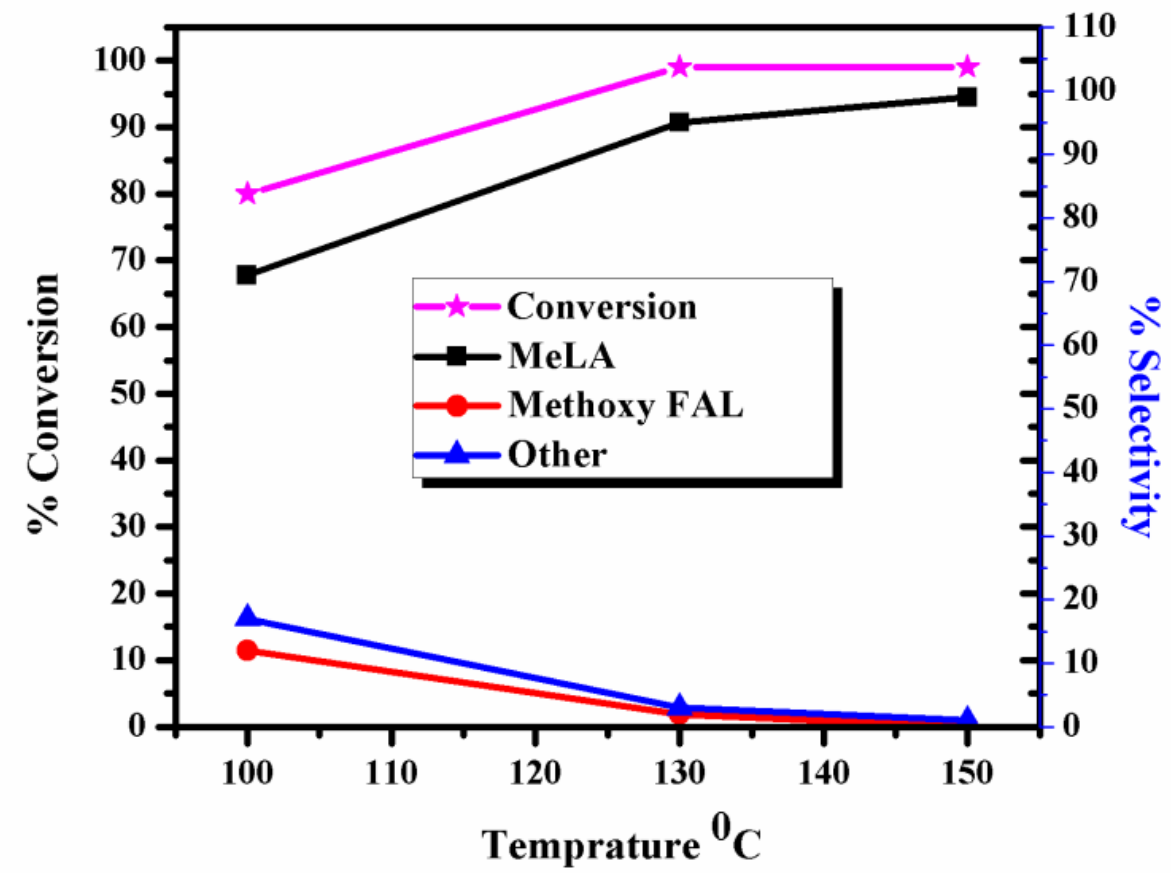

Figure 6.6. Effect of temperature on alcoholysis of furfuryl alcohol

Reaction conditions: Furfuryl alcohol, 5% (w/w); solvent, MeOH, (95 mL); temperature, 90-130^{o}C; N_2 atm, catalyst, 0.3 g (Acidic IL); reaction time, 2 h.

At higher temperature, the conversion of ethers of FAL to Me-LA was facilitated, proving the reaction pathway given in Scheme 6.1 which involves first, the etherification of FAL followed by rehydration of the intermediate ethers to Me-LA.

6.3.2.3. Effect of catalyst concentration

The study on effect of catalyst loading on the alcoholysis of furfuryl alcohol showed that the conversion of furfuryl alcohol increased from 84 to 99% with increase in catalyst loading from 0.1 to 0.3 g as shown in Figure 6.7. Moreover, the selectivity to methyl levulinate increased by 1.5 times (>80%) due to increased rehydration of the intermediate, FAL ethers. The higher catalyst concentration resulted into the higher availability of Brønsted acid sites, facilitating faster consumption of furfuryl alcohol and rehydration of the intermediates to methyl levulinate.

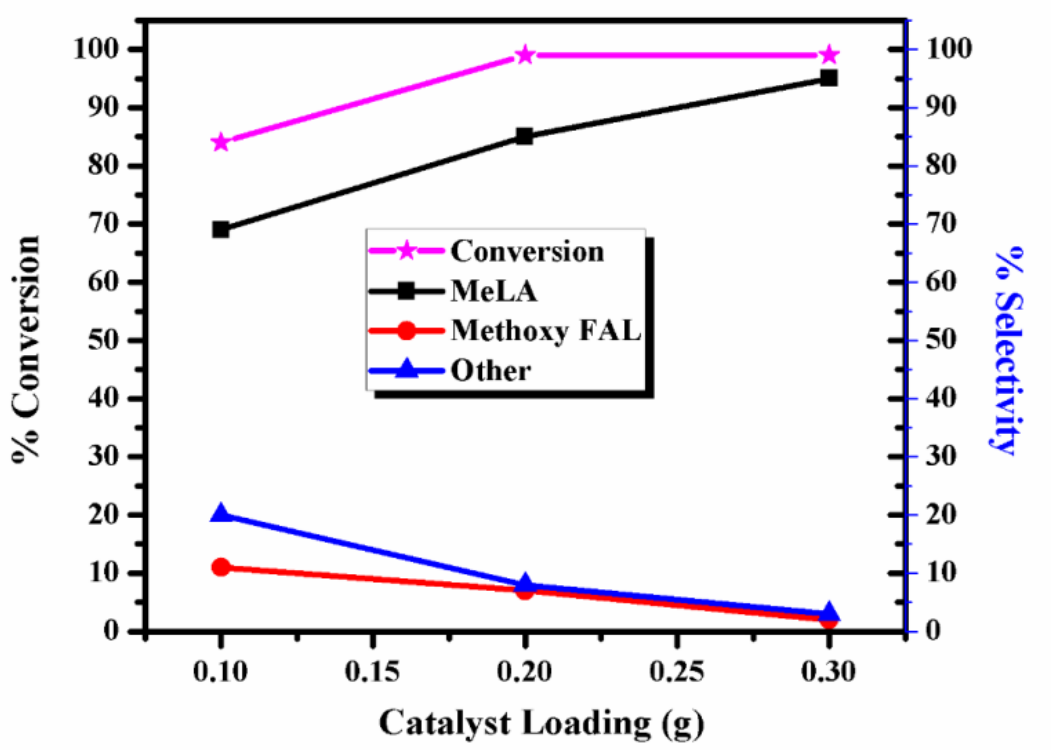

Figure 6.7. Effect of catalyst loading on alcoholysis of furfuryl alcohol

Reaction conditions: Furfuryl alcohol, 5% (w/w); solvent, MeOH, (95 mL); temperature, 130 ^{o}C; N_2 atm; reaction time, 2 h.

6.3.2.4. Effect of substrate concentration

One of the important process parameters was substrate concentration, the effect of which on conversion and selectivity pattern was studied by systematically varying the furfuryl alcohol concentration from 5 to 15% and the results are shown in Figure 6.8. With increase in substrate concentration from 5 to 15%, both the conversion of furfuryl alcohol and the Me-LA selectivity decreased significantly. At higher substrate concentration, the accumulation of higher concentration of the first step alcoholysis products viz. FAL ethers, on the active sites retarded further rehydration to Me-LA. The substrate concentration of 5% was the optimum to obtain complete conversion and suppression of methoxy FAL intermediates. This minimum substrate concentration can be compensated for higher productivity as our catalyst system was found to show more than three reuses as discussed later.

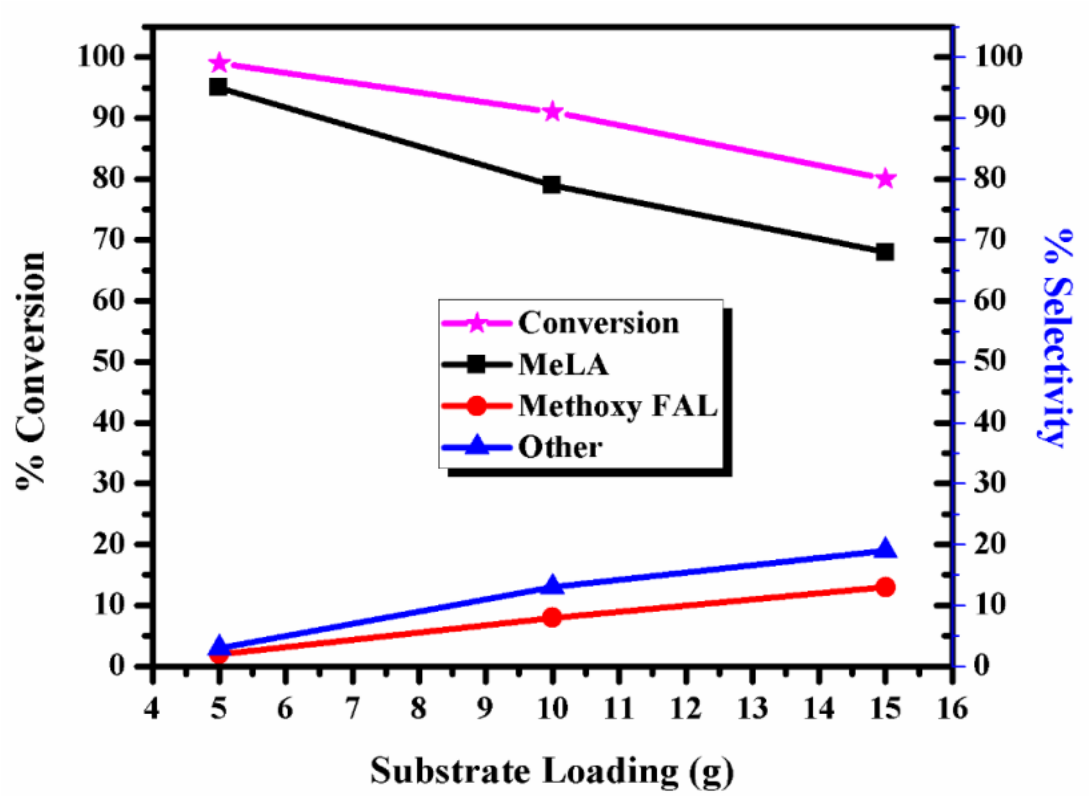

Figure 6.8. Effect of substrate loading on alcoholysis of furfuryl alcohol

Reaction conditions: Furfuryl alcohol, 5-15% (w/w); solvent, MeOH, (95 mL); temperature, 130 ^{o}C; N_2 atm, catalyst, 0.3 g (Acidic IL); reaction time, 2 h.

6.3.3. Alcoholysis followed by hydrogenation of furfuryl alcohol to GVL via LA esters

6.3.3.1. Batch Activity

Encouraged by the results on modified ILs for efficient alcoholysis of furfuryl alcohol to Me-levulinate, we thought it most desirable to obtain GVL directly from furfuryl alcohol in a single pot synthesis.

Table 6.2. Screening of catalysts for alcoholysis/hydrogenation of furfuryl alcohol

Entry	Catalyst	Additive	Conversion (%)	Selectivity (%)				
				MeLA	GVL	4-HMeLA	FAL Ethers	Others
1	5% Ru/C	H_2SO_4	99	47	31	9	13	<0.01
2	5%Ru/C	[BMIm-SH][HSO_4]	99	24	68	8	<0.01	<0.01
3	5%Ru/C	[BMIm-SH][HSO_4]*	99	12	58	1	3	26
4	5% Rh/C	[BMIm-SH][HSO_4]	99	92	2	2	4	<0.01
5	5% Re/C	[BMIm-SH][HSO_4]	99	85	9	2	4	<0.01
6	5% Pd/C	[BMIm-SH][HSO_4]	99	94	<0.01	<0.01	6	<0.01
7	5% Ir/C	[BMIm-SH][HSO_4]	99	65	6	26	3	<0.01
8	10% Ag/C	[BMIm-SH][HSO_4]	99	84	8	2	4	<0.01
9	10% Ag/ZrO_2	[BMIm-SH][HSO_4]	99	81	9	3	7	<0.01
10	5%Ru/C +	Amberlyst-15	99	76	14	6	14	<0.01
11	5% Ru/C+	SO_4-ZrO_2	99	79	18	1	2	<0.01

Reaction conditions: Furfuryl alcohol, 5% (w/w); solvent, MeOH (95 mL); temperature, 130 ^oC; N_2 atm. + H_2 pressure*, 500 psi; catalyst, 0.3+0.5 g; reaction time, 2h+3h.

For this purpose, a combination of acidic ILs and metal catalyst was used in a tandem synthesis of GVL. We therefore screened several combinations of various supported noble metals and the ILs selected from Table 6.1. All the combinations studied in this work were indeed very successful showing an excellent activity in terms of furfuryl alcohol conversion >99% Table 6.2. The selectivity to GVL varied depending on the noble metal used for the hydrogenation of the intermediate Me-LA. It is very interesting to note that under hydrogenation conditions, selectivity to GVL was only 58% and to the

intermediate ester was also only 12% while almost all the remaining (26%) byproduct was (entry 3, Table 6.2) tetrahydrofurfuryl alcohol (THFAL). THFAL was formed due to the ring hydrogenation of furfuryl alcohol and it was found to be a very stable product as observed from the conversion/selectivity vs. time profile shown in Figure 6.9.

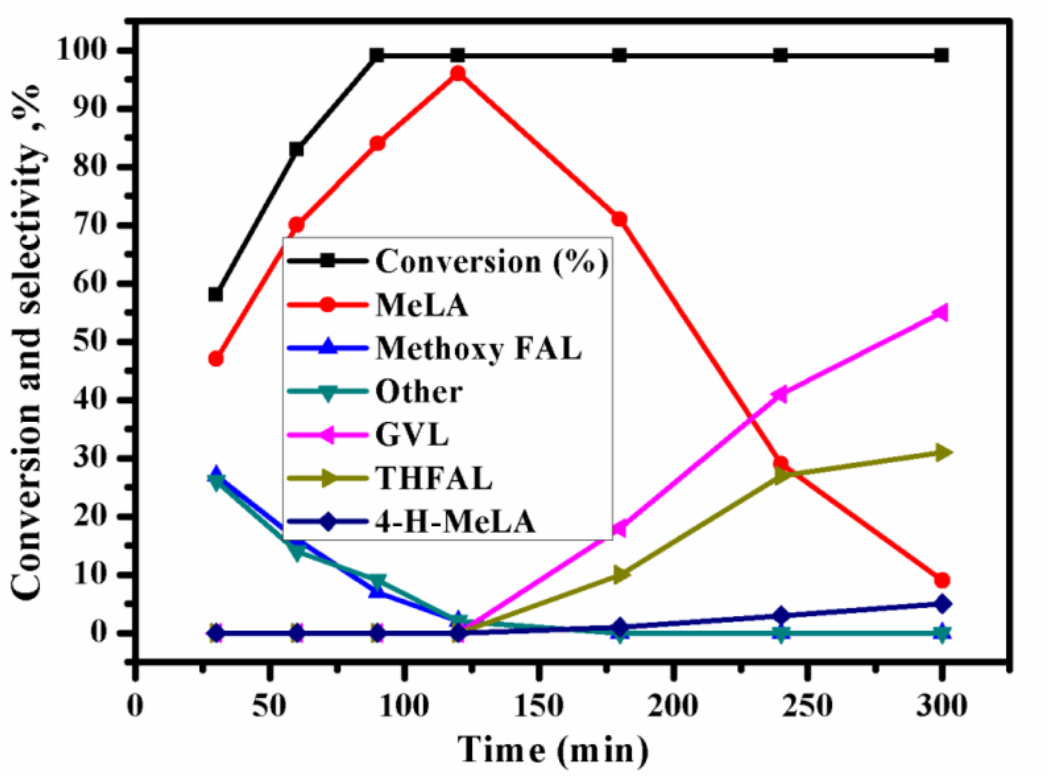

Figure 6.9. CT profile for direct hydrogenation of furfuryl alcohol

Reaction conditions: Furfuryl alcohol, 5% (w/w); solvent, MeOH (95 mL); temperature, 403 K; H_2 pressure, 500 psi; catalyst, 0.3 (acidic IL) +0.75 g (5% metal catalyst); reaction time, 5 h.

A novel strategy adopted by us involved conducting the initial alcoholysis reaction under an N_2 atmosphere for 2 h after which N_2 was replaced by H_2. This time period of changeover was arrived at from the optimum time of alcoholysis as studied previously (Table 6.1). This approach worked very well to completely suppress the ring hydrogenation product, THFAL (entry 2, Table 6.2), enhancing the selectivities to the desired products such as MeLA and GVL. Hence, further studies were carried out initially under N_2 and then replacing it by H_2. Under these conditions, among several

noble metal catalysts, 5% Ru/C in combination with IL [BMIm-SH][HSO_4] showed the highest selectivity to GVL (68%). For the same IL, other metals gave GVL selectivity in the range of 2–9%, which was in accordance with our earlier results [28]. The GVL selectivity is important not only from the process point of view but also it is necessary to dissolve the unwanted humin associated with cellulose hydrolysis [29]. The best performance of our Ru/C + [BMIm-SH][HSO_4] catalyst system for the direct conversion of FAL to GVL could be distinctly visible when compared with the performance of Ru/ C in combination with the best solid acids chosen from Table 6.1 (entries 10 and 11, Table 6.2). Ru/C with both amberlyst and SO_4-ZrO_2 gave <20% selectivity to GVL, as the major product was Me-LA. Our catalyst showed ten times higher activity (TOF, 160 h^{-1}) than the reported catalysts such as Ru/C + H_2SO_4 for the synthesis of GVL shown in Table 6.3.

Table 6.3. Comparison study of our Ru/C with other reported catalysts systems for synthesis of GVL

Entry	Catalysts	Substrate	Time (h)	Conversion (%)	Selectivity (GVL) (%)	TOF (h^{-1})
1	10%Ru/C+ [BMIm-SH][HSO_4]	Furfuryl alcohol	5	99	>95	53[a] (160)[b]
2	5%Ru/C	Levulinic acid	24	90	>99	15[a]
3	10% Ru/C + TFA	Fructose	8	99	62	7[a]

[a] The total turnover frequency is calculated on the basis of moles of Ru on support
[b]. Numbers in parenthesis refer to the TON estimated on the basis of dispersion of Ru atoms

This was because of deactivation of Ru catalyst due to sulfur leaching from H_2SO_4, which was evidenced by an intense peak at 169.3 eV of S 2p as seen from Figure 6.10 [30, 31].

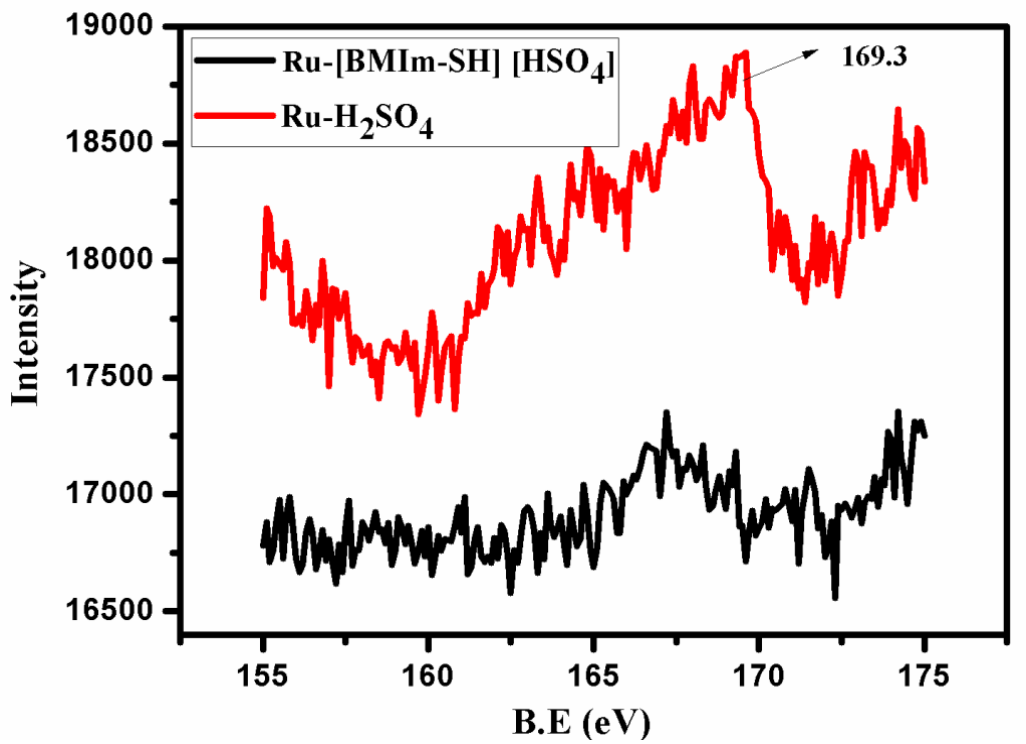

Figure 6.10. XPS study of used Ru/C catalysts

6.3.4. Reaction parameters study for tandem reaction

6.3.4.1. Effect of Ru/IL ratio

Since both acid as well as metal sites are important for the direct conversion of FAL to GVL, the effect of compositions of 5% Ru/C + ILs was also studied. For this purpose, loading of 5% Ru/C was varied from 0.25 g to 0.75 g at a constant loading IL of 0.3 g. Figure 6.11 shows that for all the loadings of Ru, the conversion of FAL remained constant at >99% while the product selectivity was significantly affected. With an increase in 5% Ru/C catalyst loading from 0.25 to 0.75 g, the selectivity to hydrogenation product GVL gradually increased from 35 to 83% at the cost of Me-LA indicating that an optimum Ru catalyst loading was necessary to achieve the highest selectivity to GVL. In another control experiment, IL loading was decreased to 0.15 g which resulted in significant lowering of the furfuryl alcohol conversion to 80%. More importantly, Me-LA selectivity was also minimum (10%) which in turn adversely affected the selectivity to GVL.

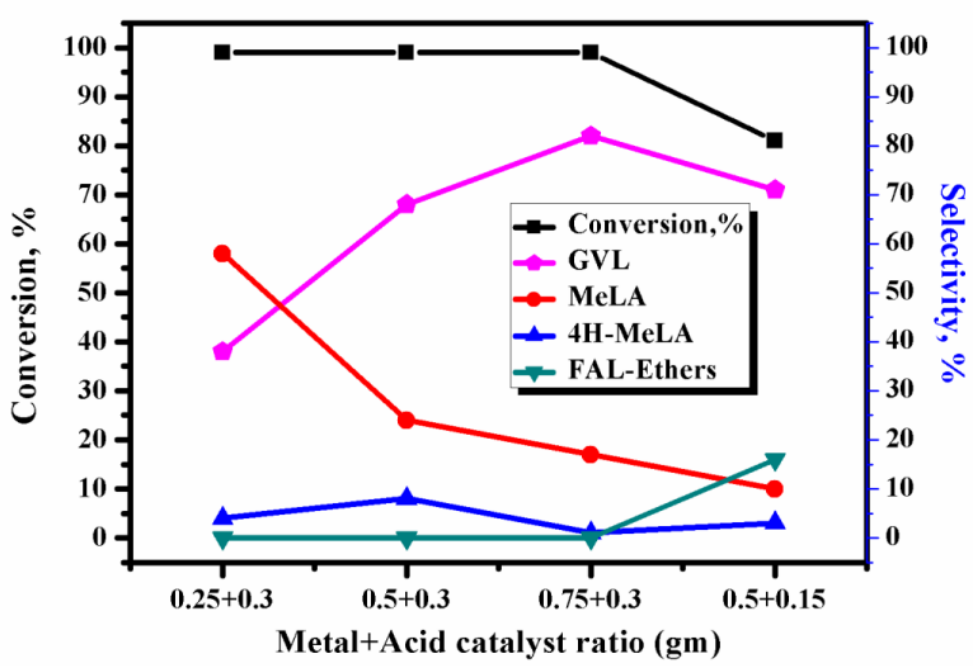

Figure 6.11. Effect of catalyst ratio on hydrogenation of furfuryl alcohol to GVL **Reaction conditions:** Furfuryl alcohol, 5% (w/w); solvent, MeOH (95 mL); temperature, 130 ^{o}C; H_2 pressure, 500 psi; catalyst, 0.15-0.3g (acidic IL) +0.25-0.75g (5% metal catalyst); reaction time, 5 h.

This study suggests that the direct conversion of furfuryl alcohol to GVL involves acid catalyzed first step alcoholysis of furfuryl alcohol to Me-LA followed by its metal catalyzed hydrogenation to 4- hydroxy methyl levulinate and subsequent cyclization to GVL (Scheme 6.2). During the cyclization, R–O is released as the corresponding alcohol, methanol in this case.

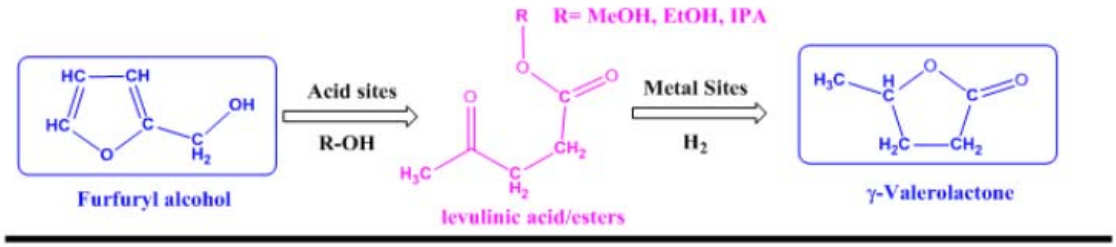

Scheme 6.2. Direct conversion of furfuryl alcohol to GVL

6.3.4.2. Effect of hydrogen pressure

In order to maximize the selectivity to GVL, hydrogen pressure was varied from 250 to 750 psi and the results are shown in Figure 6.12.

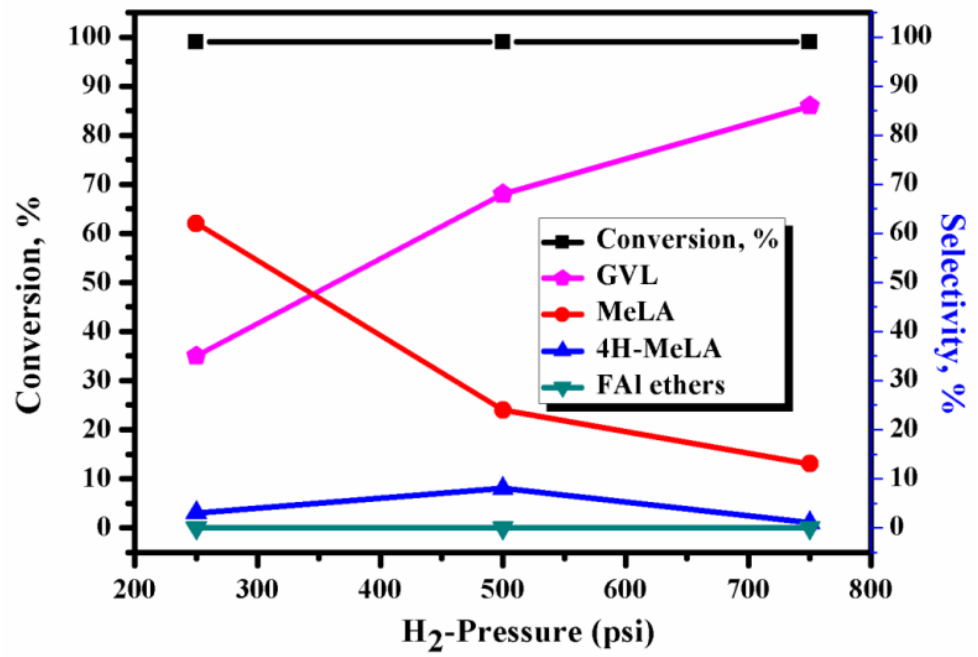

Figure 6.12. Effect of hydrogen pressure on hydrogenation of furfuryl alcohol to GVL **Reaction conditions:** Furfuryl alcohol, 5% (w/w); solvent, MeOH (95 mL); temperature, 130 ^{o}C; H_2 pressure, 250-750 psi; catalyst, 0.3g (acidic IL) +0.5g (5% metal catalyst); reaction time, 5 h.

A complete conversion of furfuryl alcohol was achieved over the entire range of H_2 pressures studied in this work. The H_2 pressure effect was very positive to enhance the selectivity to GVL from 35 to 85% with complete disappearance of FAL ethers. However, even at the highest H_2 pressure of 750 psi, marginal Me-LA and 4-MeLA remained unreacted indicating that rather than higher H_2 concentration, a higher extent of metal sites would be necessary for complete hydrogenation of the intermediates to GVL.

6.3.4.3. Effect of metal loading

The effect of active metal (Ru) loading on carbon was varied in the range of 5–10% with a constant amount of IL. As can be seen from Figure 6.13, conversion of the intermediate methyl LA increased from 76 to 95% with an increase in selectivity to GVL up to 94% for the active metal (Ru) loading of 10% on the carbon support. Thus, the availability of active metal content plays an important role in hydrogenation of methyl levulinate to GVL.

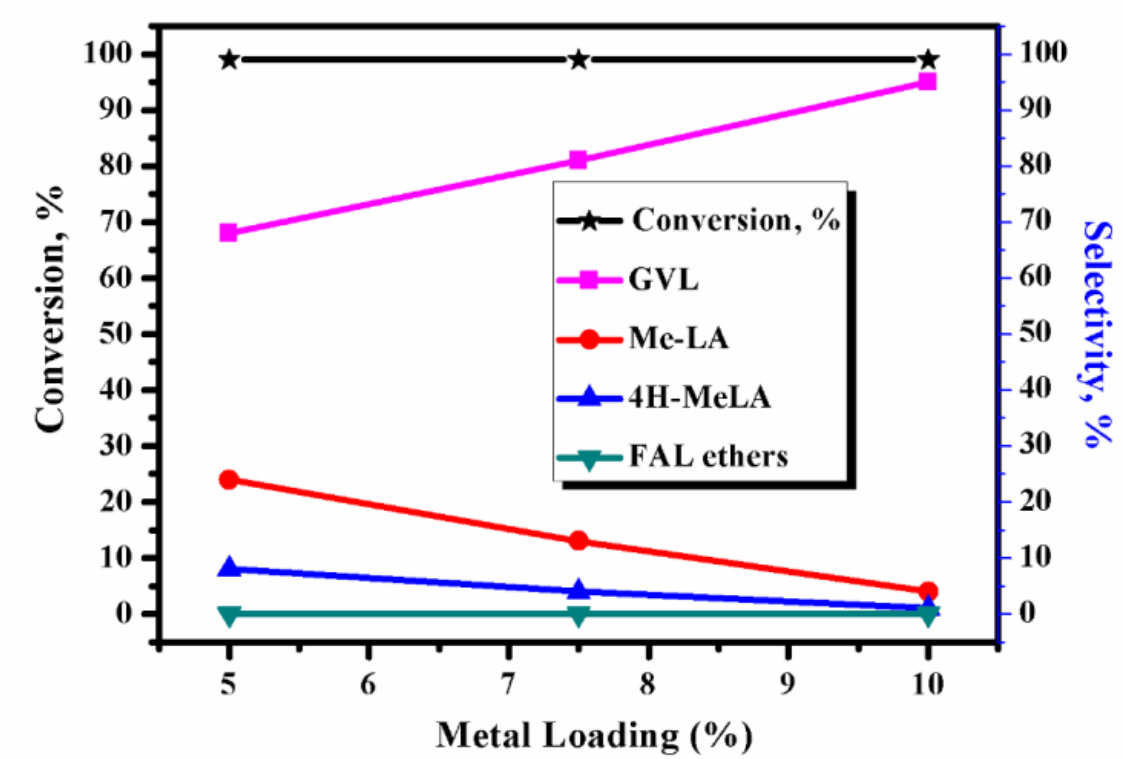

Figure 6.13. Effect of metal loading on hydrogenation of furfuryl alcohol to GVL

Reaction conditions: Furfuryl alcohol, 5% (w/w); solvent, MeOH (95 mL); temperature, 130 ^{o}C; H_2 pressure, 500 psi; catalyst, 0.3g (acidic IL) +0.5g (5-10% metal catalyst); reaction time, 5h.

6.3.4.4. Concentration Vs time study

The role of acidic and metal sites could be further understood for the direct single pot conversion of furfuryl alcohol to GVL under nitrogen and hydrogen atmosphere. Figure 6.14 shows the conversion and selectivity vs. time pattern for a single pot conversion of

furfuryl alcohol to GVL over acidic as well as metal sites. Initially, under an N_2 atmosphere, Brønsted acid sites of IL gave complete formation of methyl levulinate within the first 2 h of the reaction with complete conversion of furfuryl alcohol while changeover from N_2 to H_2 facilitated the hydrogenation of MeLA to 4-hydroxy MeLA followed by its cyclization to GVL. However, under only hydrogenation conditions, the ring hydrogenation product THF alcohol was obtained to the extent of 25–31% which remained stable, affecting the selectivity to GVL (entry 3, Table 6.2).

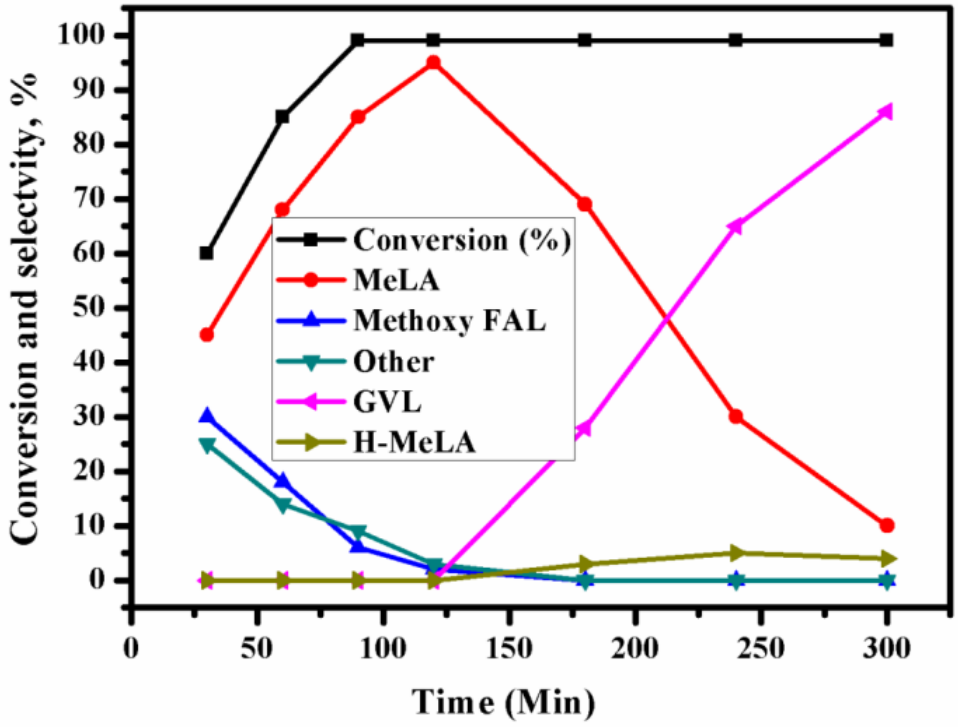

Figure 6.14. CT profile for furfuryl alcohol alcoholysis and hydrogenation

Reaction conditions: Furfuryl alcohol, 5% (w/w); solvent, MeOH (95 mL); temperature, 130 ^{o}C; N_2 atm. + H_2 pressure, 500 psi; catalyst, 0.3 (acidic IL) +0.75 g (5%metal catalyst); reaction time, 2h+3h.

The mechanistic pathway for alcoholysis of furfuryl alcohol to methyl levulinate catalyzed by IL in alcoholic medium involves first the formation of methoxy FAL followed by ring hydration in the form of 1,4- addition to form the intermediate A formed by subsequent deprotonation and the evolution of alkyl alcohol gave rise to the 1,3- diene B as shown in Scheme 6.3. Protonation of this diene yielded the cyclic oxonium compound, C. By electron-pair transfer, the cyclic oxonium compound was converted

into exocyclic oxonium D, which was attacked by water to form compound E, which then isomerized to form levulinate as the final product. In a single pot tandem approach we could achieve GVL synthesis from FAL..

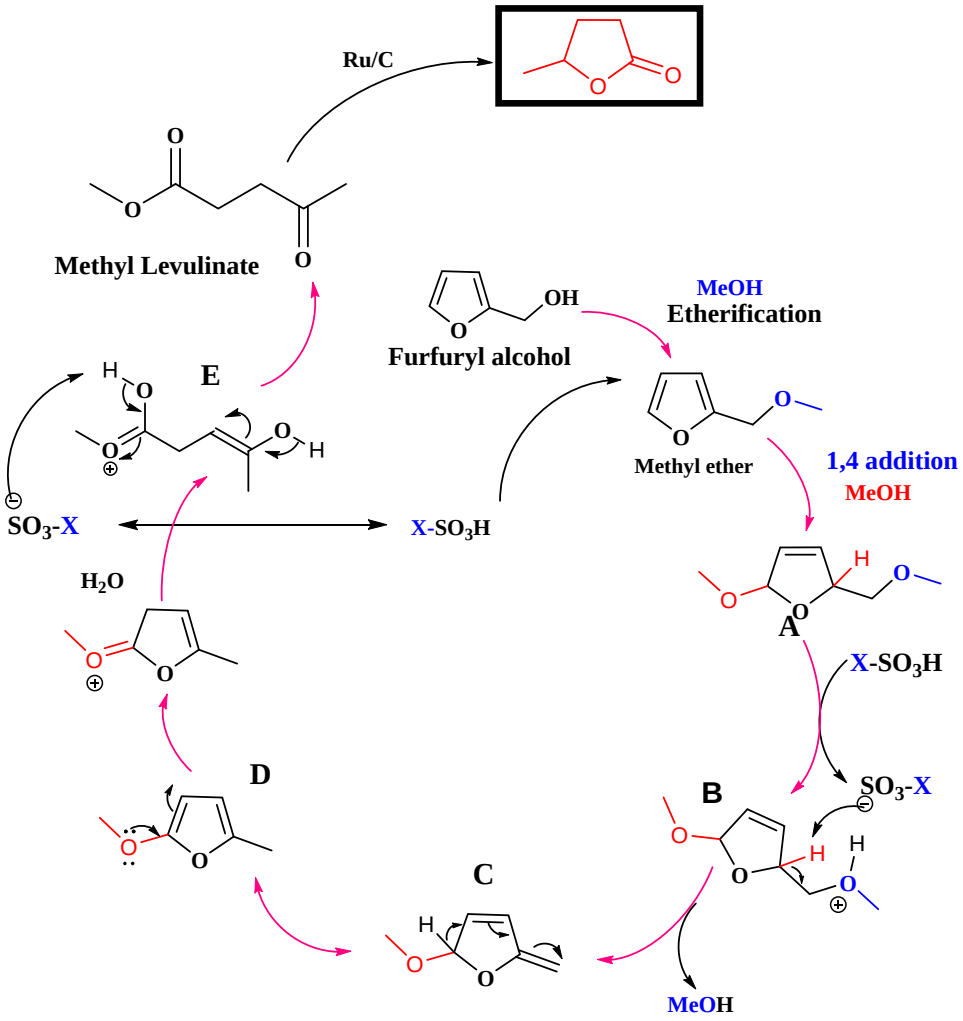

Scheme 6.3. Plausible mechanistic pathway for MeLA formation

6.3.5. Catalyst recycle study

The recycle experiments for [BMIm-SH][HSO4] catalyst for alcoholysis were also carried out at 130 °C. After completion of the reaction, methanol was evaporated using a rotavapour. To this concentrated solution, 80 mL of ethyl acetate was added and the IL was extracted with three portions 40 mL each of distilled water, in a separating funnel.

After evaporation of the aqueous layer, IL catalyst was recovered for its reuse in the subsequent alcoholysis experiment. This procedure was repeated up to the third recycle of the catalyst which showed the consistent activity as shown in Figure 6.15. A decrease in selectivity to methyl levulinate from 99 to 83% associated with the corresponding increase in intermediate selectivity was observed due to handling loss from time to time extraction. This was confirmed by adding a makeup amount (~20%) of the catalyst after the third recycle due to which the original selectivity to methyl levulinate was regained in the fourth recycle.

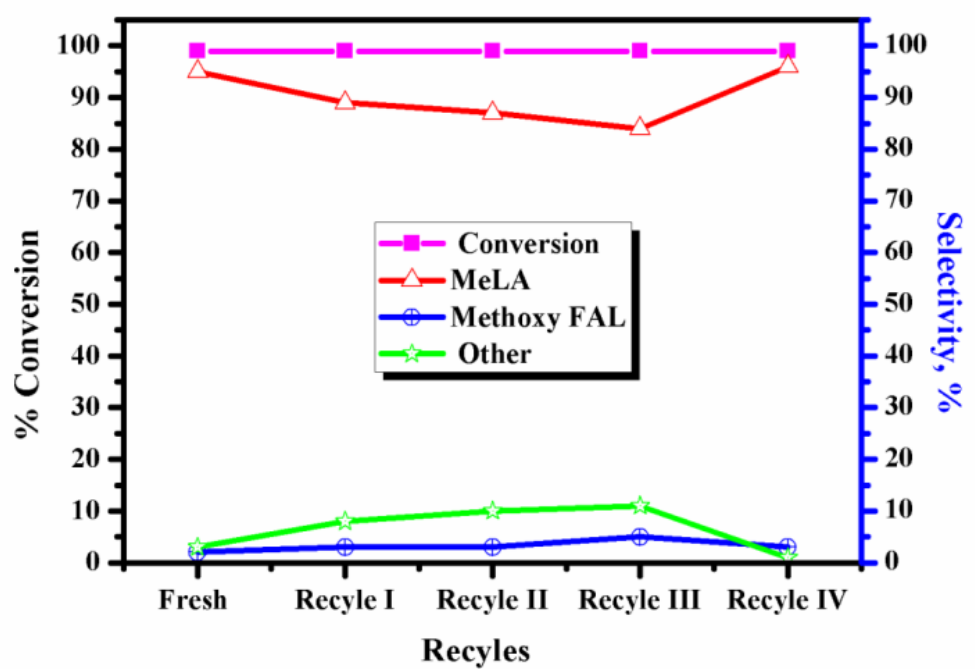

Figure 6.15. Catalyst recycle study for alcoholysis of furfuryl alcohol to methyl levulinate (B) direct hydrogenation of FAL to GVL

Reaction conditions: Furfuryl alcohol, 5% (w/w); solvent, MeOH (95 mL); temperature, 130 ^{o}C; N_2 atm, catalyst, 0.3 g [BMIm-SH][HSO4]; reaction time, 2 h; catalyst,

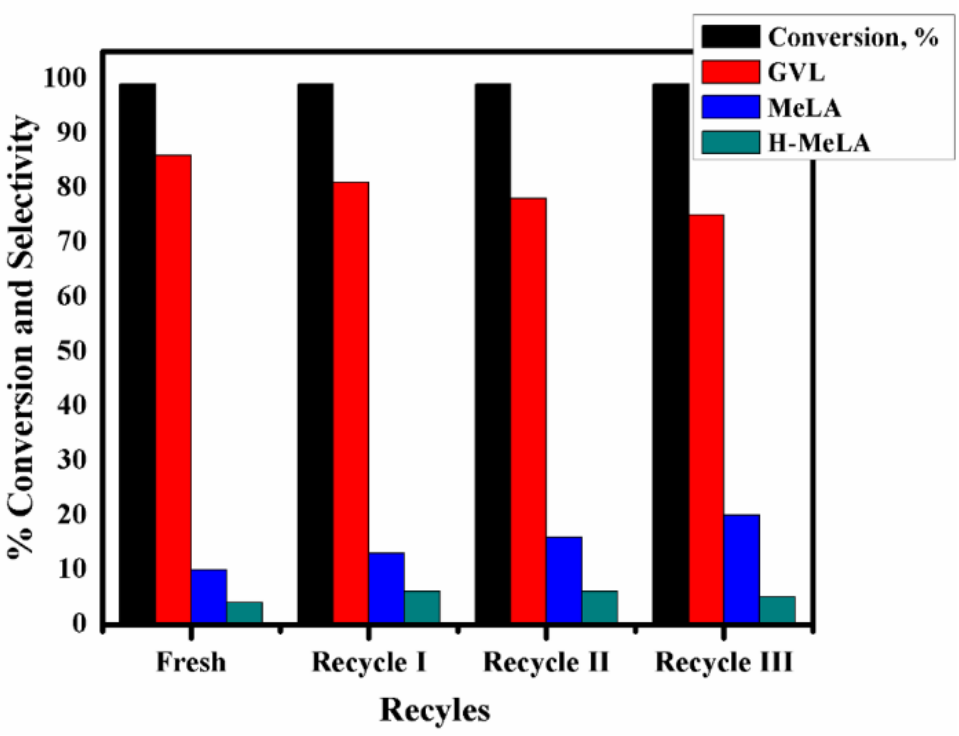

Figure 6.16. Catalyst recycle study for direct hydrogenation of FAL to GVL

Reaction conditions: Furfuryl alcohol, 5% (w/w); solvent, MeOH (95 mL); temperature, 130 ^{o}C; N_2 atm, catalyst, 0.3 g + 0.5 g [BMIm-SH][HSO4] + Ru/C; reaction time, 2 h; H_2 pressure, 500 psi; catalyst, 0.75 g;

The results of a catalyst recycle study for a single pot conversion of furfuryl alcohol to GVL are also shown in Figure 6.16. Both the activity and selectivity were consistent for 5% Ru/C in combination with [BMIm-SH][HSO_4] up to three recycles, confirming the stability of our catalyst system under reaction conditions. GC analysis of the organic layer showed GVL with 100% purity while the aqueous layer did not show any GVL Figures 6.17 and 6.18. This confirms the easy protocol of solvent extraction for the recovery of pure product (GVL).

NATIONAL CHEMICAL LABORATORY PUNE
Dr.Homi Babha Road Pune
Chemical Engg & process Dev

Method filename:	E:\solvent\LA\Cont 6.mth
Method name:	Amol
Analysed:	10-07-13 14:00
Printed:	11-Jul-13 11:13
Chromatogram filename:	E:\solvent\LA\Ethyl acetate GVL.dat

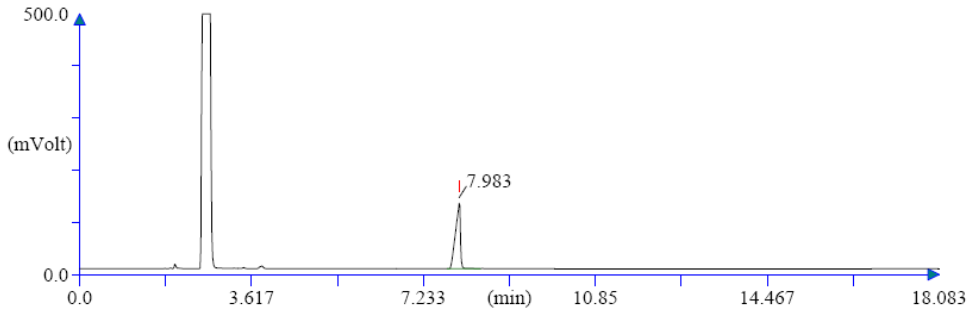

Retention Time (min)	Area (.1*uV*sec)	Area % (%)	Component Name
7.983	9053859	100.000	GVL
	9053859		

Warning Chromatogram has been subjected to manual integration.

Figure 6.17. GC spectra of extracted GVL

NATIONAL CHEMICAL LABORATORY PUNE
Dr.Homi Babha Road Pune
Chemical Engg & process Dev

Method filename:	E:\solvent\LA\Cont 6.mth
Method name:	Amol
Analysed:	10-07-13 17:52
Printed:	11-Jul-13 11:15
Chromatogram filename:	E:\solvent\LA\1§Amol001.dat

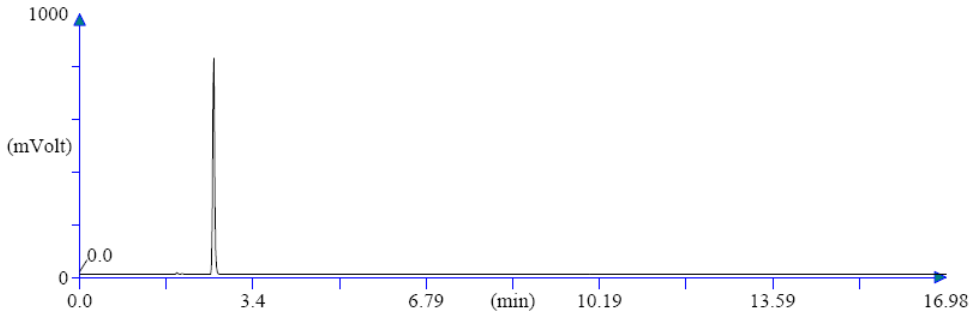

Retention Time (min)	Area (.1*uV*sec)	Area % (%)	Component Name

Warning Chromatogram has been subjected to manual integration.

Figure 6.18. GC spectra of aqueous layer for GVL

6.4. Conclusion

A novel tandem approach for direct conversion of furfuryl alcohol to GVL via the alcoholysis/hydrogenation sequence was demonstrated by designing sulfonic acid-functionalized ionic liquids (SO3H-ILs) and 5% Ru/C catalyst system. Furfuryl alcohol conversion as high as 99% could be achieved with ILs modified with HSO_4 and Cl-HSO3 anions in the alcoholysis reaction. The catalyst could be further tuned by increasing the alkyl chain of IL 1-methyl imidazole with 1,4-sultone to give an enhanced selectivity of 95% to methyl levulinate. Combining furfural alcoholysis with a subsequent hydrogenation of Me-LA in a single pot synthesis using our catalyst system comprising [BMIm-SH][HSO_4] + 5% Ru/C successfully resulted in the formation of GVL with 68% selectivity and complete conversion of furfuryl alcohol. Under the hydrogenation conditions, the ring hydrogenation to THFAL is a competing reaction adversely affecting the GVL selectivity; hence, the first stage alcoholysis can be carried out under N_2 and then changeover to H_2 eliminates the THFAL formation. Among the various parameters studied in this work, an increase in Ru loading from 5 to 10% dramatically enhanced the GVL selectivity from 68 to 94%, indicating that the availability of active metal sites is more significant in the tandem reactions of alcoholysis and hydrogenation of methyl levulinate. 5% Ru/C in combination with IL could be satisfactorily recycled three times with consistent performance, confirming its stability under reaction conditions.

6.5. References

1. G. W. Huber, S. Iborra, A. Corma, Chem. Rev.106 (2006) 4044.
2. J. O. Metzger, Angew. Chem. Int. Ed. 45 (2006) 696.
3. M. Stocker, Angew. Chem. Int. Ed. 2008, 47, 9200–9211.
4. F. M. A. Geilen, B. Engendahl, A. Harwardt, W. Marquardt, J. Klankermayer, W. Leitner, Angew. Chem.123 (2011) 6963.
5. L. Petrus, M. A. Noordermeer, Green Chem.8 (2006) 861.
6. R. Palkovits, Angew. Chem. Int. Ed.49 (2010) 4336.
7. M. Mascal, E. B. Nikitin, Angew. Chem. Int. Ed.47 (2008) 7924.
8. A. M. Hengne, C. V. Rode, Green Chem.14 (2012) 1064.
9. G. W. Huber, J. N. Chheda, C. J. Barrett, J. A. Dumesic, Science308 (2005) 1446.
10. J. P. Lange, E. V. der Heide, J. V. Buijtenen, R. Price, ChemSusChem5 (2012) 150.
11. J. P. Lange, Biofuels Bioprod. Biorefin.1 (2007) 39.
12. J. P. Lange, R. Price, P. M. Ayoub, J. Louis, L. Petrus, L. Clarke, H. Gosselink, Angew. Chem. Int. Ed. 49 (2010) 4479.
13. J. J. Bozell, L. Moens, D. C. Elliott, Y. Wang,G. G. Neuenschwander, S. W. Fitzpatrick, R. J. Bilski, J. L. Jarnefeld, Resour. Conserv. Recycl.28 (2000) 227.
14. B. Girisuta, B. Danon, R. Manurung, L. P. B. M. Janssen, H. J. Heeres, Bioresour. Technol.99 (2008) 8367.
15. P. Gallezot, Chem. Soc. Rev.41 (2012) 1538.
16. J. Q. Bond, D. M. Alonso, D. Wang, R. M. West, J. A. Dumesic, Science327 (2010) 1110.
17. I. T. Horvath, H. Mehdi, V. Fabos, L. Boda, L. T. Mika, Green Chem. 10(2008) 238.
18. H. Mehdi, V. Fabos, R. Tuba, A. Bodor, L. T. Mika, I. T. Horvath, Top. Catal.48 (2008) 49.
19. J. C. Serrano-Ruiz, R. Luque, A. Sepulveda-Escribano, Chem. Soc. Rev.40 (2011) 5266.

20. J. F. Tolan, B. Kamm, P. R. Gruber, M. Kamm, Biorefineries Industrial Processes and Products, Status Quo and Future Directions ed., Wiley-VCH, Weinheim, (2006) 193.
21. J. P. Lange, D. Wouter, V. D. Graaf, R. J. Haan, ChemSusChem 2(2009) 437.
22. Z. Zhang, K. Dong, Z. Zhao, ChemSusChem4 (2011) 112.
23. E. I.Grbz, S. G. Wettstein, J. A. Dumesic, ChemSusChem5 (2012) 383.
24. K. Tominaga, A. Mori, Y. Fukushima, S. Shimada, K. Sato, Green Chem., 13(2011)810.
25. S. Saravanamurugan, O. N. V. Buu, A. Riisager, ChemSusChem4 (2011) 723.
26. Z. Wu, S. Ge, C. Ren, M. Zhang, A. Yip, C. Xu, Green Chem.14 (2012) 3336.
27. G. M. Maldonado, R. S. Assary, J. Dumesic, L. A. Curtiss, Energy Environ. Sci.5 (2012) 6981.
28. A. M. Hengne, N. S. Biradar, C. V. Rode, Catal. Lett. 142 (2012) 779.
29. E. I. Gurbuz, J. M. R. Gallo, D. M. Alonso, S. G. Wettstein, W. Y. Lim, J. A. Dumesic, Angew. Chem. Int. Ed.52 (2013) 1270.
30. T. Miyazawa, S. Koso, K. Kunimori, K. Tomishige, Appl. Catal. A 329(2007) 30.
31. M. Osada, N. Hiyoshi, O. Sato, K. Arai, M. Shirai, Energy Fuels22 (2008) 845.

Chapter 7

Summary and Conclusions

7. Summary and Conclusions

In this thesis, a detailed study on developing various non-noble catalytic systems, their characterization and evaluation for the hydrogenation and alcoholysis-hydrogenation of levulinic acid and furfuryl alcohol, respectively, to γ-valerolactone (GVL) has been carried out. Both levulinic acid and furfuryl alcohol although used as model compounds in this work, are bio-derived C_5/C_6 platform molecules and GVL is an important product having wide range applications in energy as well as such as commodity chemical sectors. The study also involves preparation of noble metal catalysts for understanding the role of support in the activity and stability of the catalysts. Levulinic acid /ester hydrogenolysis route to GVL was studied using with and without external hydrogen source. The highlights of this Ph.D. work includes (i) the development of a non-noble metal Cu-ZrO_2 nanocomposite for levulinic acid hydrogenation via in situ esterification route, suppressing almost completely the leaching of active metal function, (ii) Ni based catalyst for CTH of levulinic acid using isopropanol as a solvent as well as a H_2 donor, (iii) development of a bi-metallic Ag-Ni catalyst for CTH of LA + formic acid mixture, in which synergism of a co-metal played an important role in generating hydrogen, (iv) tandem approach involving alcoholysis-hydrogenation sequence of furfuryl alcohol to GVL. The main conclusions of this work are summarized below.

- Initially, several supported noble metal catalysts were prepared, characterized and screened for MeLA hydrogenation to GVL, to understand the role of support. Among the screened catalysts, Ru/C was found to be the most efficient catalyst. TPR and XPS studies revealed that the formation of Ru^0 species was in higher extent on carbon support as compared to that on SiO_2 and Al_2O_3 supports. The encapsulation of Ru with silica and/or formation of stable species such as $Ru(OH)_3$ on the surface of oxide supports prevented the formation of metallic Ru.

- In order to make commercial application of LA hydrogenation to GVL process viable, non-noble metal nanocomposite catalysts were developed for the first time by incorporating Zr and Al with copper, for this sustainable process. This catalyst was prepared by a simple co-precipitation/digestion protocol which gave copper

particle size in a range of 10–14 nm, without using any template or a stabilizer. Both XRD and Raman spectroscopy confirmed the formation of the Cu–ZrO_2 nanocomposite and also the presence of mixed oxide phases along with Cu^0. Both Cu-Al as well as Cu-ZrO_2 catalysts showed complete conversion of LA and its ester with >90% selectivity to GVL. Interestingly, only Cu–ZrO_2 catalyst could be recycled efficiently four times for LA hydrogenation in methanol, with almost no leaching of the active metal. In methanol, the hydrogenation was found to proceed via the first step of the trans-esterification to the corresponding ester followed by its *in situ* hydrogenation to GVL.

- After studying LA hydrogenation using an external H_2 source, we also successfully developed two different catalyst systems for catalytic transfer hydrogenation (CTH) of LA using IPA and FA as H_2 donors. Two different catalytic pathways being operated for these two systems. In case of Ni-MMT catalyst using IPA as a hydrogen donor, the acidic MMT support catalyzes the LA esterification in presence of the secondary alcohol which is also an efficient H_2 donor for CTH while, the hydrogenation is being catalyzing metallic Ni sites. In another CTH system using aqueous LA:FA mixture, bimetallic and magnetically separable Ag-Ni/ZrO_2 catalyst was found to be highly efficient. The synergism of both the metals was essential for nascent H_2 generation from formic acid and its subsequent use for the hydrogenation of LA to GVL. For both LA and its esters, hydrogenation proceeded smoothly to GVL, confirming the bifunctional role of the catalyst in cyclization of 4-hydroxy LA esters. The generality of this catalyst was well demonstrated for one pot hydrogenation of biomass derived C_3 to C_6 molecules to a variety of useful molecules with almost complete conversion and > 80% selectivity. Due to its magnetic nature, the recovery of the catalyst was very easy and could be recycled up to five times, neither losing its activity nor any metal leaching.

- In an attempt to develop an alternate route for GVL synthesis, a more atom economic and a novel tandem approach for direct conversion of furfuryl alcohol

to GVL via the alcoholysis/hydrogenation sequence was demonstrated by designing sulfonic acid-functionalized ionic liquids (SO_3H-ILs) and 5% Ru/C catalyst system. First, the alcoholysis of furfuryl alcohol was investigated in which ILs modified with HSO_4 and Cl-HSO_3 anions were designed and prepared to give almost complete conversion of furfuryl alcohol to MeLA, in methanol medium. The catalyst could be further tuned by increasing the alkyl chain of IL, 1-methyl imidazole with 1,4-sultone to give an enhanced selectivity of 95% to methyl levulinate. Combining furfuryl alcohol alcoholysis with a subsequent hydrogenation of Me-LA in a single pot synthesis using our catalyst system comprising [BMIm-SH][HSO_4] + 5% Ru/C successfully resulted in the formation of GVL with 68% selectivity and complete conversion of furfuryl alcohol. Under the hydrogenation conditions, the ring hydrogenation to THFAL is a competing reaction adversely affecting the GVL selectivity; hence, a novel strategy was developed in which, first the alcoholysis was carried out under N_2 atmosphere and then changeover to H_2 gave selective formation of GVL without THFAL. The most sensitive parameter of Ru loading dramatically enhanced the GVL selectivity from 68 to 94%, indicating that the availability of active metal sites is more significant in the tandem reactions of alcoholysis and hydrogenation of methyl levulinate. 5% Ru/C in combination with IL could be satisfactorily recycled three times with consistent performance, confirming its stability under reaction conditions.

List of Publications

Research papers in peer reviewed journals

1. **A. M. Hengne**, C. V. Rode, Cu-ZrO_2 nanocomposite catalyst for selective hydrogenation of levulinic acid and its ester to γ- valerolactone, ***Green Chem.*** 2012, 14, 1064-1072.

2. **A. M. Hengne**, N. S. Biradar, C. V. Rode, Role of supported Ru catalyst for hydrogenation of bio-derived methyl levulinate to γ-valerolactone, ***Catal. Lett.*** 2012, 142, 779-787

3. **A. M. Hengne,** S. B. Kamble, C. V. Rode, Single pot conversion of furfuryl alcohol to levulinic esters and γ-valerolactone in presence of sulfonic acid functionzed ILs and metal catalysts, ***Green Chem.*** 2013, 15, 2540–2547.

4. **A. M. Hengne**, A. V. Malawadkar, N. S. Biradar, C. V. Rode, Surface synergism of Ag-Ni /ZrO_2 nanocomposite for catalytic transfer hydrogenation of bio-derived platform molecules, under revision to ***RSC Adv.*** *(RA-ART-09-2013-045384)*

5. **A. M. Hengne**, B.S. Kadu, N. S. Biradar, R. C. Chikate, C. V. Rode, Transfer hydrogenation of levulinic acid to g-valerolactone over MMT supported Ni catalyst, *Submitted to* ***Appl. Catal. B: Environmental***.

6. A. C. Garade, **A. M. Hengne**, T. N. Deshpande, S.V. Shaligram, M. Shirai, C. V. Rode, Continuous Hydroxyalkylation of p-Cresol to 2,2′-Methylenebis(4-Methylphenol) in a Fixed Bed Reactor, ***J. OF CHEM. ENG. OF JAPAN*** 2009, 42, 782-787.

7. Rasika B. Mane, **A. M. Hengne**, A. A. Ghalwadkar, S. Vijayanand, P. H. Mohite, H. S. Potdar, C. V. Rode, Cu:Al Nano Catalyst for Selective Hydrogenolysis of Glycerol to 1, 2-Propanediol, ***Catal. Lett.*** 2010, 135, 141-147.

8. N. S. Biradar, **A. M. Hengne**, S. N. Birajdar, P.N.Joshi, C. V. Rode, Single-pot hydrogenation of furfural to tetrahydrofurfuryl alcohol over Pd/MFI catalyst, Under revision to ***ACS Sustainable Chemistry & Engineering, ID: sc-2013-00302b)***
9. N. S. Biradar, **A. M. Hengne**, C. V. Rode, Catalytic hydrogenation of furfural to tetrahydrofurfural (THF): comparison of batch and continuous process operations, submitted to ***Organic Process Research & Development.***
10. N. S. Biradar, R. K. Swami, **A. M. Hengne**, C. V. Rode, Production of furfuryl alcohol and fuel intermediates via catalytic transfer hydrogenation of furfural over metal oxides, submitted to ***Chem.Comm.***
11. C. V. Rode, A. A. Ghalwadkar, R. B. Mane, **A. M. Hengne**, S. T. Jadkar, N. S. Biradar, Selective hydrogenolysis of glycerol to 1, 2-propanediol: comparison of batch and continuous process operations, ***Organic Process Research & Development*** 2010, 14, 1385–1392.
12. R.B. Mane, A.A.Ghalwadkar, **A.M.Hengne**, Y.R.Suryawanshi, C.V.Rode, Role of promoters in copper chromite catalysts for hydrogenolysis of glycerol, ***Catal. Today*** 2011, 164, 447–450.

Patents

1. C. V. Rode, **A. M. Hengne**, Ajay A. Ghalwadkar, Rasika B. Mane, Pravin H. Mohite and Hari S. Potdar, A process for the preparation of hydroxyacetone or propylene glycol, **WO2011/138643 A2**

2. C. V. Rode, **A. M. Hengne**, Process for preparation of γ-valerolactone via catalytic hydrogenation of levulinic acid, **Filed IN 0662DEL2012, US 13/774048**.

3. C. V. Rode, N. S. Biradar, **A.M. Hengne,** Single step process for conversion of furfural to tetrahydrofuran, **Filed IN 0249DEL2013**.

Posters/Oral presentations in national/international symposia

Oral

1. A.C. Garade, A. A. Ghalwadkar, **A. M. Hengne,** C. V. Rode, Presentation (Oral): Comparison of Batch and Continuous Process Operation for Hydroxyalkylation of p-Cresol to 2, 2'-Methylenebis (4-methylphenol), Conference: - **IICHE CHEMCON 2008** held at Chandigarh, India.

2. **A.M.Hengne**, A. A. Ghalwadkar, R.B. Mane, C. V Rode, Presentation (Oral): Selective liquid phase hydrogenolysis of glycerol to 1, 2-propylene glycol over nonchromium copper nano catalyst, **Conference: - Bilateral Indo-French Symposium on Catalysis for Sustainable & Environmental Chemistry.** 11-13 July 2010.

Posters

1. **A. M. Hengne**, A.A. Ghalwadkar, P. H. Mohite, R. B. Mane, C. V. Rode, Presentation (Poster):- **Best poster award** for "Selective liquid phase dehydration of glycerol to hydroxyacetone, Conference: - Science Day held at NCL, February 2009.
2. **A. M. Hengne**, C.V.Rode, Presentation (Poster):- **Best poster award** for "Cu-ZrO_2 nanocomposite catalyst for selective hydrogenation of levulinic acid and its ester to γ- valerolactone, Conference: - Science Day held at NCL, February 2012.
3. **A. M. Hengne**, C. V.Rode, Presentation (Poster):- **Best poster award** for "Surface species of supported ruthenium catalysts in selective hydrogenation of levulinic esters for biorefinery applications, Conference: - held at NIT Jalandhar, September 2012.
4. A. A. Ghalwadkar, R. B. Mane, P. H. Mohite, **A. M. Hengne**, C. V. Rode, Presentation (Poster):- **Best poster award** "Performance of NCL catalysts for

selective hydrogenolysis of glycerol to 1, 2 propylene glycol" Conference: - Indo-Russian Joint workshop on Catalysis for Bio-mass Conversion and Environmental engineering held at NCL, Pune in January 2009.

5. A. A. Ghalwadkar, R. B. Mane, P. H. Mohite, **A. M. Hengne**, C. V. Rode, Presentation (Poster):- Best poster award for "Downstream processing of bioglycerol" Conference: - Science Day held at NCL, February 2009.
6. A. Ghalwadkar, R. B. Mane, P. H. Mohite, **A. M. Hengne,** C. V. Rode, Presentation (Poster):- "Non chromium copper catalyst for selective liquid phase hydrogenolysis of glycerol to propylene glycol, Conference: - ACEPT held at NCL, June 2009.
7. Participated in 19th National symposium on catalysis (CATSYMP-19) on "Catalysis for Sustainable Energy and Chemicals" organized by National Chemical Laboratory (India) in January 2009.